Design Procedures of Retrofitted Bridge Rail

Richard L. Wood, Ph. D.
Assistant Professor
Department of Civil Engineering
University of Nebraska-Lincoln

Yijun Liao
Graduate Research Assistant
Department of Civil Engineering
University of Nebraska-Lincoln

Mohammad Ebrahim Mohammadi
Graduate Research Assistant
Department of Civil Engineering
University of Nebraska-Lincoln

Jordan Wipf
Former Undergraduate Student Researcher
Department of Civil Engineering
University of Nebraska-Lincoln

A Report on Research Sponsored by

Nebraska Department of Roads

University of Nebraska–Lincoln

July 2016

Technical Report Documentation Page

1. Report No. 26-1121-4024-001 SPR-P1 (15) M028	2. Government Accession No.	3. Recipient's Catalog No.
4. Title and Subtitle Design Procedures of Retrofitted Bridge Rail		5. Report Date August 2016
		6. Performing Organization Code
7. Author(s) Richard L. Wood, Yijun Liao, Mohammad Ebrahim Mohammadi, and Jordan Wipf		8. Performing Organization Report No. 26-1121-4024-001
9. Performing Organization Name and Address University of Nebraska – Lincoln 1400 R Street Lincoln, NE 68588		10. Work Unit No.
		11. Contract or Grant No.
12. Sponsoring Agency Name and Address Nebraska Department of Roads 1500 Highway 2 Lincoln, NE 68502		13. Type of Report and Period Covered July 2014 – July 2016
		14. Sponsoring Agency Code SPR-P1 (15) M028 RiP Project 36241
15. Supplementary Notes		

16. Abstract

The use of shallow embedment anchors in concrete is essential for retrofit applications; however, the combination of steel anchors, chemical adhesive, and concrete acting as a single tensile mechanism creates uncertainties in anchor strength and failure modes. Differences in concrete compressive strengths and in specifications of adhesives between manufacturers increases uncertainty further. In addition to these issues, prior research conducted by others examines the behavior of such anchors with respect to cracked versus uncracked concrete, partial bonding of the embedded length, and strength reductions due to anchor proximity to edges. While it is understood, anchors require a proper installation detail, the goal of this research is to understand the failure mechanisms and capacity when such conditions cannot be met.

One example of a limiting case is a retrofitted bridge where shallow anchors are the only option. For this application, experiments were conducted to determine the failure modes and capacities for a 4.75 inch embedment depth anchors of No. 4 reinforcement bars in accordance with a retrofit special provision. Additional experimental investigations were conducted to determine what, if any, differences existed between these provisions and specifications that included partially bonded anchors, anchors installed within an edge condition, and the differences between reinforcement surface coatings (epoxy vs plain or black). Excluding the edge tests which exhibited poor performance, most anchors exhibited a combined failure mode of concrete cone with steel rupture and reached capacities of 11.5 to 12.5 kips. No discernable difference in strength capacity was observed when the anchor embedment depth was reduced from 4.75 inches to 3.5 inches.

17. Key Words anchor, fastener, bridge rail, retrofit		18. Distribution Statement	
19. Security Classif. (of this report) Unclassified	20. Security Classif. (of this page) Unclassified	21. No. of Pages 206	22. Price

Table of Contents

List of Figures

List of Tables

Acknowledgements

Funding for this project was provided by the Nebraska Department of Roads (NDOR) under project number M028 – Design Procedures for Retrofitted Bridge Rail. The authors would like to express their gratitude for the support and guidance provided by the NDOR Technical Advisory Committee as well as Dr. Philipp Marhenholtz of Power Fasteners Europe, a R&D division of Stanley Black & Decker, and Mr. Peter Hilsabeck of the UNL Structural Laboratory. Material donations were graciously donated by Stanley Black & Decker with the assistance of Mr. Jacob Olsen as well two individuals, Ms. Jahida Nadi and Mr. Robert Dettman III, at Hilti North America.

Disclaimer

The contents of this report reflect the views of the authors, who are responsible for the facts and the accuracy of the information presented herein. This document is disseminated under the sponsorship of the U.S. Department of Transportation's University Transportation Centers Program, in the interest of information exchange. The U.S. Government assumes no liability for the contents or use thereof.

Abstract

The use of shallow embedment anchors in concrete is essential for retrofit applications; however, the combination of steel anchors, chemical adhesive, and concrete acting as a single tensile mechanism creates uncertainties in anchor strength and failure modes. Differences in concrete compressive strengths and in specifications of adhesives between manufacturers increases uncertainty further. In addition to these issues, prior research conducted by others examines the behavior of such anchors with respect to cracked versus uncracked concrete, partial bonding of the embedded length, and strength reductions due to anchor proximity to edges. While it is understood, anchors require a proper installation detail, the goal of this research is to understand the failure mechanisms and capacity when such conditions cannot be met.

One example of a limiting case is a retrofitted bridge where shallow anchors are the only option. For this application, experiments were conducted to determine the failure modes and capacities for a 4.75 inch embedment depth anchors of No. 4 reinforcement bars in accordance with a retrofit special provision. Additional experimental investigations were conducted to determine what, if any, differences existed between these provisions and specifications that included partially bonded anchors, anchors installed within an edge condition, and the differences between reinforcement surface coatings (epoxy vs plain or black). Excluding the edge tests which exhibited poor performance, most anchors exhibited a combined failure mode of concrete cone with steel rupture and reached capacities of 11.5 to 12.5 kips. No discernable difference in strength capacity was observed when the anchor embedment depth was reduced from 4.75 inches to 3.5 inches.

Chapter 1 Introduction

1.1 Background

Existing bridge rail may pose a significant risk to safety because of deterioration due to age or environmental conditions, previous impacts, or inadequate crash worthiness. Such conditions may cause marked capacity reductions, resulting in undesired performance, and early failures. For certain resurfacing, restoration, and rehabilitation projects (RRR) of bridge structures, it is economically unwise to perform a redecking due to inadequate bridge rail only. Bridge rail retrofit projects, as illustrated in Figure 1.1, utilizing post-installed anchorage in the existing concrete bridge decks. Connected to these anchorage is a new cast-in-place rail system that provides an economical, efficient, and safe solution. This is only provided that the post-installed anchorage used to secure the retrofitted rail to the bridge deck has sufficient capacity to withstand the design forces induced by a vehicular collision (e.g., TL-3).

(a) (b)

Figure 1.1 Bridge rail retrofit: (a) deteriorated steel rail, (b) retrofitted concrete rail

Unfortunately, concrete is a complex, heterogeneous, composite material with intrinsic variability. The anchorage system, consisting of reinforcement steel, chemical adhesive, and concrete, exhibits higher capacity uncertainties. This uncertainty is exacerbated in shallow embedment anchorage applications, where the design equations are invalid. The anchorage system may fail in various mechanisms due to the numerous materials. The desired failure mechanisms of such a system are ductile to permit load redistribution in the event of an extreme load (i.e., vehicular collision). Ductile failures are characteristic of steel rupture in lieu of concrete and adhesive failures. However, the failure mechanisms of shallow anchors are not well understood.

Extensive research on shallow embedded anchors has been conducted by others. The resultant data sets are useful for determining probable capacities and failure modes for tested anchor products and configurations. This has led to manufacturer and code-compliant capacities for design applications. However, brittle failure modes, which are common in shallow anchorage, result in larger penalty factors and reduced design capacities since they must account for uncertainty and experimental scatter. To ensure these products can be utilized where it is anticipated that the design capacities will be lowered, the shallow embedment anchorage configuration needs to be experimentally verified.

An experimental campaign was conducted to confirm the shallow embedment provision of a No. 3 epoxy-coated reinforcement bar at depths of 4.75 inches (12.1 cm) and 3.5 inches (8.9 cm). The current desired embedment depth is 4.75 inches; however, this is infeasible for tapered or thin concrete decks where the depth of concrete at the location of the anchors is less than 6.5 inches (16.5 cm). The strength of No. 3 reinforcement steel at 4.5 inches is sufficient, but if the

depth is reduced to 3.5 inches, the strength reduction is not well predicted. A standard plan view of the setup is shown in Figure 1.2.

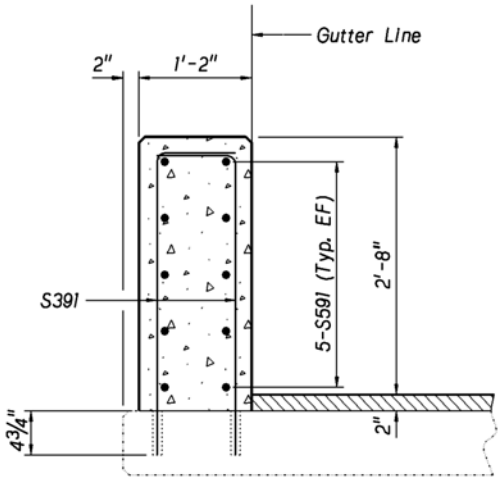

Figure 1.2 NDOR bridge rail retrofit special provision

The experimental campaign was divided into two primary phases. The first phase utilized five repeats for three configurations. Due to the compressive strength of the concrete being larger than what was anticipated in the field (5700 psi versus 3000-4000 psi in the field), an additional set of two slabs were constructed for the second phase, which explored seven different configurations. Phase two testing was comprised of a range of adhesives from different manufacturers, plain versus epoxy reinforcement steel, and partially bonded specimens. One additional test configuration of anchors located at the free edge was spot checked. While it was not anticipated that anchors at the edge would experience tensions associated with the direct impact of a vehicle, secondary loading associated with load distribution and dynamic cycling may induce tension into these anchors. Within this configuration of 4 inches (10.2 cm) of clear cover to the free edge, a stark reduction was observed while all other configurations had similar strengths. In summary, 39 anchorage pullout tests were conducted utilizing three different concrete slabs.

1.2 Objective

The primary project goal was to experimentally verify the capacity of the shallow embedment depth anchors as specified in the NDOR bridge rail retrofit special provision. This included the current specified depth of 4.75 inches as well as a reduced embedment depth of 3.5 inches for tapered or thin bridge decks.

1.3 Organization of the Report

This report documents the development of an experimentation campaign to verify the adequacy of the shallow embedded anchors. Chapter 1 of this report outlines the project and its focus. Chapter 2 provides an experimental introduction, which includes a summary literature review of shallow embedment depth anchors and the resultant test matrix. Chapter 3 documents the experimental setup, including the apparatus, instrumentation, and data acquisition for recording and analysis. Chapter 4 presents the experimental and analytical results of the concrete cylinders, concrete cores from phase two, and all of the associated anchorage specimens. The last section, Chapter 5, outlines the final recommendations and directions for future research.

Chapter 2 Experimental Introduction

2.1 Introduction

A brief literature review was conducted on factors that influence the capacity of epoxy anchorage, which were essential to the project's goal and possible alternative configurations. The primary experimental configurations focused on embedment depths of 3.5 and 4.75 in, with further tests including alternative installation configurations that could benefit capacity and desired failure mode, such as partial debonding of the anchor, as well as unforeseen configurations, such as edge anchors under tension loads as a result of load redistribution and rebound after a vehicular impact. The specific parameters of each configuration in the test matrix were developed following insight from previous research, referenced below. The anticipated demands were quantified using the TL-4 loading from MASH 350 (AASHTO, 2009) and can be later compared to the capacities found in the experimental campaign. In addition, the bond strength and concrete breakout design capacities for the anchor configuration were determined using equations from ACI 318-14. Finally, the test matrix is presented at the conclusion of this chapter.

2.1 Literature Review

2.1.1 Influence of Installation Procedures

Certain installation conditions can significantly influence the strength of epoxy or adhesive anchorage . Examples include poorly cleaned holes and damp or moist hole conditions. For example, excess moisture in a damp hole results in a 77% reduction of the adhesive bond strength compared to an ideal dry installation. Similarly, in a comparison between cleaned and uncleaned holes, the bond strength capacity decreases by an average of 29% (Cook and Konz,

2001). Both of these conditions are non-ideal due to their resulting reduced strength capacities for adhesive anchors. See Figure 2.1 for an installation example.

Figure 2.1 Installation of an adhesive anchor within a floor slab

Additional installation conditions exist as a result of poor management. After a field study was conducted on the installation of adhesive anchorage (Grosser et al., 2011), it was noted that the project site was often missing some or all of the material specifications required to install the adhesive anchor properly. These instructions denote proper adhesive storage techniques (possibly voiding the chemical properties), correct placement techniques (partial fill from the bottom of the hole and then upward toward the top), and temperature and curing tables. It is noted that these specifications vary between manufactures and adhesive types.

Other adverse installation conditions that reduce anchorage strength include: oversized holes, improper embedment depths, and incorrect adhesive cure times, which are dependent on environmental conditions. Although a perfect installation is nearly impossible, minimizing installation errors is critical, as noted on the manufacturer's instructions on proper installation

and storage techniques. Due to these well documented issues and the known reduction in strength capacity, variations in installation technique are not tested herein.

2.1.2 Minimum Edge Distance

The distance the anchor has to a free (or unrestrained) edge will have a significant influence on the failure mode and capacity. Each individual anchor has an influence area approximately 1.5 times the embedment depth. If an anchor is located at a reduced distance from an edge, the anchor will likely exhibit a side concrete cone breakout (or side-face blowout) at the ultimate failure load. Figure 2.2 illustrates this failure mode, which is not a desired failure mode. Eligenhausen et al. (2006) developed an equation to determine the critical edge distance, denoted as c_{cr}.

$$c_{cr} = 20d\sqrt{\frac{\tau}{1450}} \quad \text{[inches]} \tag{2.1}$$

where d is the anchor diameter and τ is the bond strength of the chemical adhesive. Likewise, and based on the work done by Eligenhausen, ACI 314-14 (2014) recommends a reduction in the bond strength and the concrete breakout capacity to account for potential edge distances smaller than equation 2.2. This edge distance, c_{Na}, is defined below and in 17.4.5.1d.

$$c_{Na} = 10d\sqrt{\frac{\tau}{1100}} \quad \text{[inches]} \tag{2.2}$$

It is critical to assess whether the provided 4-inch concrete cover between the anchor face and the slab edge is adequate for the special provision for the anchor closest to the free edge. A total of three edge effect tests were conducted to quantify this effect.

Figure 2.2 Example of catastrophic side concrete breakout at St. John's Lutheran Church in Pilger, NE

2.1.3 Partially Bonded Anchorage

One potential for retrofitted applications is the use of partially bonded anchors, based on the research performed by Gurbaz and Ilki (2011). Partially bonded anchors behave differently than traditional fully bonded anchors (where the adhesive is full depth). The undesired failure mode for a fully bonded anchor within low strength concrete is concrete cone breakout and/or anchor pullout, which is a significantly brittle failure mode. In comparison, the failure mode for a partially bonded anchor may be characterized as pullout after the anchor has yielded. This potential failure is often more ductile due to the yielding or necking in the steel anchor, which is often the preferred design due to its predictability and load distribution potential. When comparing identical anchors (diameter and yield stress) at the same embedment depth, a partially bonded anchor has nearly the same tensile strength as the fully bonded anchor. This was observed when the unbonded portion is a percentage of the total embedment depth. For anchors at deeper embedment depths, partially bonded anchors were noted to have an increased tensile capacity compared to fully bonded anchors for the same embedment depths. This is illustrated in

Figure 2.3, which depicts load-displacement curves for the two different anchor installations at identical shallow embedment depths of 6.3 inches. As observed, the partially bonded anchor (where only 3.8 inches are bonded) can achieve a larger displacement demand with increased ductility before failure due to yielding within the anchor. The ultimate strength for each anchor was 16.6 and 16.3 kips for the fully bonded and partially bonded conditions, respectively. This application may be beneficial for this retrofit application to ensure a more ductile failure mode without a marked reduction in tensile capacity. To explore this application, tests were repeated five times for 60% and 80% partially-bonded anchors at an embedment depth of 3.5 inches.

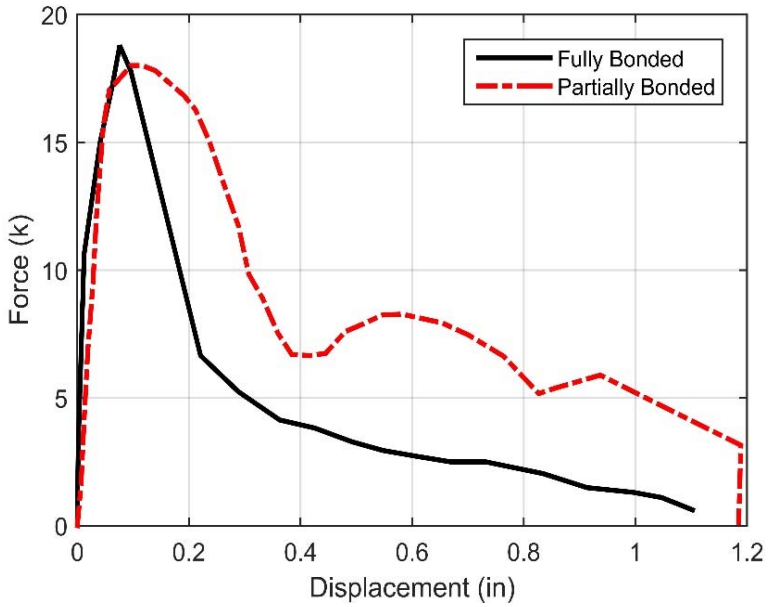

Figure 2.3 Load-displacement curves for No. 5 anchor with fully and 60% partially-bonded epoxy anchors with an embedment depth of ten times the diameter
(Digitized from Gurbaz and Ilki 2011)

2.1.4 Governing Design Code

An adhesive anchor subjected to tensile load will likely exhibit either a concrete breakout or bond failure. Under the ACI 318-14, an analyst checks for both conditions via individual equations to determine the controlling design scenario. The concrete breakout and bond strength are illustrated as equations 2.3 and 2.4, respectively. The derived capacities are assumed to be

dependent on embedment depth, diameter of the anchorage (or reinforcement bar), compressive concrete strength, and edge distance. The nominal concrete breakout design strength, N_{cb}, is quantified as:

$$N_{cb} = \frac{A_{Nc}}{A_{Nco}} \psi_{\text{ed,N}} \psi_{\text{c,N}} \psi_{\text{c}p,\text{N}} N_b \tag{2.3}$$

Likewise, the adhesive design strength, denoted as N_a, can be computed as:

$$N_a = \frac{A_{Na}}{A_{Nao}} \psi_{\text{ed,Na}} \psi_{\text{c,Na}} \psi_{\text{c}p,\text{N}} N_{ba} \tag{2.4}$$

In these equations, A_{Nc} and A_{Na} denote the project area of influence, A_{Nco} and A_{Nao} denote the project area of influence without edge effects, $\psi_{\text{ed,N}}$ and $\psi_{\text{ed,Na}}$ are parameters related to the edge effect, $\psi_{\text{c}p,\text{N}}$ and $\psi_{\text{c}p,\text{N}}$ are factors related to the cracking, and N_b and N_a are the nominal strength of the concrete breakout and adhesive bond. Note that the last subscript "c" or none relate to concrete, while the subscript "a" refers to the adhesive. Typical strength reductions of 0.75 are suggested by the ACI code. Using these aforementioned equations, the nominal concrete breakout design strength and bond design strength were calculated to be 8575 psi and 8889 psi, respectively, for a 3.5-inch embedded adhesive No. 3 anchorage in 3000 psi concrete with an adhesive strength of 2050 psi. Note that no effects of surface ribs are considered in the above calculation.

2.1.5 Design Loads via Vehicular Collision

The proposed retrofitted bridge rails are intended to sustain a TL-4 collision, as specified in MASH 350 (AASHTO, 2009). This impact is defined as a 22,050 lbf vehicle (pickup truck)

impacting the barrier at 55.9 mph with an incident angle of 15 degrees. After calculations, it was determined that this collision would produce approximately an 80 kips impact load to the barrier.

2.1.6 Anchorage Group Effects

When anchors are closely spaced, their behavior is no longer independent and is influenced by their neighbors or the group effect. The group spacing is dependent on the embedment depth of the anchors and the influence area. Anchors are code classified as an anchor group when the spacing is less than or equal to three times the embedment depth (ACI, 2014). Therefore, within this project, anchors may experience a group effect when the spacing is at 10.5 inches or less for an embedment depth of 3.5 inches. If the spacing is insufficient, a new coefficient to reduce the strength is specified in 17.4.2.4 (ACI, 2014). This can drastically reduce the capacity of the anchor for certain anchor group geometries. Eligenhausen et al. (2006) suggests that the anchor group effect will only occur when the spacing is less than 1.5 times the embedment depth. In contrast to ACI, this reduced number is based on numerical simulations and was later confirmed in extensive experimental investigations. Furthermore, it is suggested that ACI 318-14 design capacities for group effects are overly conservative.

Anchor group effects will only occur on anchors that are loaded in tension. These relate to the design loads for the anchorage under a vehicular collision. The largest anticipated tension loads are located closest to the traffic lanes, as illustrated in Figure 2.4. For the retrofitted rail scheme, an anchor group effect is only a consideration if the anchor spacing is less than or equal to three times the embedment depth, which is computed to be 10.5 inches for a 3.5-inch embedment. In addition, only the interior anchors are considered since the edge anchors are predominately loaded in compression due to the overturning moment induced by a vehicular collision (Figure 2.5). For this study, the targeted anchor spacing is 12.0 inches, so group effects are not considered.

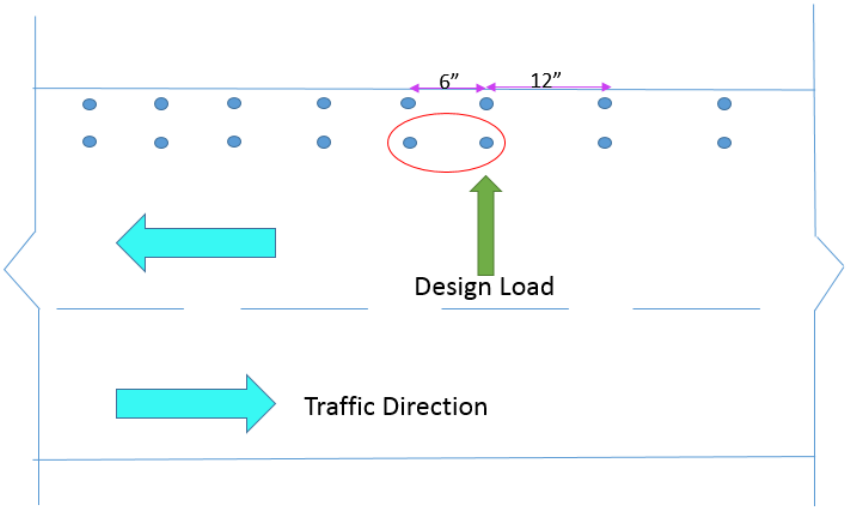

Figure 2.4 Schematic top view of an anchor group effect on a bridge rail

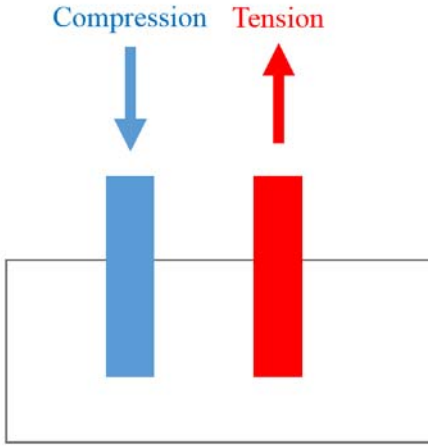

Figure 2.5 Schematic (side view) of the predominant force distribution under a vehicular collision (simplified)

2.2 Test Matrix and Summary

The finalized and iterated test matrix is presented in Table 2.1. This test matrix was constructed with the primary focus of verifying the capacities of the special provision for the retrofitted bridge rail at embedment depths of 4.75 and 3.5 inches with epoxy reinforcement. The 4.75 and 3.5-inch embedment depths are denoted as the current provision and baseline,

respectively. These essential tests were conducted with five repeats to gather a sense of the dispersion in the test data. The second priority for the test matrix was more exploratory to investigate the influence of other parameters. This includes a baseline configuration with plain (black) rebar, an alternative adhesive manufacturer, partially bonded cases with 60% and 80% configurations, and an extreme edge condition where only 4.0 inches of clear spacing is between the reinforcement bar and the free edge. Five configurations of each were sought; however, due to unexpected concrete cone failures, this was relaxed for non-critical cases. Note that in the configuration nomenclature, the following scheme was adopted: BL-AE where the first portion of letters represent the general description, such as BL=baseline, CP=current provision, and P80 and P60 for partially bonded at 80% bonded length and 60% bonded length, respectively. The final two letters indicate the adhesive and rebar type: either A or B for the adhesive and E or P for the surface coating of the rebar. This is the finalized test matrix where, due to spacing issues associated with low-strength or uncured concrete in the second set of slabs (2-1), the baseline and 60% partially bonded configurations had additional specimens added to a third slab (2-2) to ensure good data and a sufficient number of repeats. Due to significant edge breakouts, only three specimens were achievable for the edge effects series (EE).

Table 2.1 Test matrix with identified priorities

Test Number	Configuration	Description	Phase	Embedment Depth (in)	Adhesive Type	Rebar Type	Priority
1-5	BL-AE	Baseline	1	3.5	A	Epoxy	1
6-10	BL-AP	Baseline with plain rebar	1	3.5	A	**Plain**	1
11-15	CP-AE	Current provision	1	**4.75**	A	Epoxy	1
16-21	BL-AE	Baseline	2	3.5	A	Epoxy	1
22-26	CP-AE	Current provision	2	**4.75**	A	Epoxy	1
27-31	P60-AE	Partially bonded (60%)	2	3.5	A	Epoxy	2
32-34	P80-AE	Partially bonded (80%)	2	3.5	A	Epoxy	2
35-36	BL-BE	Baseline adhesive B	2	3.5	**B**	Epoxy	2
37-39	EE-AE	Edge effect	2	3.5	A	Epoxy	3

Chapter 3 Experimental Setup

3.1 Overview

In this chapter, a summary of the experimental setup is presented. This is done in a sequential fashion where the discussion starts with the concrete slabs and then the test apparatus (hydraulic jack with a built-up frame with a coupling nut). Afterwards, the selected instrumentation is discussed and the calibration procedure outlined. The selected adhesives, denoted as type A and B, are outlined as well as adhesive type C which exhibited extremely poor performance. Lastly, the methodology for the data processing is illustrated, and extraction of key parameters (stiffness, displacements, and forces) are outlined.

3.2 Concrete Slabs Construction and Detailing

In the first test phase, three mock bridge deck slab specimens with nominal dimensions of 4.0 feet (W), 8.0 feet (L) and 6.5 inch (D) using the standard 47-BD mix. This mix design provided by Concrete Industries Inc. To simulate the confining effect of reinforcement in bridge decks, the slabs were reinforced with No.5 plain reinforcement bars spaced 6 inch on center for the top and bottom mats in the longitudinal and transverse directions. The slabs are illustrated in Figures 3.1 through 3.3, where they are denoted as 1-1 (first pour, first slab), 1-2 (first pour, second slab), and 1-3 (first pour, third slab). A single side of the slab was simulated as a free edge of a bridge deck and did not have any protruding reinforcement. Note the reinforcement protrusions enabled locations to pick and move the slab throughout the lab. Twelve cylinders, 6 (D) by 12 (L) inches, were prepared for compressive strength characterization. Upon testing, the cylinders had an average compressive strength of about 5.7 ksi. As this far exceeded the desired strength of existing bridge decks (3500-4500 psi), a second set of mock bridge deck specimens were constructed, as outlined in the next subsection.

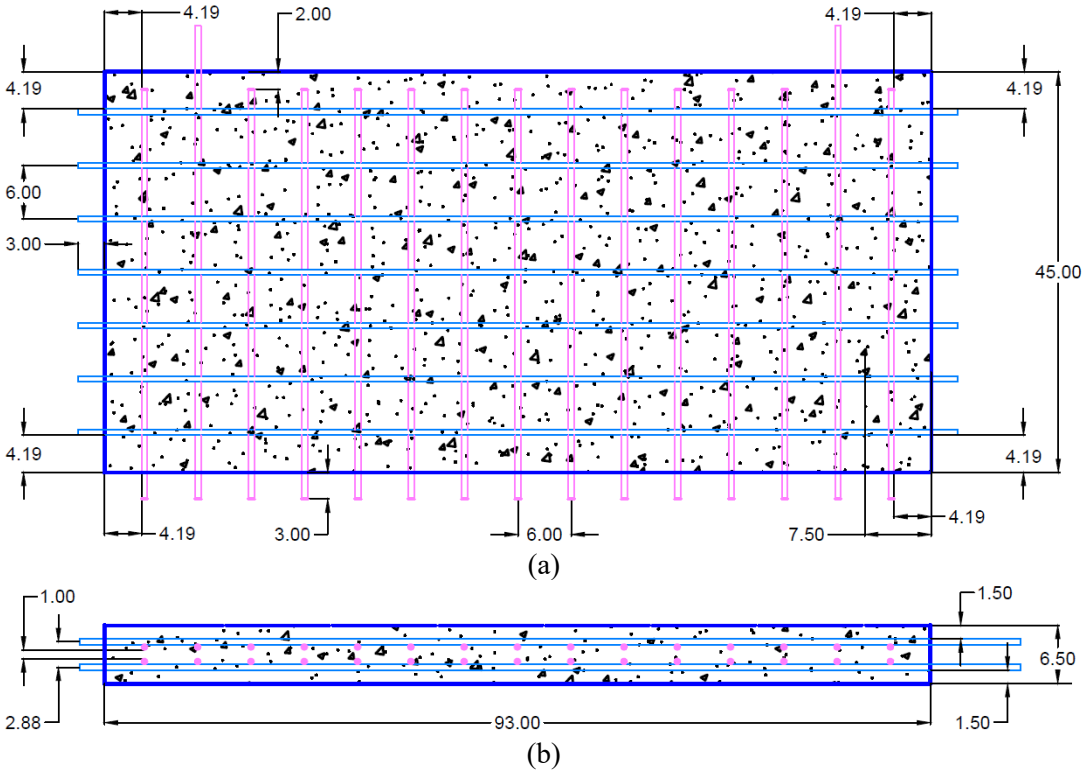

Figure 3.1 Dimensioned drawings of slabs 1-1 through 1-3: (a) top view and (b) side view

Figure 3.2 Rebar preset before the concrete placement

Figure 3.3 The final concrete slab (1-1) with identified locations for test specimens

Based on the feedback from the TAC members in October, two additional slabs were constructed with the desired lower compressive strengths. Phase two slab specimens had nominal dimensions of 7.0 feet (L), 7.0 feet (W), 6.5 inches (D). The geometry was modified from that of phase one to permit better specimen spacing within the central region of each slab. The reinforcement schedule comprised of No. 5 plain reinforcement bars spaced 6 inches on-center for each of the two mats. Like in phase one, a single free edge was maintained to simulate anchors within the edge zone. Figures 3.4 through 3.6 illustrate the phase two slabs (denoted as 2-1 and 2-2, representing the second pour first and second slabs, respectively).

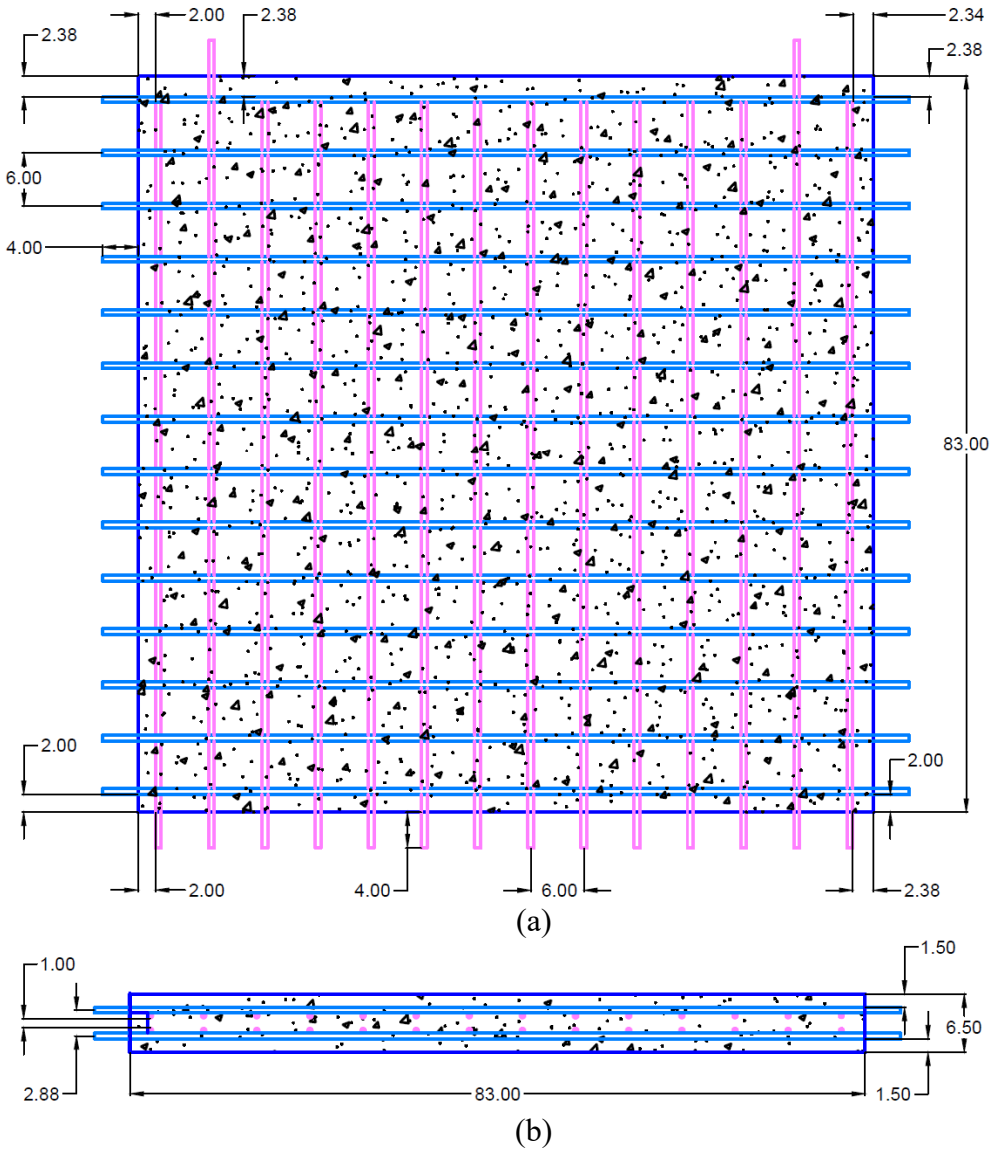

Figure 3.4 Dimensioned drawings of slabs 2-1 and 2-2: (a) top view and (b) side view

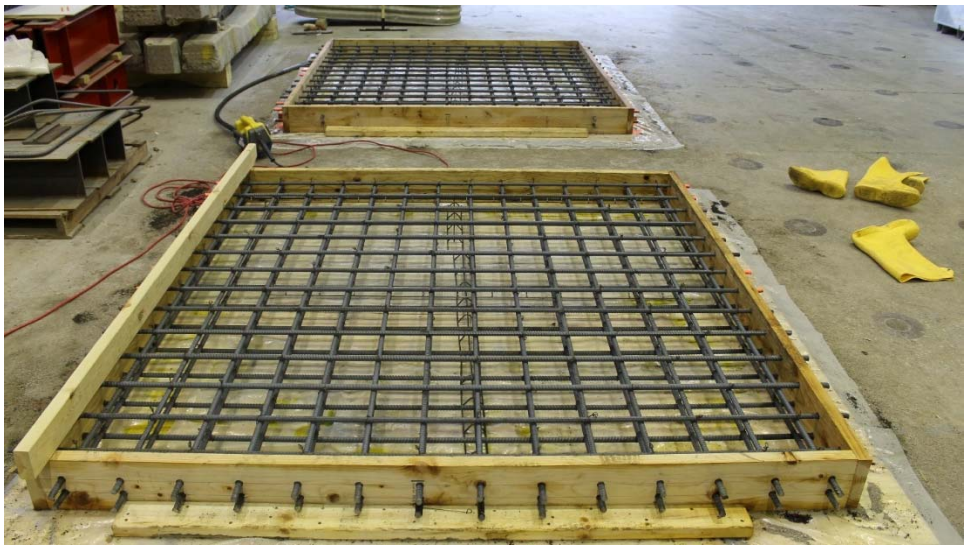

Figure 3.5 Rebar preset before the concrete placement

Figure 3.6 The final concrete slab (1-1) with identified locations for test specimens

3.3 Test Apparatus and Key Components

The experimental setup, illustrated in Figure 3.7, supplied a tension lead to the post-installed adhesive reinforcement bar without slippage. In this setup, a 120 kip (60 ton) hydraulic jack supplies a tensile load to the reinforcement bar while it reacts against the steel plate assembly

to create a clear span distance of 20.5 inches (greater than four times the embedment depth, as specified by ASTM E488 [2015]). The hydraulic jack applies the tensile force to the embedded reinforcement through a shear-bolt style rebar coupler that is welded to the end of a one-inch diameter Dywidag bar (Figure 3.8). The pressure of the hydraulic jack will indicate the tensile force. To measure the displacement, two six-inch stroke linear voltage displacement transducers (LVDTs) are supplied on each side of the test apparatus. The average of both LVDTs will be utilized in case any non-vertical displacement occurs. The LVDTs are welded to the horizontal plate and the plate bearing on the top of the hydraulic jack. Figure 3.9 shows the finalized test apparatus just before testing. Details of the hydraulic jack and the coupling nut are described in the next two subsections.

An Erico Lenton Lock Type B Shear Bolt Coupler, shown in Figure 3.7a, is designed to splice two No.3 or No.4 reinforcement bars together. In practice, this is done to reduce the overlap and development length required if they are not mechanically spliced. To prevent slippage between the embedded reinforcement bar and the coupling nut, the bolts were tightened to 30 lbf-ft, which equates to 20% of the fracture strength. Note this was done to permit the reuse of bolts and the coupling nut between specimens. Careful attention was taken at the conclusion of each specimen to inspect for slippage on both the shear bolts and the reinforcement specimen, but no slippage was observed.

The yellow Enerpac RCH-606 hydraulic jack displayed in Figure 3.9 supplies the tensile force to the reinforcement bar. The hydraulic jack has an effective area of 12.73 in^2 with a capacity of 60 tons (120 kips). When fully retracted, the jack is 12.75 inches tall by with an outside diameter of 6.25 inches. Upon full extension, the length is 18.75 inches, which indicates a full six inches of possible displacement. This displacement exceeded the anticipated

displacement range of the specimens. For precise quasi-static control of the applied force (pressure), the jack was operated via a manual hand pump.

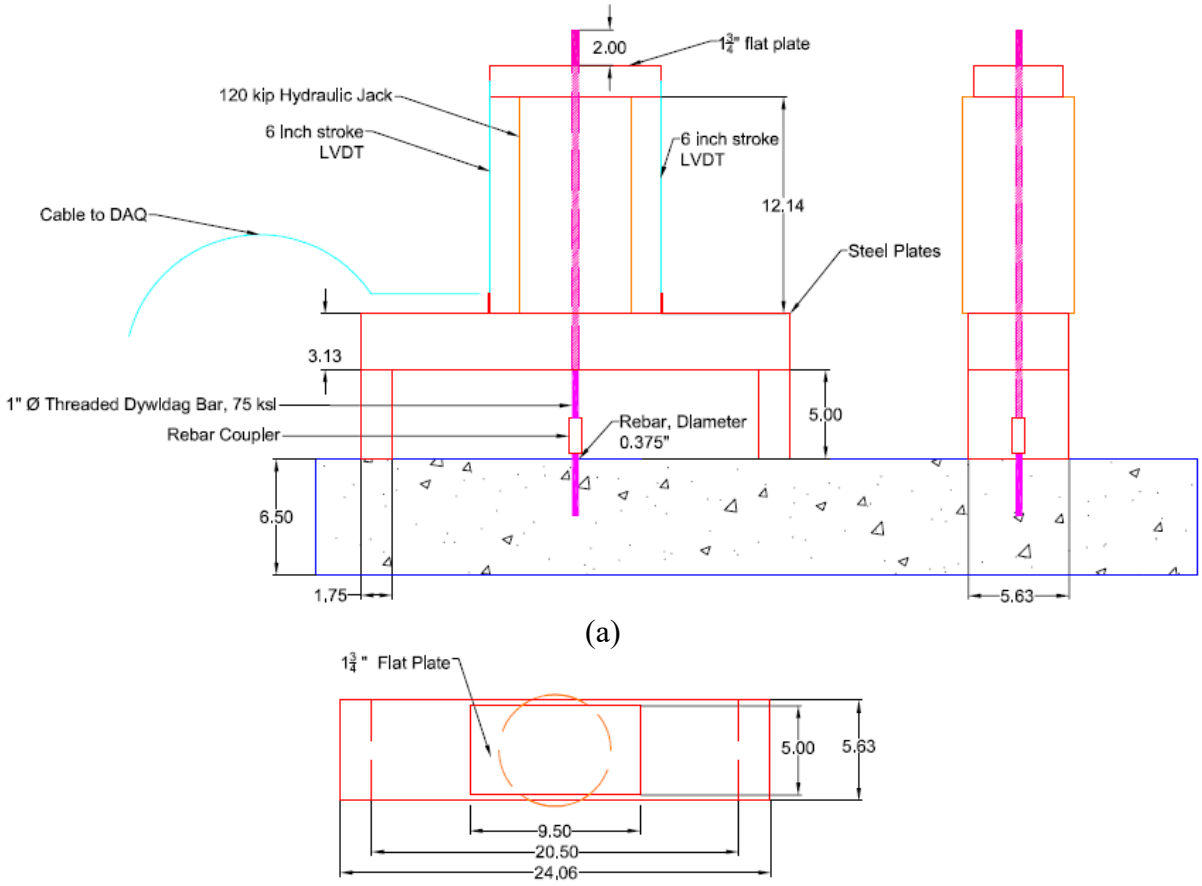

Figure 3.7 Experimental test apparatus setup where all dimensions are in inch: (a) side view and (b) top view

Figure 3.8 Rebar coupler details: (a) photo and (b) implementation drawing

Figure 3.9 Test setup with yellow hydraulic jack, rebar coupler, Dywidag, and two LVDTs

3.4 Instrumentation Selection

To measure the displacement of each specimen, two Celesco CLP 150 linear voltage displacement transducers (LVTDs) were connected to the frame on both sides of the hydraulic jack. These LVDTs have a nominal stroke of 6 inches and are specified as having nearly an

infinite resolution by the manufacturer. The potentiometers were excited with an input voltage of 5 volts and returned a scaled voltage. This scale voltage can be calibrated to provide displacement in inches. An example of a LVDT is shown in Figure 3.10.

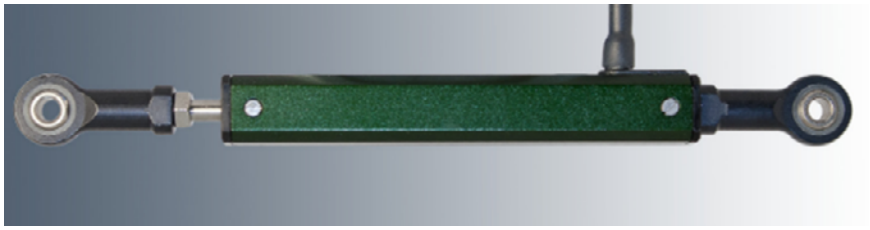

Figure 3.10 Example LVDT
(Figure courtesy of Celesco)

To quantify the tensile force induced by the hydraulic jack, an Omega PX612 pressure transducer was connected to the hydraulic assembly. According to the manufacturer, the pressure transducer is accurate within 0.4%. The pressure transducer was excited with an input voltage of 5 volts and returned a scaled voltage. The scaled voltage can be calibrated to provide pressure in terms of pounds per square inch (psi) and converted to force (lbf). Figure 3.11 shows an example of a pressure transducer.

Figure 3.11 Example pressure transducer
(Figure courtesy of Omega)

The instrumentation, which are the LVDTs and s pressure transducer, require calibration to convert scaled voltage into physical units. National Instruments (NI) provided the Signal Express platform, which is capable of the required calibration directly on the data acquisition (DAQ) device. This software platform was selected to quantify the stiffness, initial cracking, and failure mechanisms for the quasi-static test procedure. While the test is quasi-state in nature, the damage progression is dynamic; therefore, a sampling rate of 2 kHz was selected to capture this phenomenon. Note that this software package differs from other platforms used in UNL previous tests such that a high sampling rate is achievable. A screenshot of this software platform is shown in Figure 3.12.

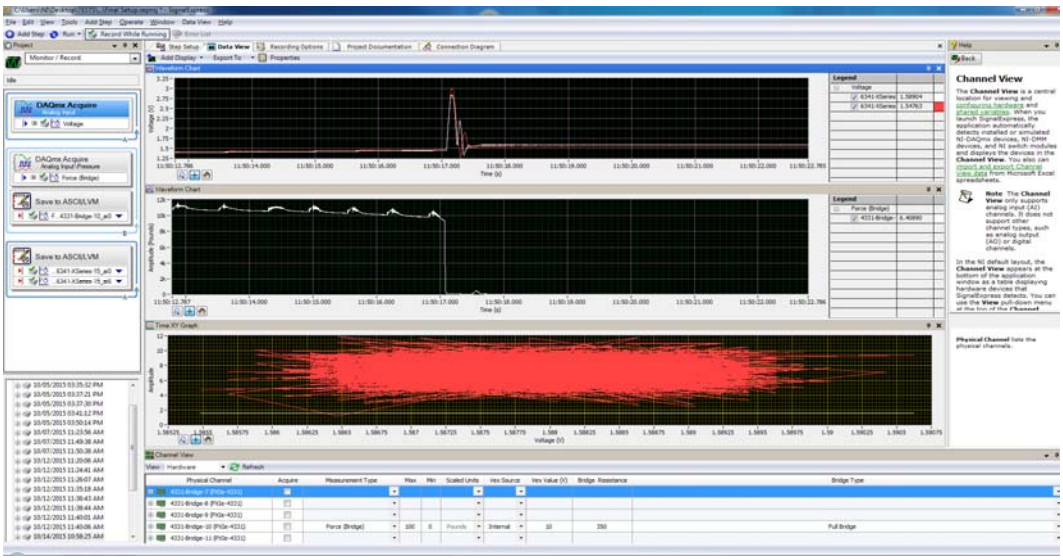

Figure 3.12 NI Signal Express software interface illustrated on the DAQ

The calibration of the LVDTS was performed via digital calipers and Signal Express. Caliper measurements were performed at one-half-inch intervals over the nominal stroke of six inches for each LVDT. The final calibration curves are illustrated in Figure 3.13. Linear regression was performed within the curves, and the curve fit was well-represented, as evidenced by r-squared

values of 1.0. The calibration of the pressure transducer was conducted by placing the hydraulic jack within the universal test frame (UTF) in the UNL structures lab. This was conducted within the NI Signal Express platform where numerous readings were taken over the targeted 25 kip range. Initially, values were obtained at 150 lbf intervals, then 500 lbf for force values in the mid-range, and increased to 5000 lfb at the higher force values (15, 20, and 25 kips). The calibration curve was found to be linear, as illustrated in Figure 3.14, and verified by an r-squared value of nearly one.

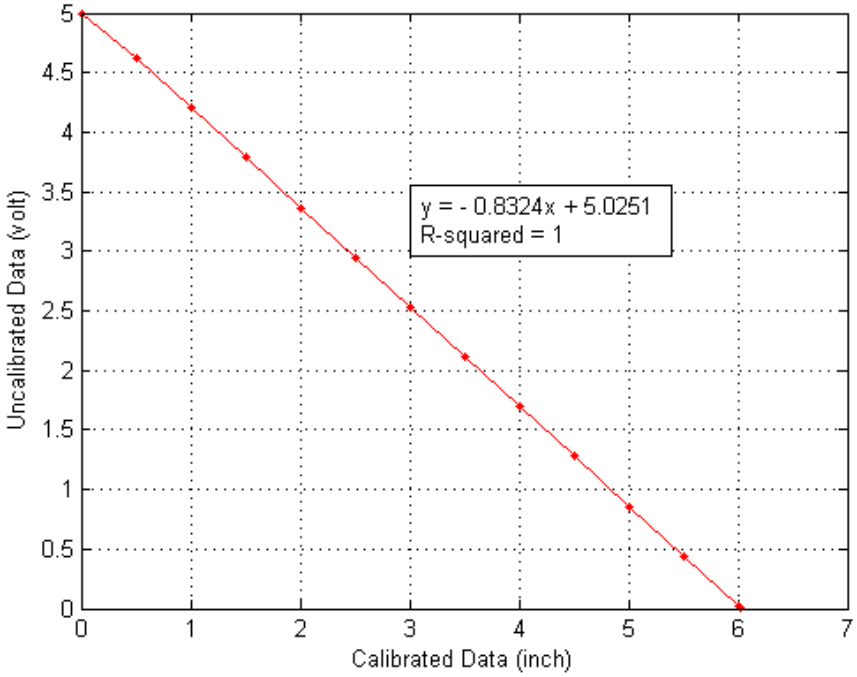

(a)

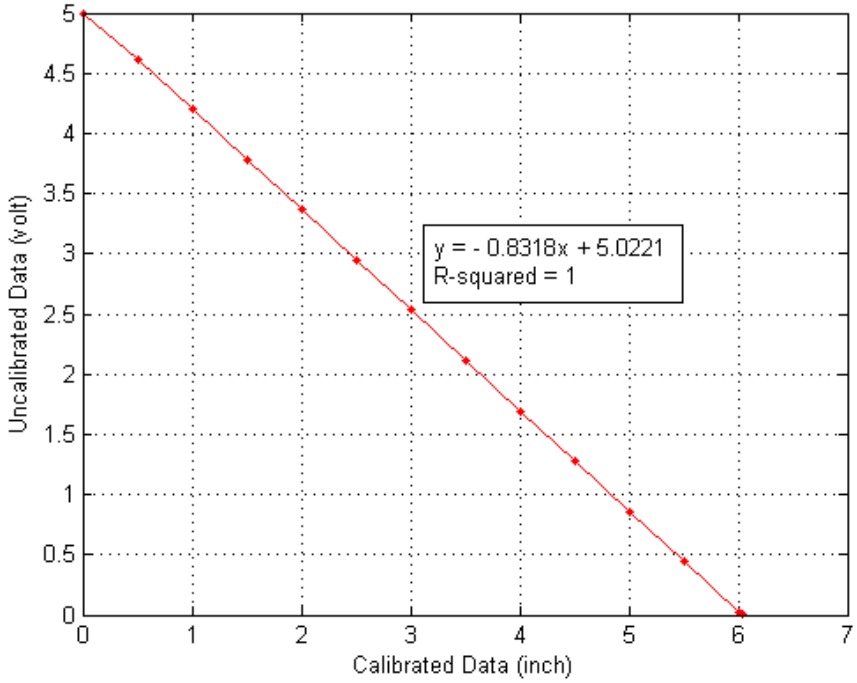

(b)

Figure 3.13 LVDT Calibration curves: (a) serial number 26686 and (b) serial number 28569

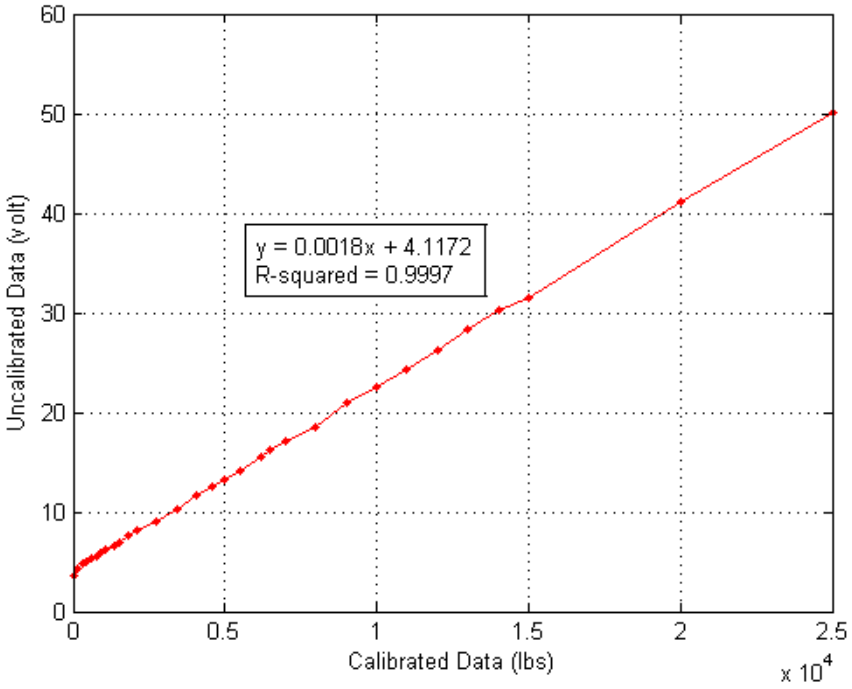

Figure 3.14 The px612 pressure sensor calibration curve

3.5 Adhesive Selection

Two different adhesives or epoxies were selected for the test matrix. This was done to investigate if the reinforcement behavior was dependent on adhesive or epoxy type. The primary adhesive was Powers PE1000+ (denoted as type A) and the secondary was Hilti HIT - RE500 (denoted as type B) for comparison purposes. Note both of these products are present on the most recent version of the NDOR approved product list (at the time of testing). Summary specifications of the two adhesives are provided in Table 3.1.

Table 3.1 Comparison of Hilti and Powers adhesives

Adhesive Type	Temp (°F)	T_{work} (min)	T_{cure} (hrs)	Bond Strength (psi)
Type A	68	30	10	2375
	86	20	6	
Type B	68	30	12	1800
	86	20	8	

A third adhesive, denoted as type C, was initially utilized in the pre-test configurations. This adhesive, Sikadur Anchorfix 2, is on the NDOR approved products list (APL) for anchorage epoxy; however, its performance was sub-par. This is a pre-mixed (single tube) adhesive that did not fully cure despite being in an ideal laboratory setting. During the pre-test trial runs, experimental configurations performed to iterate on the instrumentation and test fixture, two of the seven set anchors did not fully cure within two separate cartridges. As a result, significant reduction was observed in the tensile capacity, and upon inspection, the adhesive had a consistency similar to that of "cake frosting." The incomplete cure was in excess of the manufacturer's specifications, and all other installation requirements were either met or exceeded. While it is unknown if this was due to poor quality control, it was experienced in the middle of the cartridge in two batches. As a result, adhesive type C was eliminated from the test matrix. It is further recommended that this adhesive be re-evaluated since it is currently listed on the approved products list.

3.6 Data Analysis Methodology

With the test apparatus and the slab constructed, the only task left prior to conducting the experiments was determining how to process the data. The first step was to begin data recording, which is conducted before any forces or displacements have occurred. The first set of data points are inherently offset where an initial bias exists, so the pressure (force) and the displacements

values are zeroed out. This is done using a constant mean value of each channel during the pre-test window. Graphs of this process are shown in Figures 3.16 and 3.17. Figure 3.16 illustrates approximately a 0.9-inch displacement offset and 0.10 kip force offsets. The offsets are automatically corrected for each specimen, where an example of which is shown in Figure 3.17. Complete Figures for the entire test matrix are shown in Appendix A.

The next steps deal with the method of extracting the key points. Since the pressure in the hydraulic ram is supplied using a manual pump, the resultant force-displacement curve is not very smooth; the hydraulic ram relaxes due to gravity between oscillations of the handle. It is beneficial to smooth the data out and represent the bounding curve for a given displacement value, also known as the backbone curve. This is done automatically following each test. The first process uses a Butterworth filter and smoothing function to remove the high frequency noise in the data in terms of a low-pass filter, which is dependent on the other activities in the lab. The result after the removal of the high frequency noise is shown in Figure 3.17. With this smoothed curve, it is now necessary to determine the backbone curve, which is characterized as the maximum force for each displacement value. The filtered data after the backbone extraction is displaced in Figure 3.18 for a subset of the data where numerous relaxations occurred. Note the smoothness of the curve following the filtering and backbone extraction. Using this set of Figures, the maximum force and displacement can be found. The ultimate displacement and force is defined at breakage (bond slip or concrete cone) or 80% of the post peak strength if rupture is not achieved, as in the case of a ductile failure (yielding).

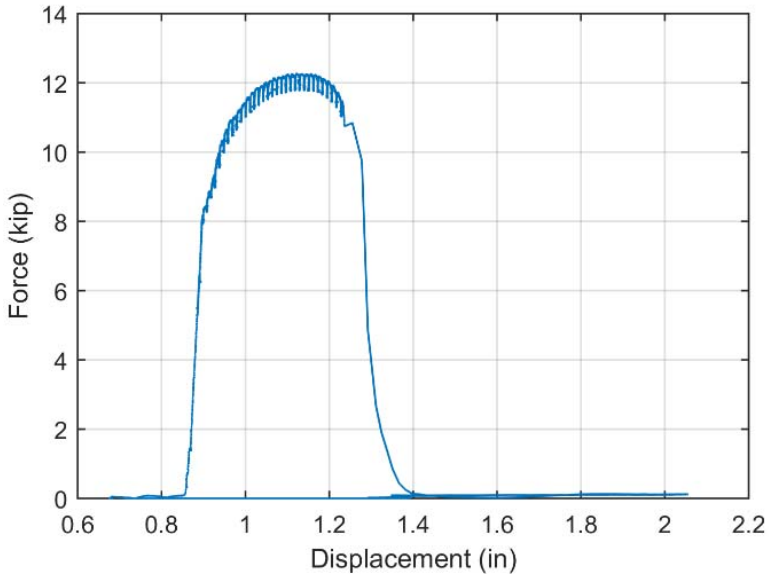

Figure 3.15 Force-displacement time history that requires bias correction

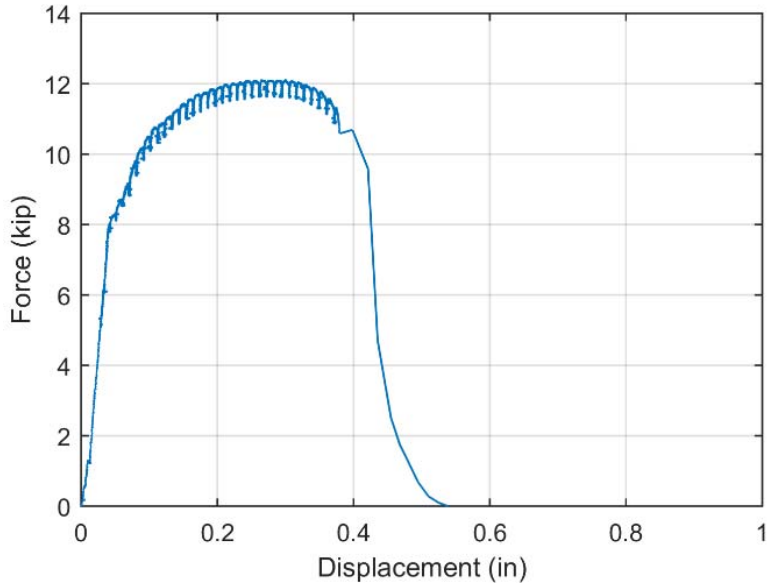

Figure 3.16 Force-displacement time history after correction for the initial bias

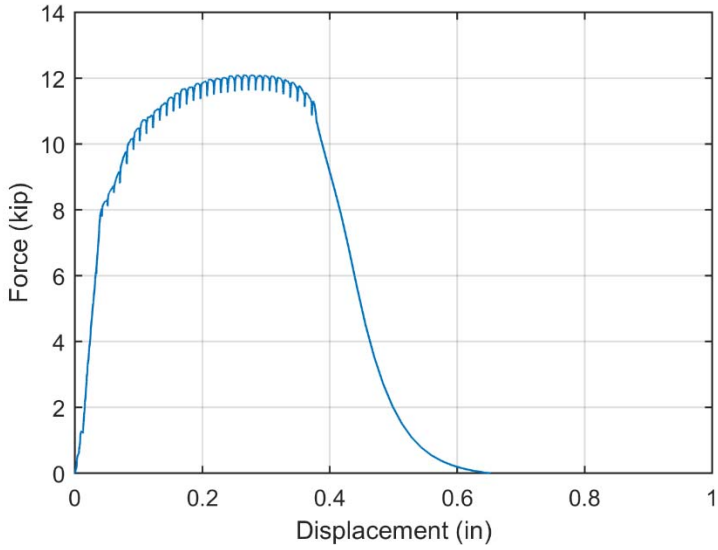

Figure 3.17 Filtered data plot

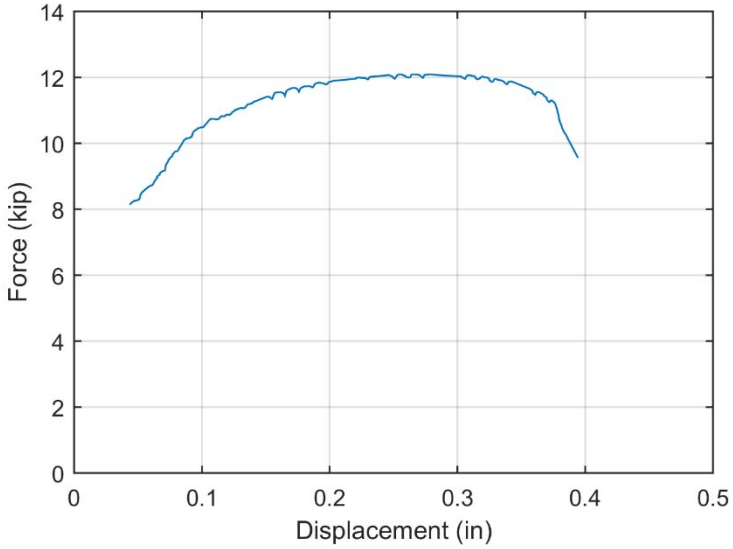

Figure 3.18 Backbone extraction curve

Additional parameters of stiffness, yielding displacement and force, and ductility were also sought. These parameters provide insight into the anchorage's behavior under a given load. The stiffness is computed as the significant value from the first derivative plot. This is the tangent stiffness, which is often higher when compared to the secant stiffness at yielding. An

example of the first derivative is shown in Figure 3.19. To indicate the point of significant yielding, the second derivative is computed, which also represents the curvature. The point of significant deviation is thereby indicated to be the point of yielding (refer to Figure 3.20). One complete force-displacement response with the points of yielding and maximum values is illustrated in Figure 3.21.

The final key point computed for each specimen is the ductility. Ductility is the ratio of the ultimate displacement normalized by that of the yield displacement. This is a direct quantity that relates to the specimen's ability to undergo nonlinear displacement after yielding. While ductility is not always needed, particularly beyond that of the maximum force, it permits load redistribution and limits catastrophic or sudden failure. This quantity is determined from previously identified quantities. In the example in Figure 3.21, the ductility is approximately 8.

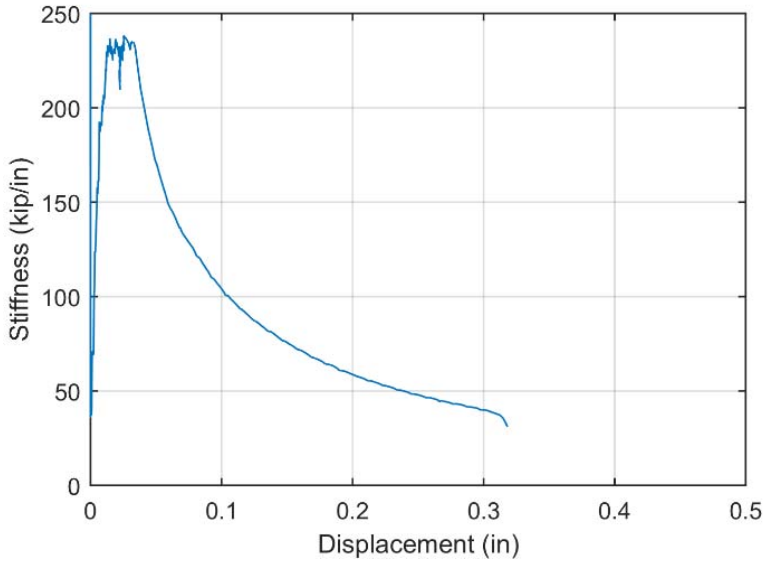

Figure 3.19 First derivative or the tangent stiffness

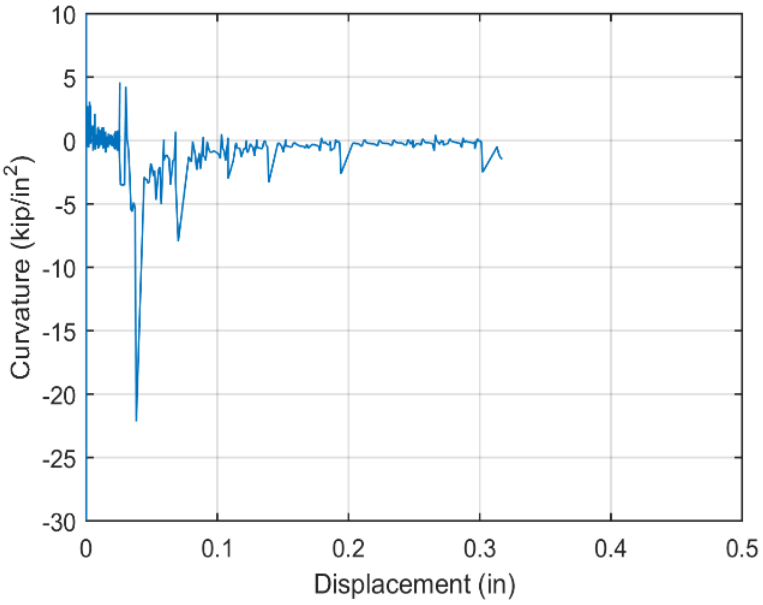

Figure 3.20 Second derivative or the curvature

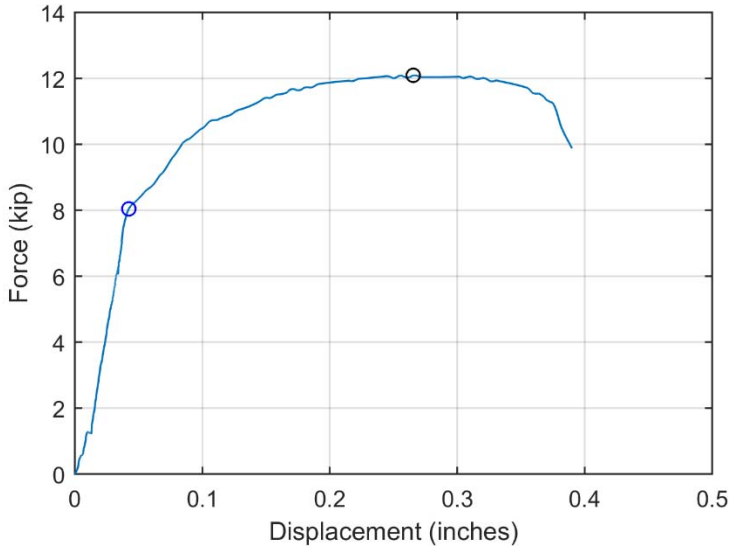

Figure 3.21 Filtered curve with yielding and maximum force

3.7 Summary

This chapter presented the concrete mock bridge deck specimens' test apparatus, instrumentation, and data processing. Note that when the two phases of tests were conducted, the results from the second set of slabs (2-1 and 2-2) were of most interest for this project. The procedure outlined here was utilized for the 45 specimens discussed in the chapter 4 summary.

Chapter 4 Experimental Results

4.1 Overview

In this chapter of the report, the experimental process and the results are discussed. The procedure for each test is quickly summarized prior to the discussion of the results, followed by a short discussion of phase one and its limitations. Due to the high compressive strength values for the concrete specimens in phase one, phase two is of most interest since it represents anticipated concrete strengths for possible bridge rail retrofit installation. The focus is on phase two and a compressive comparison outlines its key findings. Note complete experimental results may be obtained in Appendices A, B, and C.

4.2 Specimen Procedure

Before any of the installed anchorage is loaded in tension, each embedded reinforcement bar is prepared. The first step is to set up the coupler on the reinforcement. Before tightening, the hydraulics are released by opening the manual release valve such that the pressure is nominally zero. Then the shear bolts on the reinforcement bar coupler are tightened to a maximum of 30 ft-lbf. The built-up test apparatus is carefully lifted over the reinforcement bar into place. After the apparatus is in its approximate position, the horizontal plate is checked for levelness and shimmed as necessary. Then, the LVDTs, one on each side, are connected after they are checked for plumb in both directions. If the LVDTs are not plumb, additional washers are applied as needed. When this is completed, the specimen and the test apparatus are ready for the tensile loads. The loading of each specimen was done using a manual hydraulic pump, as discussed in Chapter 3. Each specimen is photographed before and after each test, and the DAQ's operation is confirmed with a sampling rate of 2 kHz. Each specimen is loaded in tension until failure.

Failure is either defined as mechanical (anchor pullout) or excessive force reduction past the peak load (80%).

4.3 Phase One Summary

In the first phase of the experimental campaign, three sets were achieved, namely: BL-AP, BL-AE, and CP-AE. The first series corresponds to the baseline configuration (3.5-inch depth) with plain reinforcement (black) secured with adhesive type A. The second series is similar to the first; however, it utilizes epoxy reinforcement (green). The third series achieved in phase one was the current provision (4.75-inch depth) with epoxy reinforcement secured with adhesive type A. Before the details are presented for each specimen, the characterization of the compression is discussed.

Concrete cylinders constructed during the first pour permit the characterization of the compressive strength. In accordance with ASTM C31/C31M (2015), the cylinder length is specified to be twice the diameter, while the cylinder diameter shall be at least 3 times the nominal maximum size of the coarse aggregate. This specification was met for the 6 (D) by 12 (W) inch cylinders. During the application of the compressive loads, the load rate is specified as 35 ± 7psi/second. The load rate is continually applied until failure.

In accordance to the specification, 12 cylinders were constructed during the first phase of testing. These were divided into six cylinders for slab 1-1 and three each for slabs 1-2 and 1-3. During the specimen testing for slab 1-1, the corresponding first three cylinders were broken. The compressive strengths were 6.0 ksi, 5.6 ksi, and 4.5 ksi, with a mean value of 5.8 ksi. A graphical display of the cylinder compressive strength is illustrated in Figure 4.1. This is a higher than expected value, and as a result, only three quick specimen groups were conducted. Complete details can be found in Appendix C.

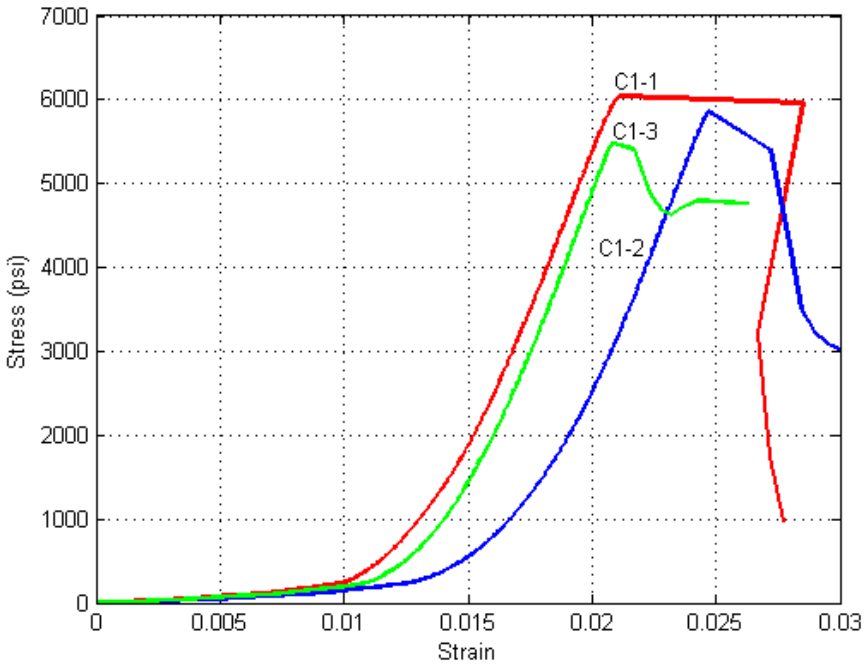

Figure 4.1 Compressive stress strain curves for slab 1-1 cylinders in phase one

The summary of results for first three specimen groups of phase one are presented here for completeness. Recall that the compressive strength of this concrete specimen at the time of testing was 5.8 ksi. This is higher than what is typical for an existing bridge deck and therefore these results are only presented for comparative purposes. They are inconclusive for the application of the retrofitted bridge rail. The typical failure mode for all series is a combined failure mode of concrete cone and steel rupture. Two examples are shown in Figures 4.2 and 4.3 for the BL-AE and CP-AE series, respectively. Group summary details can be found in Figures 4.4 through 4.6 and Tables 4.1 through 4.3. The maximum force capacities per group was within 2% of each other and centered around 12.1 kips.

Characteristic values of each specimen group can be calculated in accordance with ACI 355.4 (ACI, 2011). This is calculated using the computed values of the mean maximum force and its coefficient of variation. The computed values are 11.87, 11.46, and 12.17 kips, which correspond to BL-AP, BL-AE, and CP-AE, respectively. This indicates that for a 3.5-inch

embedment depth, the plain or non-epoxy surface coated reinforcement has a slightly higher strength. When comparing the 3.5-inch vs 4.75-inch depth, only a 0.7 kip force reduction (5.8%) is observed. Since the concrete strength is higher than what is anticipated in the field, no clear recommendation can be made.

Figure 4.2 Representative failure mode for BL-AP of combined failure in 5.8 ksi compressive strength concrete

Figure 4.3 Representative failure mode for CP-AE in 5.8 ksi compressive strength concrete

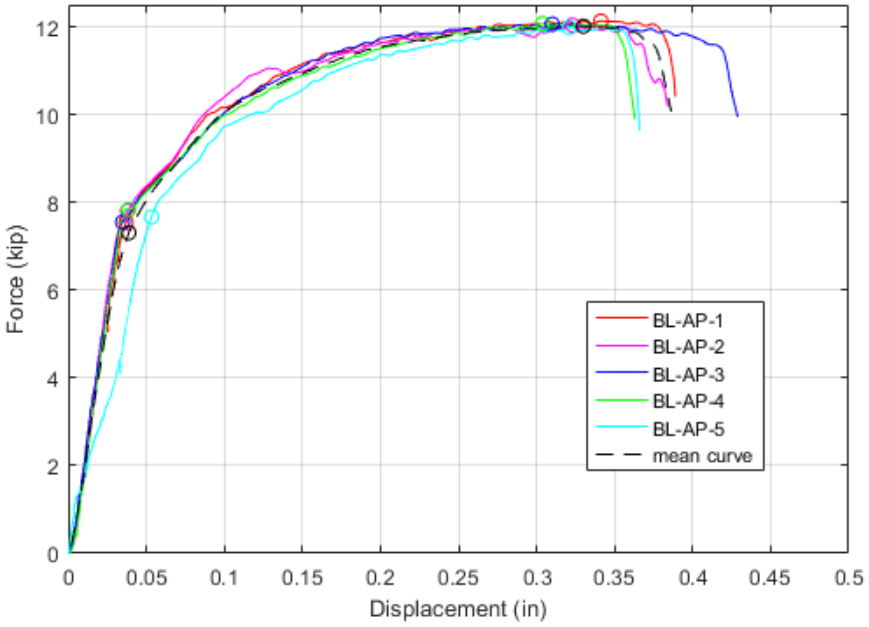

Figure 4.4 Specimen group comparison for BL-AP and its representative mean curve in 5.8 ksi compressive strength concrete

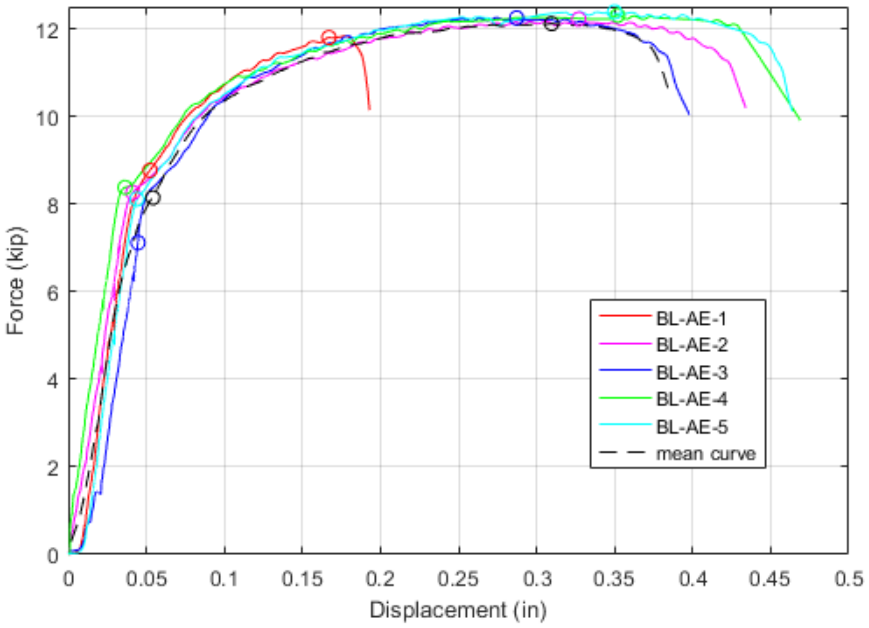

Figure 4.5 Specimen group comparison for BL-AE and its representative mean curve in 5.8 ksi compressive strength concrete

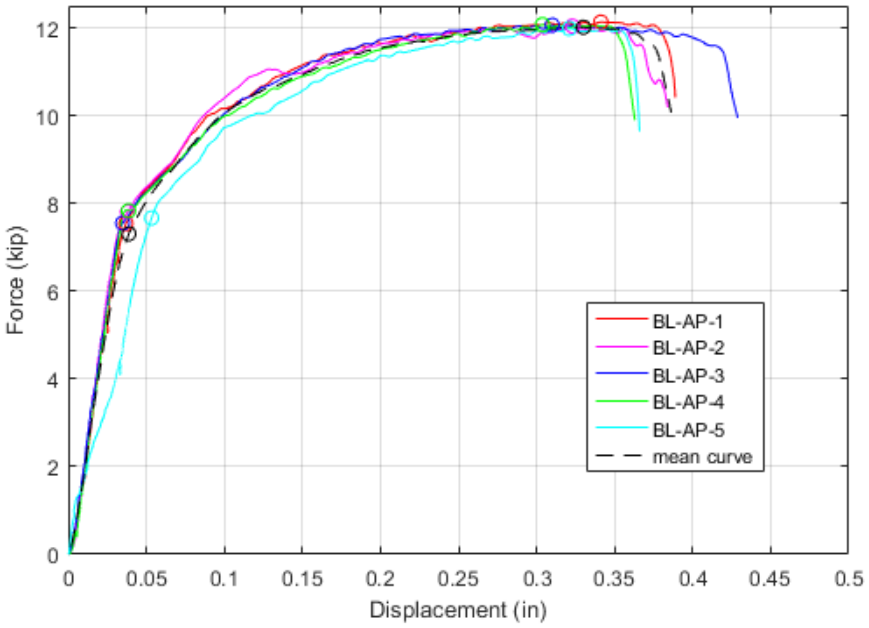

Figure 4.6 Representative failure mode for CP-AE in 5.8 ksi compressive strength concrete

Table 4.1 Specimen group summary and key points for BL-AP in 5.8 ksi compressive strength concrete

Test Name	Stiffness (kip/in)	F_y (kip)	Δ_y (in)	F_{max} (kip)	Δ_{max} (in)	F_u (kip)	Δ_u (in)	μ (in/in)
BL-AP-1	222.04	7.54	0.037	12.13	0.341	9.68	0.389	10.52
BL-AP-2	239.50	7.80	0.038	12.04	0.323	9.63	0.384	10.11
BL-AP-3	231.97	7.55	0.035	12.06	0.310	9.74	0.430	12.29
BL-AP-4	227.10	7.83	0.039	12.07	0.304	9.69	0.365	9.36
BL-AP-5	275.00	7.66	0.053	11.98	0.321	9.59	0.366	6.91
Mean	209.74	7.29	0.039	12.02	0.337	10.36	0.385	9.87
Standard Deviation	18.06	0.12	6.4e-3	0.05	0.068	0.04	0.020	1.75
Coefficient of Variation	0.088	0.018	0.180	0.0045	0.044	0.0060	0.068	0.20

Table 4.2 Specimen group summary and key points for BL-AE in 5.8 ksi compressive strength concrete

Test Name	Stiffness (kip/in)	F_y (kip)	Δ_y (in)	F_{max} (kip)	Δ_{max} (in)	F_u (kip)	Δ_u (in)	μ (in/in)
BL-AE-1	197.35	8.07	0.042	11.83	0.178	9.45	0.193	4.60
BL-AE-2	230.81	8.26	0.041	12.17	0.305	9.89	0.437	10.56
BL-AE-3	165.10	8.05	0.043	12.25	0.352	9.74	0.402	9.35
BL-AE-4	230.20	8.38	0.036	12.30	0.352	9.80	0.470	12.92
BL-AE-5	185.60	8.11	0.044	12.38	0.327	9.97	0.466	10.59
Mean	185.58	8.14	0.054	12.11	0.310	10.51	0.385	7.11
Standard Deviation	28.62	0.14	0.0031	0.21	0.073	0.20	0.12	3.08
Coefficient of Variation	0.140	0.017	0.076	0.018	0.24	0.020	0.290	0.320

Table 4.3 Specimen group summary and key points for CP-AE in 5.8 ksi compressive strength concrete

Test Name	Stiffness (kip/in)	F_y (kip)	Δ_y (in)	F_{max} (kip)	Δ_{max} (in)	F_u (kip)	Δ_u (in)	μ (in/in)
CP-AE-1	212.86	8.21	0.041	12.25	0.268	9.63	0.413	10.07
CP-AE-2	213.34	8.12	0.039	12.33	0.302	9.76	0.397	10.18
CP-AE-3	236.72	8.01	0.033	12.26	0.285	9.78	0.403	12.21
CP-AE-4	227.70	8.23	0.038	12.29	0.304	9.75	0.410	10.79
CP-AE-5	244.33	7.94	0.033	12.32	0.279	9.90	0.406	12.30
Mean	221.99	8.16	0.040	12.27	0.285	9.82	0.394	9.85
Standard Deviation	13.98	0.13	0.0036	0.035	0.015	0.096	0.0062	1.08
Coefficient of Variation	0.062	0.016	0.099	0.003	0.053	0.0098	0.015	0.097

4.4 Phase Two Overview

In accordance with ASTM C31/C31M specifications, a total of nine cylinders were constructed for the second phase of testing. They were divided into three cylinders for each of the two slabs and one during the transition between the slabs. Note for phase two, these slabs are denoted as 2-1 and 2-2. At fourteen days, the cylinders were checked for their compressive strength, which was found to be a mean value of 4.9 ksi (Table 4.4 and Figure 4.3). Therefore, all phase two reinforcement specimens were installed immediately to permit testing within 48 hours. During the initial specimen testing of phase two, large concrete cones were observed. These large cones could be the result of incomplete concrete curing and lower than anticipated concrete curing. Therefore, three cylinders were tested for their tensile strength and cores were taken from each slab. As anticipated, the tension strength was approximately 7% of the compressive strength, which is lower than the 10% anticipated value. The cored sections demonstrated an average compressive strength of 4.4 ksi for slab 2-1 (Figure 4.8) and 4.1 ksi for slab 2-2 (Figure 4.9). These values are somewhat high; however, they are comparative to older bridge decks with sound concrete. It is expected that the variation of the compressive strength is between 3.5 and 4.5 ksi since compressive strengths age with the structure. Complete details can be found in Appendices A and B.

Table 4.4 Summary of compressive strengths for phase two

`	**Cylinder Tensile Strength (psi)**	**Cylinder Compressive Strength (psi)**	**Cored Slab 2-1 Compressive Strength (psi)**	**Cored Slab 2-2 Compressive Strength (psi)**
1	318.98	4900.45	4141.34	4565.28
2	335.07	5118.68	4560.28	3820.99
3	*n/a*	4743.56	4565.28	3991.60
Mean	327.03	4920.90	4422.30	4125.95
Tension/Compression Ratio (%)	*NA*	6.65%	7.39%	7.93%

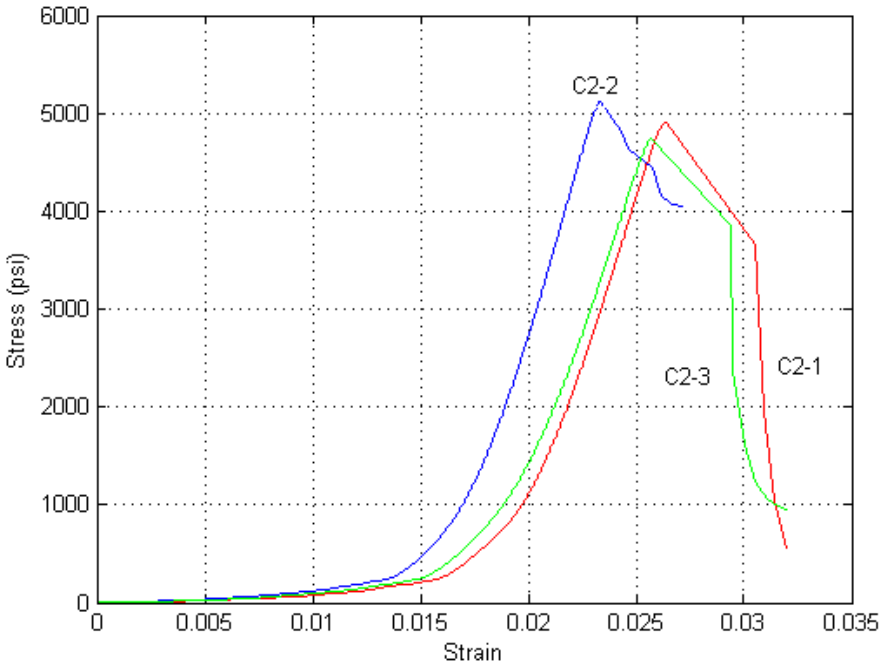

Figure 4.7 Compressive stress strain curves for slabs 2-1 and 2-2 cylinders

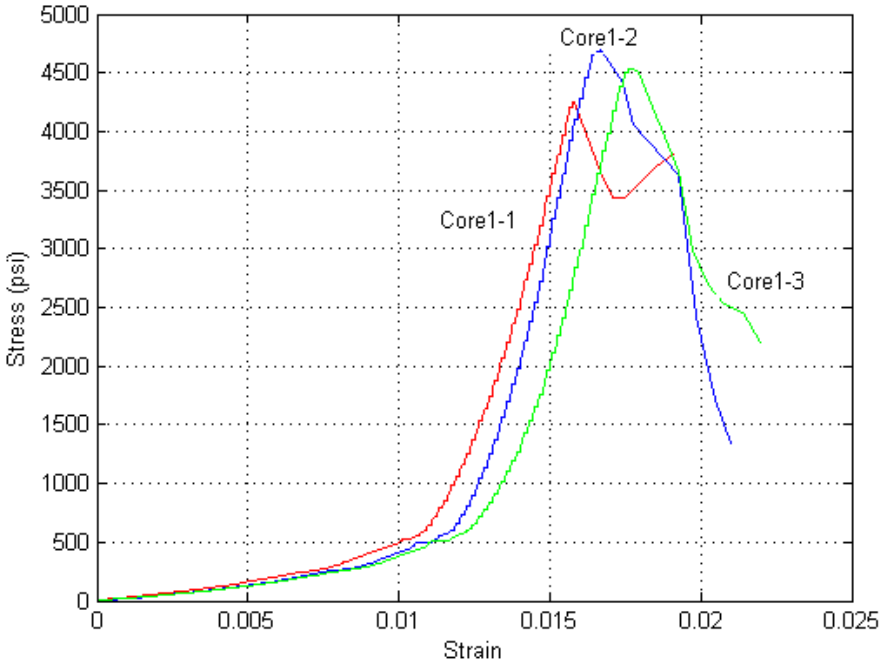

Figure 4.8 Compressive stress strain curves for slab 2-1 cores

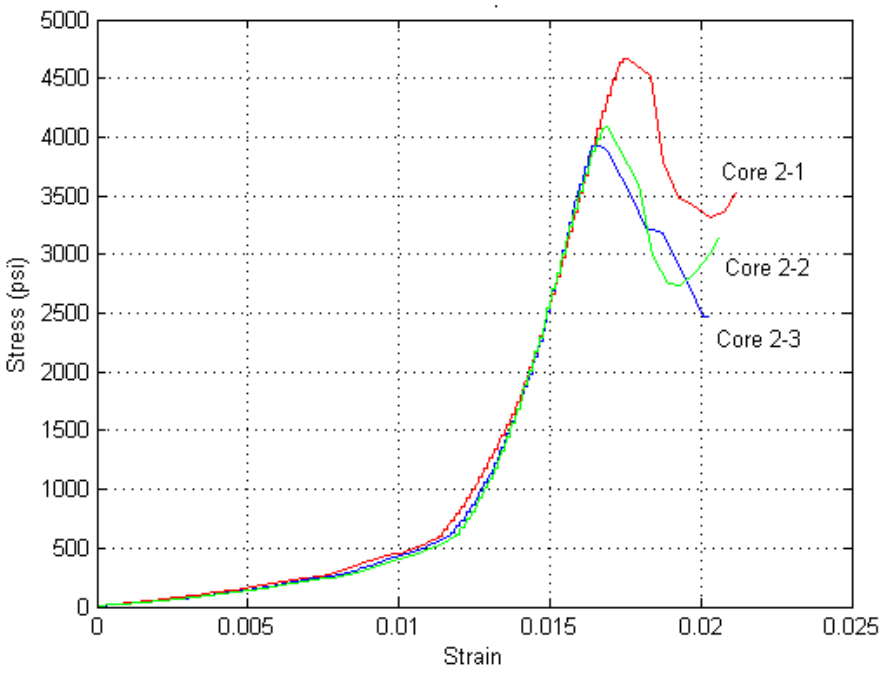

Figure 4.9 Compressive stress strain curves for slab 2-2 cores

4.5 Summary of BL-AE

The first specimen group that was considered in phase two was BL-AE, which was the baseline configuration (3.5-inch embedment depth) with epoxy reinforcement that was secured with adhesive type A. The typical failure mode of these specimens was a combined failure mode, as displayed in Figure 4.10. This combined failure mode is comprised of concrete cone breakout, steel necking or yielding, and steel rupture. Due its experimental history of steel yielding, these specimens experienced a fair amount of ductility (Figure 4.11). The mean parameters were computed for stiffness, yielding, yield force, and yield displacement at 209 kip/in, 8.0 kips, and 0.04 inches, respectively. The additional parameters were the maximum force, associated maximum force displacement, ultimate force, and ultimate displacement of 12.1 kips, 0.32 inches, 9.9 kips, and 0.38 inches. By comparing the yield and ultimate displacement, the mean

ductility was found to be 9.9. In accordance with ACI 355.4 (ACI, 2011), the characteristic strength is 11.7 kips. A summary is shown in Table 4.5.

Figure 4.10 Representative failure mode for BL-AE of combined failure (concrete breakout and steel rupture)

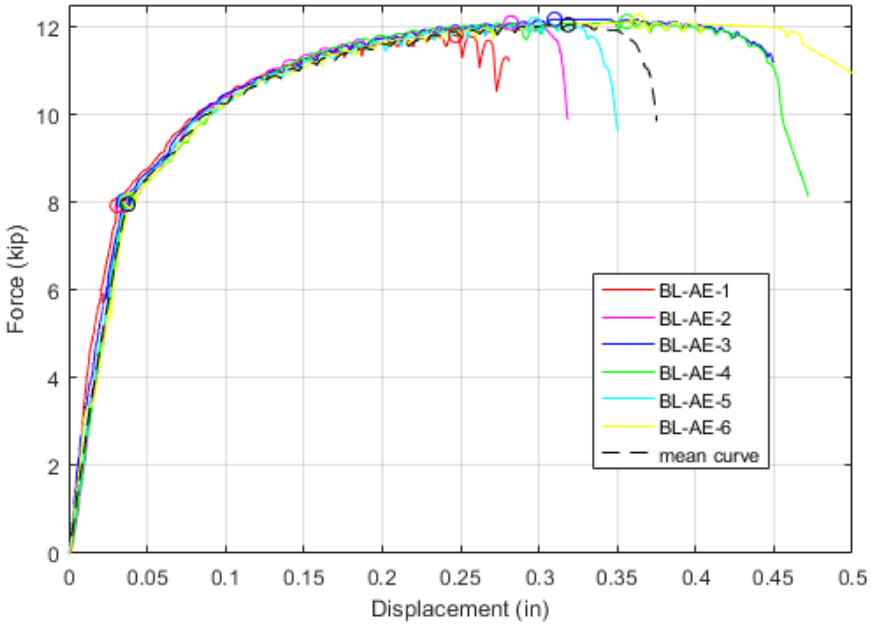

Figure 4.11 Specimen group comparison for BL-AE and its representative mean curve

Figure 4.5 Specimen group summary and key points for BL-AE

Test Name	Stiffness (kip/in)	F_y (kip)	Δ_y (in)	F_{max} (kip)	Δ_{max} (in)	F_u (kip)	Δ_u (in)	μ (in/in)
BL-AE-1	255.81	7.93	0.031	11.8	0.247	11.21	0.281	9.06
BL-AE-2	232.94	7.92	0.034	12.09	0.282	9.88	0.318	9.35
BL-AE-3	229.43	8.03	0.035	12.17	0.31	11.38	0.45	12.86
BL-AE-4	217.03	8.03	0.037	12.12	0.356	8.13	0.472	12.76
BL-AE-5	222.22	8.00	0.036	12.05	0.297	9.61	0.35	9.72
BL-AE-6	201.75	8.07	0.04	12.12	0.363	9.65	0.507	12.68
Mean	209.47	7.96	0.038	12.05	0.319	9.85	0.375	9.87
Standard Deviation	18.05	0.06	0.03	0.13	0.044	1.09	0.09	1.87
Coefficient of Variation	0.079	0.0075	0.085	0.011	0.14	0.11	0.23	0.17

4.6 Summary of CP-AE

The second specimen group within phase two was CP-AE, which is the current provision configuration (4.75-inch embedment depth) with epoxy reinforcement that was secured with adhesive type A. The typical failure mode of these specimens was a combined failure mode, as displayed in Figure 4.12. This combined failure mode was comprised of concrete cone breakout, steel necking or yielding, and steel rupture. This failure mode was also nearly identical to that of BL-AE. As in the previous specimens, these specimens experienced a fair amount of ductility (Figure 4.13). The mean parameters were computed for stiffness, yielding, yield force, and yield displacement as 154 kip/in, 8.1 kips, and 0.05 inches, respectively. The additional parameters were the maximum force, associated maximum force displacement, ultimate force, and ultimate displacement of 12.0 kips, 0.34 inches, 9.5 kips, and 0.38 inches. By comparing the yield and ultimate displacement, the mean ductility was 7.8. In accordance with ACI 355.4, the characteristic strength was 11.8 kips. A summary is shown in Table 4.6. Note that these values are very similar to the results of the shorter embedment depth of 3.5 inches. Despite the mean value for CP-AE being slightly higher than BL-AE, the characteristic strength is just slightly higher because of the smaller standard deviation.

Figure 4.12 Representative failure mode for CP-AE of combined failure (concrete breakout and steel rupture)

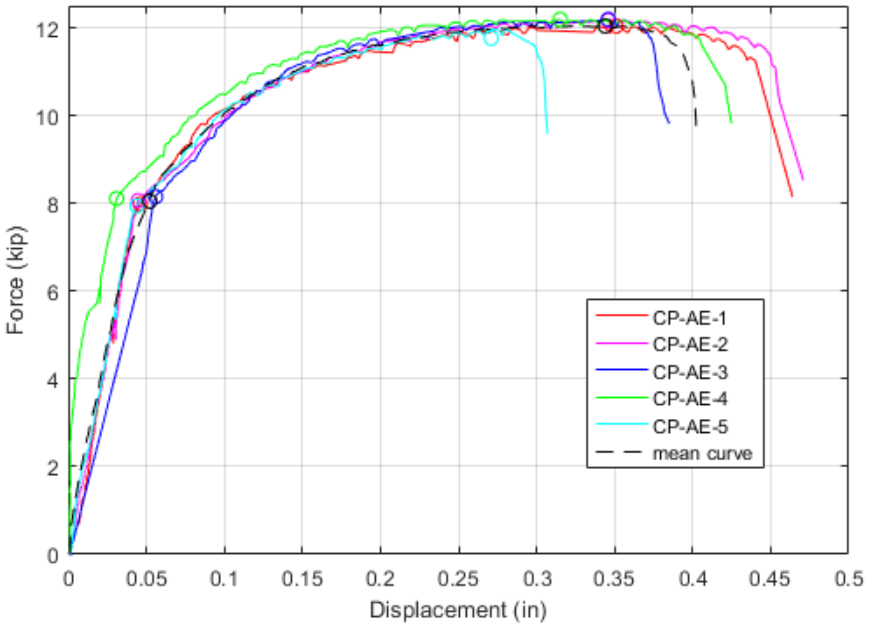

Figure 4.13 Specimen group comparison for CP-AE and its representative mean curve

Table 4.6 Specimen group summary and key points for CP-AE

Test Name	Stiffness (kip/in)	F_y (kip)	Δ_y (in)	F_{max} (kip)	Δ_{max} (in)	F_u (kip)	Δ_u (in)	μ (in/in)
CP-AE-1	173.7	7.99	0.046	12.03	0.352	8.14	0.44	10.09
CP-AE-2	179.11	8.06	0.045	12.17	0.346	10.29	0.456	10.13
CP-AE-3	145.54	8.15	0.056	12.19	0.346	9.81	0.385	6.88
CP-AE-4	261.61	8.11	0.031	12.19	0.315	9.82	0.425	13.71
CP-AE-5	180.45	7.94	0.044	11.96	0.273	9.59	0.307	6.98
Mean	154.81	8.05	0.052	12.04	0.344	9.53	0.403	7.75
Standard Deviation	43.29	0.086	0.0089	0.11	0.033	0.82	0.06	2.81
Coefficient of Variation	0.23	0.011	0.20	0.0088	0.1	0.086	0.15	0.29

4.7 Summary of P60-AE

The next specimen group within phase two was P60-AE, which was a partially bonded reinforcement bar (60% bonded over the 3.5-inch embedment). This also utilized epoxy reinforcement that was secured with adhesive type A. The typical failure mode of these specimens was steel rupture, as displayed in Figure 4.14. Since the failure mode was steel rupture, a fair amount of ductility was observed (Figure 4.15). The mean parameters were computed for stiffness, yielding, yield force, and yield displacement as 158 kip/in, 8.1 kips, and 0.05 inches, respectively. The additional parameters were the maximum force, associated maximum force displacement, ultimate force, and ultimate displacement of 11.8 kips, 0.36 inches, 9.8 kips, and 0.44 inches. By comparing the yield and ultimate displacement, the mean ductility was 8.6. In accordance with ACI 355.4, the characteristic strength was 11.5 kips. A summary is shown in Table 4.7. This group's results are similar to those of BL-AE, however no noted improvement in ductility was observed.

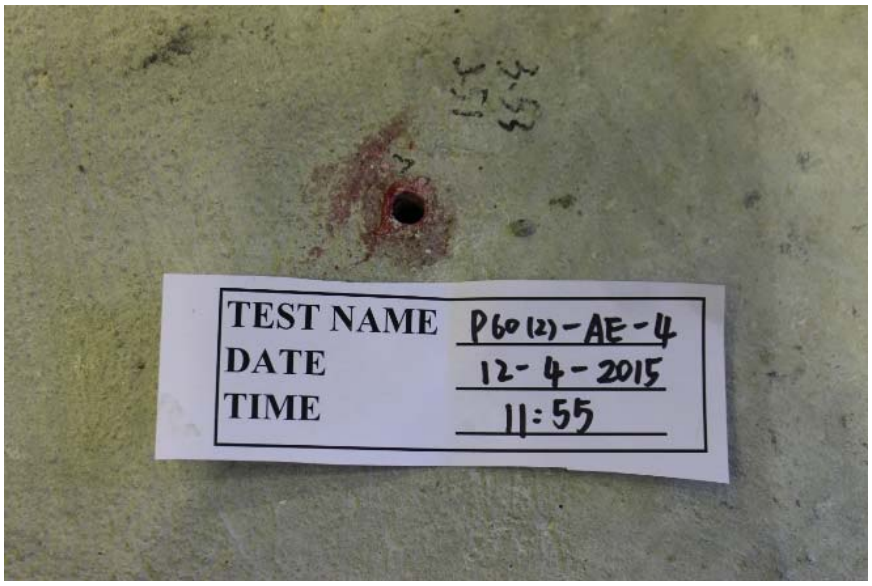

Figure 4.14 Representative failure mode for P60-AE of steel rupture failure

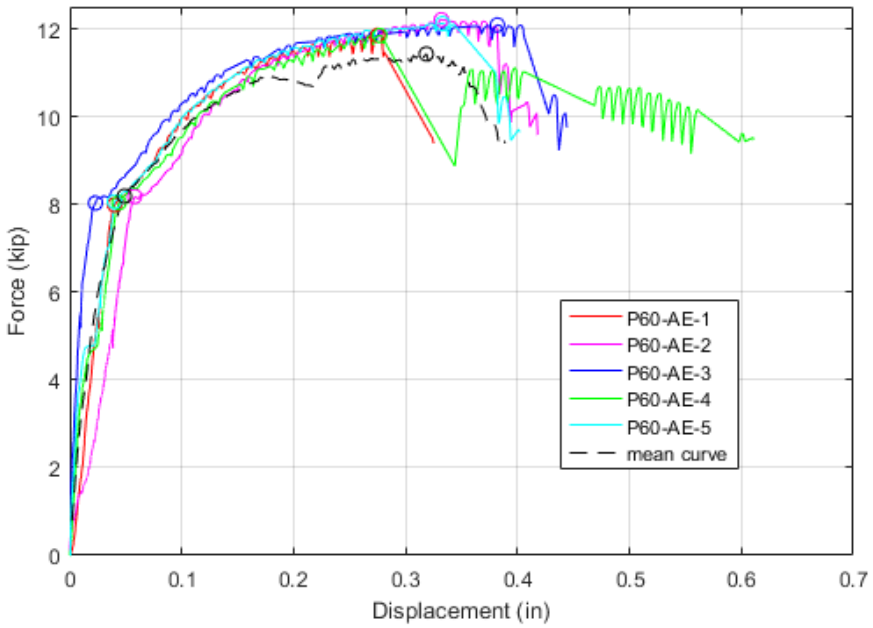

Figure 4.15 Specimen group comparison for P60-AE and its representative mean curve

Table 4.7 Specimen group summary and key points for P60-AE

Test Name	Stiffness (kip/in)	F_y (kip)	Δ_y (in)	F_{max} (kip)	Δ_{max} (in)	F_u (kip)	Δ_u (in)	μ (in/in)
P60-AE-1	199.75	7.99	0.04	11.85	0.275	9.39	0.325	8.13
P60-AE-2	141.03	8.18	0.058	12.21	0.332	9.58	0.418	7.21
P60-AE-3	349.13	8.03	0.023	12.09	0.382	9.75	0.444	9.3
P60-AE-4	187.73	8.04	0.044	11.85	0.277	9.47	0.611	13.89
P60-AE-5	201.5	8.06	0.04	12.12	0.333	9.64	0.402	10.05
Mean	158.04	8.06	0.051	11.75	0.36	9.78	0.439	8.61
Standard Deviation	78.45	0.072	0.013	0.16	0.045	0.14	0.11	2.57
Coefficient of Variation	0.36	0.0089	0.30	0.014	0.14	0.015	0.24	0.26

4.8 Summary of P80-AE

The next specimen was a slight variation of the partially bonded series. This group within phase two was P80-AE that was a partially bonded reinforcement bar (80% bonded over the 3.5-inch embedment). This also utilized epoxy reinforcement that was secured with adhesive type A. The typical failure mode of these specimens was steel rupture, as displayed in Figure 4.16. Since the failure mode was steel rupture, a fair amount of ductility was observed (Figure 4.17). The mean parameters were computed for stiffness, yielding, yield force, yield displacement at 194 kip/in, 7.4 kips, and 0.04 inches, respectively. The additional parameters were the maximum force, associated maximum force displacement, ultimate force, and ultimate displacement of 11.5 kips, 0.20 inches, 9.5 kips, and 0.29 inches. By comparing the yield and ultimate displacement, the mean ductility was 7.6. In accordance with ACI 355.4, the characteristic strength was 7.9 kips. This characteristic strength was significantly penalized since only three specimens were achievable. A summary is shown in Table 4.8. This group's results were similar to those of P60-AE and no notable improvement of BL-AE was observed.

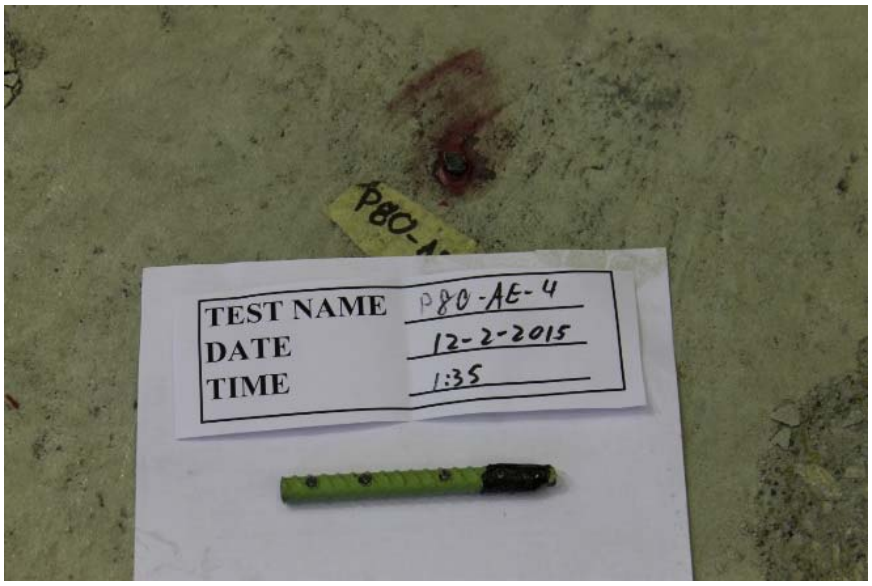

Figure 4.16 Representative failure mode for P80-AE of steel rupture

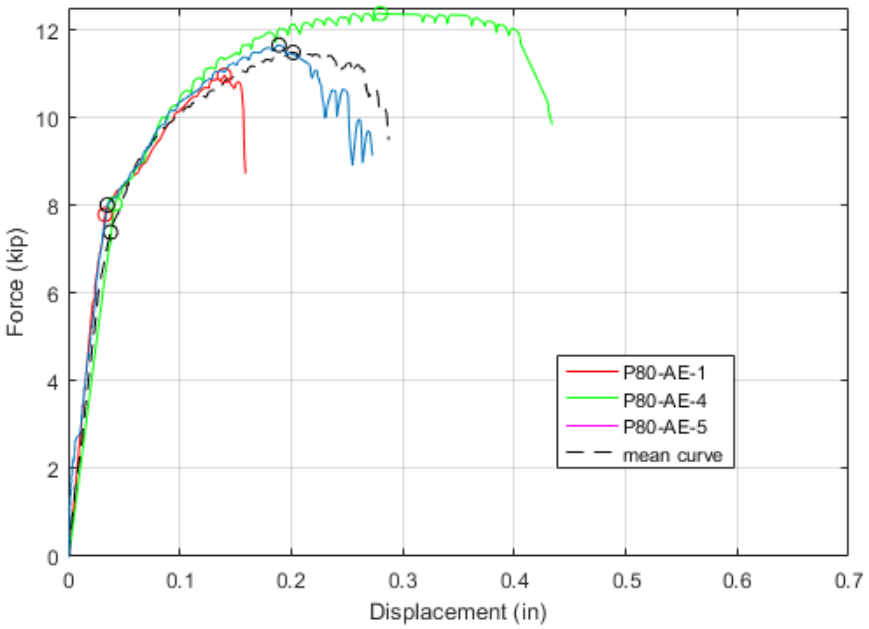

Figure 4.17 Specimen group comparison for P80-AE and its representative mean curve

Table 4.8 Specimen group summary and key points for P80-AE

Test Name	Stiffness (kip/in)	F_y (kip)	Δ_y (in)	F_{max} (kip)	Δ_{max} (in)	F_u (kip)	Δ_u (in)	μ (in/in)
P80-AE-1	236.06	7.79	0.033	10.96	0.140	9.13	0.158	4.79
P80-AE-4	191.43	8.04	0.042	12.37	0.280	9.85	0.434	10.33
P80-AE-5	228.86	8.01	0.035	11.65	0.189	9.33	0.270	7.71
Mean	194.47	7.39	0.038	11.48	0.202	9.49	0.287	7.55
Standard Deviation	23.96	0.137	0.0047	0.71	0.071	0.37	0.14	2.77
Coefficient of Variation	0.11	0.017	0.13	0.061	0.35	0.039	0.48	0.36

4.9 Summary of BL-BE

The following specimen group was BL-BE, which had the baseline configuration (3.5-inch embedment depth) with epoxy reinforcement that was secured with adhesive type B. Note that the only difference between BL-AE and BL-BE was the chosen manufacturer adhesive. The typical failure mode of these specimens was a combined failure mode, as displayed in Figure 4.18. This combined failure mode was comprised of concrete cone breakout, steel necking or yielding, and steel rupture. This failure mode was also nearly identical to that of BL-AE, indicating no significant dependency on selected adhesive or epoxy. As in the previous specimens, these specimens experienced a fair amount of ductility (Figure 4.19). The mean parameters were computed for stiffness, yielding, yield force, and yield displacement at 235 kip/in, 8.0 kips, and 0.03 inches, respectively. The additional parameters were the maximum force, associated maximum force displacement, ultimate force, and ultimate displacement of 11.8 kips, 0.28 inches, 10.0 kips, and 0.33 inches. By comparing the yield and ultimate displacement, the mean ductility was 10.9. Since test were only conducted on two specimens, no characteristic strength can be compared. A summary is shown in Table 4.9. Note that the maximum force is similar to that of adhesive A, but the displacement demands are much smaller. This indicates a more rigid adhesive system for adhesive type B.

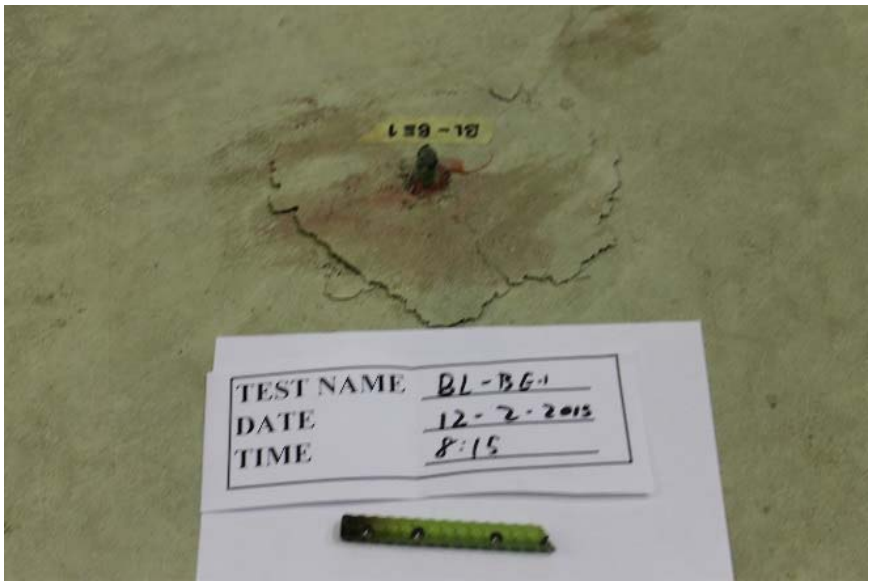

Figure 4.18 Representative failure mode for BL-BE of combined failure (concrete breakout and steel rupture)

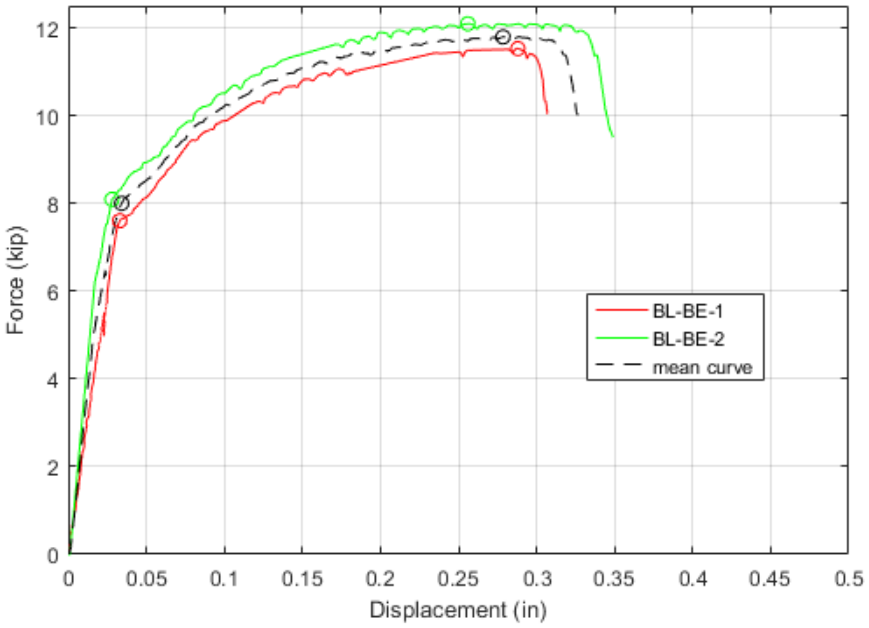

Figure 4.19 Specimen group comparison for BL-BE and its representative mean curve

Table 4.9 Specimen group summary and key points for BL-BE

Test Name	Stiffness (kip/in)	F_y (kip)	Δ_y (in)	F_{max} (kip)	Δ_{max} (in)	F_u (kip)	Δ_u (in)	μ (in/in)
BL-BE-1	230.3	7.60	0.033	11.53	0.288	10.03	0.307	9.3
BL-BE-2	288.93	8.09	0.028	12.09	0.256	9.51	0.349	12.46
Mean	235.29	8.00	0.034	11.79	0.279	10.01	0.327	10.88
Standard Deviation	41.46	0.35	0.035	0.4	0.023	0.37	0.03	2.23
Coefficient of Variation	0.16	0.044	0.12	0.034	0.083	0.038	0.091	0.21

4.10 Summary of EE-AE

The final specimen group within phase two was EE-AE, which was the baseline configuration with a minimum clear edge distance of 4.0 inches with epoxy reinforcement that was secured with adhesive type A. The embedment depth was 3.5 inches. The typical failure mode of these specimens was a concrete cone and side breakout, as displayed in Figure 4.20. This failure is particularly brittle and consequently, only contains a small amount of ductility (Figure 4.21). The mean parameters were computed for stiffness, yielding, yield force, and yield displacement at 143 kip/in, 8.0 kips, and 0.06 inches, respectively. The additional parameters were the maximum force, associated maximum force displacement, ultimate force, and ultimate displacement of 9.9 kips, 0.12 inches, 7.2 kips, and 0.15 inches. Comparing the yield and ultimate displacement, the mean ductility was only 2.6. In accordance with ACI 355.4, the characteristic strength was 3.7 kips, which was significantly reduced from that of the mean value due to the small number of specimens (three). A summary is shown in Table 4.10. A significant reduction (15%) in the mean maximum force was observed due to the proximity to the free edge.

Figure 4.20 Representative failure mode for EE-AE of side concrete blowout

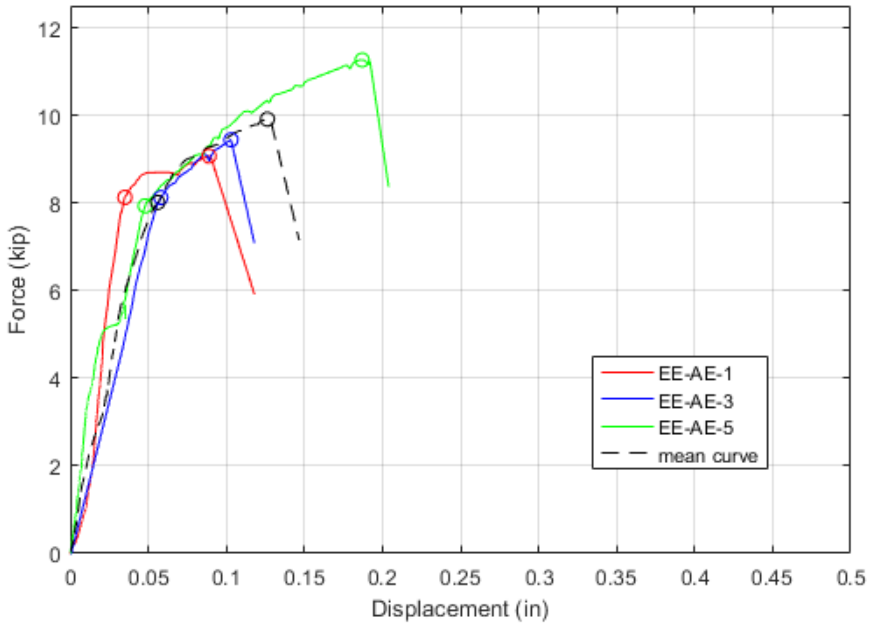

Figure 4.21 Specimen group comparison for EE-AE and its representative mean curve

Table 4.10 Specimen group summary and key points for EE-AE

Test Name	Stiffness (kip/in)	F_y (kip)	Δ_y (in)	F_{max} (kip)	Δ_{max} (in)	F_u (kip)	Δ_u (in)	μ (in/in)
EE-AE-1	232.29	8.13	0.035	9.07	0.089	6	0.118	3.37
EE-AE-3	140	8.12	0.058	9.44	0.103	7.08	0.118	2.03
EE-AE-5	165.21	7.93	0.048	11.26	0.187	8.37	0.204	2.25
Mean	143.04	8.01	0.056	9.91	0.126	7.15	0.147	2.63
Standard Deviation	47.7	0.11	0.012	1.17	0.053	1.19	0.05	0.72
Coefficient of Variation	0.27	0.014	0.25	0.12	0.42	0.17	0.34	0.28

4.11 Discussion and Summary

The previous sections, 4.3-4.10, present details for each group of specimens tested during phase two. This section discusses the comparison between the mean curves from each group in phase two. The focus is only on phase two, which is most representative of compressive strengths anticipated in existing concrete bridge decks. Figure 4.22 illustrates the mean force-displacement curve for each of the groups. Likewise, Table 4.11 identifies the mean key points. An inspection of the yield point revealed no discernable differences except for the P80-AE series. However, the initial stiffness does vary and may consequently result in notable differences in the yield displacement values. As the tensile load increases, the differences between the groups became more evident. The first group to reach its maximum value and subsequently fail was the EE-AE series. This series is defined by much smaller force and displacement capacities due to the large concrete cones and side breakouts. The remaining series continued to a minimum maximum force capacity of 11.5 kips. The current provision of a 4.75-inch embedment depth is characterized by a mean maximum force capacity of 12.0 kips, which is equal to the baseline configuration (3.5-inch embedment) of 12.0 kips. Adhesive type B, from an alternative manufacturer, experienced similar behavior for a maximum force capacity of 11.8 kips. The partially bonded series did experience a lower force capacity. At failure, the partially

bonded series also did not experience any larger ductility demands. While partially bonding the specimen did change the failure to steel rupture, the ductility did not increase. Therefore, partially unbonding the reinforcement bars is not recommended. Examination shows that the ductility of the current provision and the baseline case are similar in value.

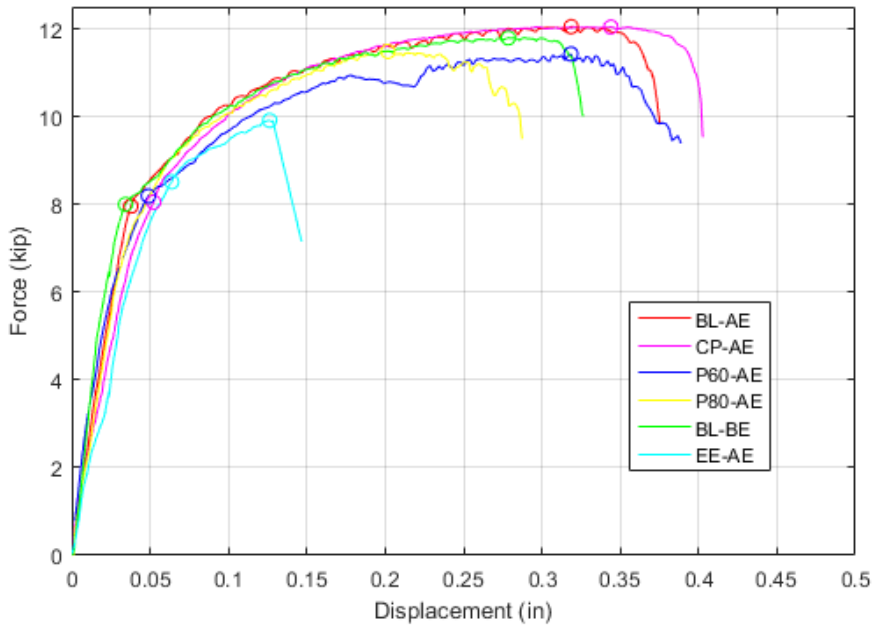

Figure 4.22 Mean group comparison force-displacement relationships

Table 4.11 Mean group comparison and key points

Group Name	Stiffness (kip/in)	F_y (kip)	Δ_y (in)	F_{max} (kip)	Δ_{max} (in)	F_u (kip)	Δ_u (in)	μ (in/in)	Characteristic Strength (kip)
BL-AE	209.47	7.96	0.038	12.05	0.319	9.85	0.375	9.87	11.65
CP-AE	154.81	8.05	0.052	12.04	0.344	9.53	0.403	7.75	11.75
P60-AE	158.04	8.06	0.051	11.75	0.360	9.78	0.439	8.61	11.46
P80-AE	194.47	7.39	0.038	11.48	0.202	9.49	0.287	7.55	7.92(1)
BL-BE	235.29	8.00	0.034	11.79	0.279	10.01	0.327	9.62	n/a
EE-AE	143.04	8.01	0.056	9.91	0.126	7.15	0.147	2.63	3.70(1)

(1) The P80-AE and EE-AE series are significantly penalized in the computation of the characteristic strengths due to a low sample size.

The last point of discussion relates to the current provision (4.75 inches) and the baseline configurations (3.5 inches) via the characteristic strength in accordance with ACI 355.4 (ACI, 2011). While the baseline case produced a very slightly larger maximum force value, the characteristic value was slightly lower: 11.75 kips vs 11.65 kips. This is a result of the larger standard deviation for the baseline case at the maximum force point. These values are identified as 0.11 versus 0.13 kips. By reviewing these two configurations, the baseline and the current provision cases are nearly statistically equivalent and no significant differences were observed in their failure mechanisms. Therefore, a 3.5-inch embedment depth for a No. 3 epoxy reinforcement bar is nearly equivalent to an embedment depth of 4.75 inches. This is true for the yield force and the maximum force capacities. This experimental campaign demonstrates that a reduced embedment depth of 3.5 inches is sufficient to meet the current demands.

Chapter 5 Recommendations and Conclusions

5.1 Project Motivation and Experimental Summary

The project's objective was to experimentally verify the capacity of the shallow embedment depth anchors as specified in the NDOR bridge rail retrofit special provision. This included the current specified depth of 4.75 inches as well as a reduced embedment depth of 3.5 inches for tapered or thin bridge decks. While the strength capacity of the anchors (No. 3 reinforcement bars) embedded at 4.75 inches is sufficient for design, the reduced embedment depth is not well predicted in strength capacity and failure mode. To address this need, an experimental campaign was conducted to verify the capacity of anchors embedded at both embedment depths.

The compressive strength of the concrete slabs during initial testing (5.8 ksi) was higher than that anticipated for slabs in the field. As a result, only three configurations of anchorage groups were tested. While no discernable differences in capacity were observed between anchorage groups of 4.75 and 3.5 inch embedment depths, no recommendations are reported from this first phase of testing due to the compressive strength of the concrete. As a result, a second phase of testing was conducted which incorporated lower strength.

In the second phase of testing, the effects of four primary variables on anchorage group capacity were explored: 1) embedment depth, 2) adhesive, 3) bond (full vs partial), and 4) edge distance. The current provision (4.75-inch embedment depth) and the baseline configuration (3.5-inch embedment) achieved the same mean maximum force capacity of 12.0 kips with similar ductility and concrete breakout failure modes. Variation of the adhesive (types A and B) did not result in significant differences in capacity or failure mode for the baseline configuration (11.8 kips). However, partially bonded anchors of the baseline embedment depth were found to

have slightly reduced capacity (11.6 kips) and a transition to steel rupture as the failure mode. Despite this change in failure mode, no significant increase in the ductility was observed. The most significant variable in this study was found to be edge distance, where the lowest capacities were observed for anchorage groups within 4 inches from the free edge (9.9 kips). This was due to the generation of large concrete cones and side breakout failure modes of the concrete slabs. It is noted that in all other test configurations with larger edge distances, the minimum peak force capacity was 11.5 kips.

5.2 Summary of Findings and Recommendations for Implementation

As informed by the second phase of the experimental campaign, two conclusions can be drawn. First, the effect of partially bonding the reinforcement is not recommended despite similar strength capacity. While the failure mechanism was steel rupture, no significant increase in ductility was noted. Consequently, this is not recommended due to the additional complications of debonding anchorage in the field.

The second recommendation relates to the current provision (4.75 inches) and the baseline configurations (3.5 inches). The characteristic strengths for the current provision and the baseline configuration were found to be 11.75 and 11.65 kips, respectively, as computed in accordance with ACI 355.4 (ACI, 2011). The slightly lower value of the baseline configuration can be attributed to the larger standard deviation in the experimental capacity values. The baseline and the current provision cases are nearly statistically equivalent and no significant differences were observed in their failure mechanisms. Therefore, a 3.5-inch embedment depth for a No. 3 epoxy reinforcement bar (60 ksi) is nearly equivalent to an embedment depth of 4.75 inches for both yield and maximum force capacities. To this end, the experimental campaign as

outlined in Chapters 3 and 4 demonstrates that a reduced embedment depth of 3.5 inches is sufficient to meet the current demands.

5.3 Recommendations for Future Research

This study examined the tensile behavior of two embedment depths of No. 3 reinforcement installed into mock bridge specimens. To further understand these systems, the following additional research areas may be investigated:

1) Dynamic loading of the anchorage. The capacity of anchors can be assessed under static loads, however higher strain rates may occur during a vehicular collision and the inertial effects may become significant. This can be tested either mechanically or via a simulated crash test protocol.
2) Shear capacity of the anchorage. While the anchors are primarily loaded in tension, shear forces are also present and may not be negligible. Often shear and tension capacities are tested independently, however the shear capacity of the various configurations was not evaluated in this study.
3) Anchor capacity in real structures. This study explored the capacity of embedded anchors in mock bridge specimens. These concrete specimens were constructed in a laboratory under ideal curing and placement conditions. The concrete base material in retrofitted bridge deck is likely to contain small cracks due to shrinkage and other material abnormalities, which is likely to impact the concrete strength and the potential failure modes.

References

American Association of State Highway and Transportation Officials. (2009). "*Manual for Assessing Safety Hardware" MASH 350,* Washington, D.C.

American Concrete Institute. (2011). "*Qualification of Post-Installed Adhesive Anchors in Concrete" ACI 355.4-11,* Farmington Hills, Michigan.

American Concrete Institute. (2014). "*Building code requirements for structural concrete" ACI 318-14*, Farmington Hills, Michigan.

American Society for Testing and Materials International (ASTM). (2013). *Standard Test Method for Obtaining and Testing Drilled Cores and Sawed Beams of Concrete,* ASTM C42, Conshohocken, Pennsylvania.

American Society for Testing and Materials International (ASTM). (2015). *Standard Test Methods for Strength of Anchors in Concrete Elements,* ASTM E488, Conshohocken, Pennsylvania.

Cook, R., and Konz, R.C. (2001). "Factors Influencing Bond Strength of Adhesive Anchors." ACI Structural Journal, 98(1): 76-86.

Eligenhausen, R., Cook, R. A., Appl, J. (2006). "Behavior and Design of Adhesive Bonded Anchors." *ACI Structural Journal,* 103(6), 822-831.

Eligenhausen, R., Mallée, R, and Silva, J.F. (2006). Anchorage in Concrete Construction. First Edition. Ernst & Sohn, Berlin, Germany, 391pp.

Gurbaz, T., and Ilki, A. (2011). "Pullout Performance of Fully and Partially Bonded Retrofit Anchors in Low-Strength Concrete." *ACI Structural Journal,* 108(1), 61-70.

Williams, W. F., Buth, C. E., Menges, W. L. (2006). *Adhesive Anchors for Retrofit/Repair of Bridge Rails*, Texas Transportation Institute, The Texas A&M University System, College Station, Texas.

Appendix A – Summary of Phase Two Test Results

A.1 Raw and Filtered Data

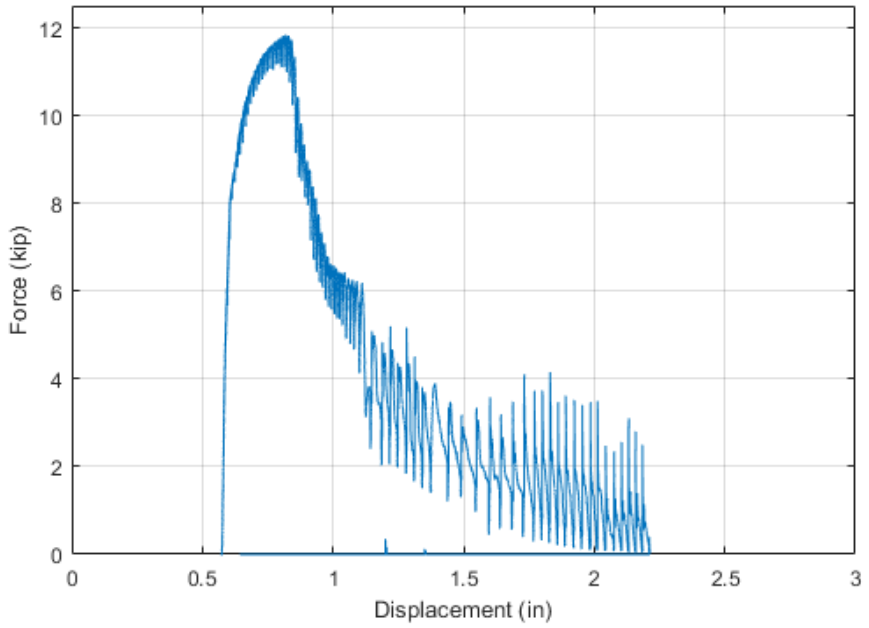

Figure A.1 Unfiltered force versus displacement relationship of BL-AE-1

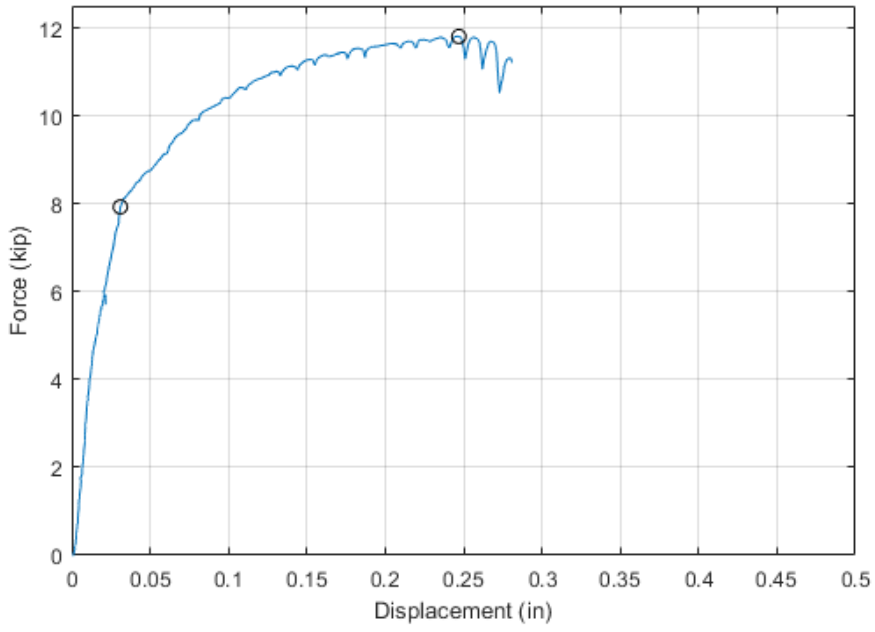

Figure A.2 Force versus displacement relationship of BL-AE-1

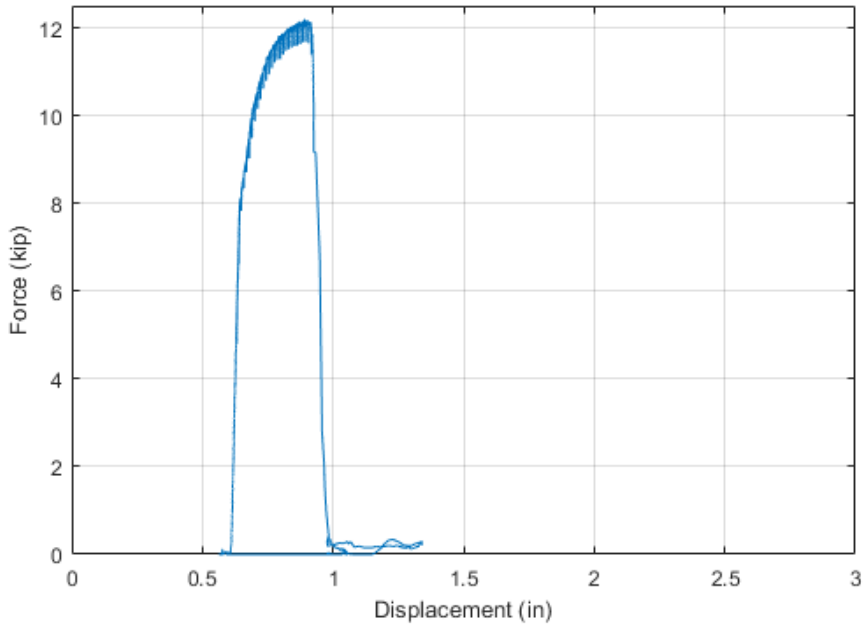

Figure A.3 Unfiltered force versus displacement relationship of BL-AE-2

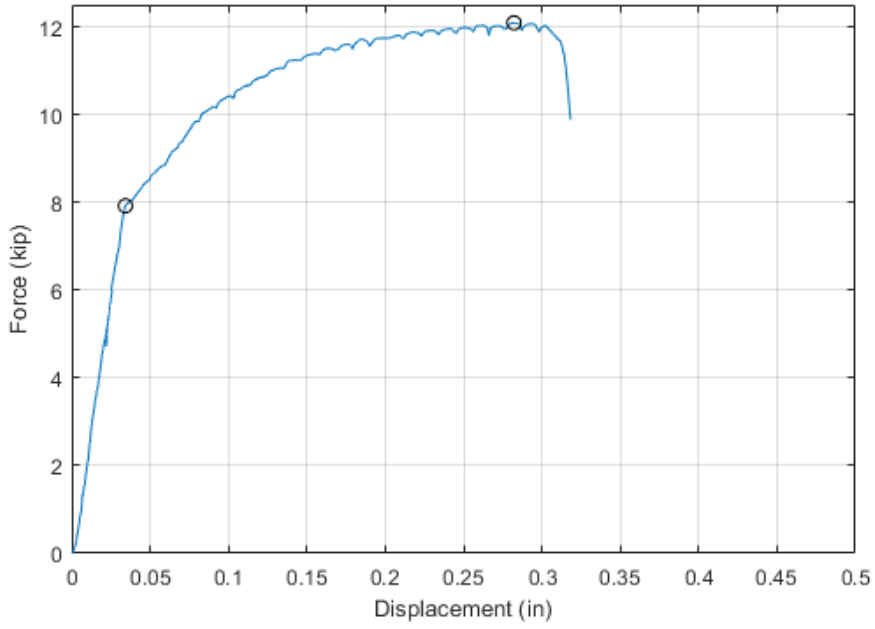

Figure A.4 Force versus displacement relationship of BL-AE-2

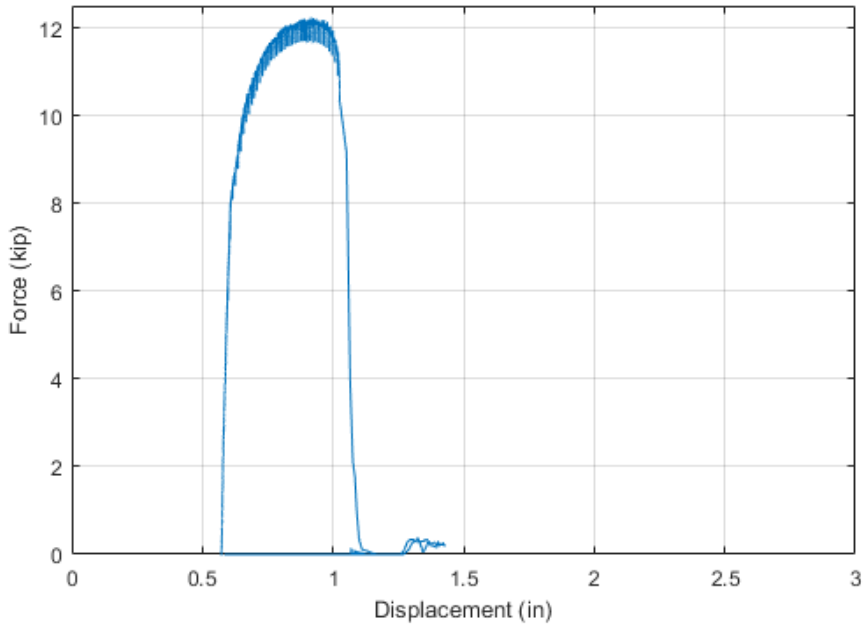

Figure A.5 Unfiltered force versus displacement relationship of BL-AE-3

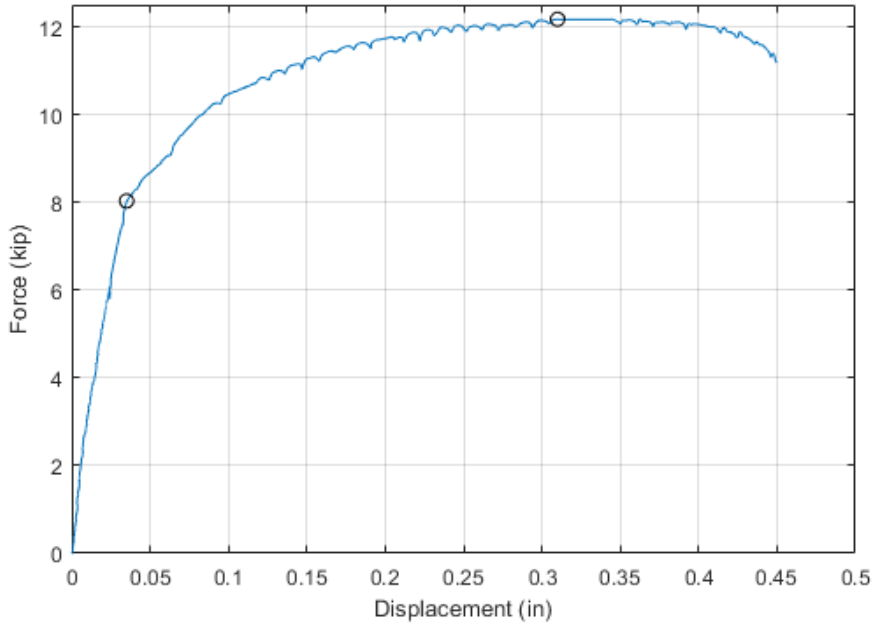

Figure A.6 Force versus displacement relationship of BL-AE-3

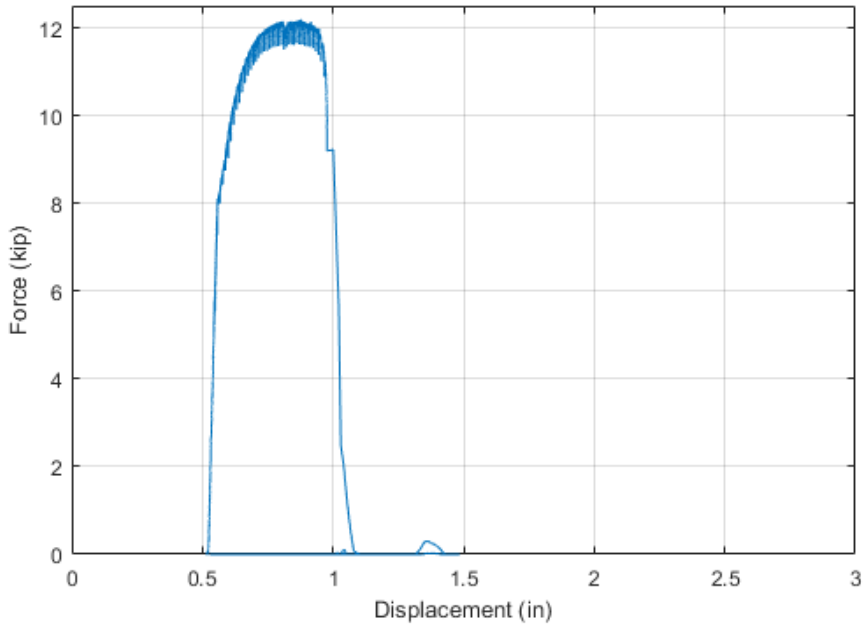

Figure A.7 Unfiltered force versus displacement relationship of BL-AE-4

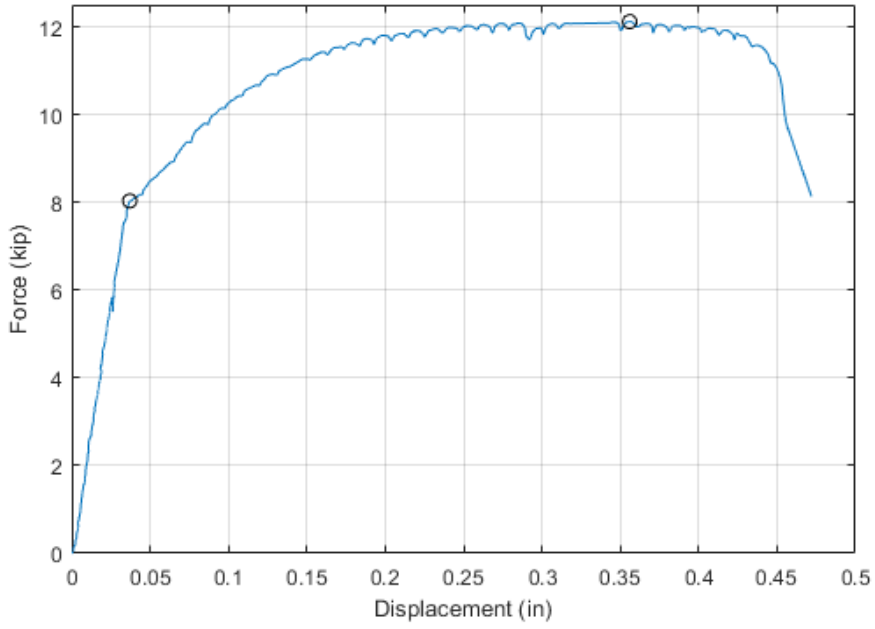

Figure A.8 Force versus displacement relationship of BL-AE-4

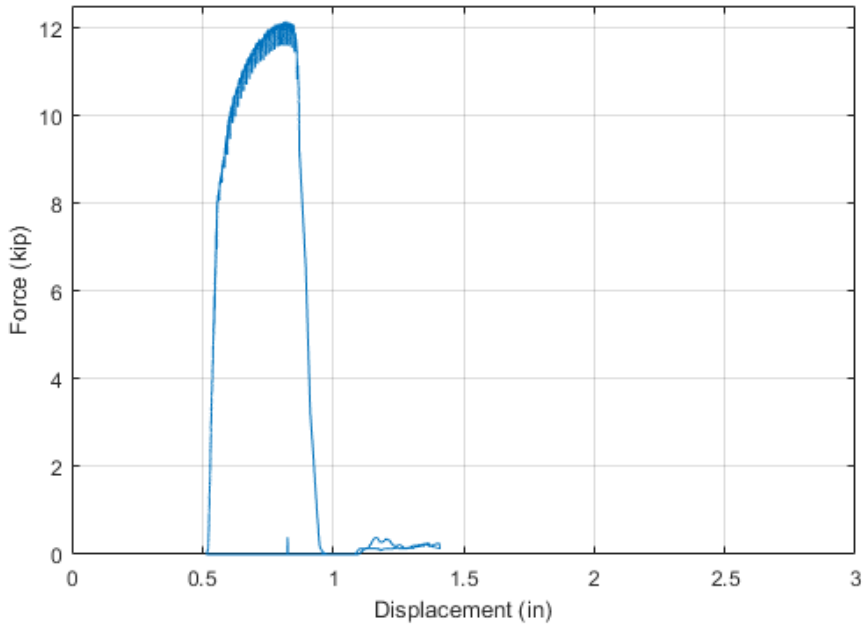

Figure A.9 Unfiltered force versus displacement relationship of BL-AE-5

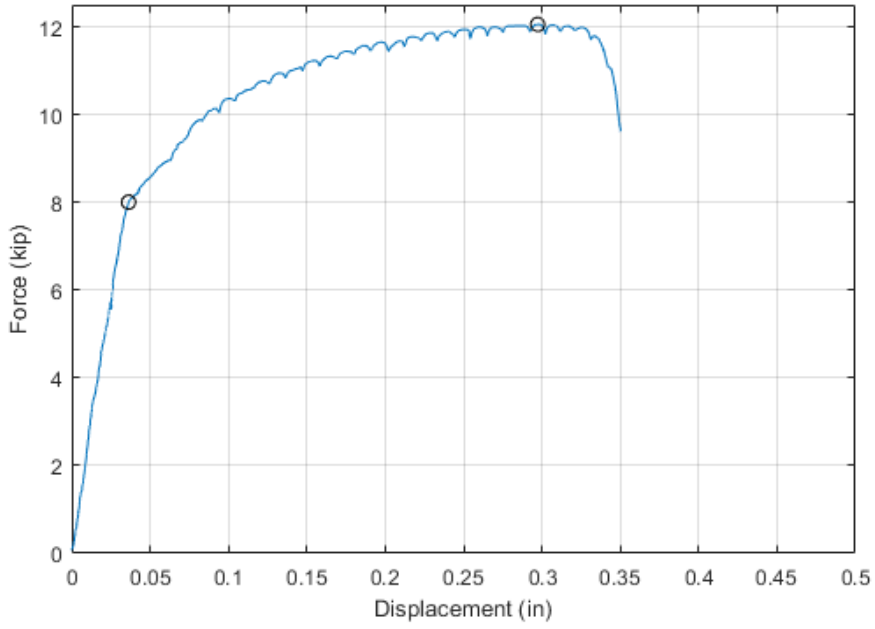

Figure A.10 Force versus displacement relationship of BL-AE-5

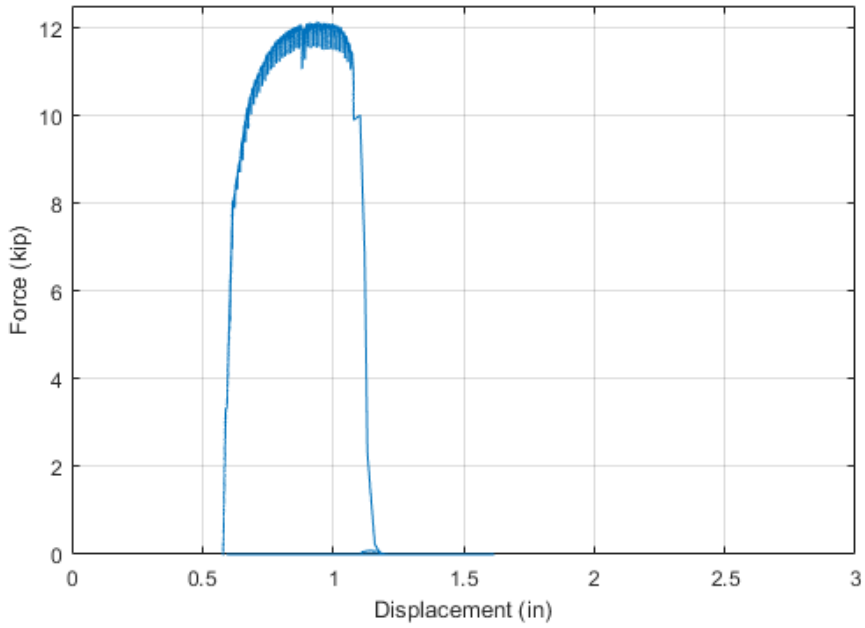

Figure A.11 Unfiltered force versus displacement relationship of BL-AE-6

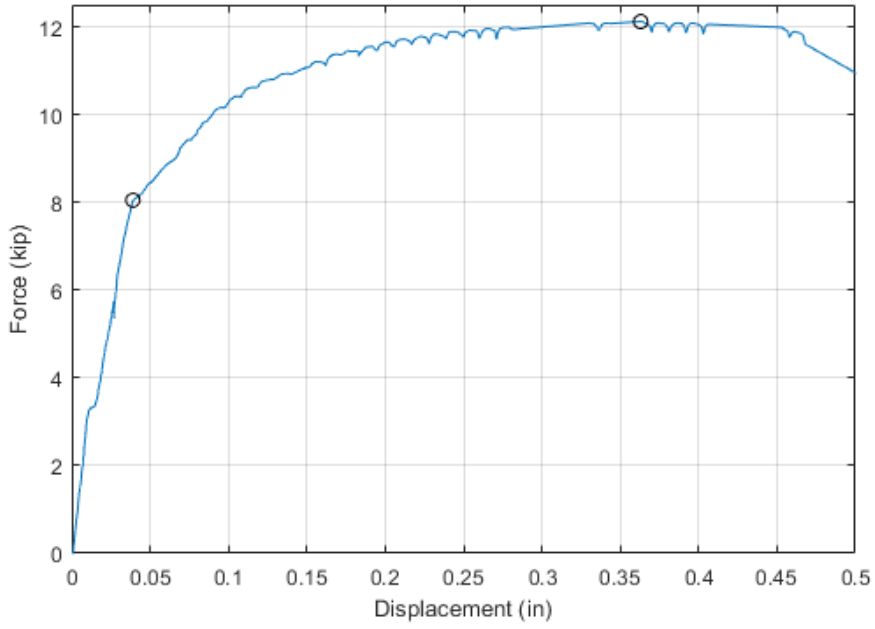

Figure A.12 Force versus displacement relationship of BL-AE-6

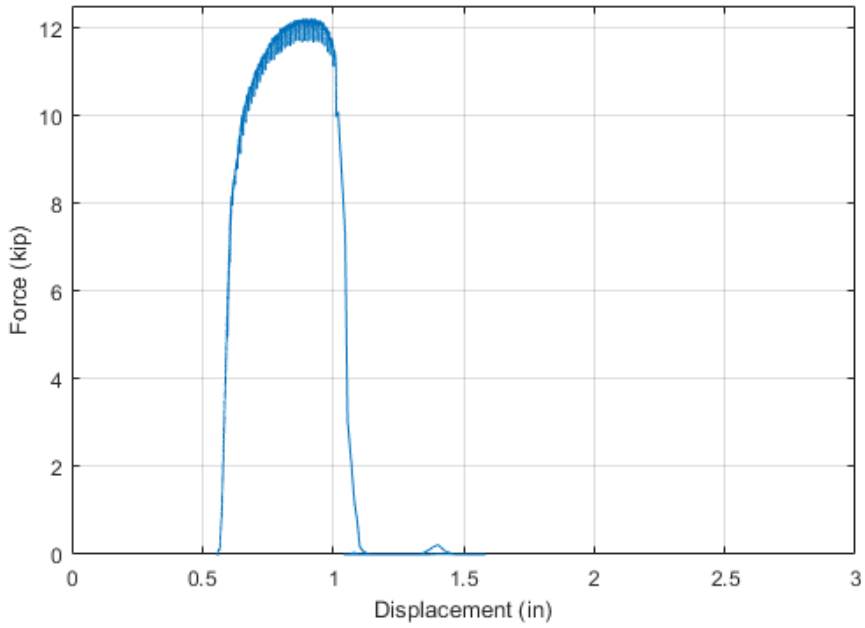

Figure A.13 Unfiltered force versus displacement relationship of CP-AE-1

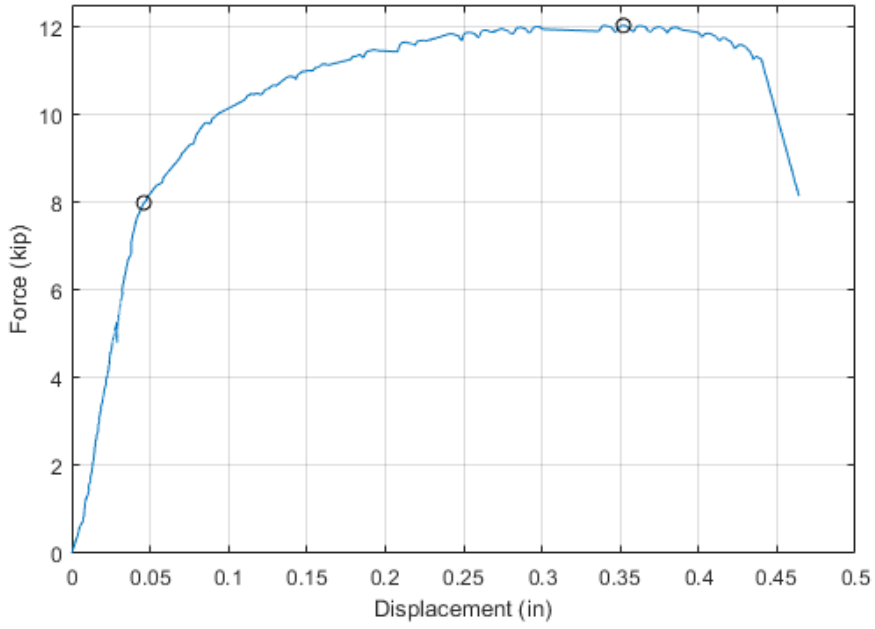

Figure A.14 Force versus displacement relationship of CP-AE-1

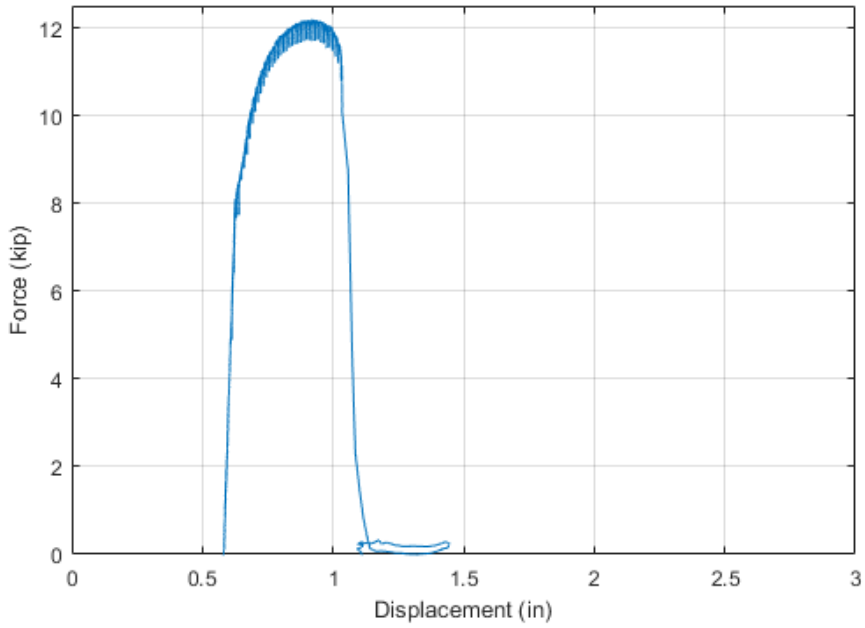

Figure A.15 Unfiltered force versus displacement relationship of CP-AE-2

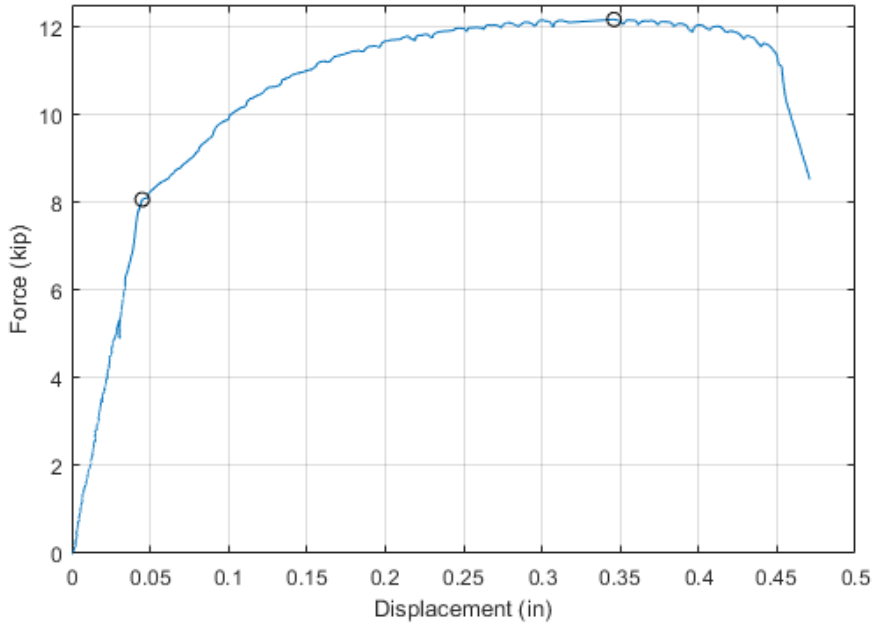

Figure A.16 Force versus displacement relationship of CP-AE-2

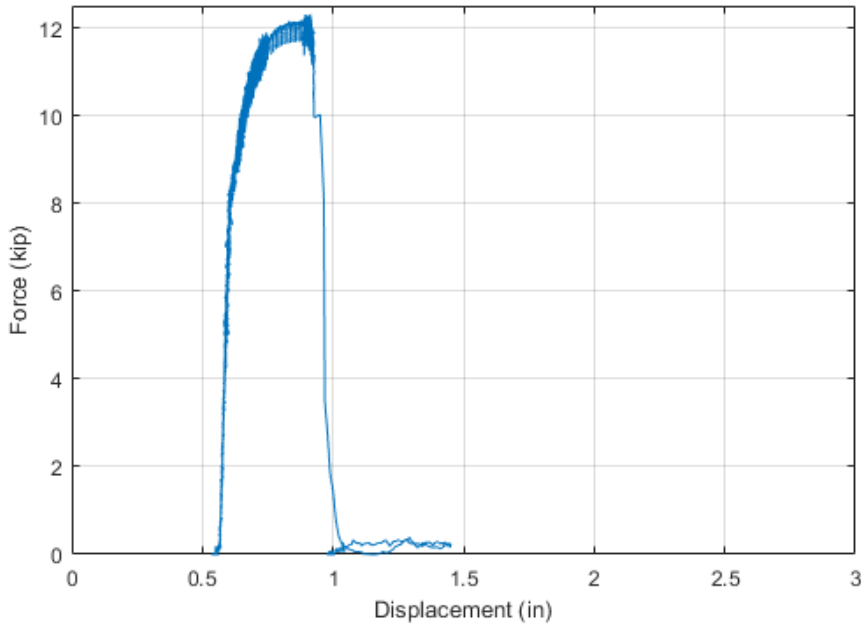

Figure A.17 Unfiltered force versus displacement relationship of CP-AE-3

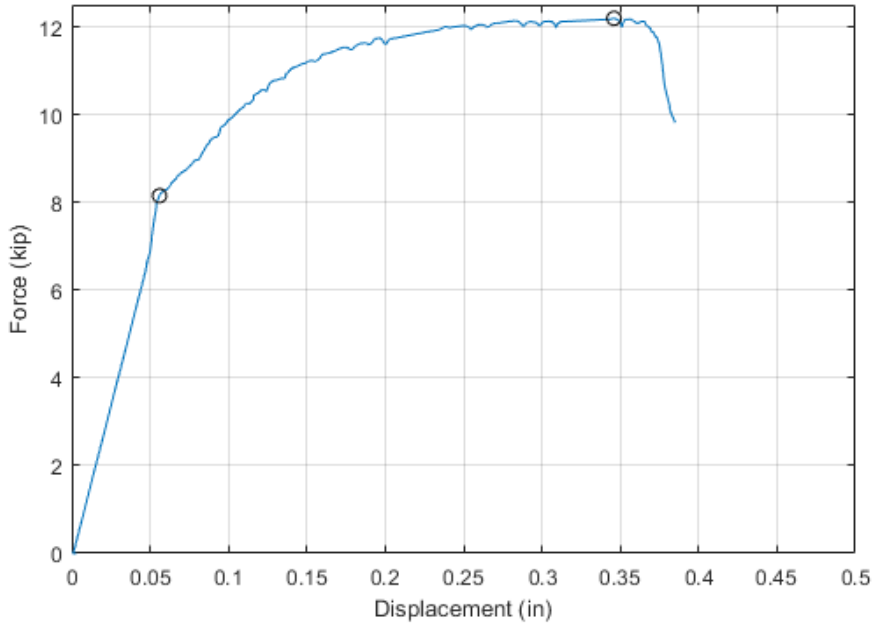

Figure A.18 Force versus displacement relationship of CP-AE-3

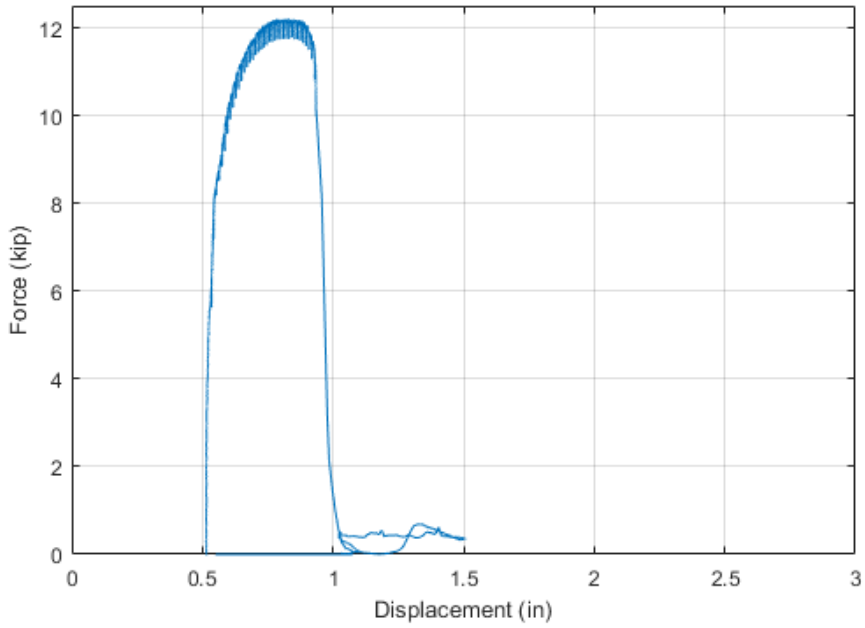

Figure A.19 Unfiltered force versus displacement relationship of CP-AE-4

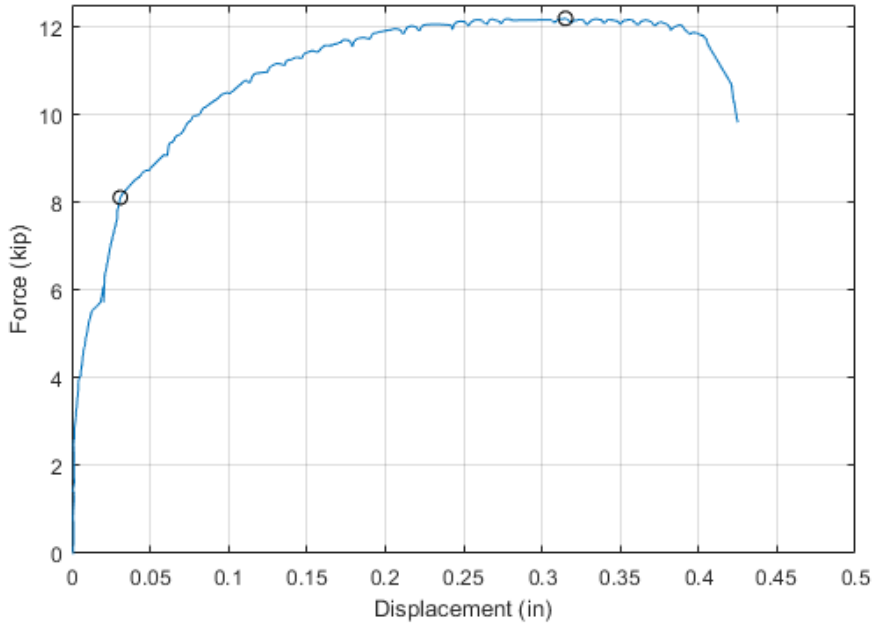

Figure A.20 Force versus displacement relationship of CP-AE-4

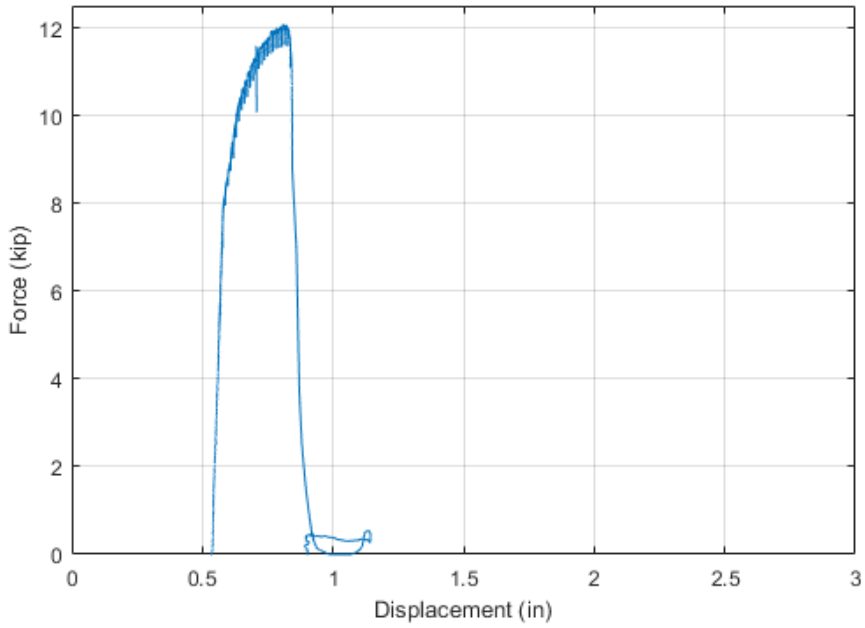

Figure A.21 Unfiltered force versus displacement relationship of CP-AE-5

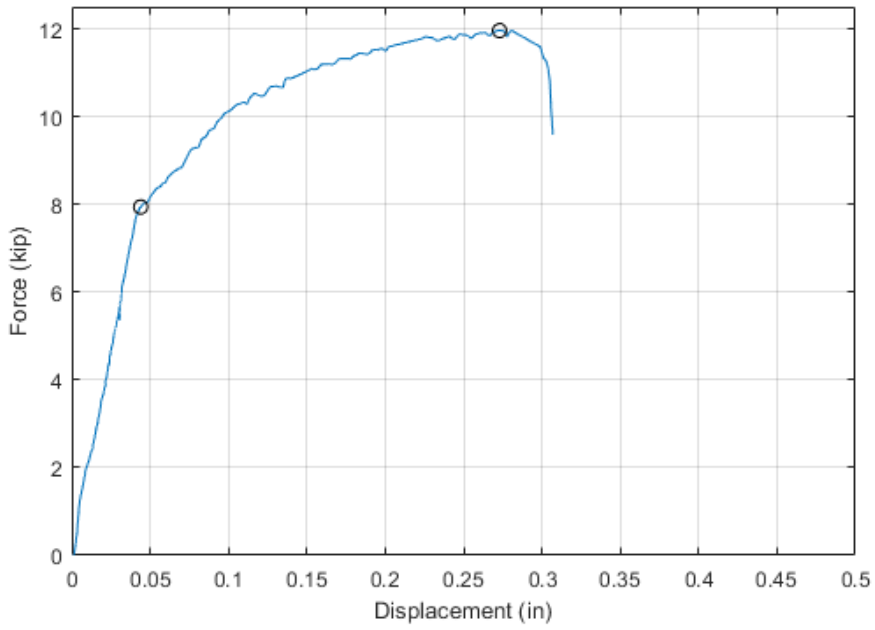

Figure A.22 Force versus displacement relationship of CP-AE-5

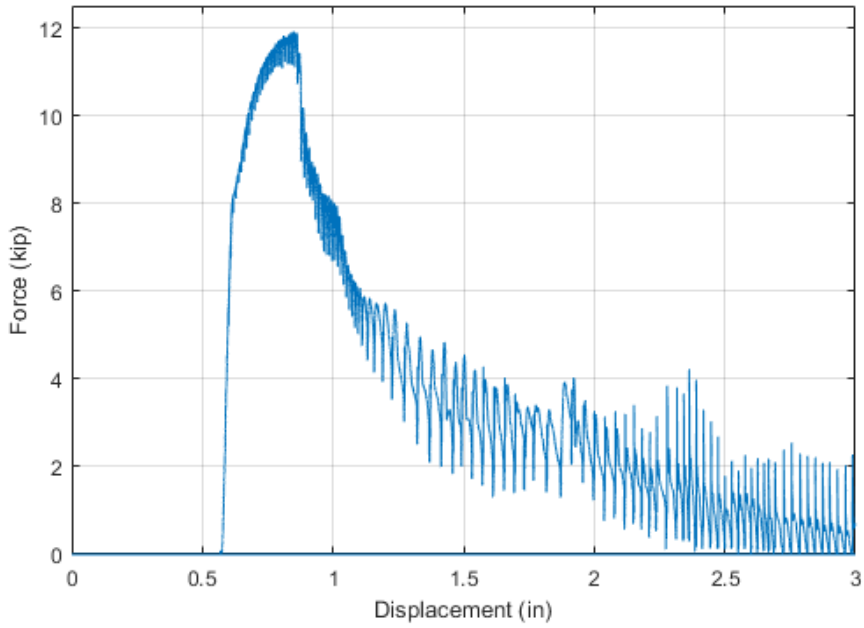

Figure A.23 Unfiltered force versus displacement relationship of P60-AE-1

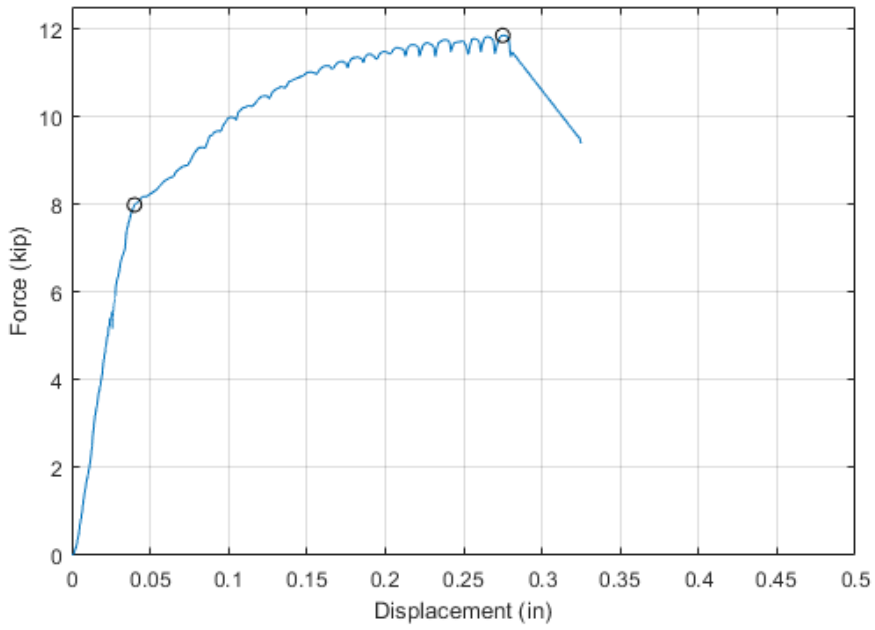

Figure A.24 Force versus displacement relationship of P60-AE-1

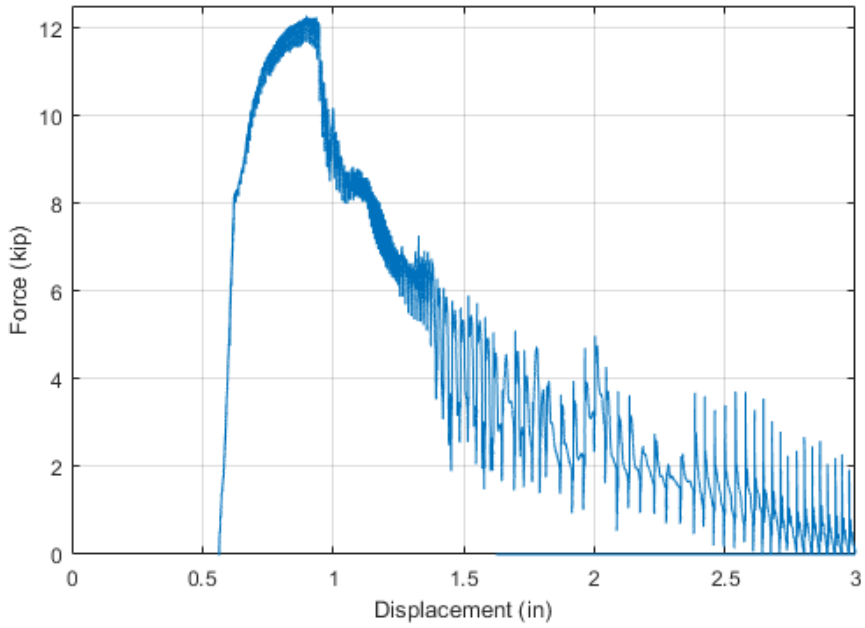

Figure A.25 Unfiltered force versus displacement relationship of P60-AE-2

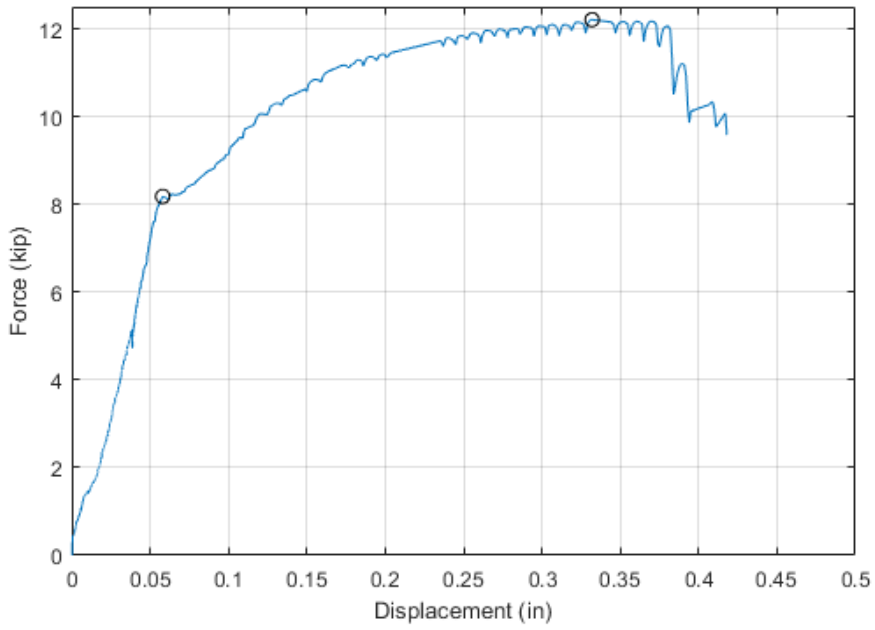

Figure A.26 Force versus displacement relationship of P60-AE-2

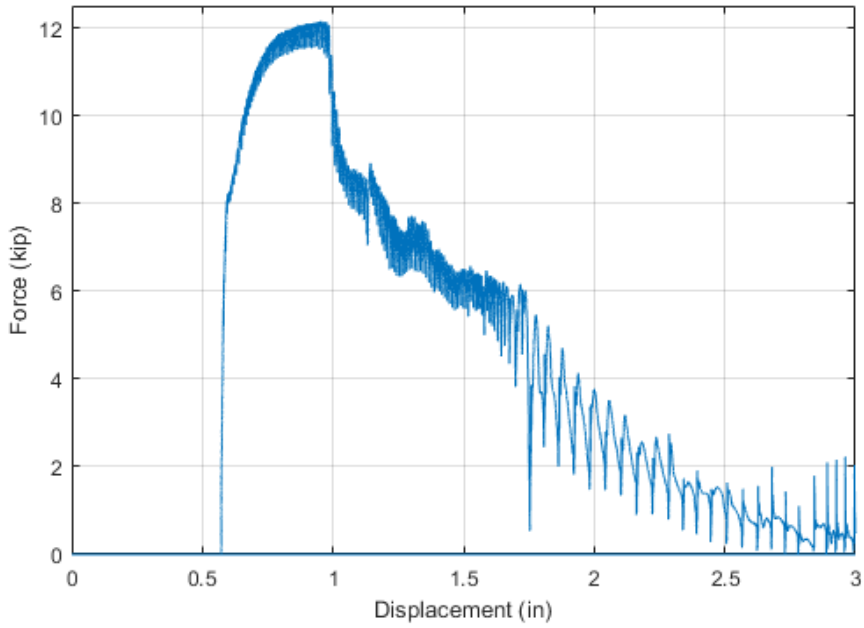

Figure A.27 Unfiltered force versus displacement relationship of P60-AE-3

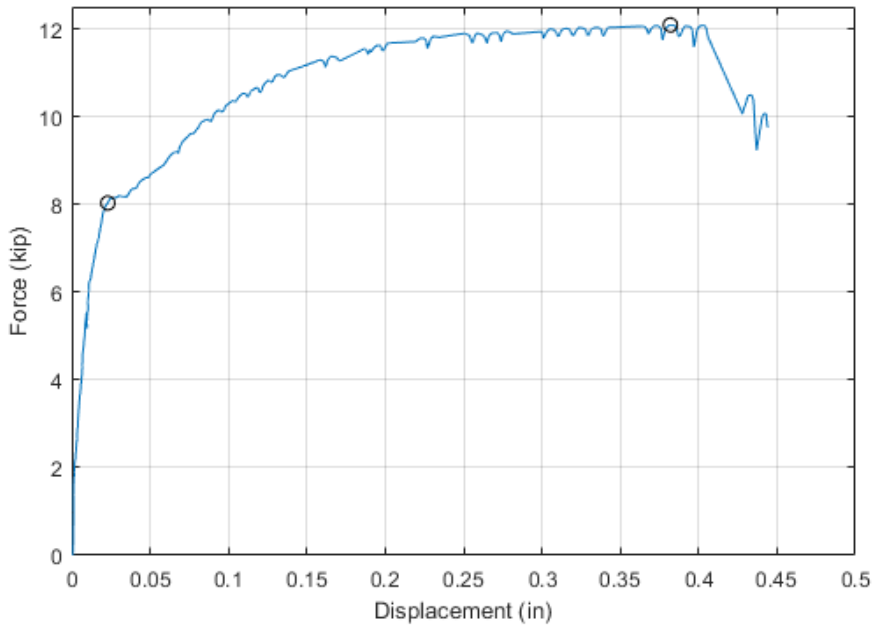

Figure A.28 Force versus displacement relationship of P60-AE-3

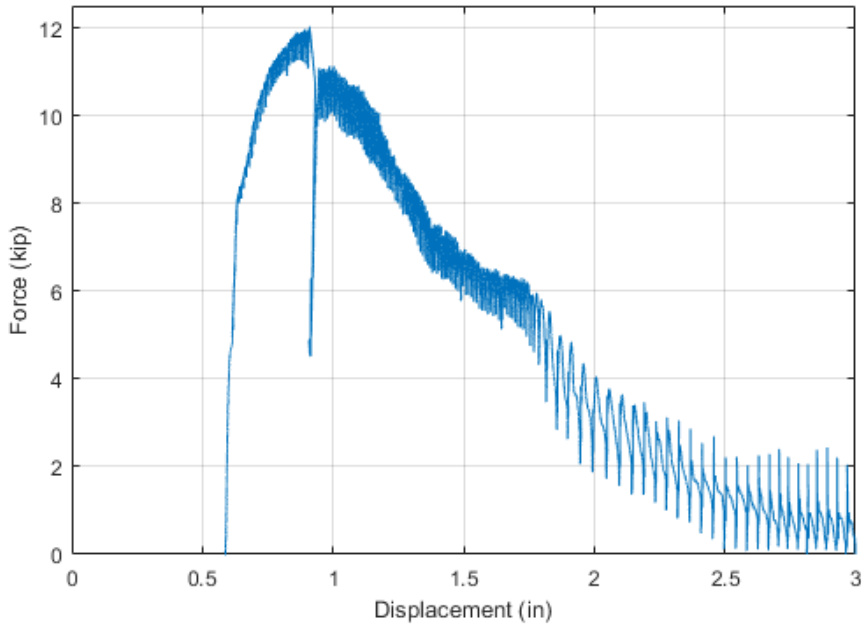

Figure A.29 Unfiltered force versus displacement relationship of P60-AE-4

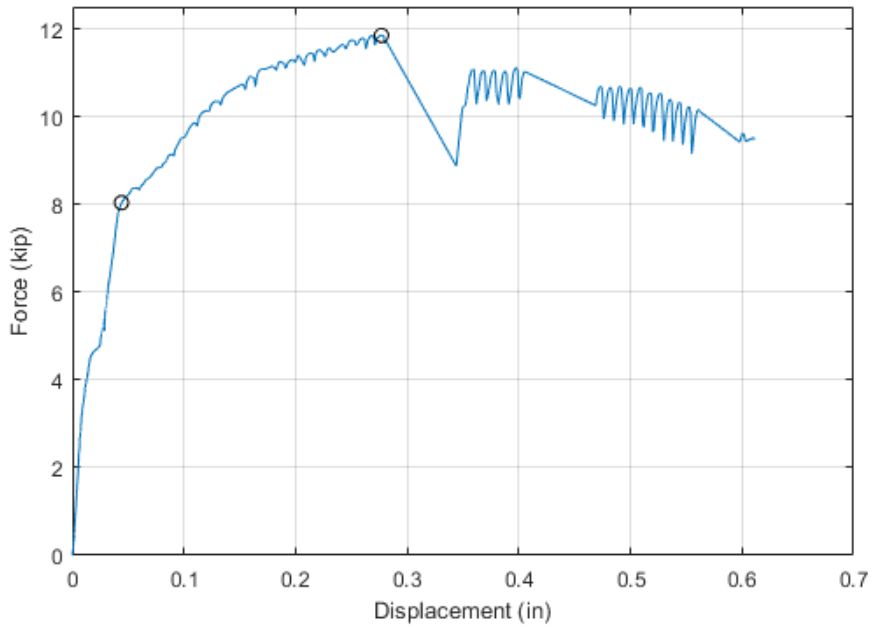

Figure A.30 Force versus displacement relationship of P60-AE-4

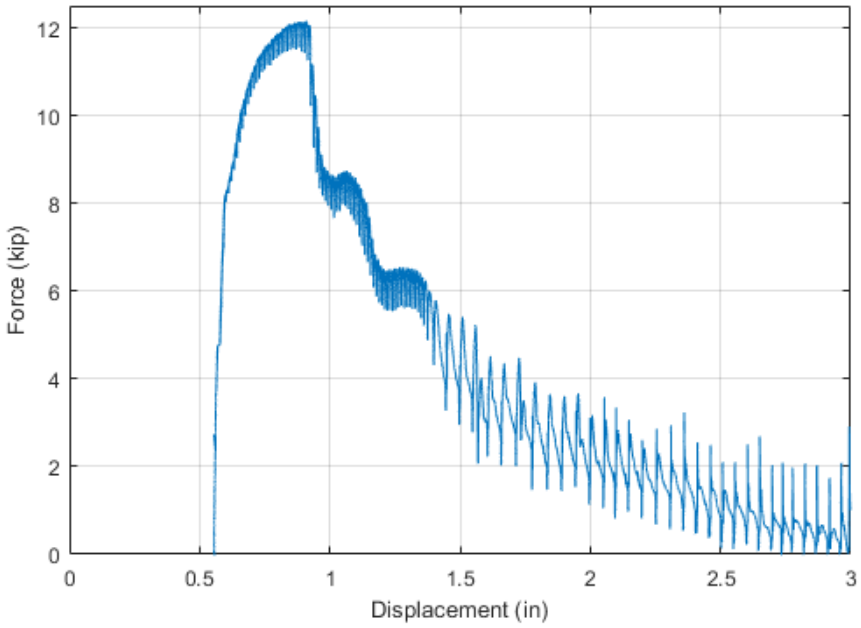

Figure A.31 Unfiltered force versus displacement relationship of P60-AE-5

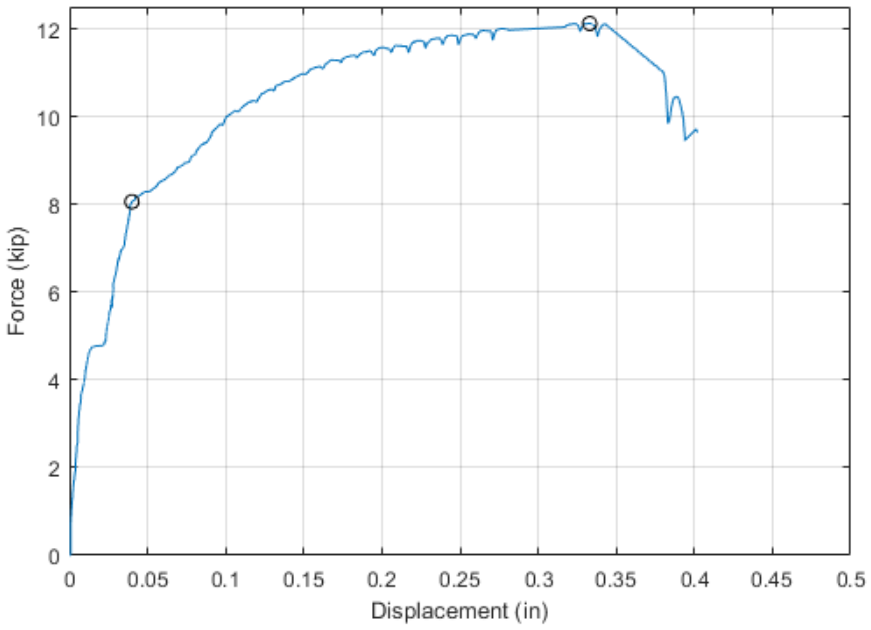

Figure A.32 Force versus displacement relationship of P60-AE-5

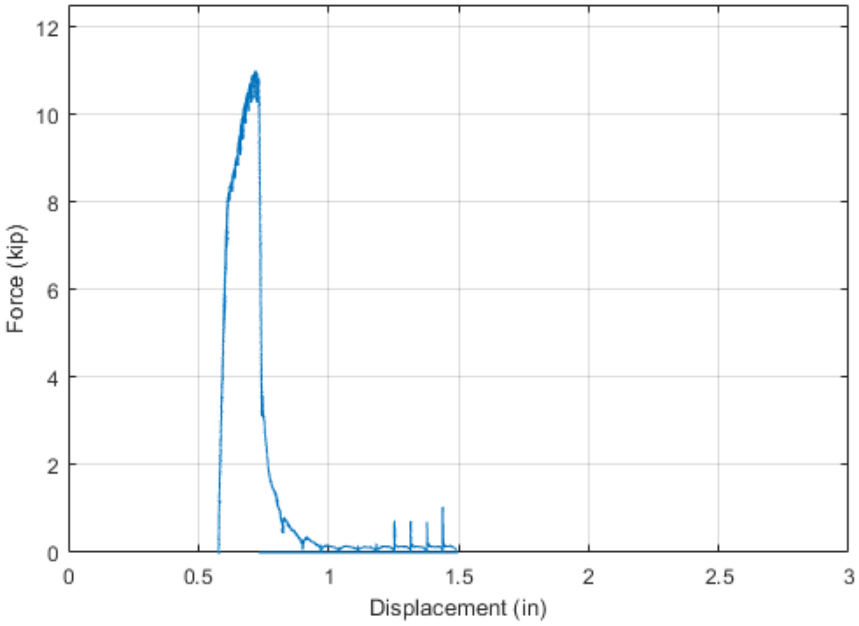

Figure A.33 Unfiltered force versus displacement relationship of P80-AE-1

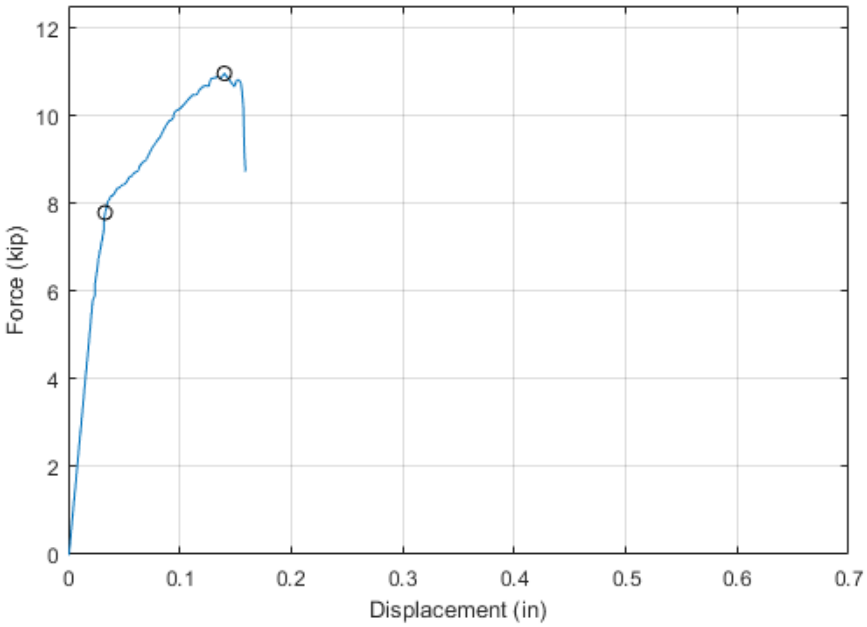

Figure A.34 Force versus displacement relationship of P80-AE-1

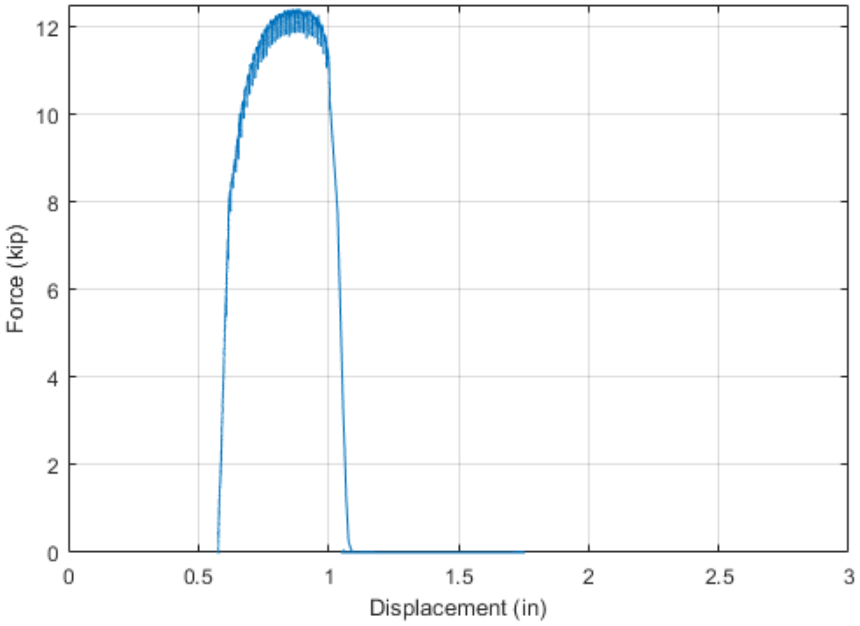

Figure A.35 Unfiltered force versus displacement relationship of P80-AE-4

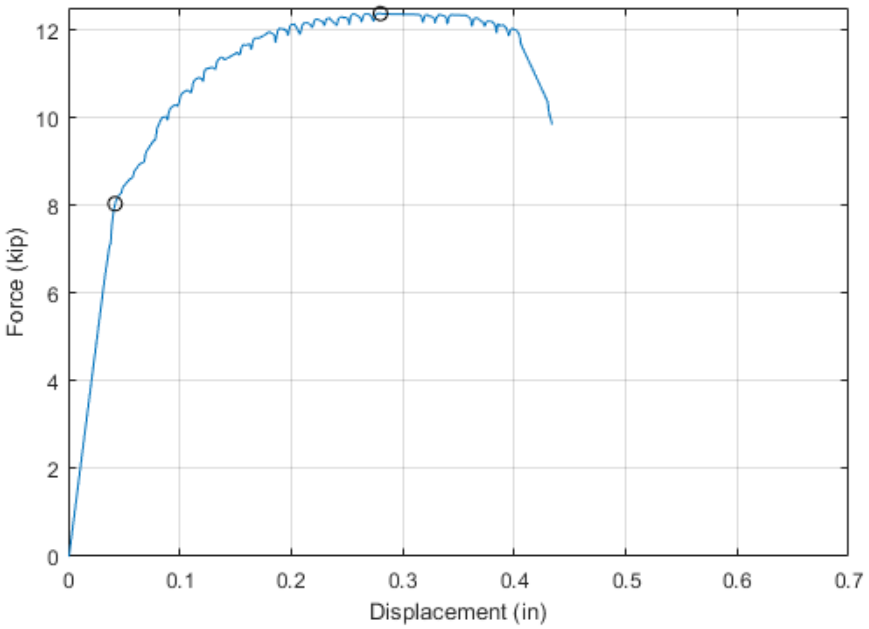

Figure A.36 Force versus displacement relationship of P80-AE-4

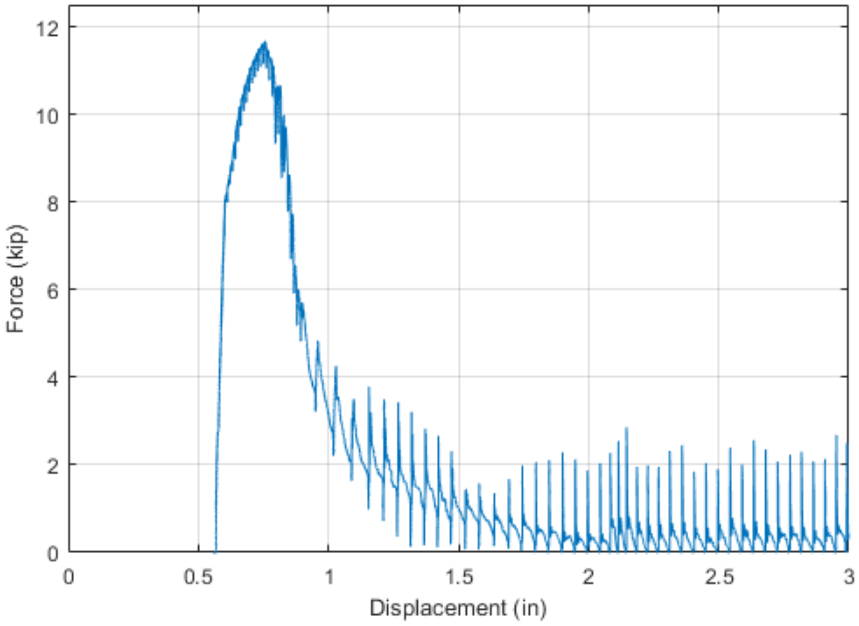

Figure A.37 Unfiltered force versus displacement relationship of P80-AE-5

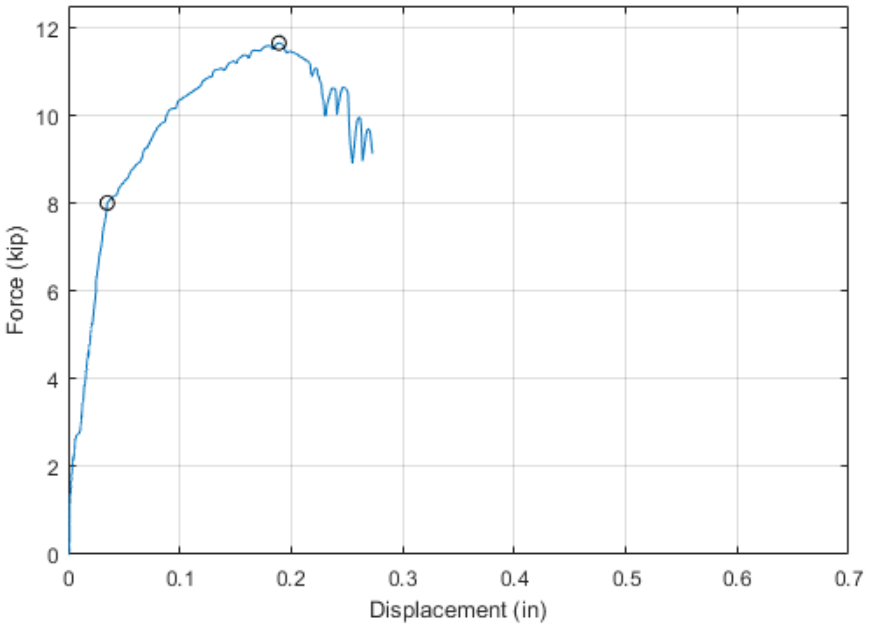

Figure A.38 Force versus displacement relationship of P80-AE-5

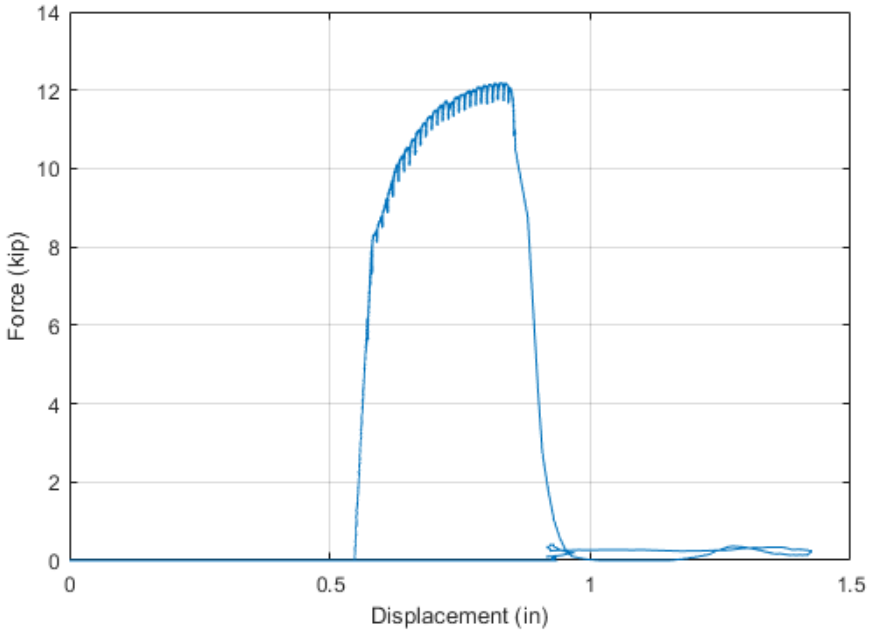

Figure A.39 Unfiltered force versus displacement relationship of BL-BE-1

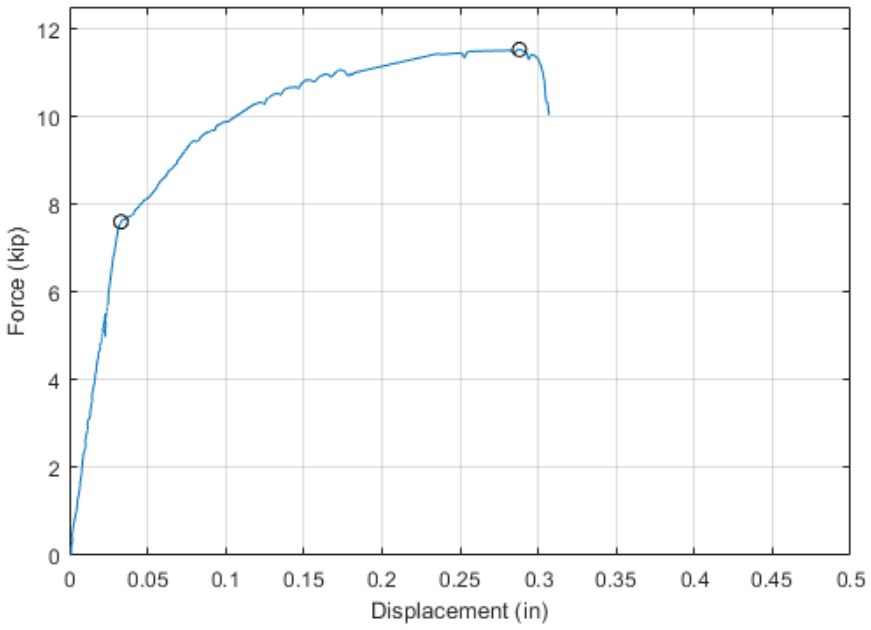

Figure A.40 Force versus displacement relationship of BL-BE-1

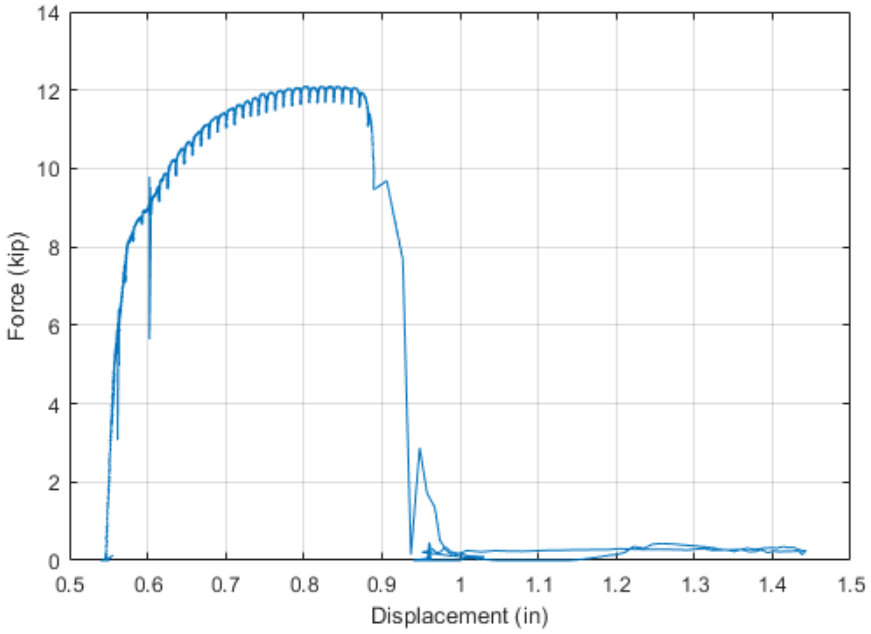

Figure A.41 Unfiltered force versus displacement relationship of BL-BE-2

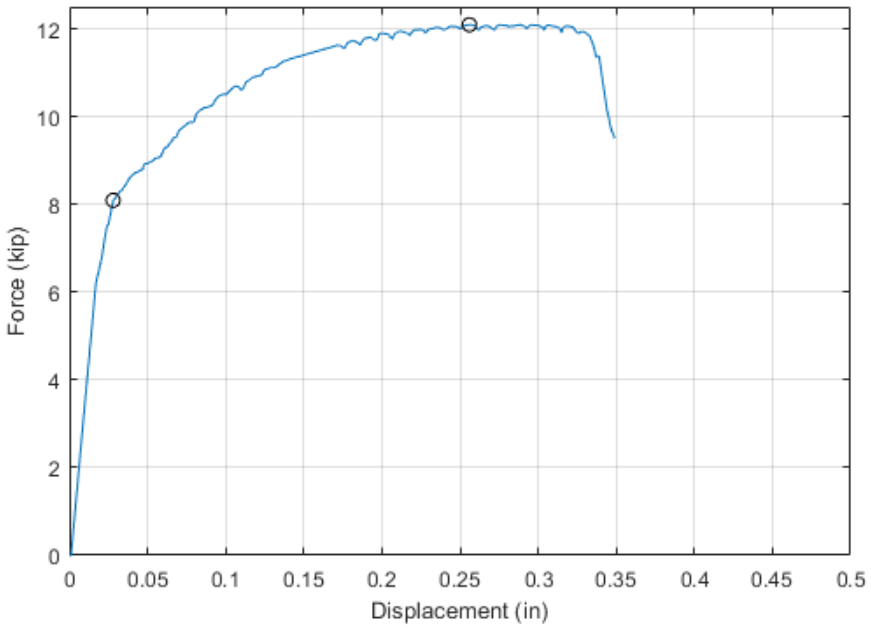

Figure A.42 Force versus displacement relationship of BL-BE-2

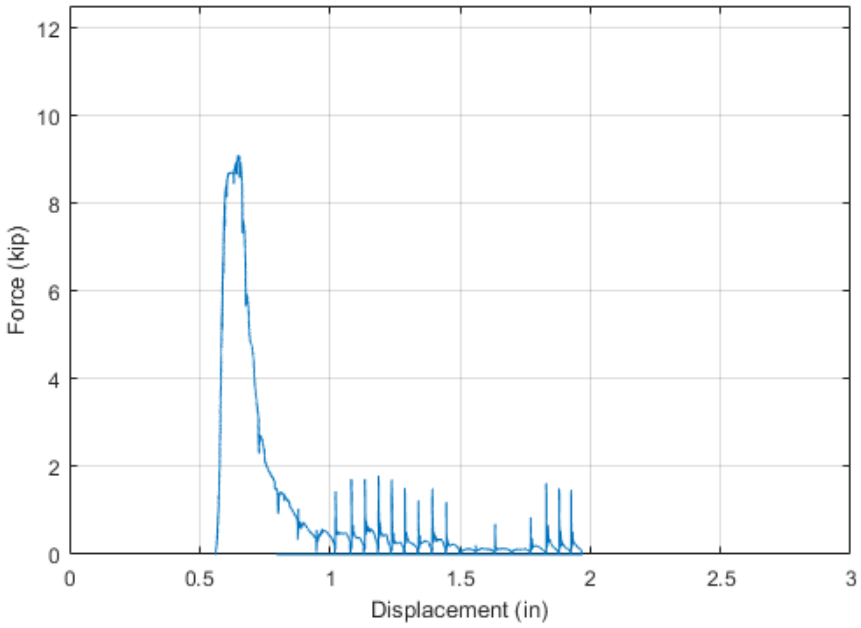

Figure A.43 Unfiltered force versus displacement relationship of EE-AE-1

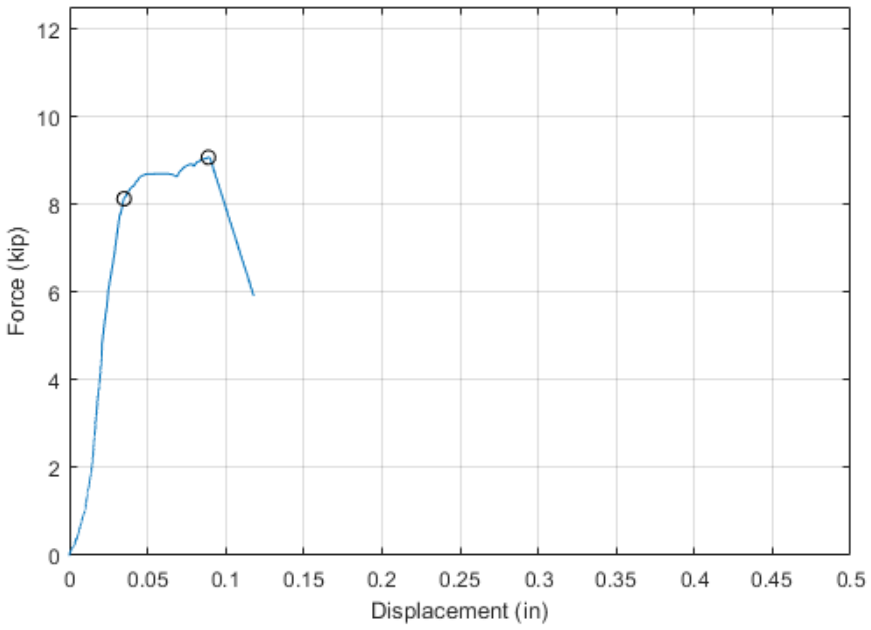

Figure A.44 Force versus displacement relationship of EE-AE-1

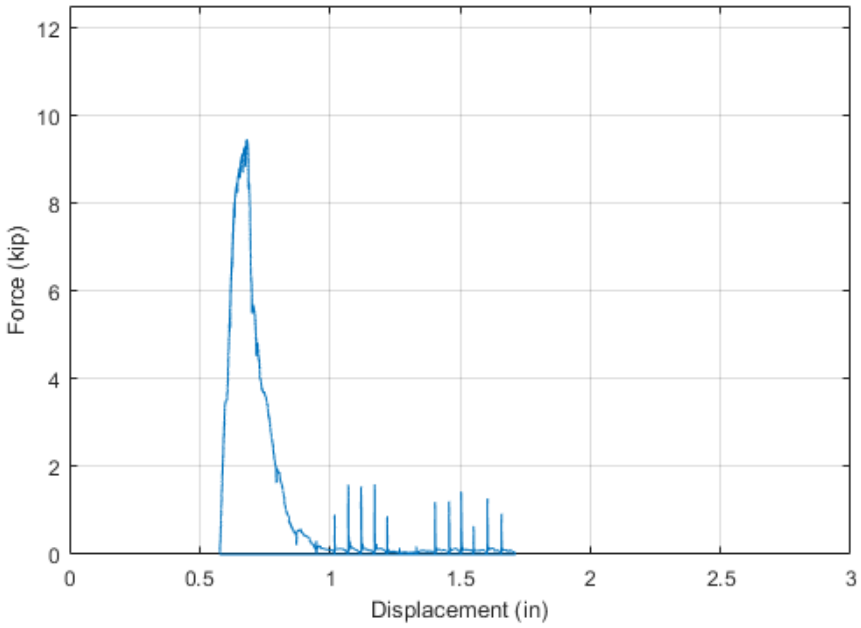

Figure A.45 Unfiltered force versus displacement relationship of EE-AE-3

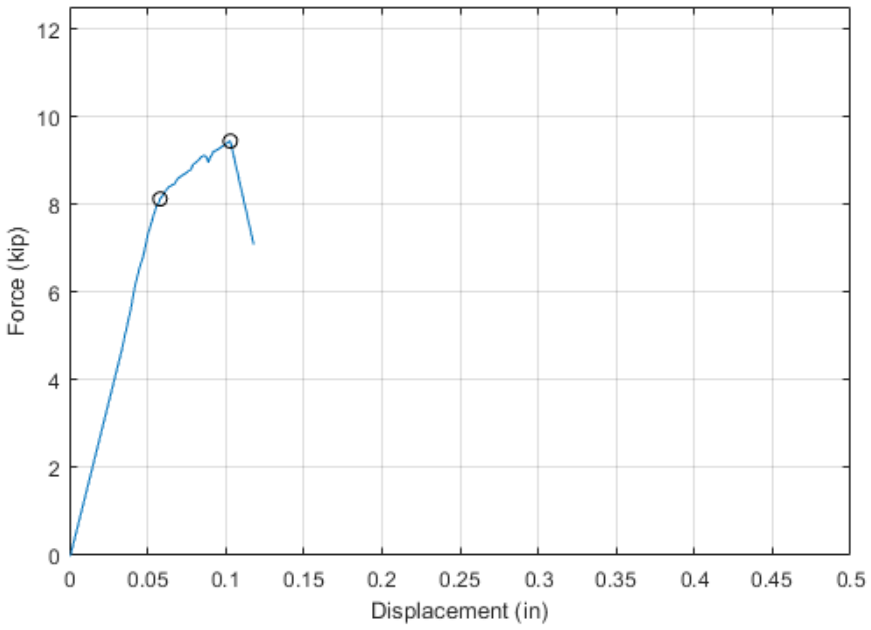

Figure A.46 Force versus displacement relationship of EE-AE-3

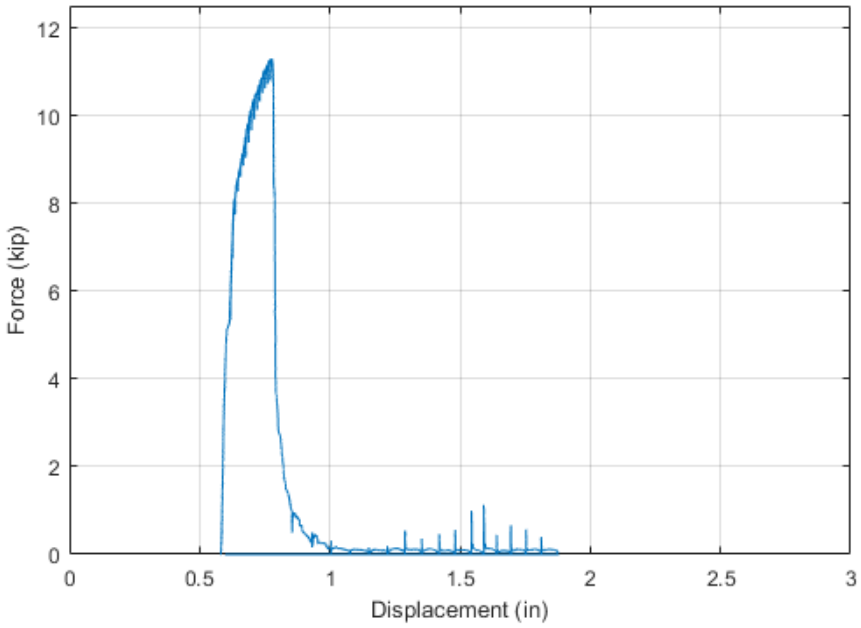

Figure A.47 Unfiltered force versus displacement relationship of EE-AE-5

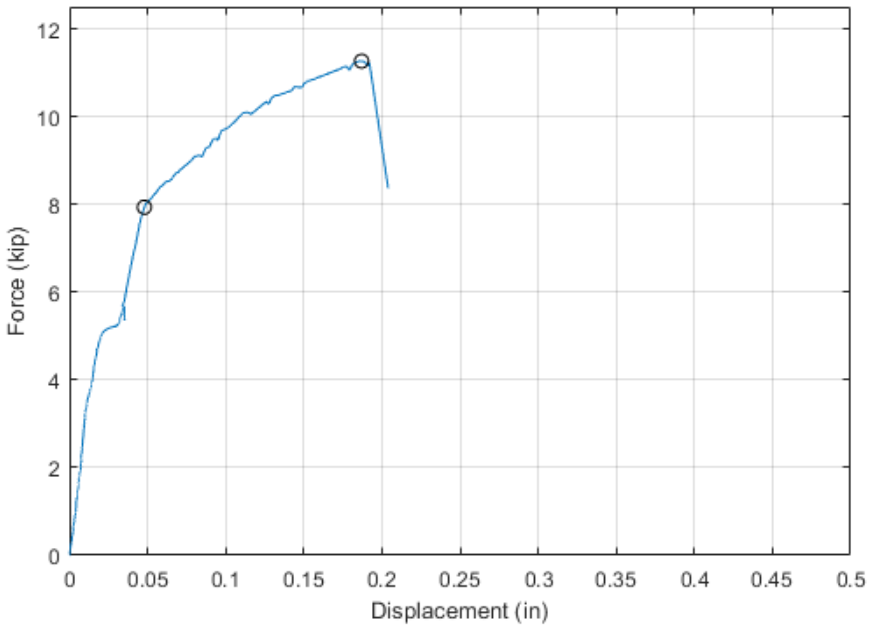

Figure A.48 Force versus displacement relationship of EE-AE-5

A.2 First Derivative and Stiffness Identification

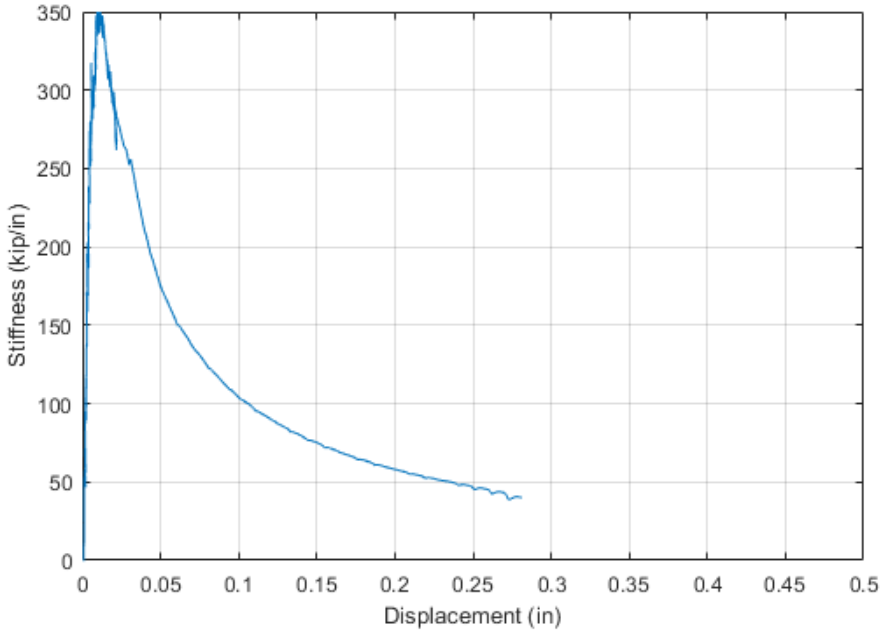

Figure A.49 Tangent stiffness (first derivative) versus displacement relationship of BL-AE-1

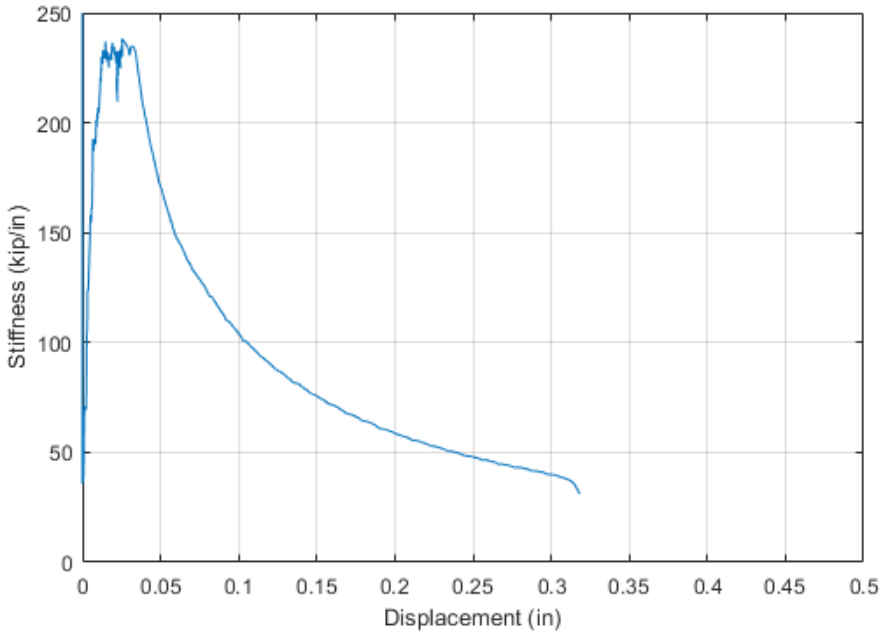

Figure A.50 Tangent stiffness (first derivative) versus displacement relationship of BL-AE-2

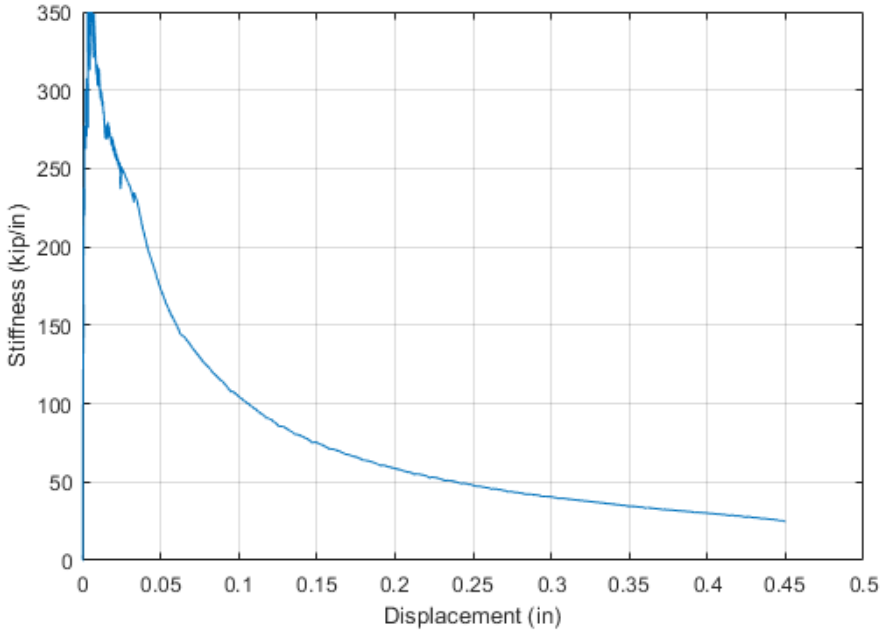

Figure A.51 Tangent stiffness (first derivative) versus displacement relationship of BL-AE-3

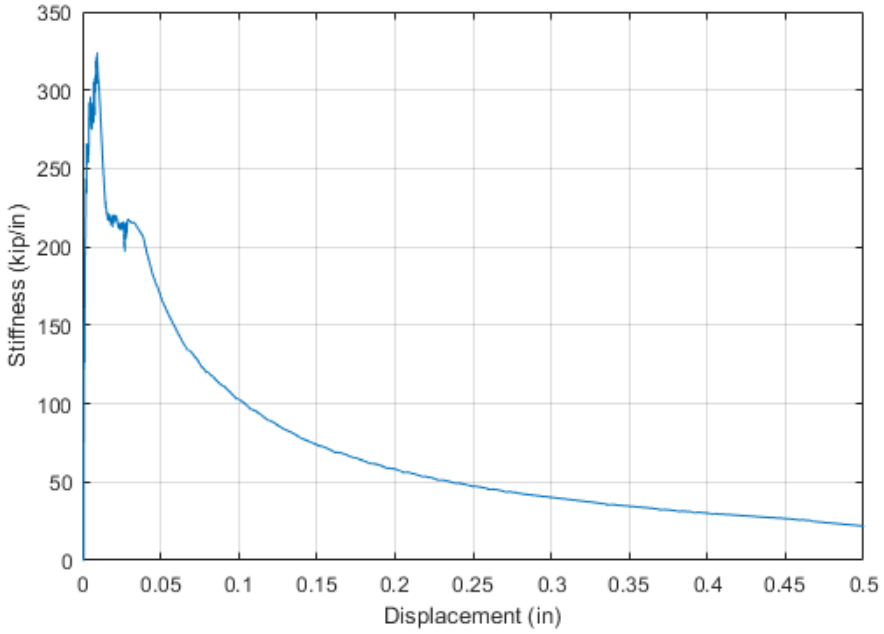

Figure A.52 Tangent stiffness (first derivative) versus displacement relationship of BL-AE-4

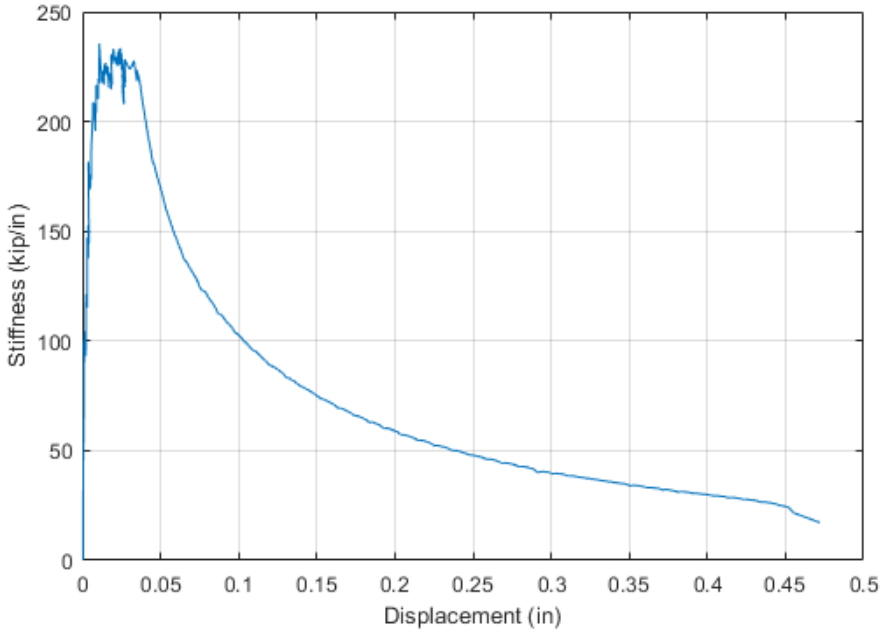

Figure A.53 Tangent stiffness (first derivative) versus displacement relationship of BL-AE-5

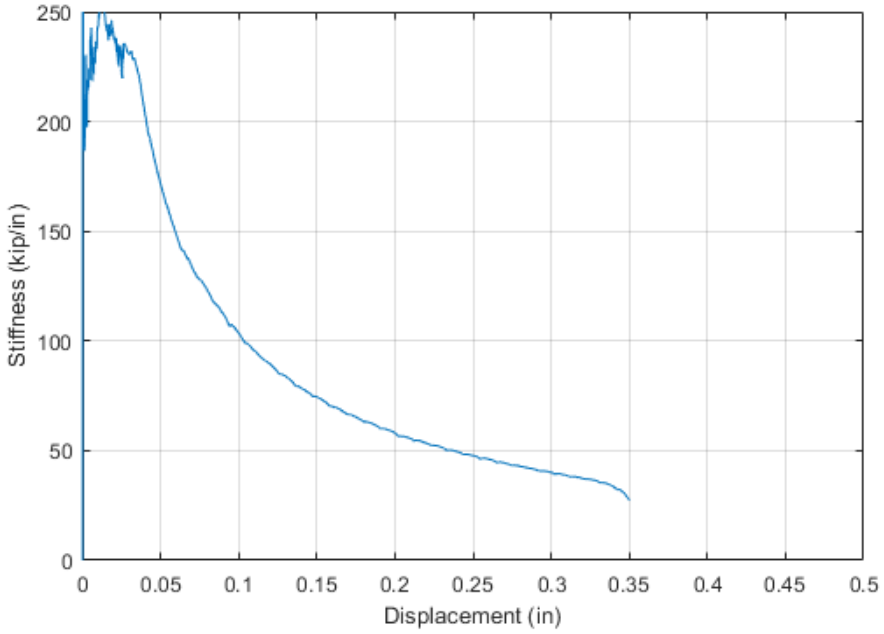

Figure A.54 Tangent stiffness (first derivative) versus displacement relationship of BL-AE-6

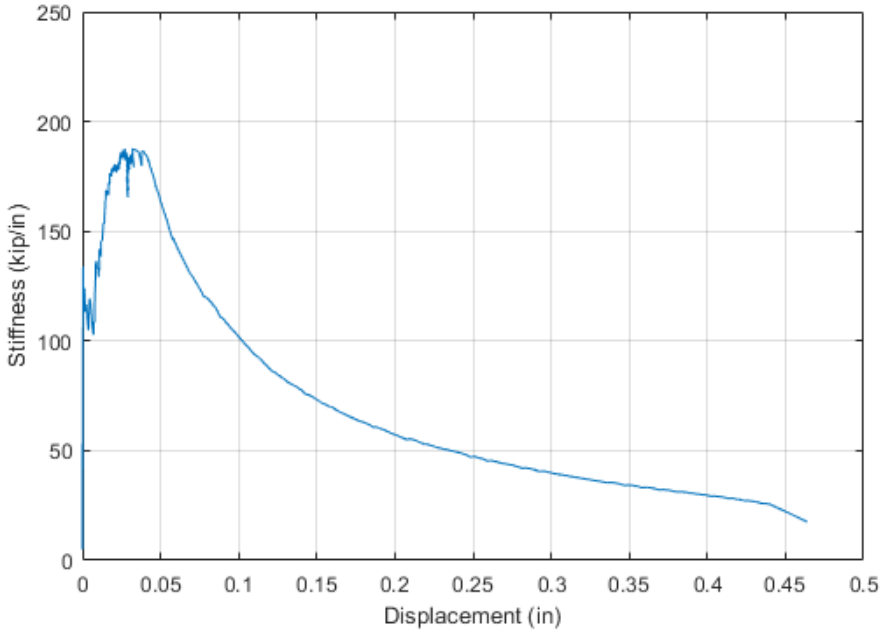

Figure A.55 Tangent stiffness (first derivative) versus displacement relationship of CP-AE-1

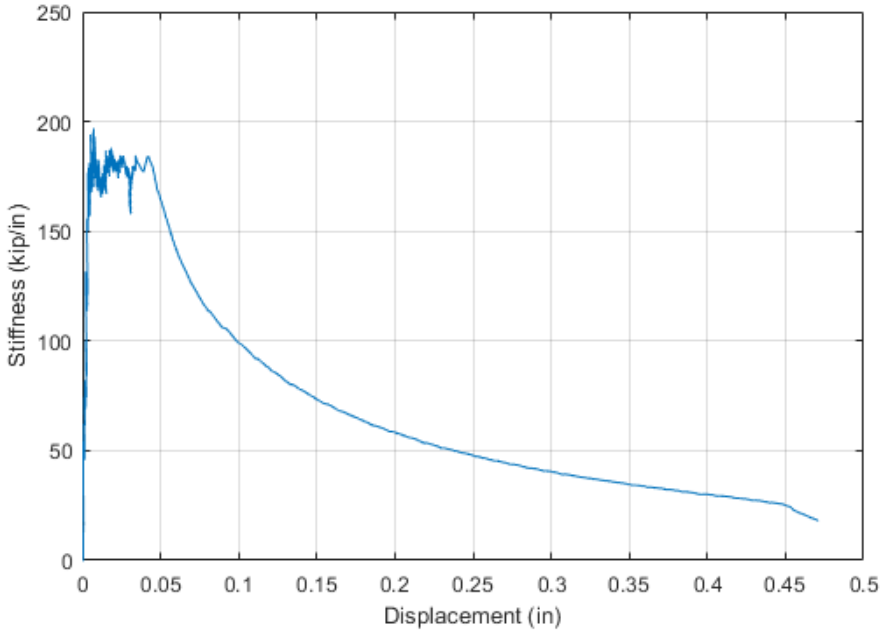

Figure A.56 Tangent stiffness (first derivative) versus displacement relationship of CP-AE-2

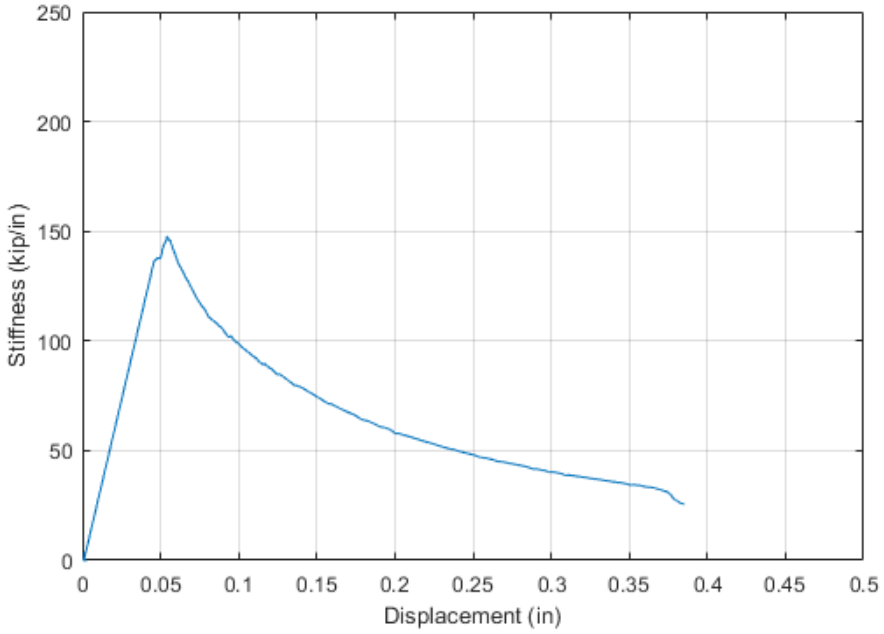

Figure A.57 Tangent stiffness (first derivative) versus displacement relationship of CP-AE-3

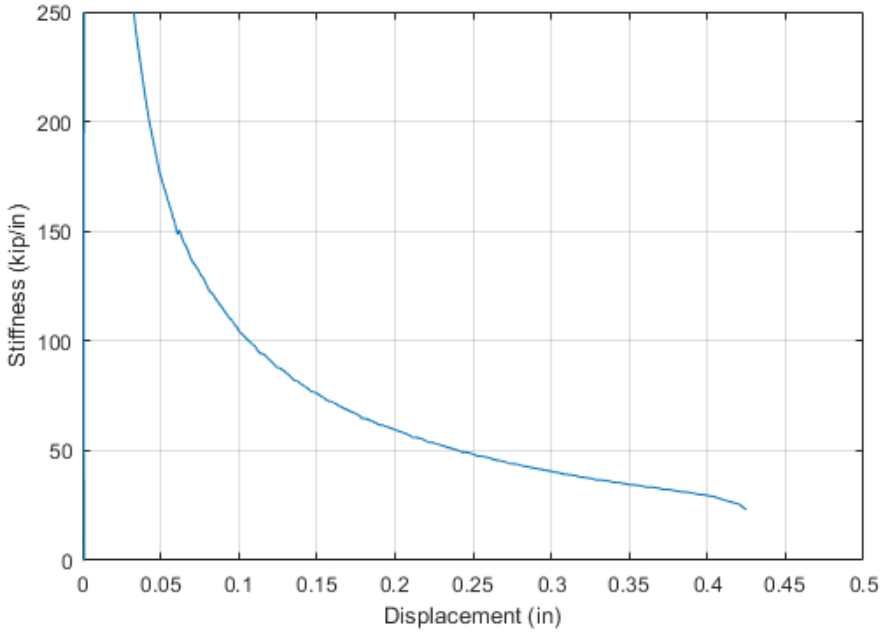

Figure A.58 Tangent stiffness (first derivative) versus displacement relationship of CP-AE-4

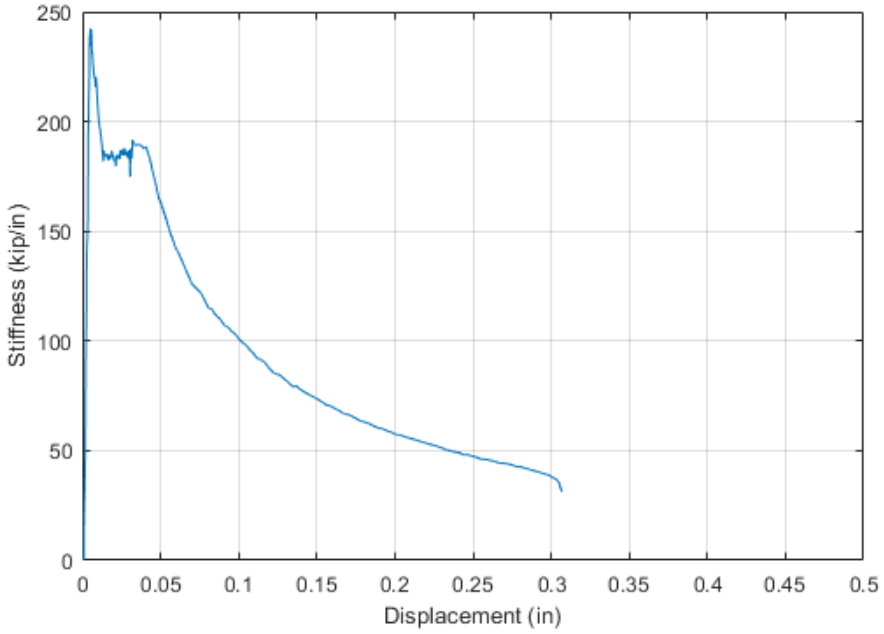

Figure A.59 Tangent stiffness (first derivative) versus displacement relationship of CP-AE-5

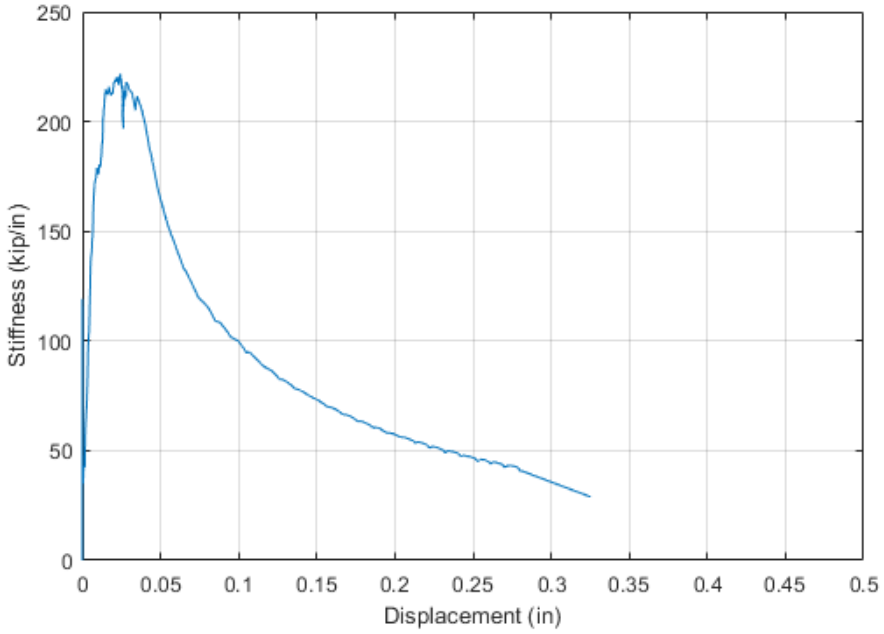

Figure A.60 Tangent stiffness (first derivative) versus displacement relationship of P60-AE-1

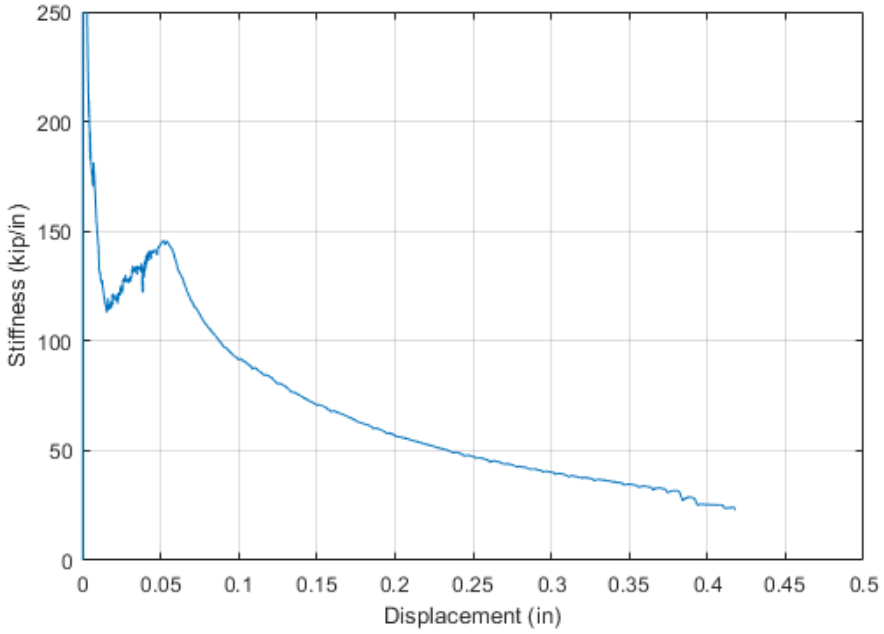

Figure A.61 Tangent stiffness (first derivative) versus displacement relationship of P60-AE-2

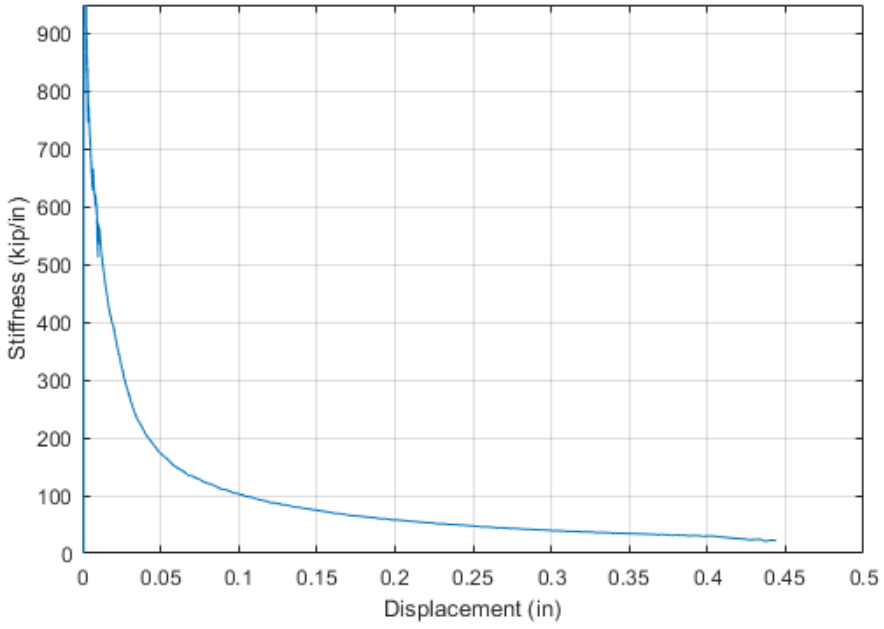

Figure A.62 Tangent stiffness (first derivative) versus displacement relationship of P60-AE-3

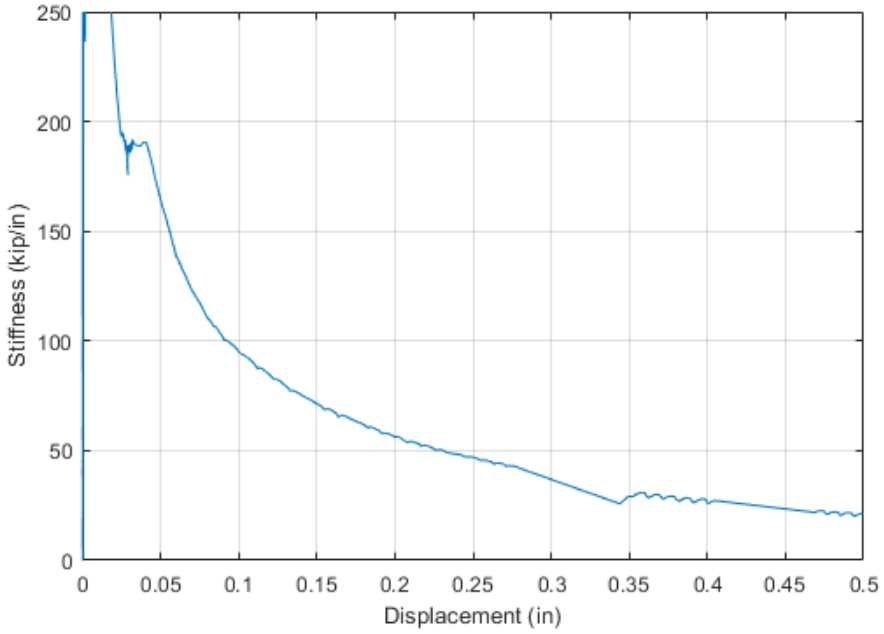

Figure A.63 Tangent stiffness (first derivative) versus displacement relationship of P60-AE-4

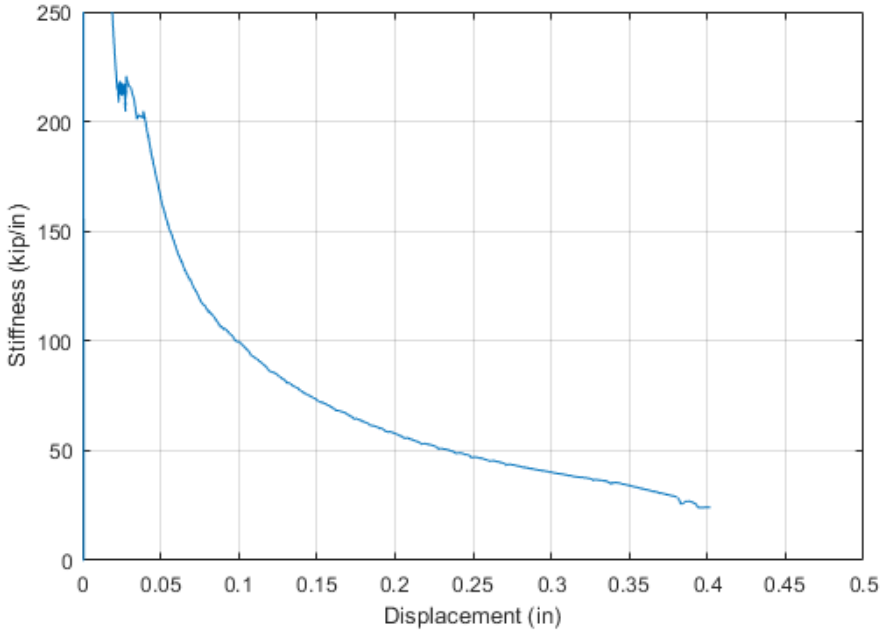

Figure A.64 Tangent stiffness (first derivative) versus displacement relationship of P60-AE-5

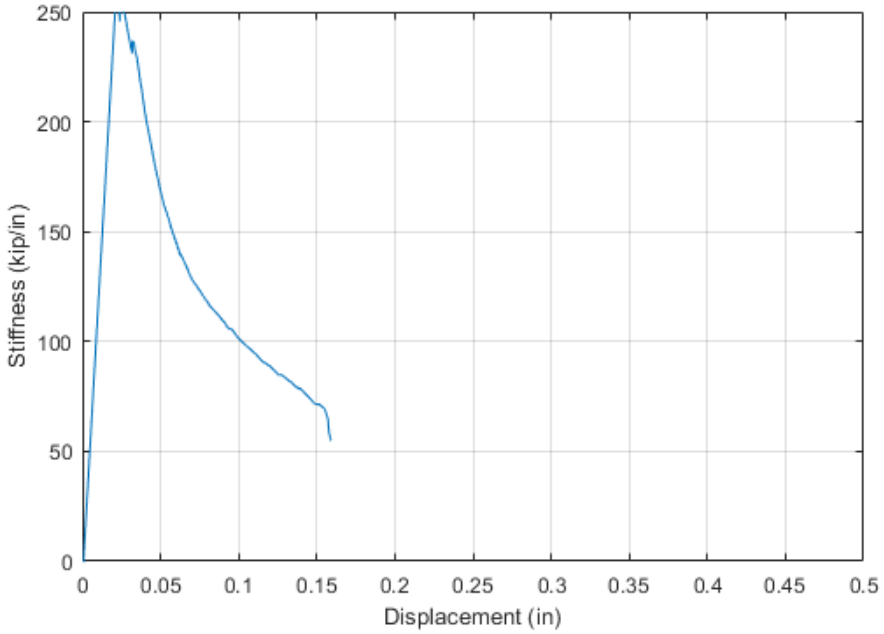

Figure A.65 Tangent stiffness (first derivative) versus displacement relationship of P80-AE-1

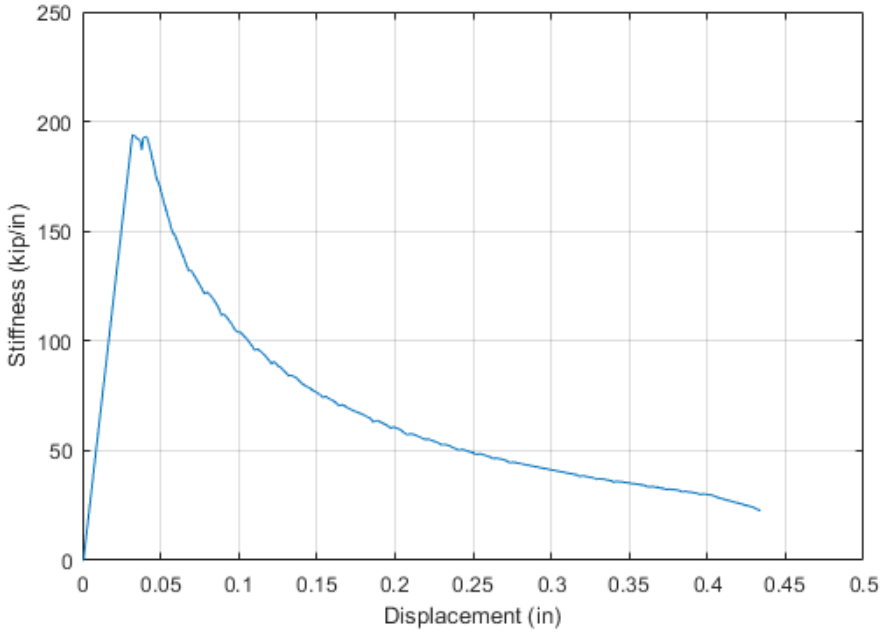

Figure A.66 Tangent stiffness (first derivative) versus displacement relationship of P80-AE-4

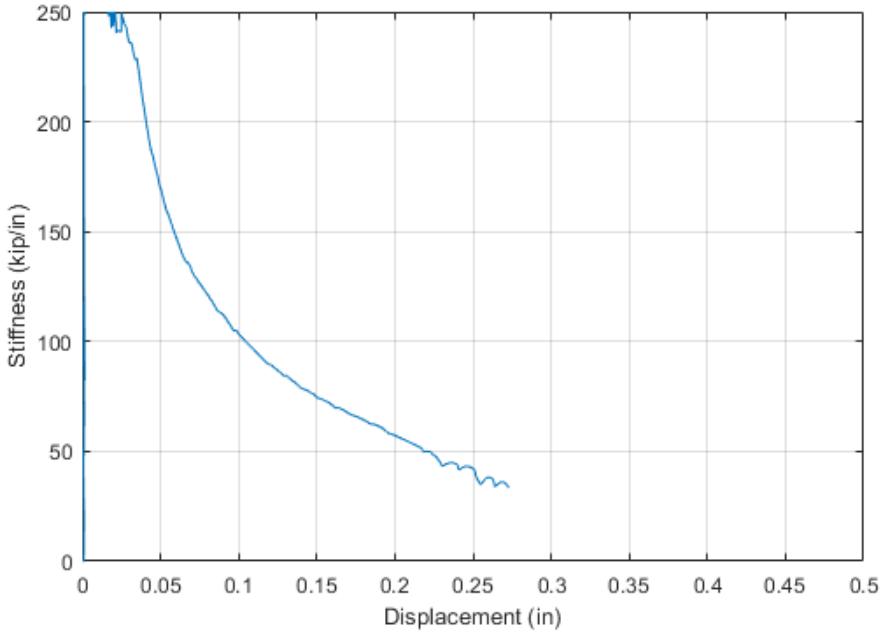

Figure A.67 Tangent stiffness (first derivative) versus displacement relationship of P80-AE-5

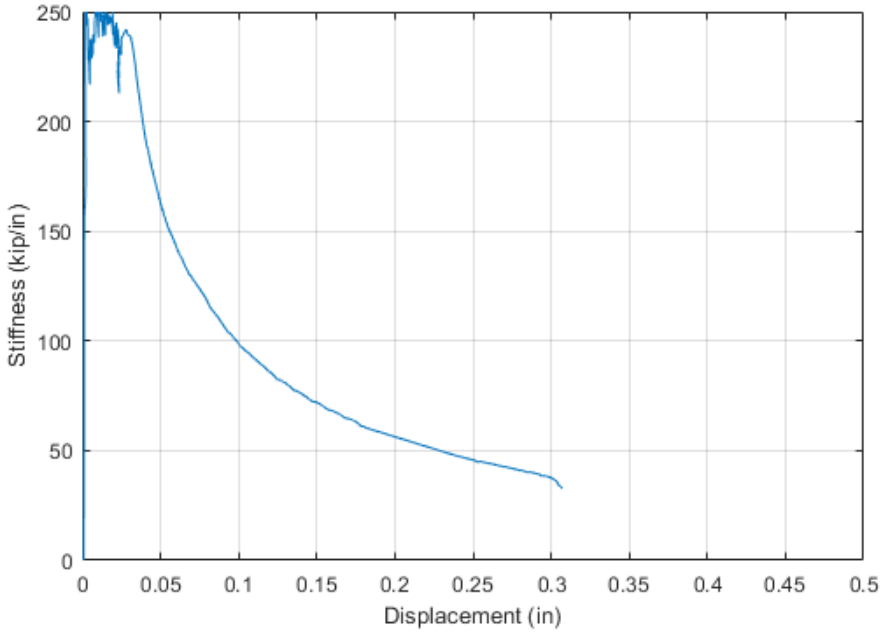

Figure A.68 Tangent stiffness (first derivative) versus displacement relationship of BL-BE-1

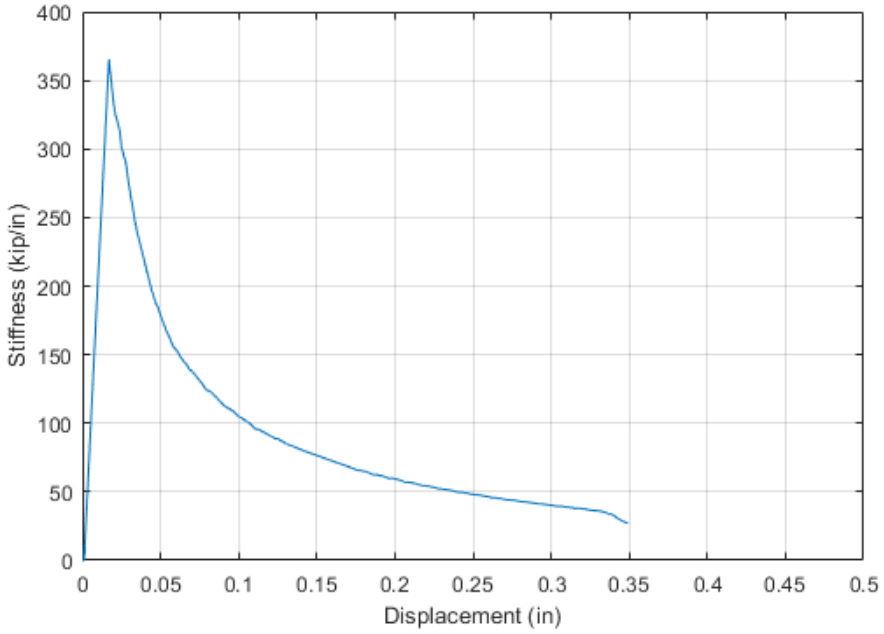

Figure A.69 Tangent stiffness (first derivative) versus displacement relationship of BL-BE-2

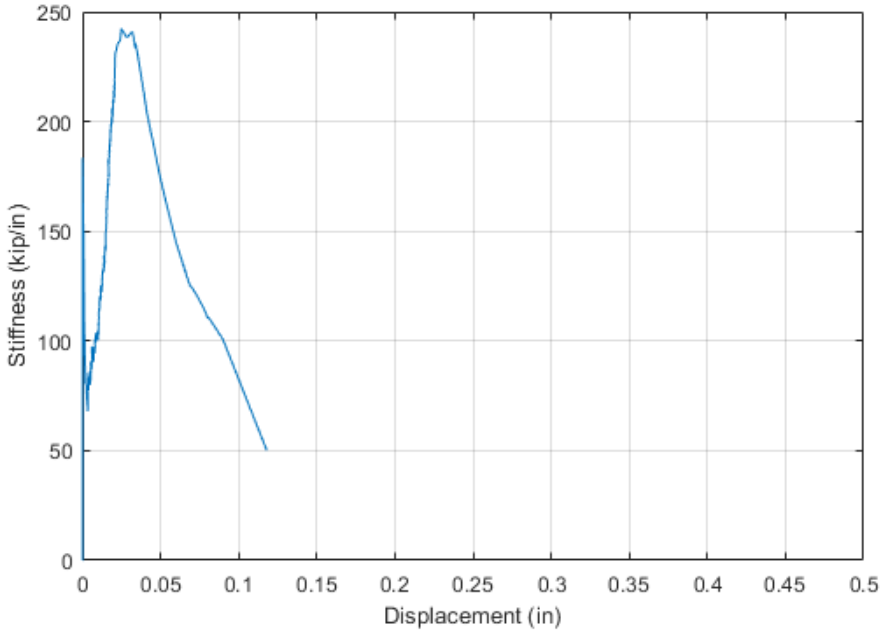

Figure A.70 Tangent stiffness (first derivative) versus displacement relationship of EE-AE-1

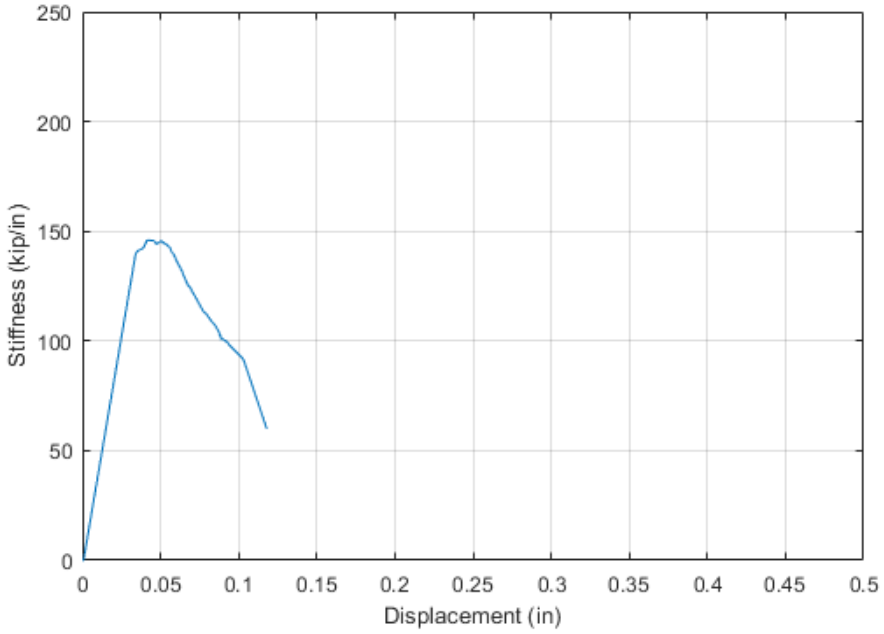

Figure A.71 Tangent stiffness (first derivative) versus displacement relationship of EE-AE-3

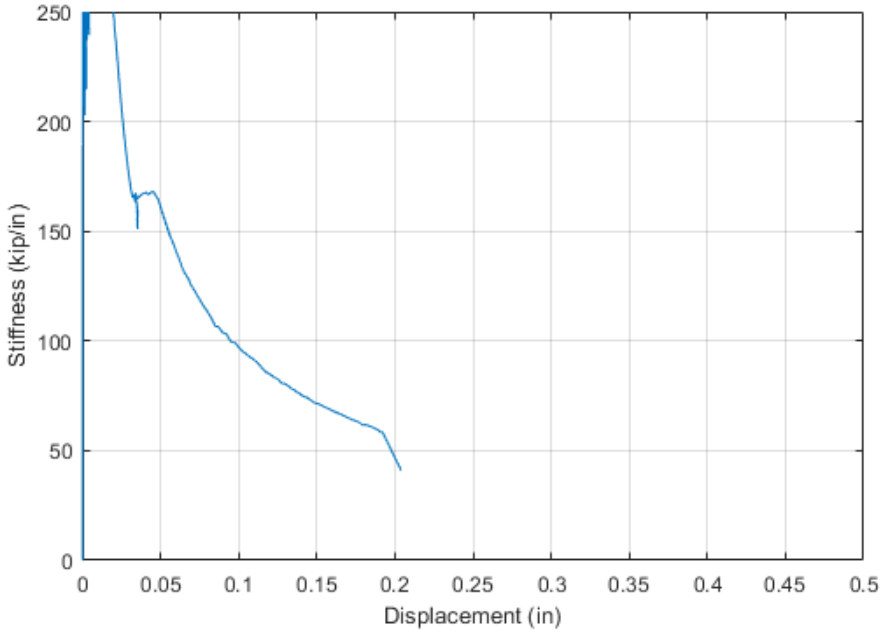

Figure A.72 Tangent stiffness (first derivative) versus displacement relationship of EE-AE-5

A.3 Second Derivative to Indicate Significant Yielding

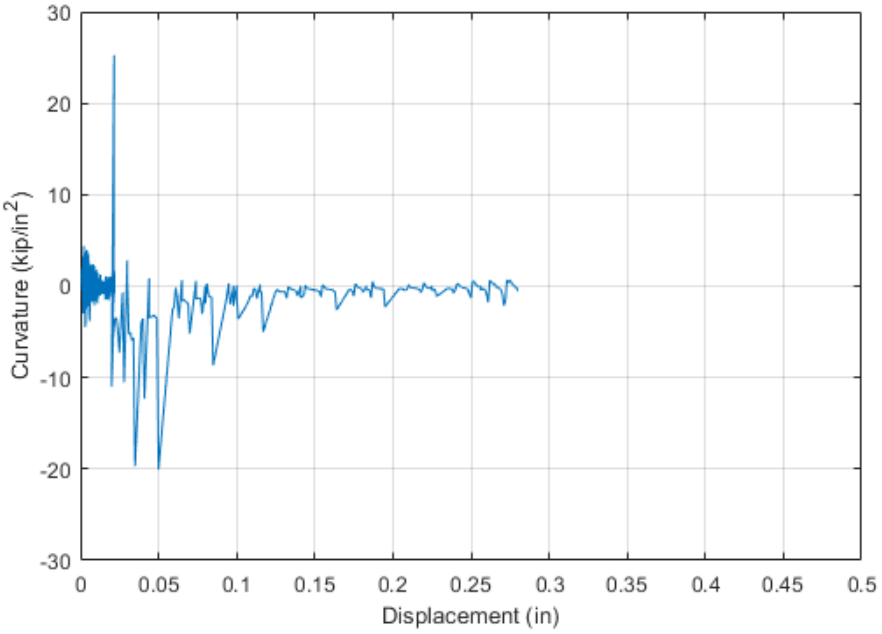

Figure A.73 Curvature (second derivative) versus displacement relationship of BL-AE-1

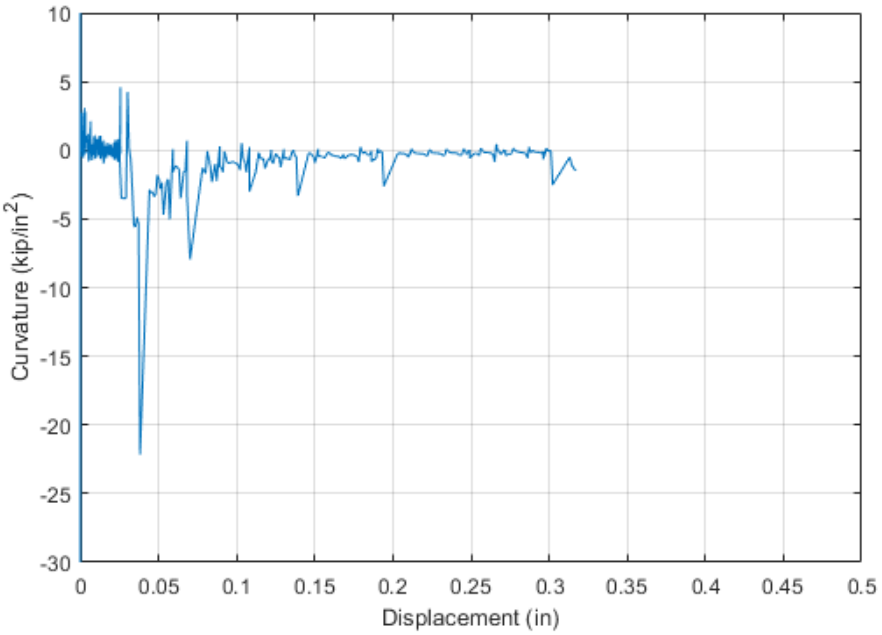

Figure A.74 Curvature (second derivative) versus displacement relationship of BL-AE-2

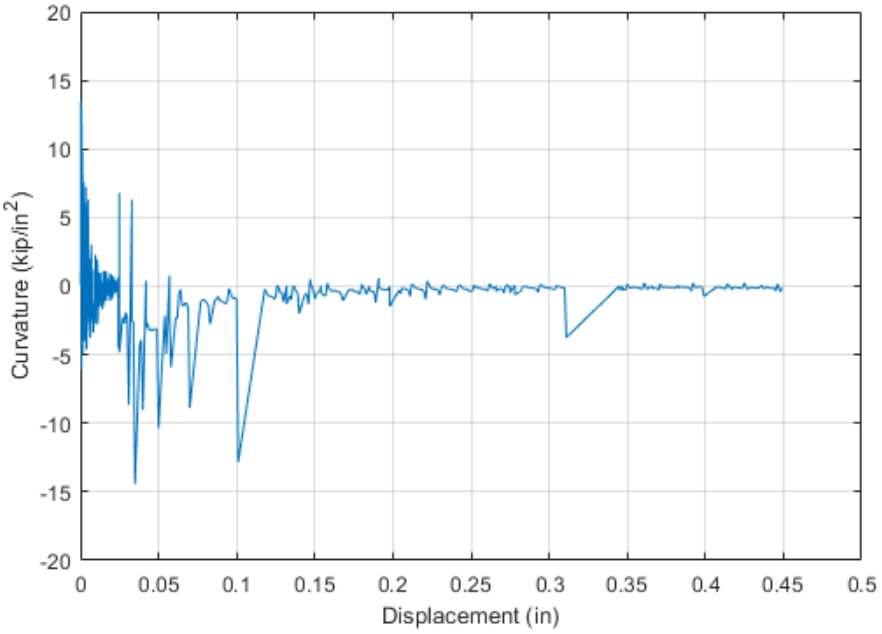

Figure A.75 Curvature (second derivative) versus displacement relationship of BL-AE-3

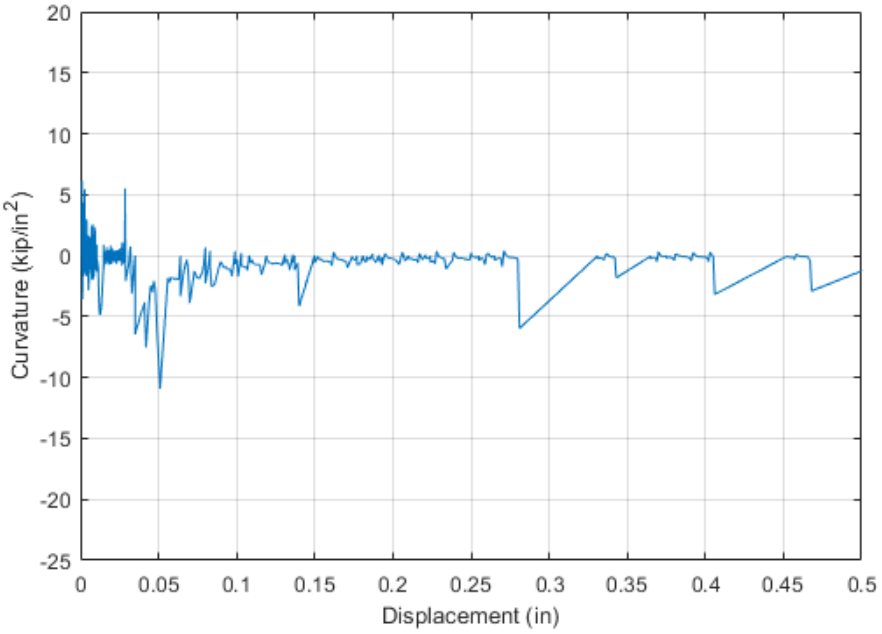

Figure A.76 Curvature (second derivative) versus displacement relationship of BL-AE-4

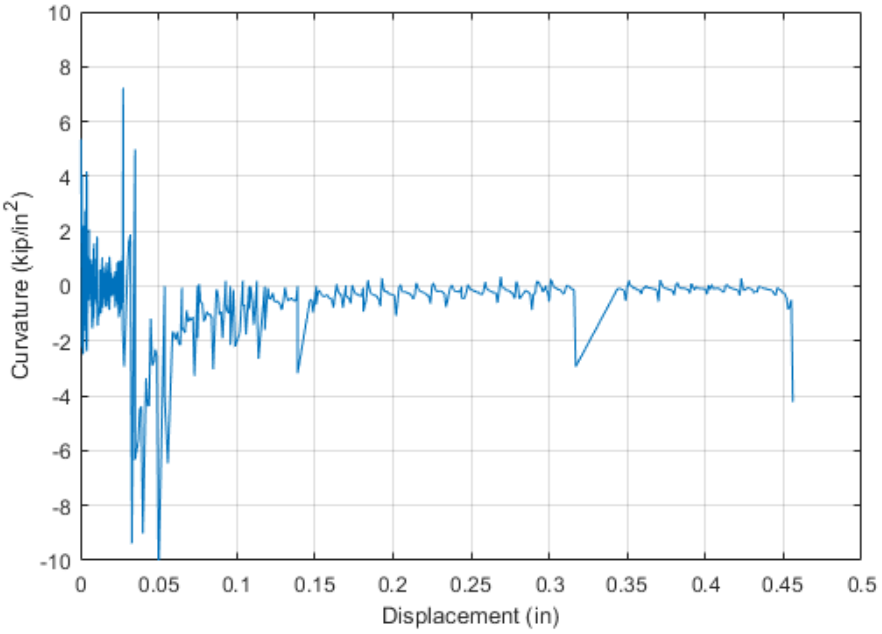

Figure A.77 Curvature (second derivative) versus displacement relationship of BL-AE-5

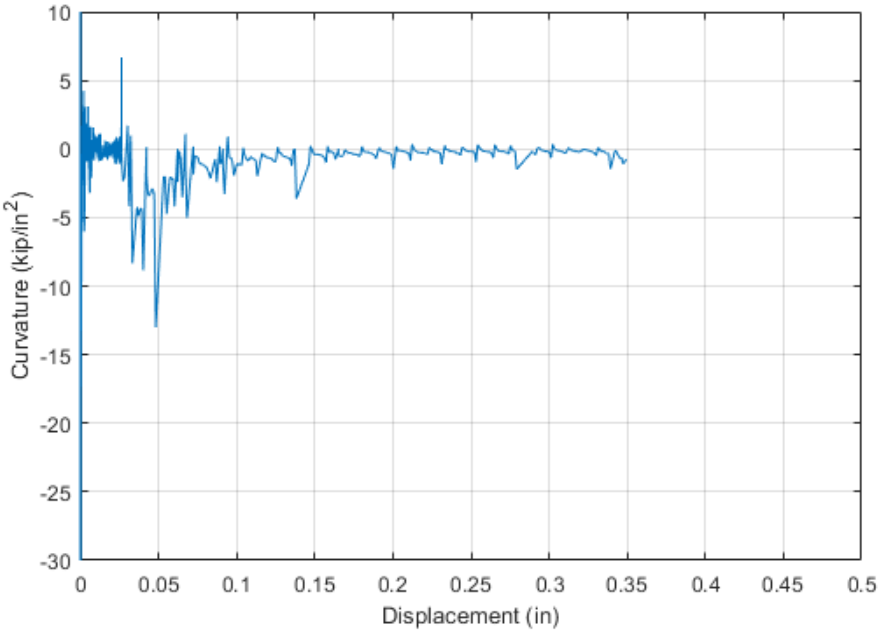

Figure A.78 Curvature (second derivative) versus displacement relationship of BL-AE-6

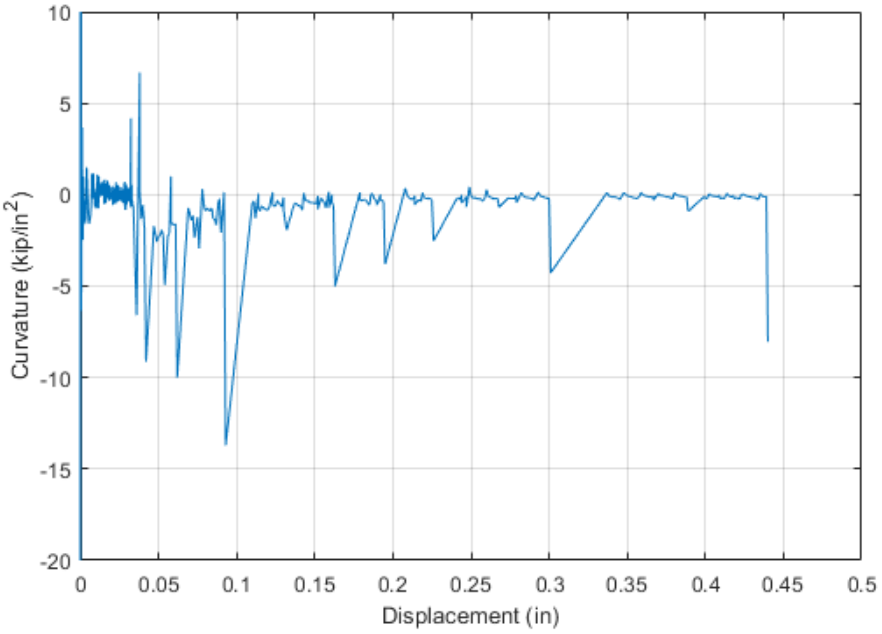

Figure A.79 Curvature (second derivative) versus displacement relationship of CP-AE-1

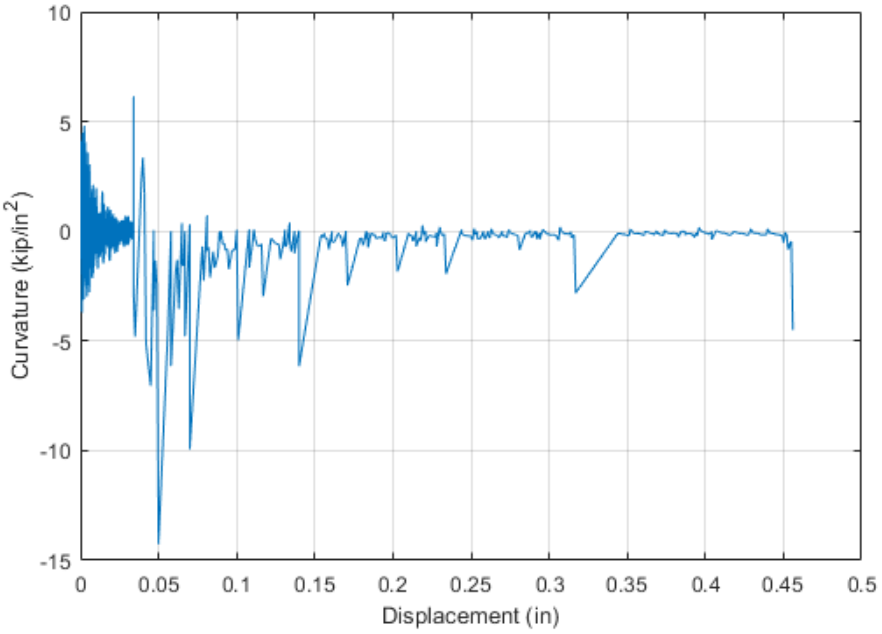

Figure A.80 Curvature (second derivative) versus displacement relationship of CP-AE-2

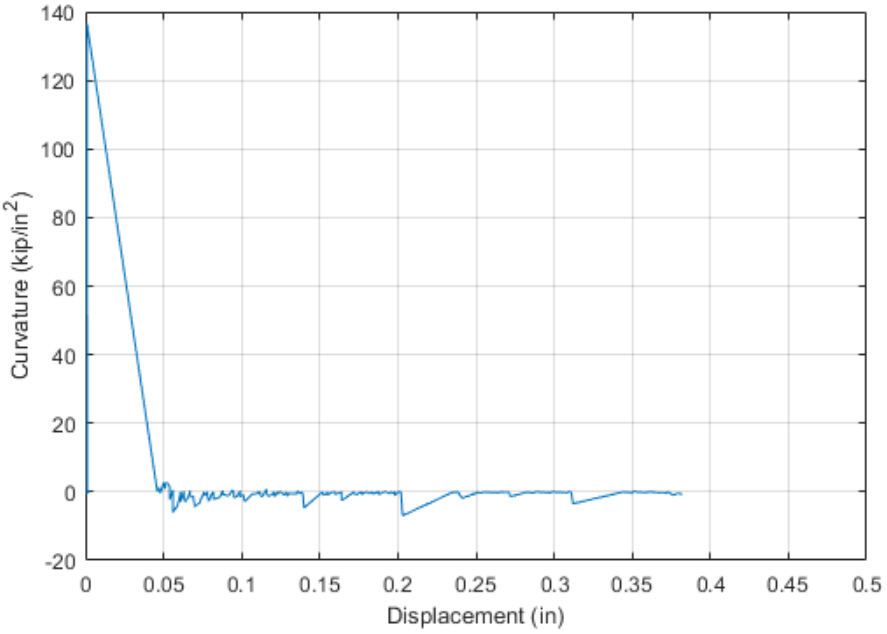

Figure A.81 Curvature (second derivative) versus displacement relationship of CP-AE-3

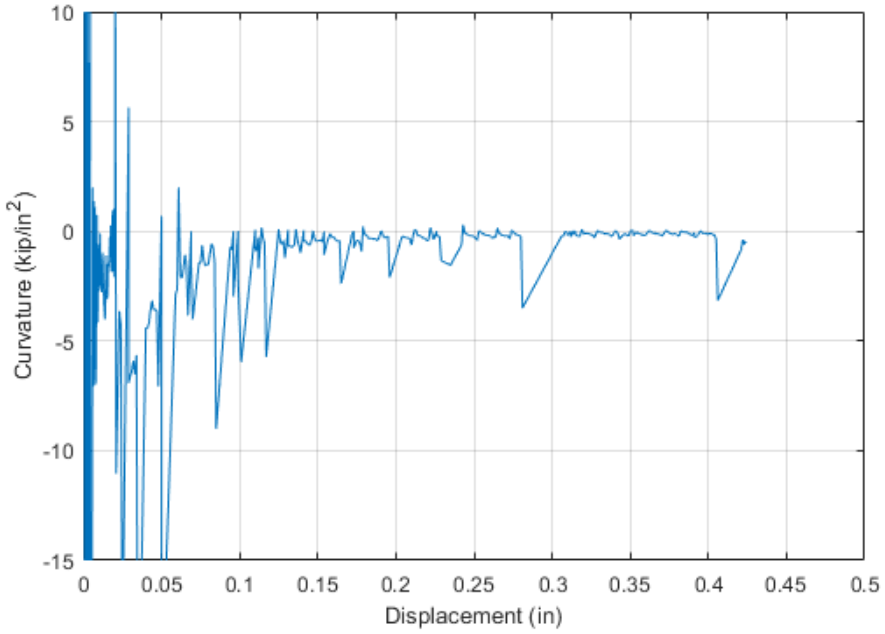

Figure A.82 Curvature (second derivative) versus displacement relationship of CP-AE-4

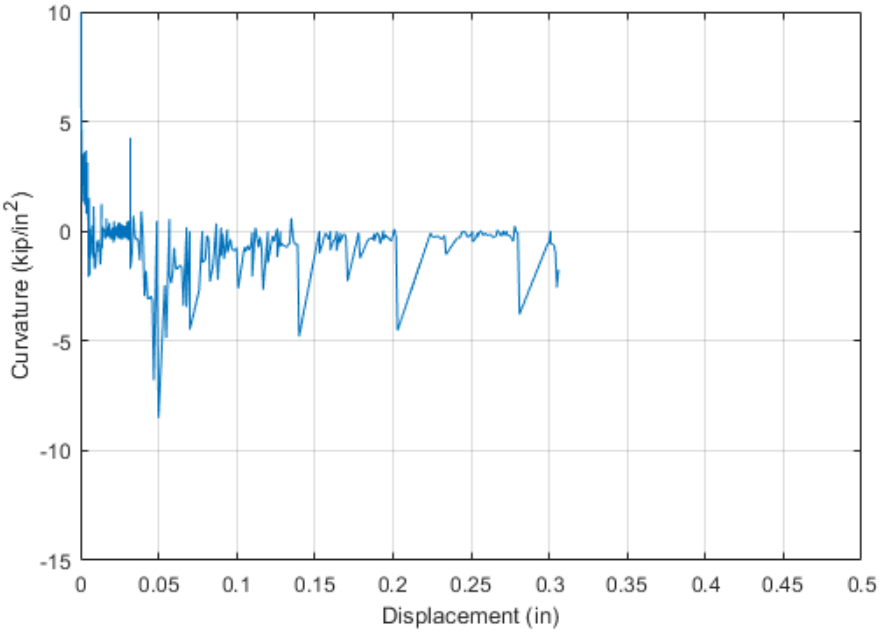

Figure A.83 Curvature (second derivative) versus displacement relationship of CP-AE-5

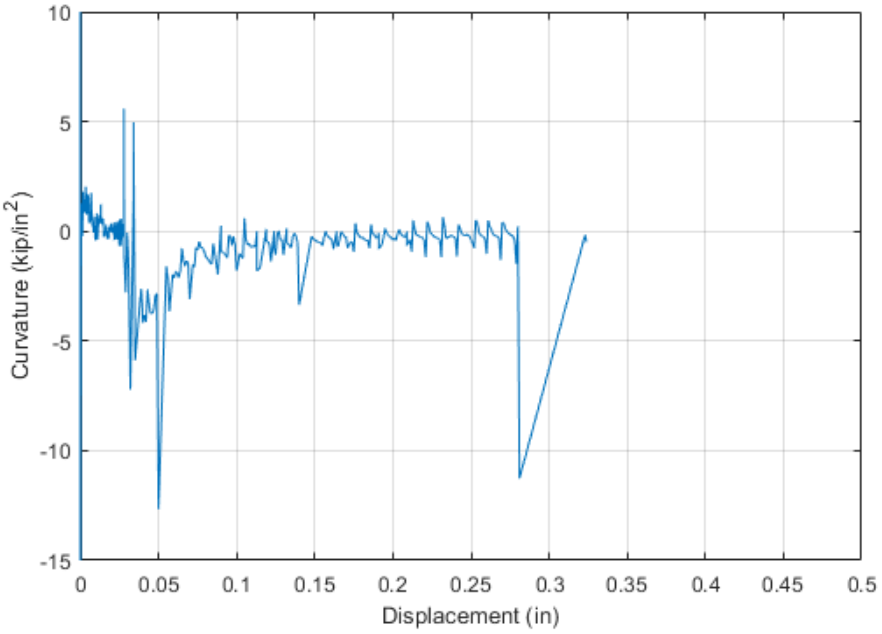

Figure A.84 Curvature (second derivative) versus displacement relationship of P60-AE-1

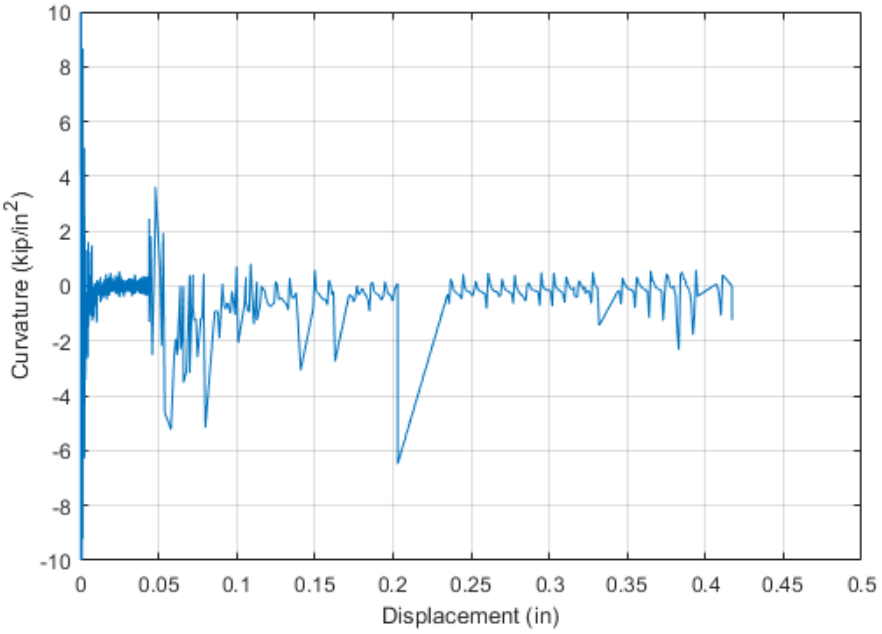

Figure A.85 Curvature (second derivative) versus displacement relationship of P60-AE-2

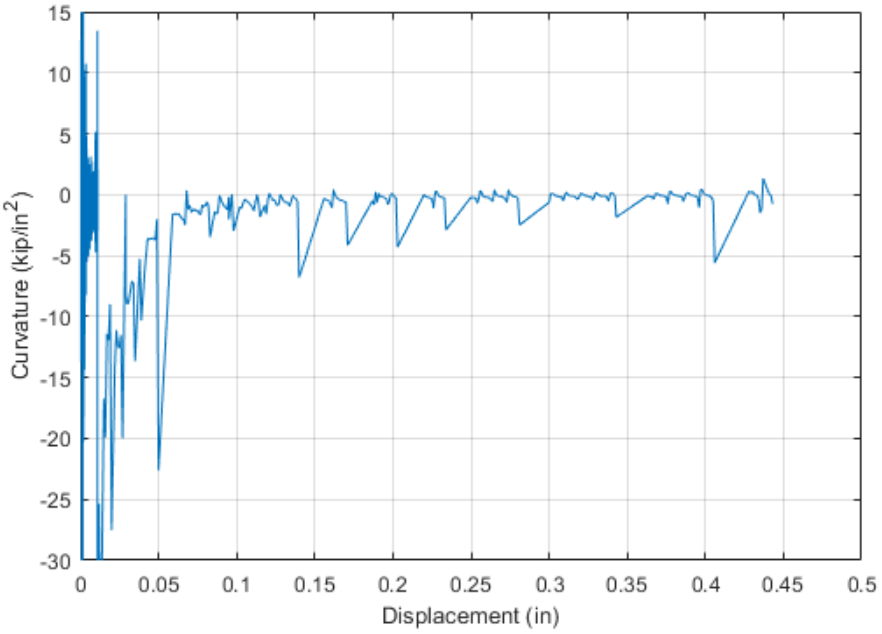

Figure A.86 Curvature (second derivative) versus displacement relationship of P60-AE-3

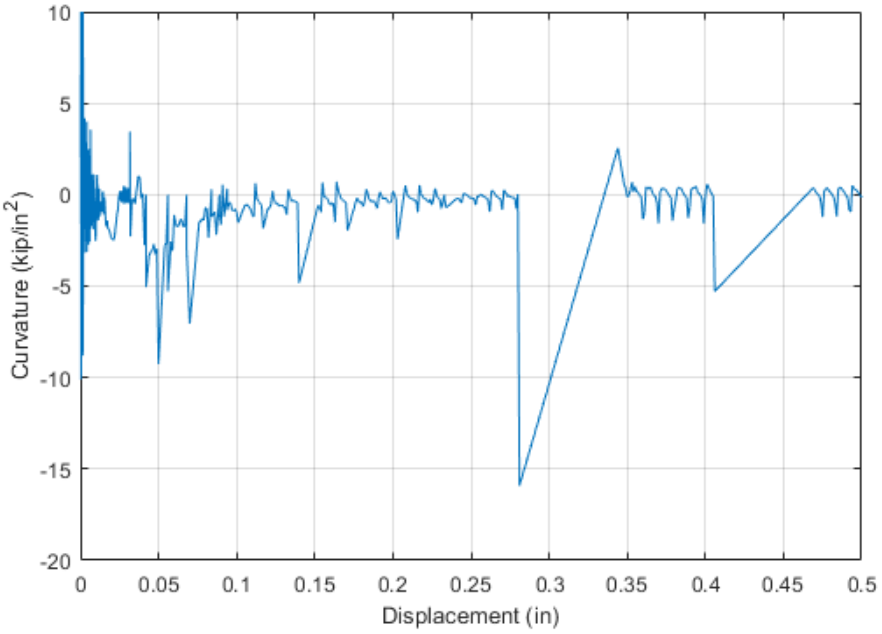

Figure A.87 Curvature (second derivative) versus displacement relationship of P60-AE-4

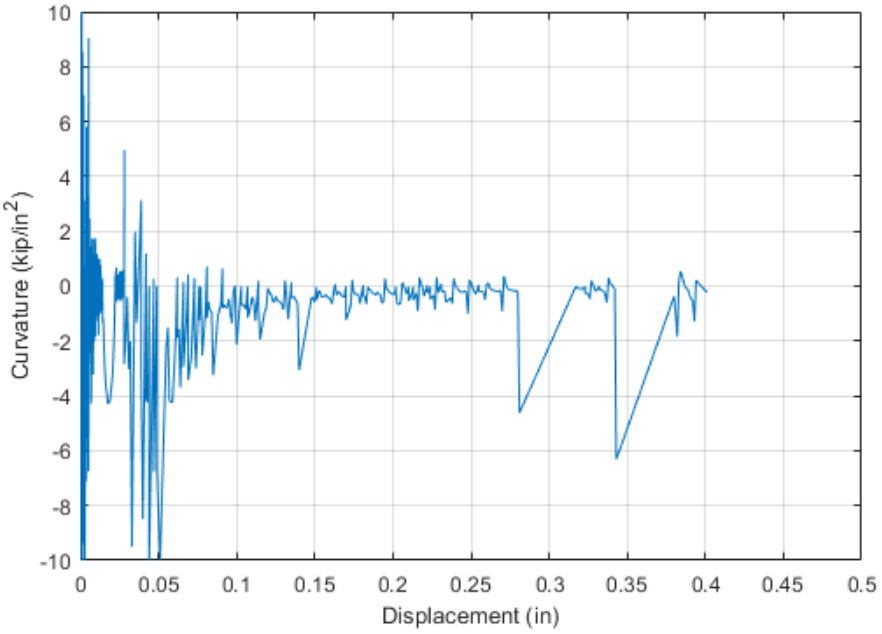

Figure A.88 Curvature (second derivative) versus displacement relationship of P60-AE-5

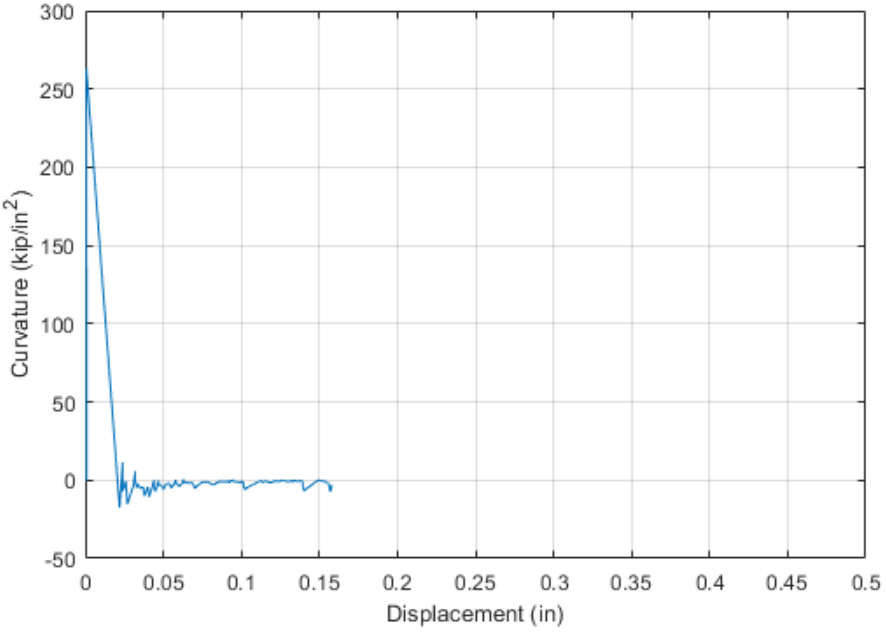

Figure A.89 Curvature (second derivative) versus displacement relationship of P80-AE-1

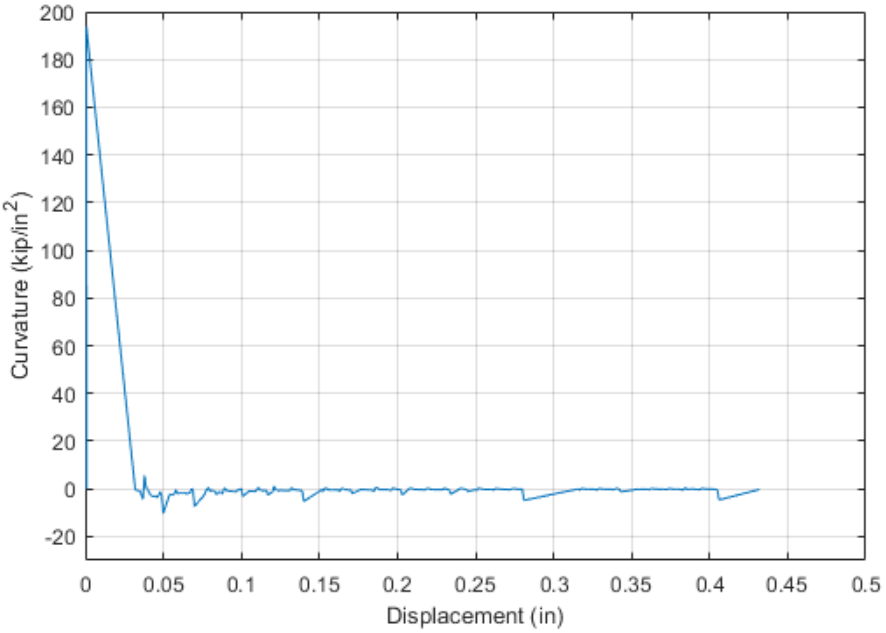

Figure A.90 Curvature (second derivative) versus displacement relationship of P80-AE-4

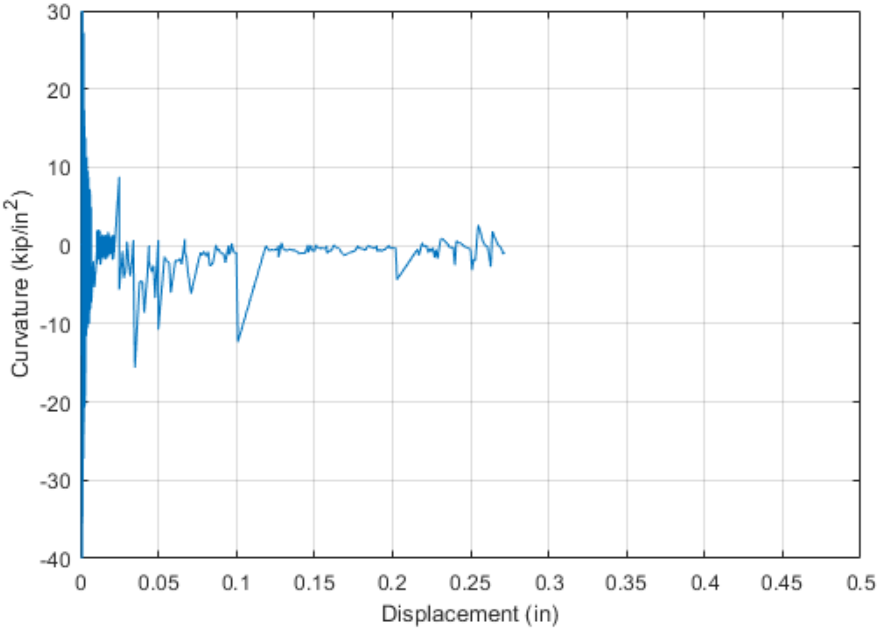

Figure A.91 Curvature (second derivative) versus displacement relationship of P80-AE-5

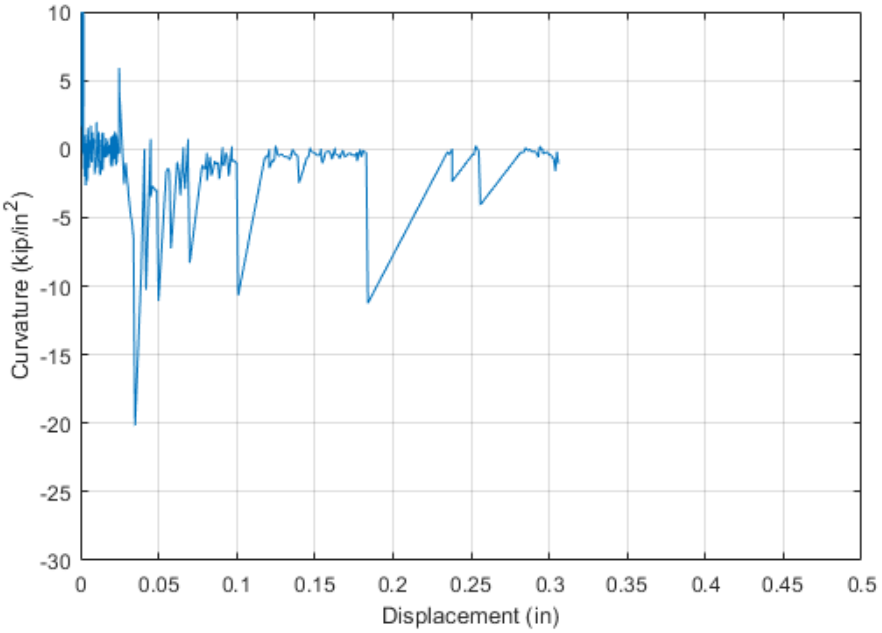

Figure A.92 Curvature (second derivative) versus displacement relationship of BL-BE-1

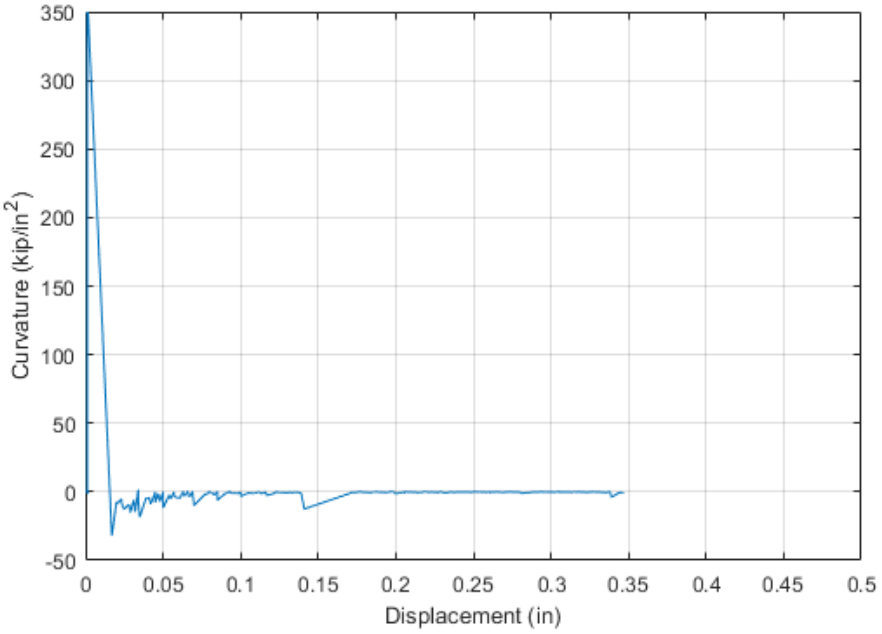

Figure A.93 Curvature (second derivative) versus displacement relationship of BL-BE-2

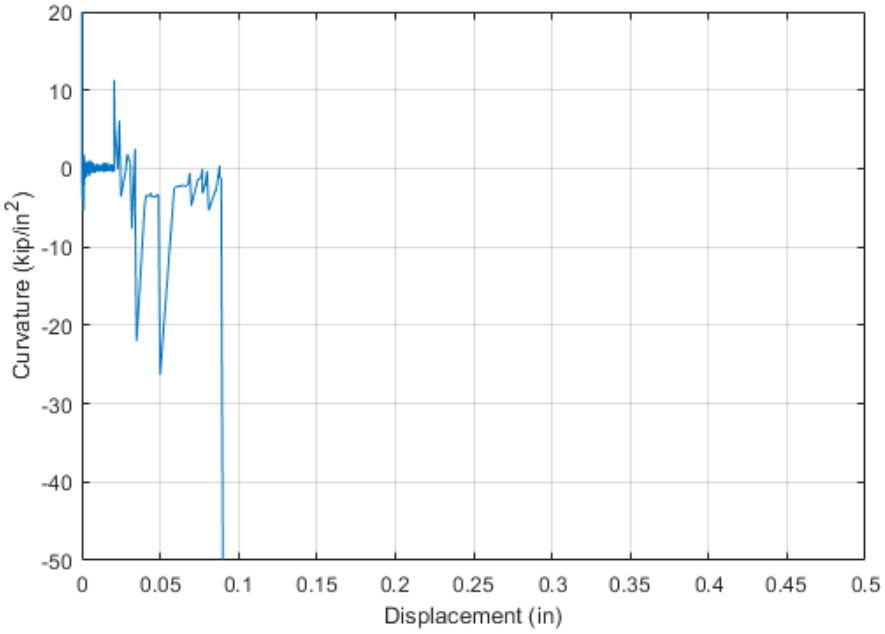

Figure A.94 Curvature (second derivative) versus displacement relationship of EE-AE-1

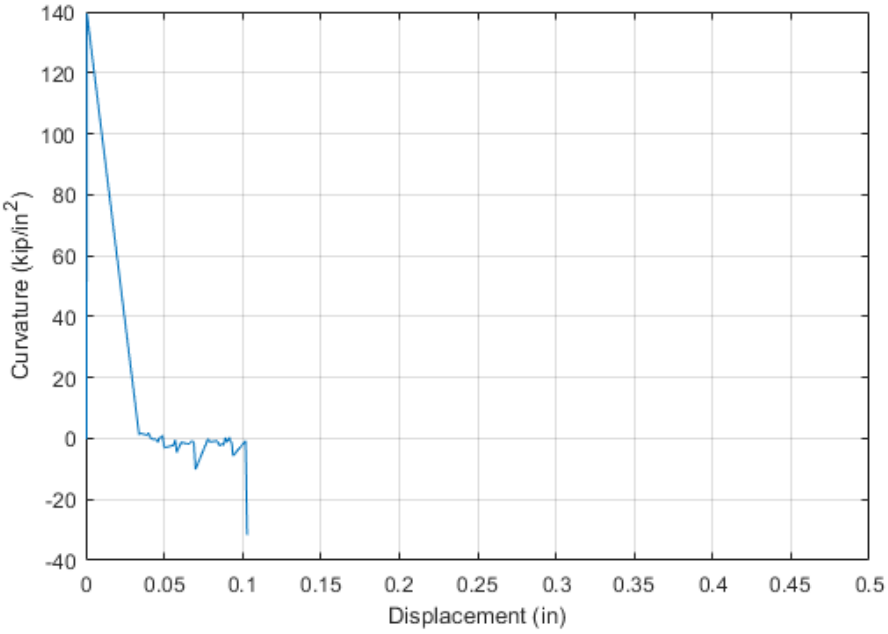

Figure A.95 Curvature (second derivative) versus displacement relationship of EE-AE-3

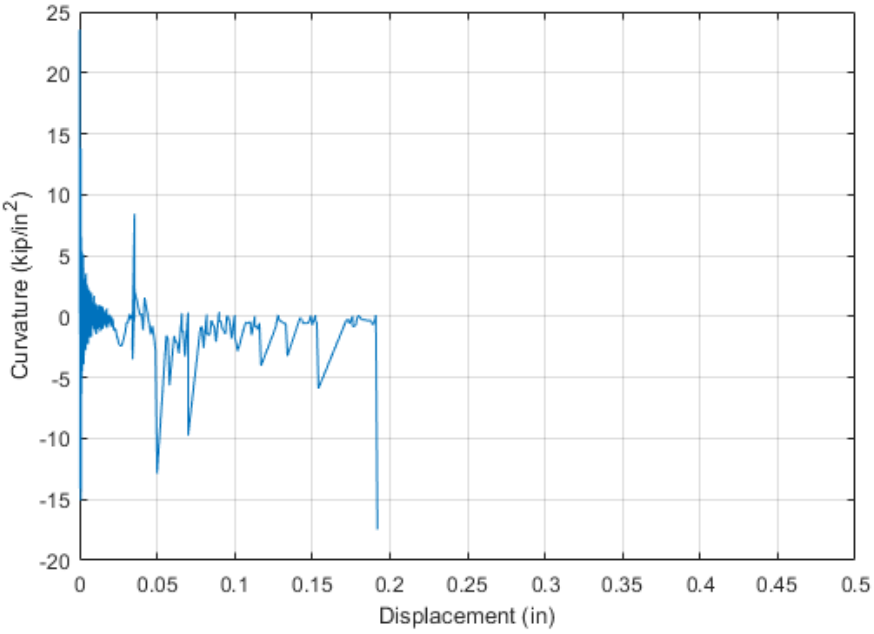

Figure A.96 Curvature (second derivative) versus displacement relationship of EE-AE-5

A.4 Summary of Key Parameters by Configuration

Table A.1 Summary of BL-AE specimens

Test Name	Stiffness (kip/in)	F_y (kip)	Δ_y (in)	F_{max} (kip)	Δ_{max} (in)	F_u (kip)	Δ_u (in)	μ (in/in)
BL-AE-1	255.81	7.93	0.031	11.8	0.247	11.21	0.281	9.06
BL-AE-2	232.94	7.92	0.034	12.09	0.282	9.88	0.318	9.35
BL-AE-3	229.43	8.03	0.035	12.17	0.31	11.38	0.45	12.86
BL-AE-4	217.03	8.03	0.037	12.12	0.356	8.13	0.472	12.76
BL-AE-5	222.22	8	0.036	12.05	0.297	9.61	0.35	9.72
BL-AE-6	201.75	8.07	0.04	12.12	0.363	9.65	0.507	12.68
Mean	209.47	7.96	0.038	12.05	0.319	9.85	0.375	9.87
Standard Deviation	18.05	0.06	0.03	0.13	0.044	1.09	0.09	1.87
Coefficient of Variation	0.079	0.0075	0.085	0.011	0.14	0.11	0.23	0.17

Table A.2 Summary of CP-AE specimens

Test Name	Stiffness (kip/in)	F_y (kip)	Δ_y (in)	F_{max} (kip)	Δ_{max} (in)	F_u (kip)	Δ_u (in)	μ (in/in)
CP-AE-1	173.7	7.99	0.046	12.03	0.352	8.14	0.44	10.09
CP-AE-2	179.11	8.06	0.045	12.17	0.346	10.29	0.456	10.13
CP-AE-3	145.54	8.15	0.056	12.19	0.346	9.81	0.385	6.88
CP-AE-4	261.61	8.11	0.031	12.19	0.315	9.82	0.425	13.71
CP-AE-5	180.45	7.94	0.044	11.96	0.273	9.59	0.307	6.98
Mean	154.81	8.05	0.052	12.04	0.344	9.53	0.403	7.75
Standard Deviation	43.29	0.086	0.0089	0.11	0.033	0.82	0.06	2.81
Coefficient of Variation	0.23	0.011	0.20	0.0088	0.1	0.086	0.15	0.29

Table A.3 Summary of P60-AE specimens

Test Name	Stiffness (kip/in)	F_y (kip)	Δ_y (in)	F_{max} (kip)	Δ_{max} (in)	F_u (kip)	Δ_u (in)	μ (in/in)
P60-AE-1	199.75	7.99	0.04	11.85	0.275	9.39	0.325	8.13
P60-AE-2	141.03	8.18	0.058	12.21	0.332	9.58	0.418	7.21
P60-AE-3	349.13	8.03	0.023	12.09	0.382	9.75	0.444	9.3
P60-AE-4	187.73	8.04	0.044	11.85	0.277	9.47	0.611	13.89
P60-AE-5	201.5	8.06	0.04	12.12	0.333	9.64	0.402	10.05
Mean	158.04	8.06	0.051	11.75	0.36	9.78	0.439	8.61
Standard Deviation	78.45	0.072	0.013	0.16	0.045	0.14	0.11	2.57
Coefficient of Variation	0.36	0.0089	0.30	0.014	0.14	0.015	0.24	0.26

Table A.4 Summary of P80-AE specimens

Test Name	Stiffness (kip/in)	F_y (kip)	Δ_y (in)	F_{max} (kip)	Δ_{max} (in)	F_u (kip)	Δ_u (in)	μ (in/in)
P80-AE-1	236.06	7.79	0.033	10.96	0.140	9.13	0.158	4.79
P80-AE-4	191.43	8.04	0.042	12.37	0.280	9.85	0.434	10.33
P80-AE-5	228.86	8.01	0.035	11.65	0.189	9.33	0.270	7.71
Mean	194.47	7.39	0.038	11.48	0.202	9.49	0.287	7.55
Standard Deviation	23.96	0.137	0.0047	0.71	0.071	0.37	0.14	2.77
Coefficient of Variation	0.11	0.017	0.13	0.061	0.35	0.039	0.48	0.36

Table A.5 Summary of BL-BE specimens

Test Name	Stiffness (kip/in)	F_y (kip)	Δ_y (in)	F_{max} (kip)	Δ_{max} (in)	F_u (kip)	Δ_u (in)	μ (in/in)
BL-BE-1	230.3	7.60	0.033	11.53	0.288	10.03	0.307	9.3
BL-BE-2	288.93	8.09	0.028	12.09	0.256	9.51	0.349	12.46
Mean	235.29	8.00	0.034	11.79	0.279	10.01	0.327	9.62
Standard Deviation	41.46	0.35	0.035	0.4	0.023	0.37	0.03	2.23
Coefficient of Variation	0.16	0.044	0.12	0.034	0.083	0.038	0.091	0.21

Table A.6 Summary of EE-AE specimens

Test Name	Stiffness (kip/in)	F_y (kip)	Δ_y (in)	F_{max} (kip)	Δ_{max} (in)	F_u (kip)	Δ_u (in)	μ (in/in)
EE-AE-1	232.29	8.13	0.035	9.07	0.089	6	0.118	3.37
EE-AE-3	140	8.12	0.058	9.44	0.103	7.08	0.118	2.03
EE-AE-5	165.21	7.93	0.048	11.26	0.187	8.37	0.204	2.25
Mean	143.04	8.01	0.056	9.91	0.126	7.15	0.147	2.63
Standard Deviation	47.7	0.11	0.012	1.17	0.053	1.19	0.05	0.72
Coefficient of Variation	0.27	0.014	0.25	0.12	0.42	0.17	0.34	0.28

A.5 Summary Plots by Configuration

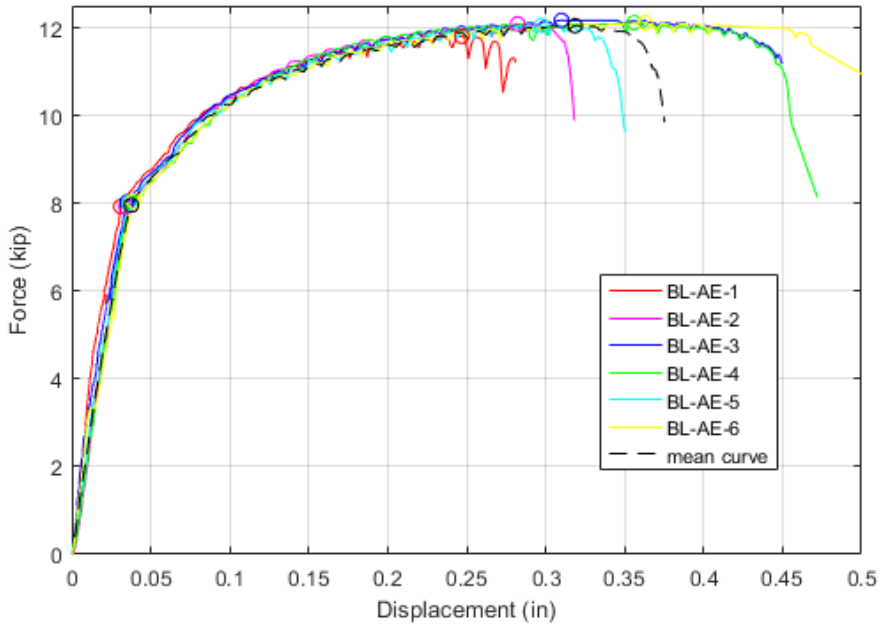

Figure A.97 BL-AE group comparison: individual test specimens against the mean response

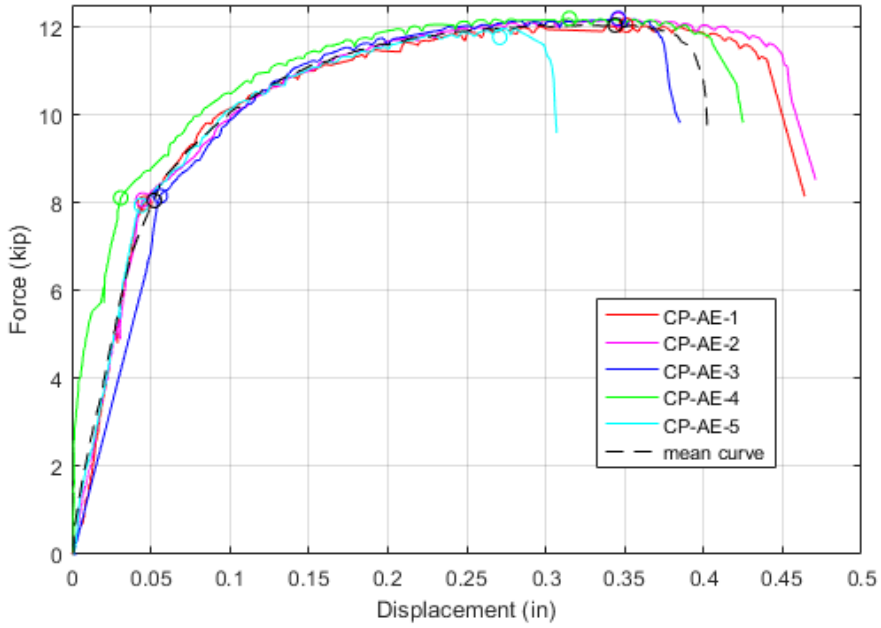

Figure A.98 CP-AE group comparison: individual test specimens against the mean response

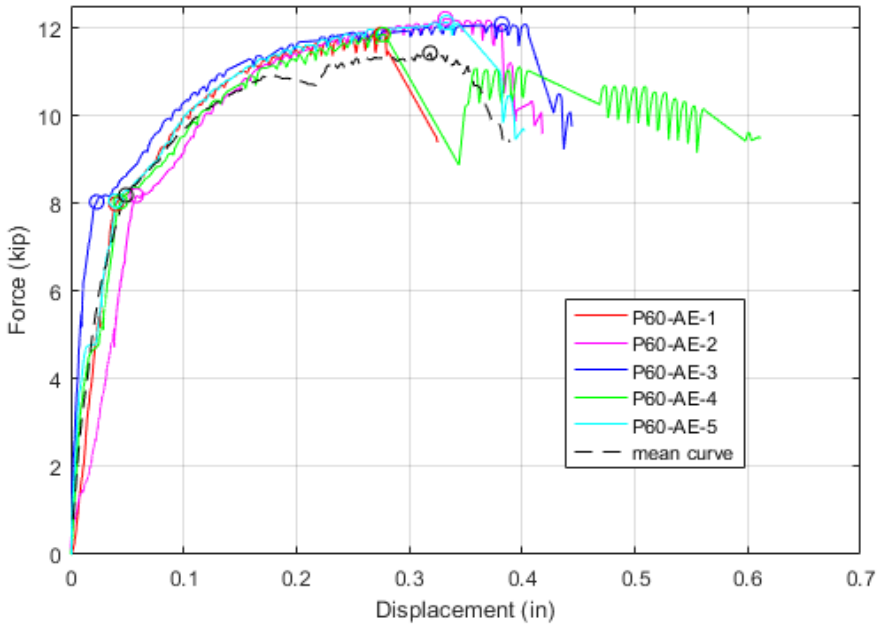

Figure A.99 P60-AE group comparison: individual test specimens against the mean response
Note: the maximum x-value is increased to account for P60-AE-3.

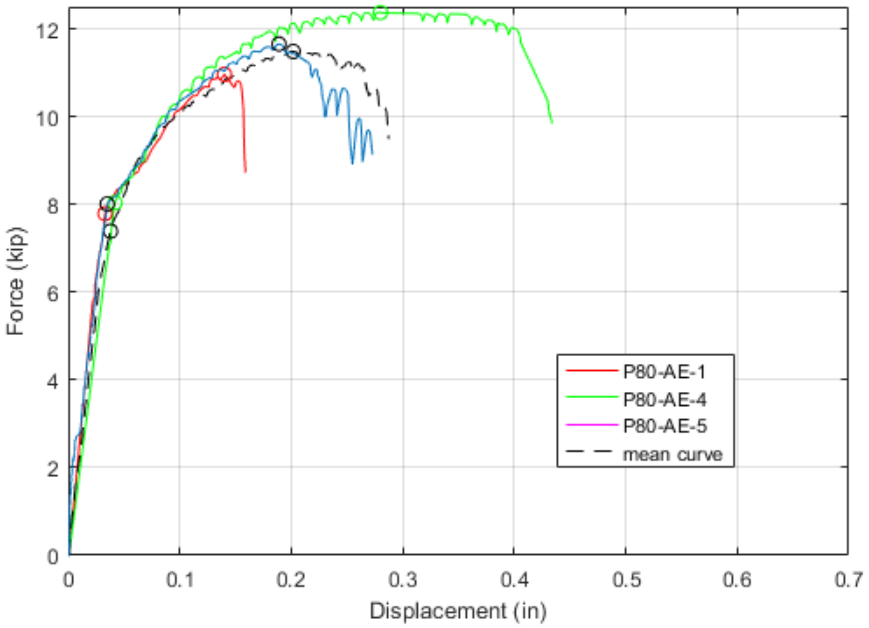

Figure A.100 P80-AE group comparison: individual test specimens against the mean response

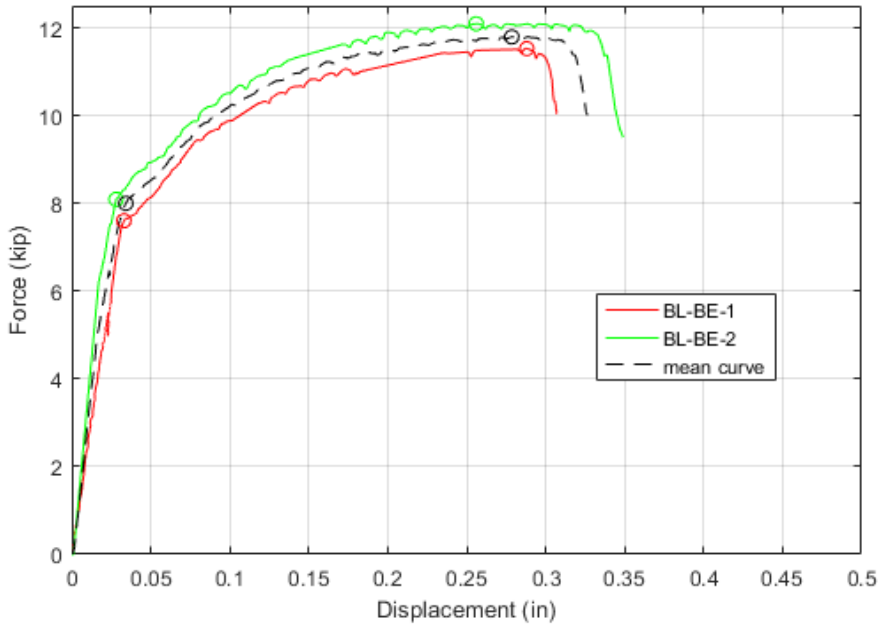

Figure A.101 BL-BE group comparison: individual test specimens against the mean response

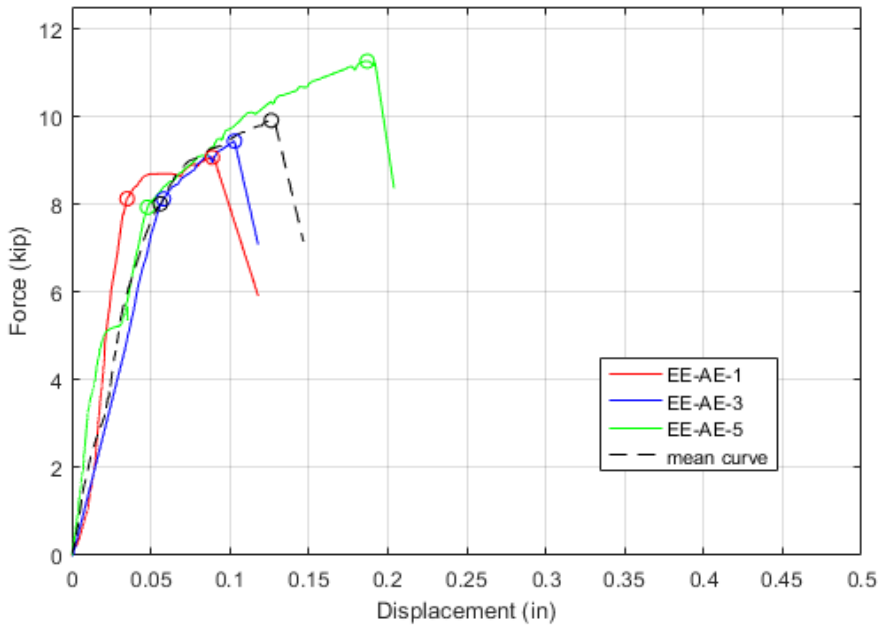

Figure A.102 EE-AE group comparison: individual test specimens against the mean response

Appendix B – Phase Two Specimen Photos

B.1 Configuration BL-AE

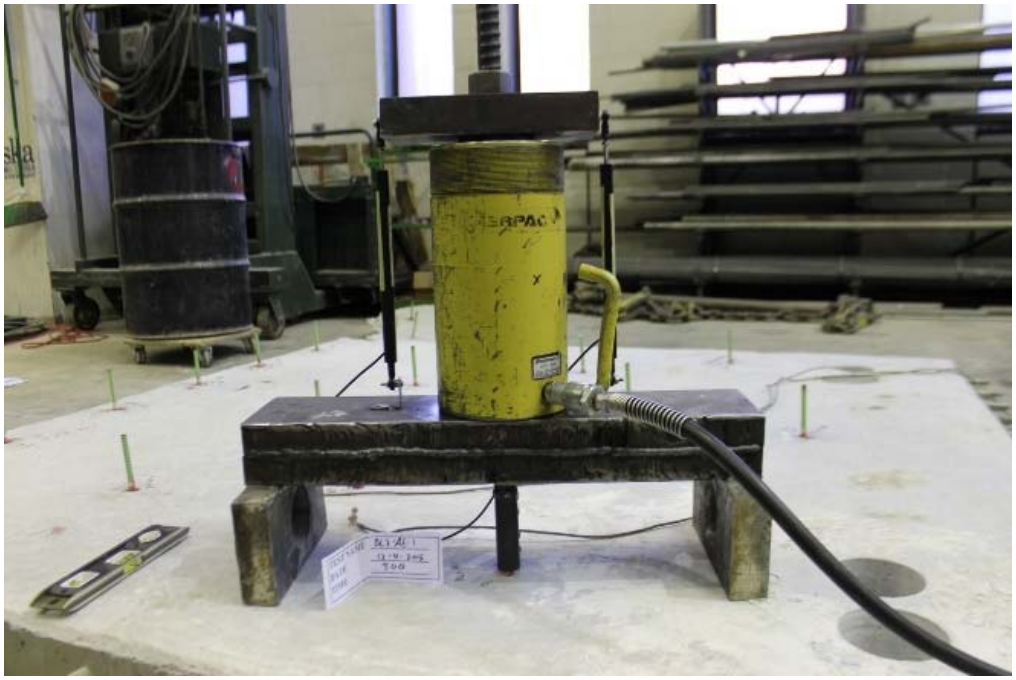

Figure B.1 Complete assembly and specimen prior to testing for BL-AE-1

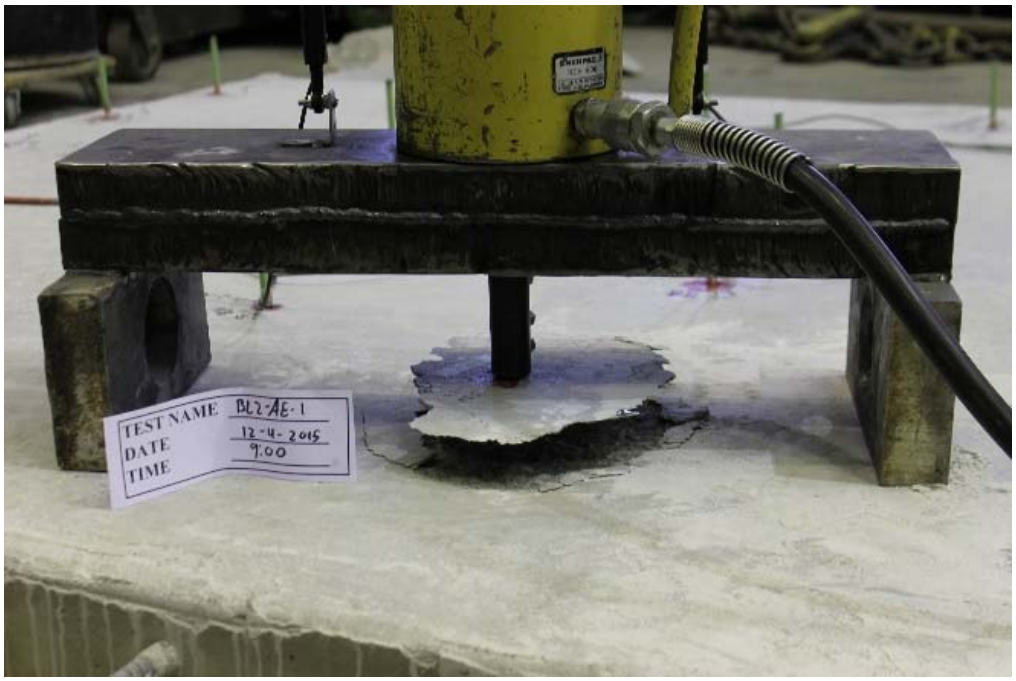

Figure B.2 Detailed view of the reinforcement at failure for BL-AE-1

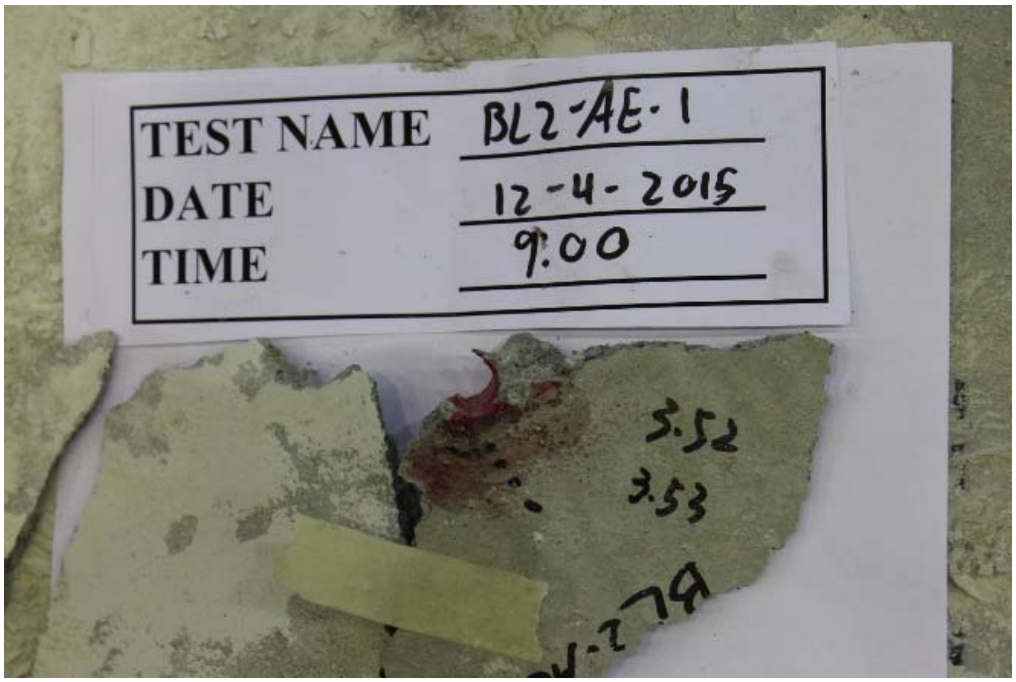

Figure B.3 Specimen details after testing for BL-AE-1

Figure B.4 Complete assembly and specimen prior to testing for BL-AE-2

Figure B.5 Detailed view of the reinforcement at failure for BL-AE-2

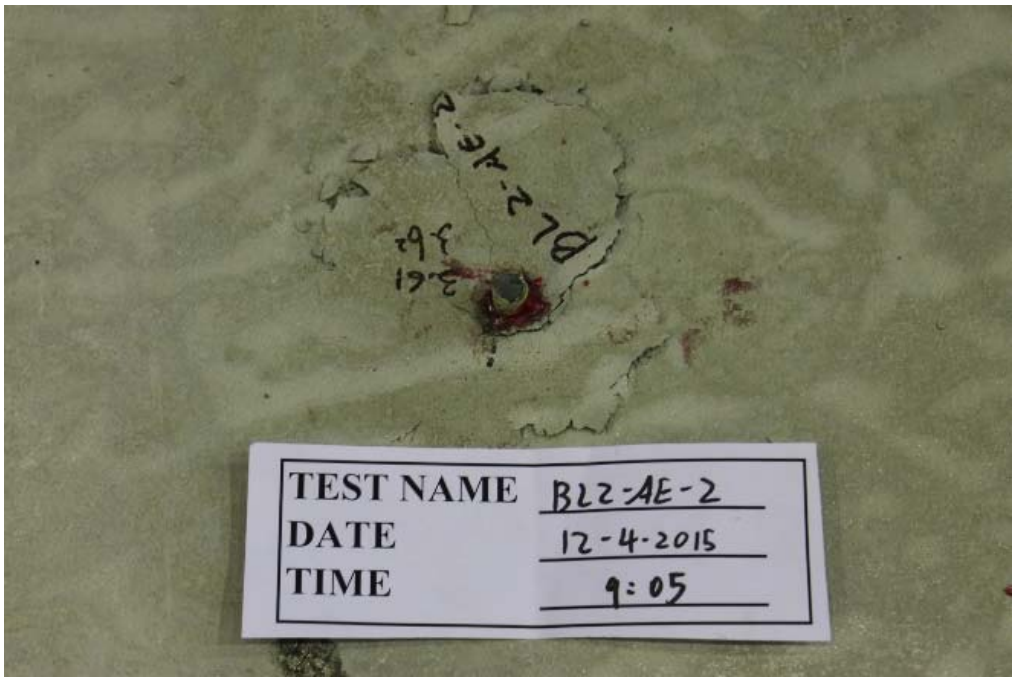

Figure B.6 Specimen details after testing for BL-AE-2

Figure B.7 Complete assembly and specimen prior to testing for BL-AE-3

Figure B.8 Detailed view of the reinforcement at failure for BL-AE-3

Figure B.9 Specimen details after testing for BL-AE-3

Figure B.10 Complete assembly and specimen prior to testing for BL-AE-4

Figure B.11 Detailed view of the reinforcement at failure for BL-AE-4

Figure B.12 Specimen details after testing for BL-AE-4

Figure B.13 Complete assembly and specimen prior to testing for BL-AE-5

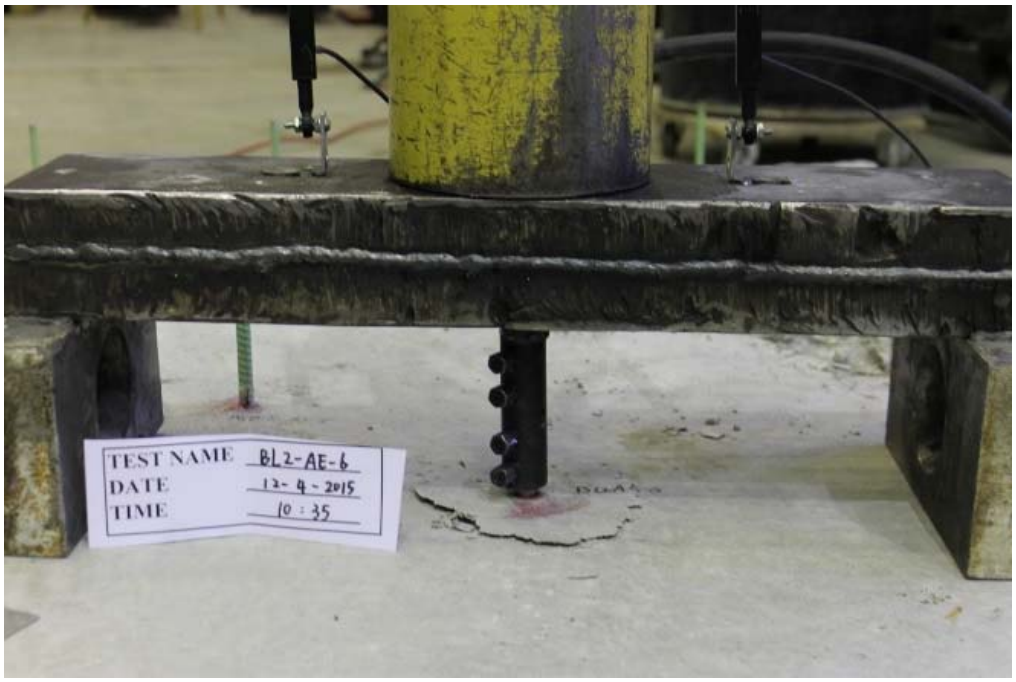

Figure B.14 Detailed view of the reinforcement at failure for BL-AE-5

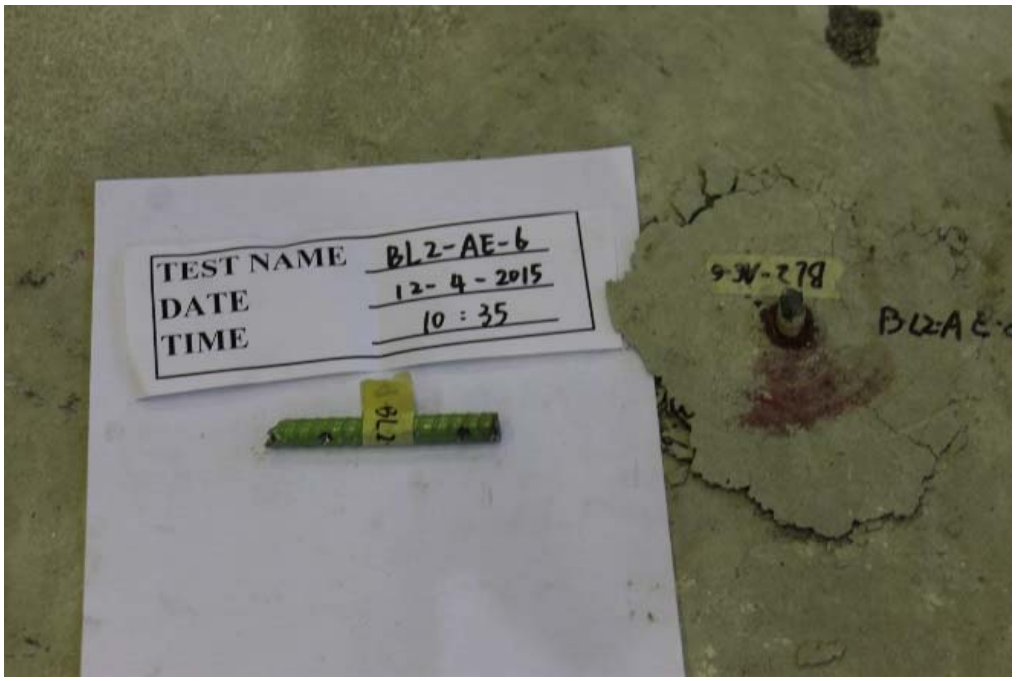

Figure B.15 Specimen details after testing for BL-AE-5

Figure B.16 Complete assembly and specimen prior to testing for BL-AE-6

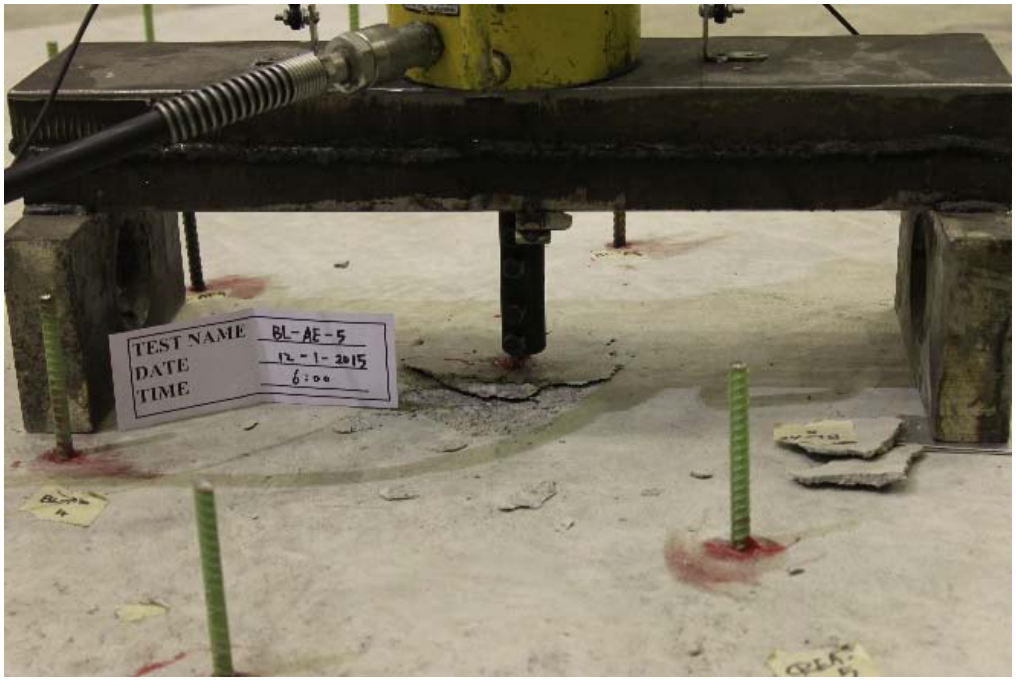

Figure B.17 Detailed view of the reinforcement at failure for BL-AE-6

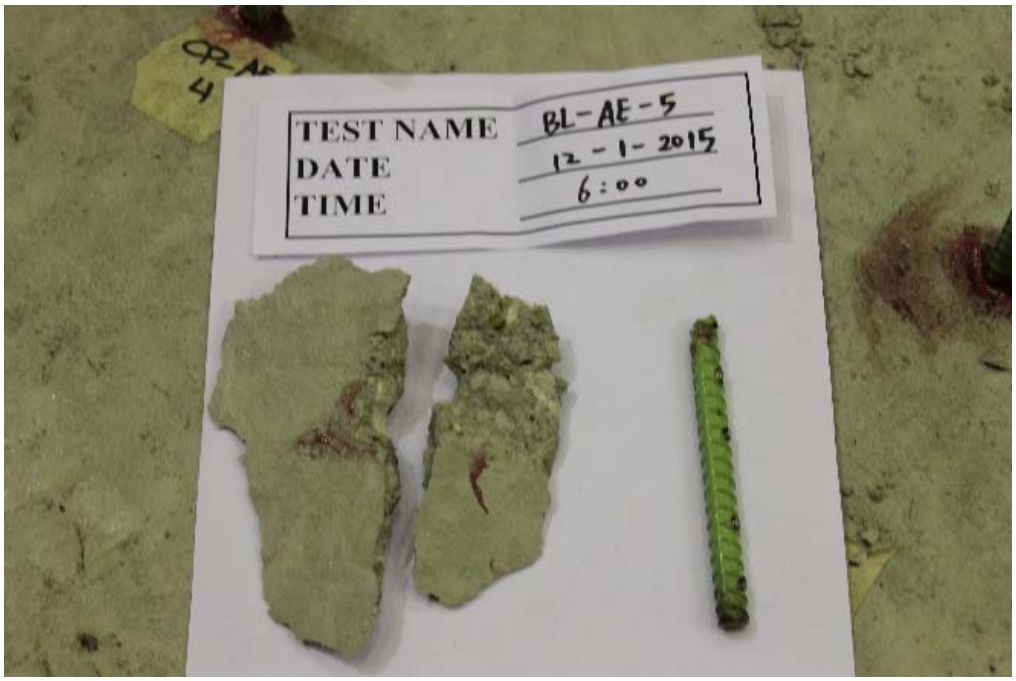

Figure B.18 Specimen details after testing for BL-AE-6

B.2 Configuration CP-AE

Figure B.19 Complete assembly and specimen prior to testing for CP-AE-1

Figure B.20 Detailed view of the reinforcement at failure for CP-AE-1

Figure B.21 Specimen details after testing for CP-AE-1

Figure B.22 Complete assembly and specimen prior to testing for CP-AE-2

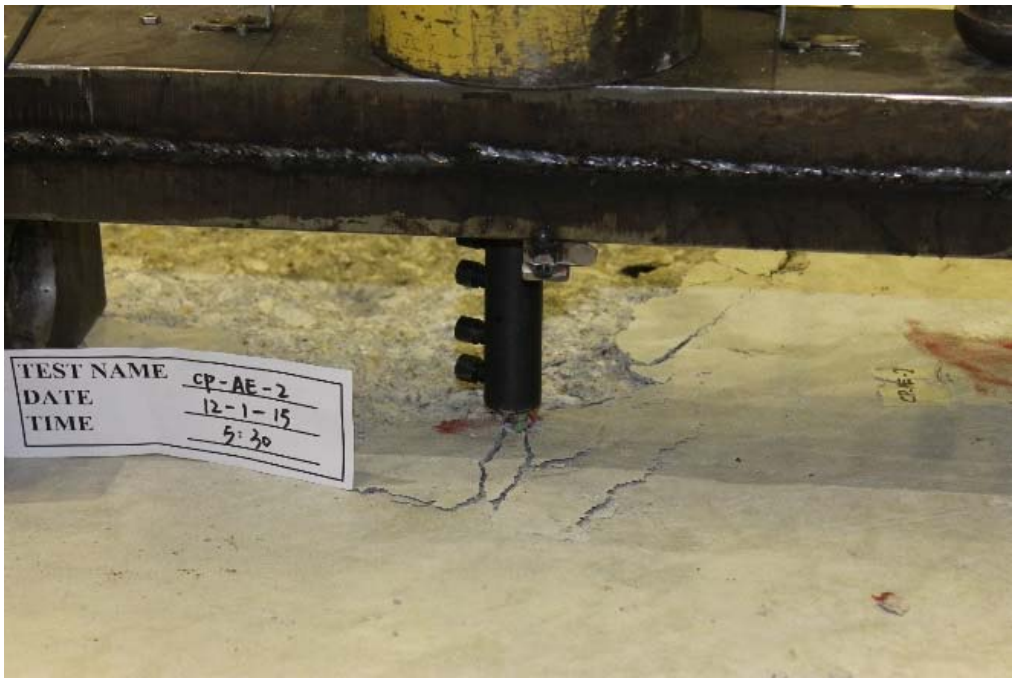

Figure B.23 Detailed view of the reinforcement at failure for CP-AE-2

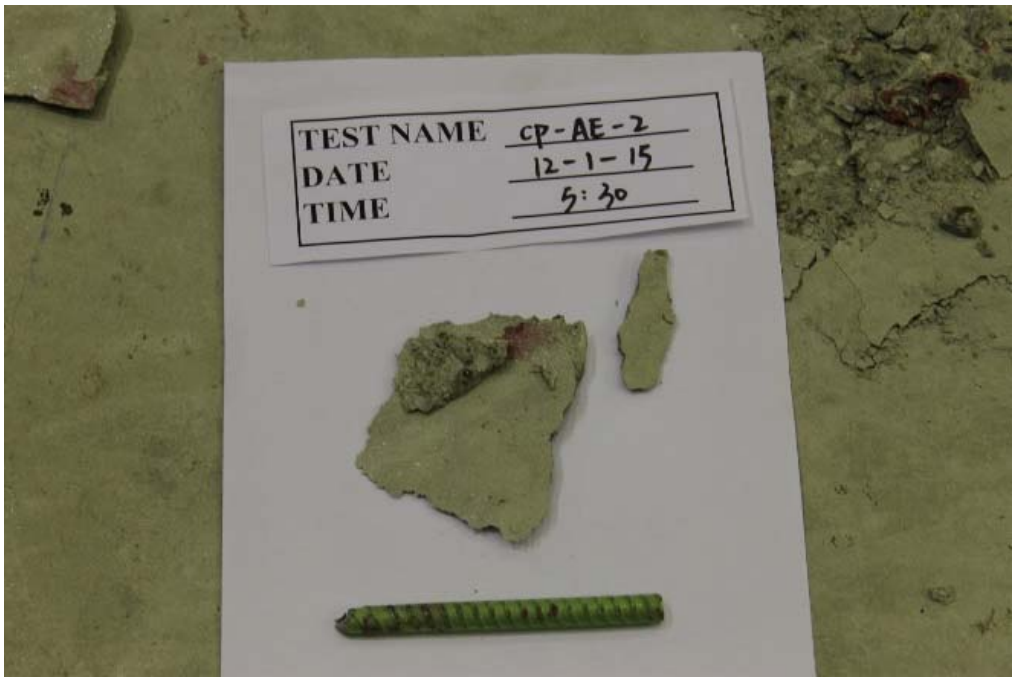

Figure B.24 Specimen details after testing for CP-AE-2

Figure B.25 Complete assembly and specimen prior to testing for CP-AE-3

Figure B.26 Detailed view of the reinforcement at failure for CP-AE-3

Figure B.27 Specimen details after testing for CP-AE-3

Figure B.28 Complete assembly and specimen prior to testing for CP-AE-4

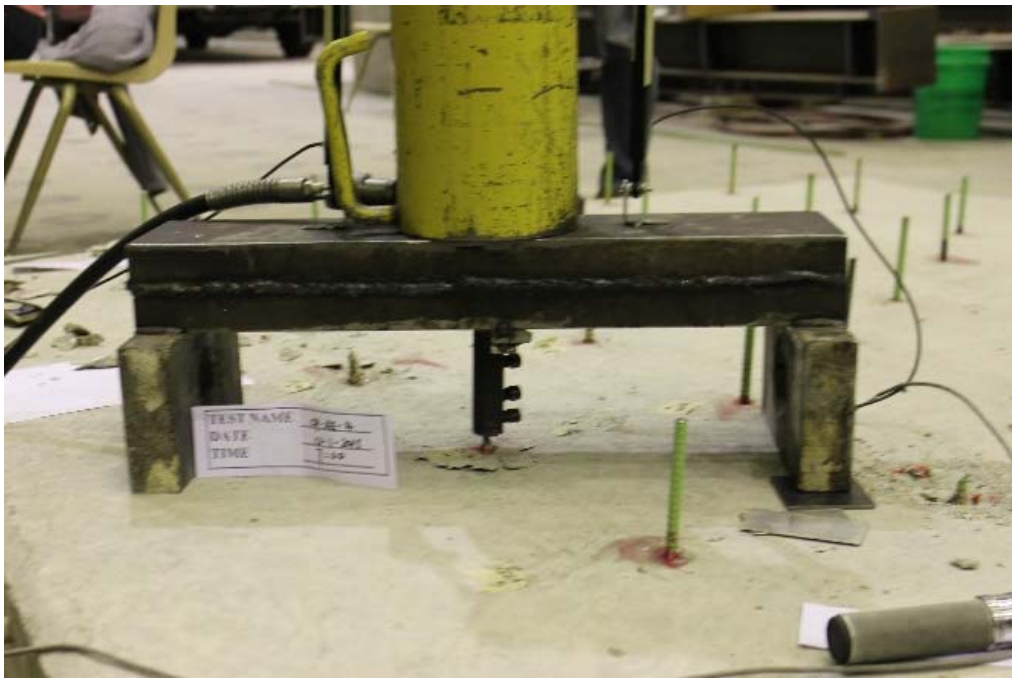

Figure B.29 Detailed view of the reinforcement at failure for CP-AE-4

Figure B.30 Specimen details after testing for CP-AE-4

Figure B.31 Complete assembly and specimen prior to testing for CP-AE-5

Figure B.32 Detailed view of the reinforcement at failure for CP-AE-5

B.3 Configuration P60-AE

Figure B.33 Complete assembly and specimen prior to testing for P60-AE-1

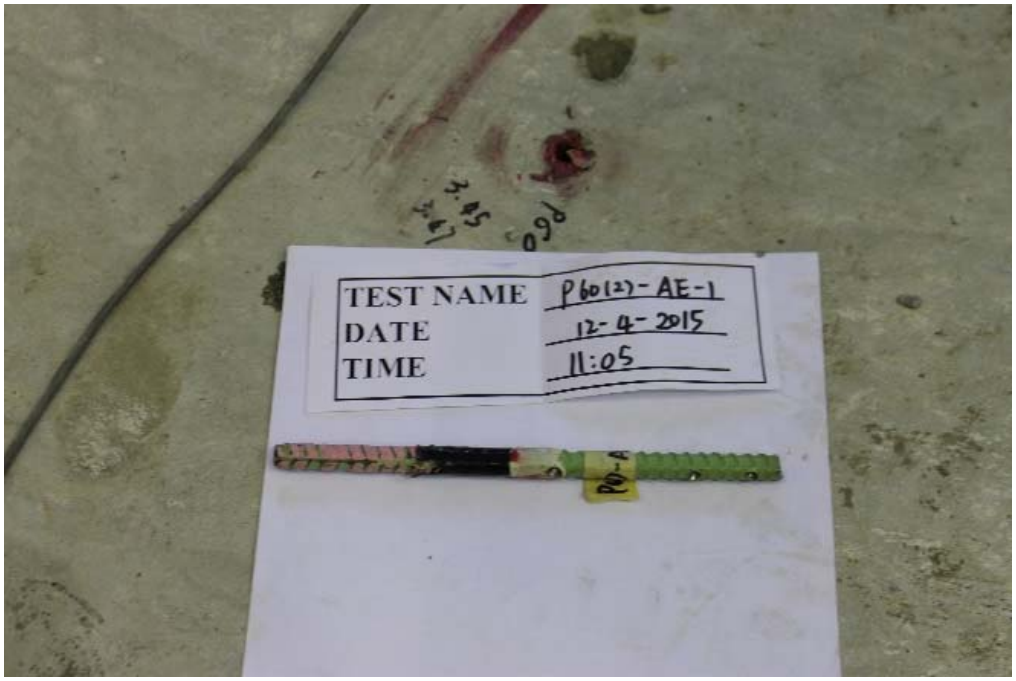

Figure B.34 Specimen details after testing for P60-AE-1

Figure B.35 Complete assembly and specimen prior to testing for P60-AE-2

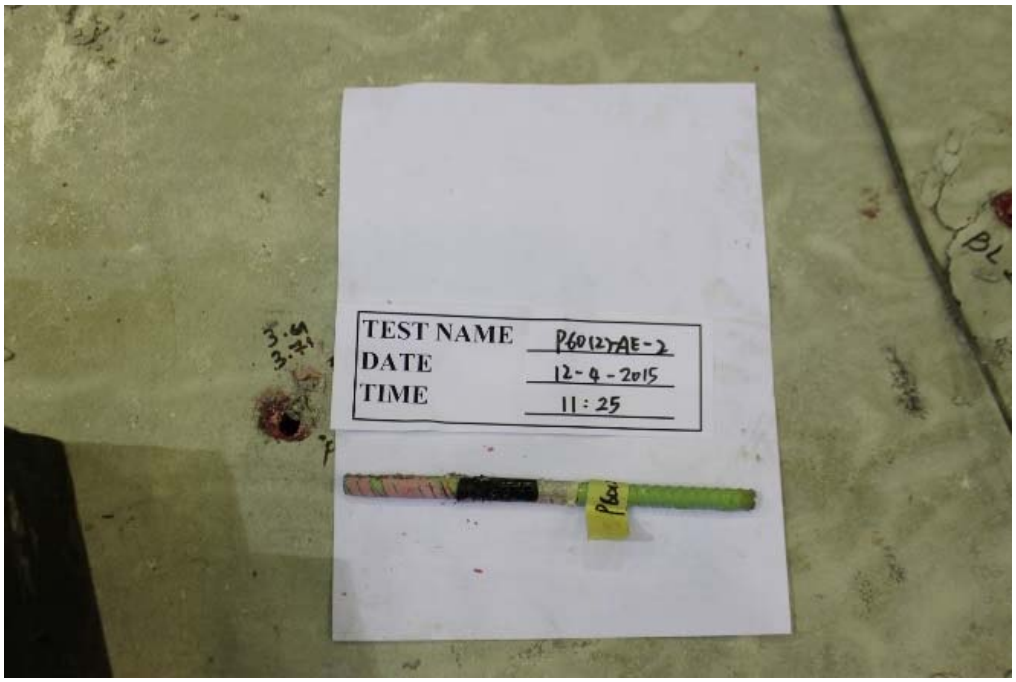

Figure B.36 Specimen details after testing for P60-AE-2

Figure B.37 Complete assembly and specimen prior to testing for P60-AE-3

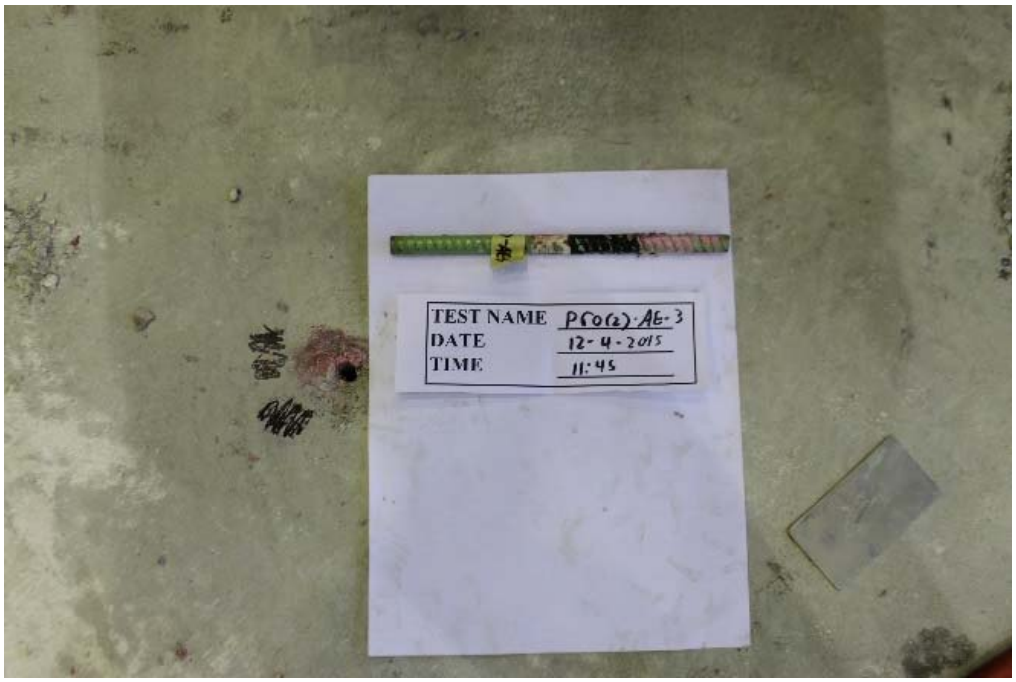

Figure B.38 Specimen details after testing for P60-AE-3

Figure B.39 Complete assembly and specimen prior to testing for P60-AE-4

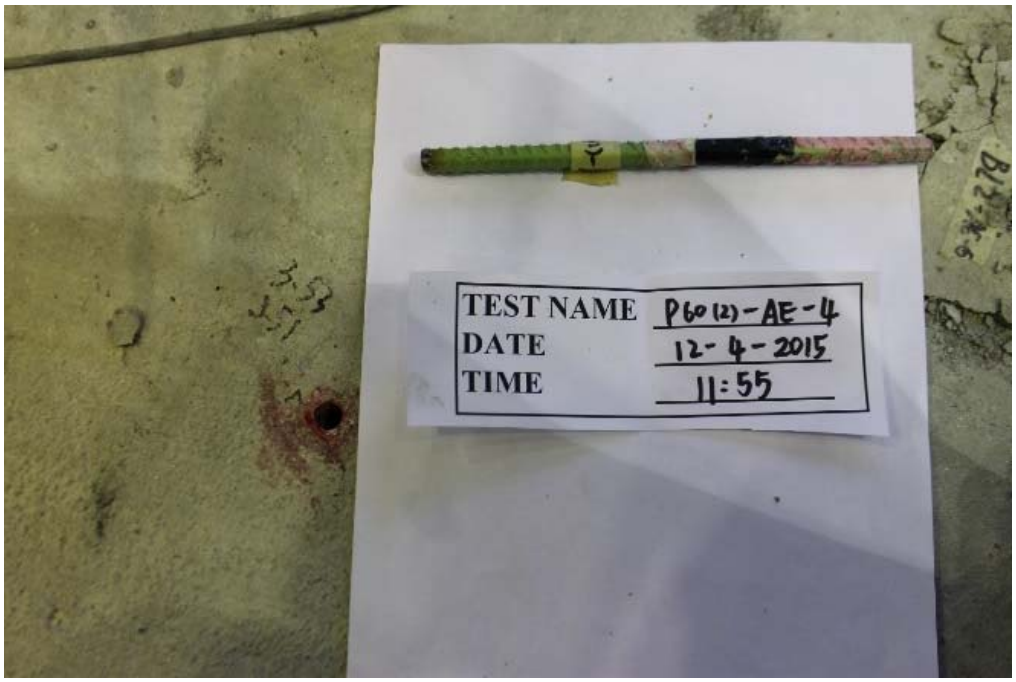

Figure B.40 Specimen details after testing for P60-AE-4

Figure B.41 Complete assembly and specimen prior to testing for P60-AE-5

Figure B.42 Detailed view of the reinforcement at failure for P60-AE-5

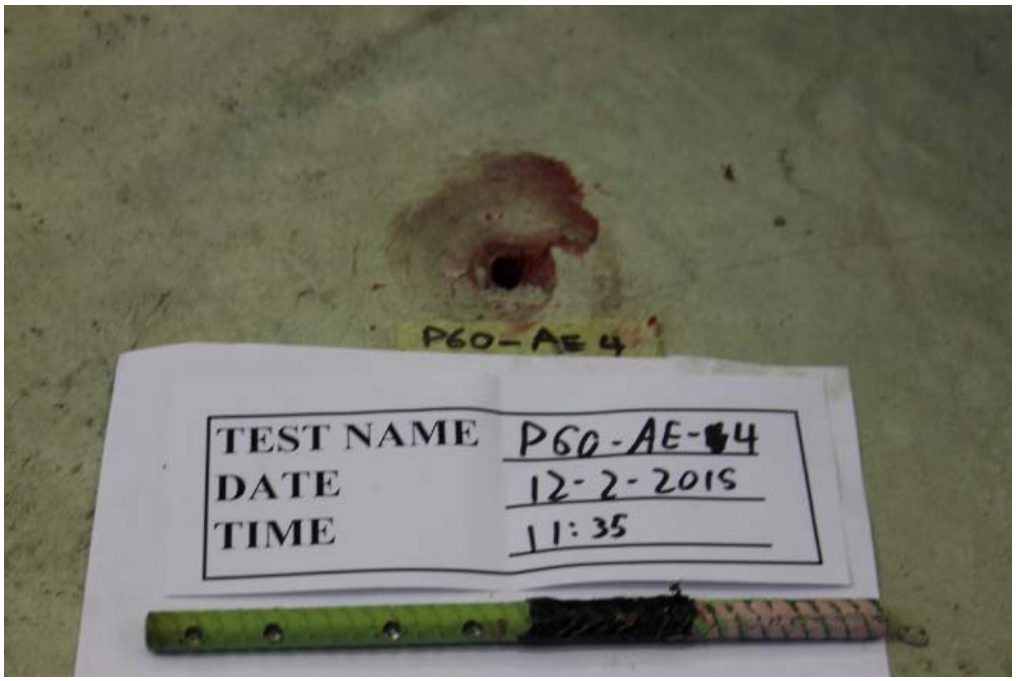

Figure B.43 Specimen details after testing for P60-AE-5

B.4 Configuration P80-AE

Figure B.44 Complete assembly and specimen prior to testing for P80-AE-4

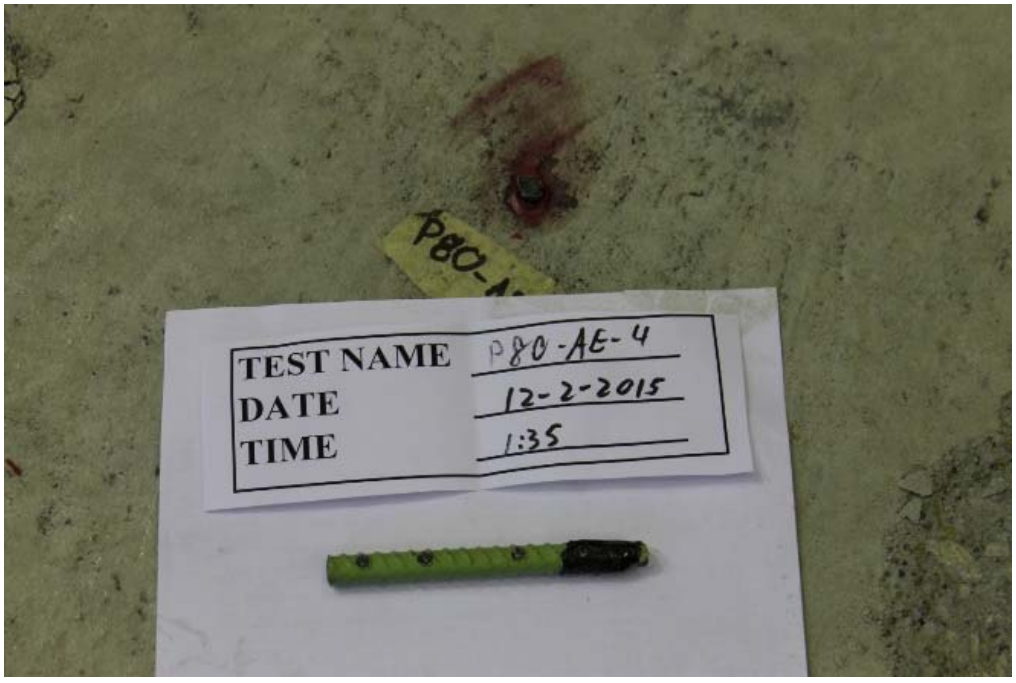

Figure B.45 Specimen details after testing for P80-AE-4

Figure B.46 Complete assembly and specimen prior to testing for P80-AE-5

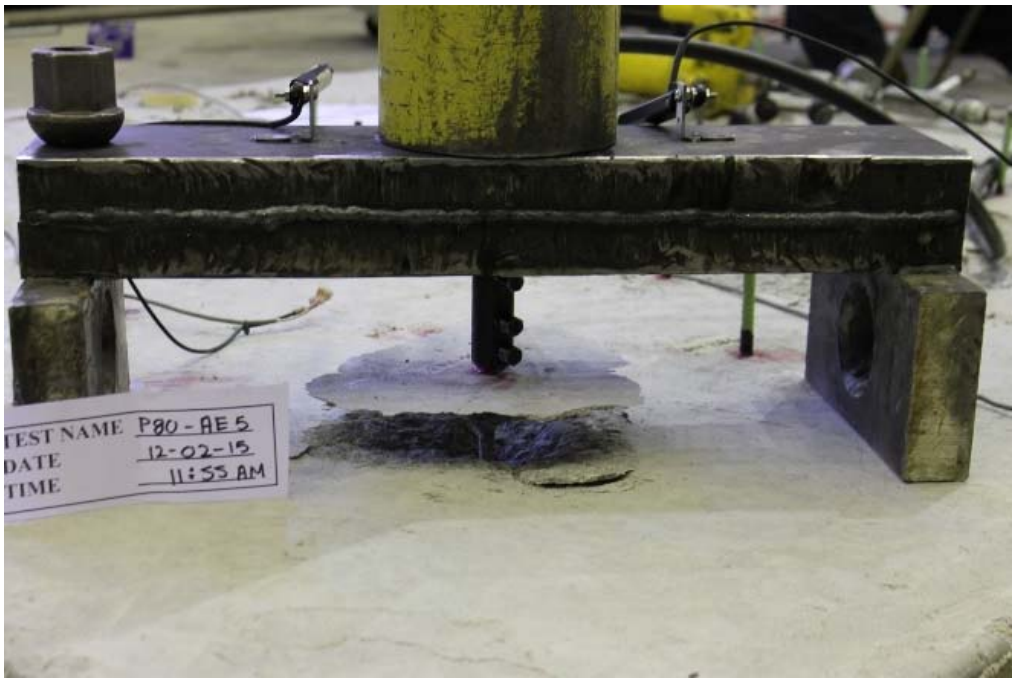

Figure B.47 Detailed view of the reinforcement at failure for P80-AE-5

Figure B.48 Specimen details after testing for P80-AE-5

B.5 Configuration BL-BE

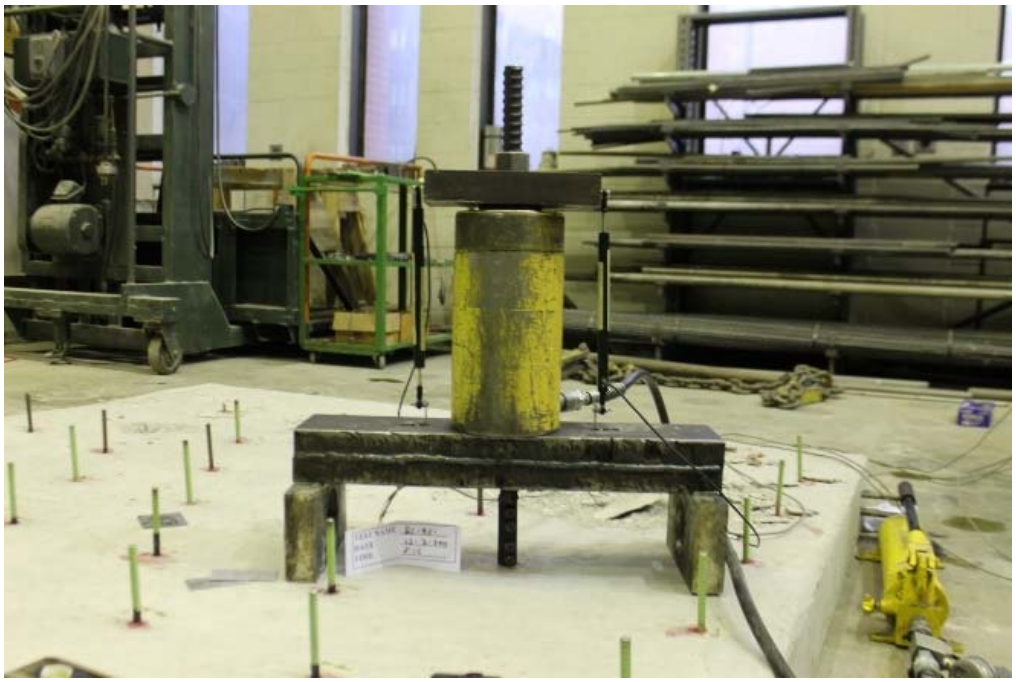

Figure B.49 Complete assembly and specimen prior to testing for BL-BE-1

Figure B.50 Detailed view of the reinforcement at failure for BL-BE-1

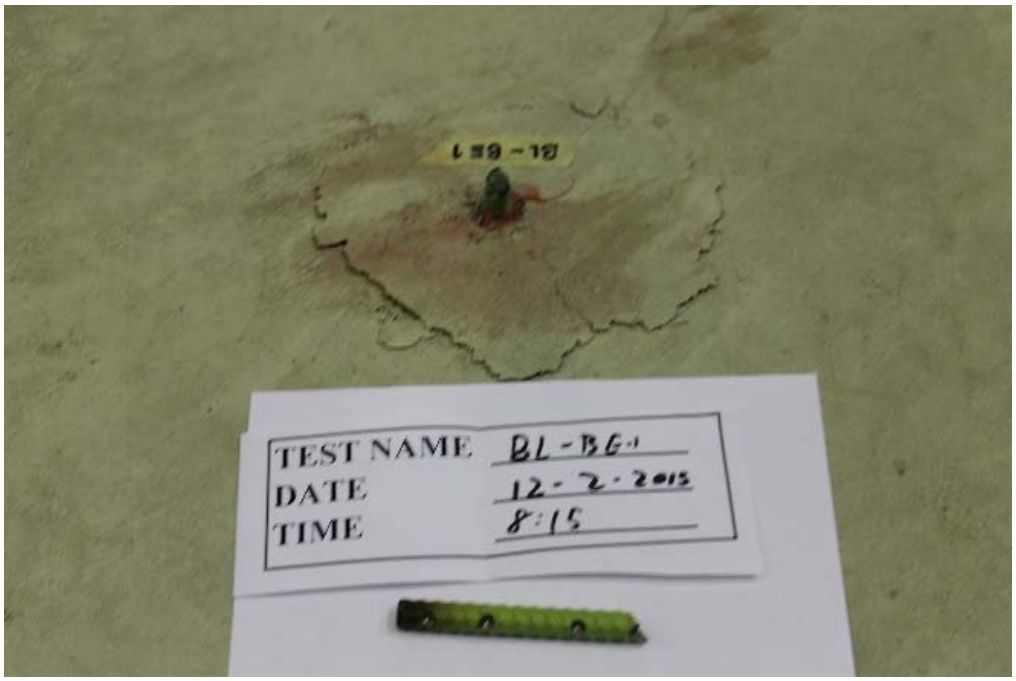

Figure B.51 Specimen details after testing for BL-BE-1

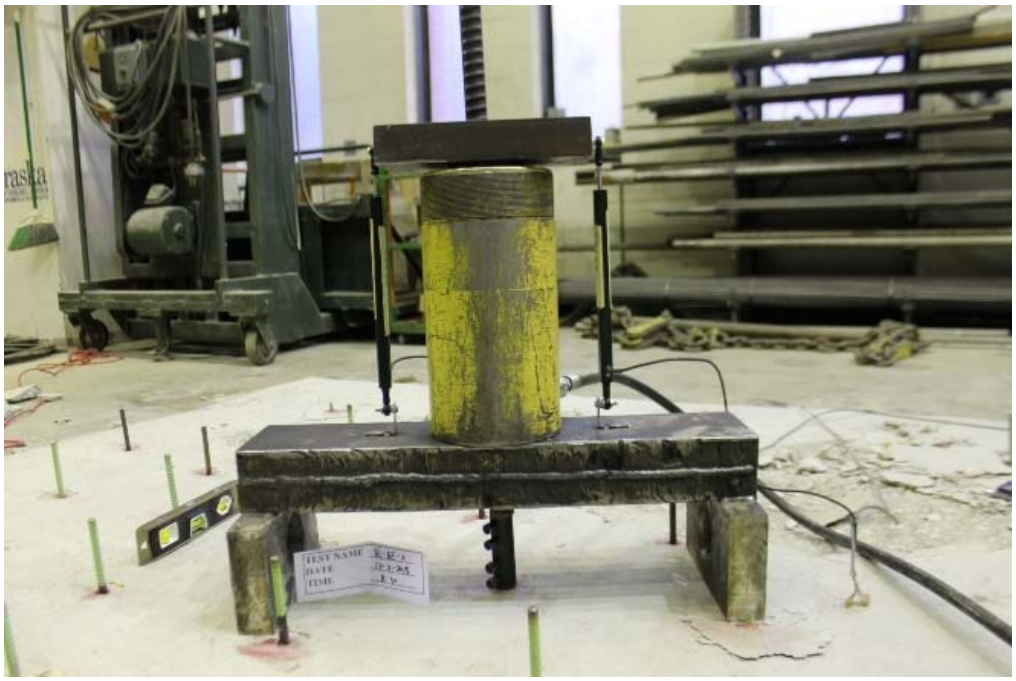

Figure B.52 Complete assembly and specimen prior to testing for BL-BE-2

Figure B.53 Detailed view of the reinforcement at failure for BL-BE-2

Figure B.54 Specimen details after testing for BL-BE-2

B.6 Configuration EE-AE

Figure B.55 Complete assembly and specimen prior to testing for EE-AE-1

Figure B.56 Detailed view of the reinforcement at failure for EE-AE-1

Figure B.57 Specimen details after testing for EE-AE-1

Figure B.58 Complete assembly and specimen prior to testing for EE-AE-3

Figure B.59 Detailed view of the reinforcement at failure for EE-AE-3

Figure B.60 Specimen details after testing for EE-AE-3

Figure B.61 Complete assembly and specimen prior to testing for EE-AE-5

Figure B.62 Detailed view of the reinforcement at failure for EE-AE-5

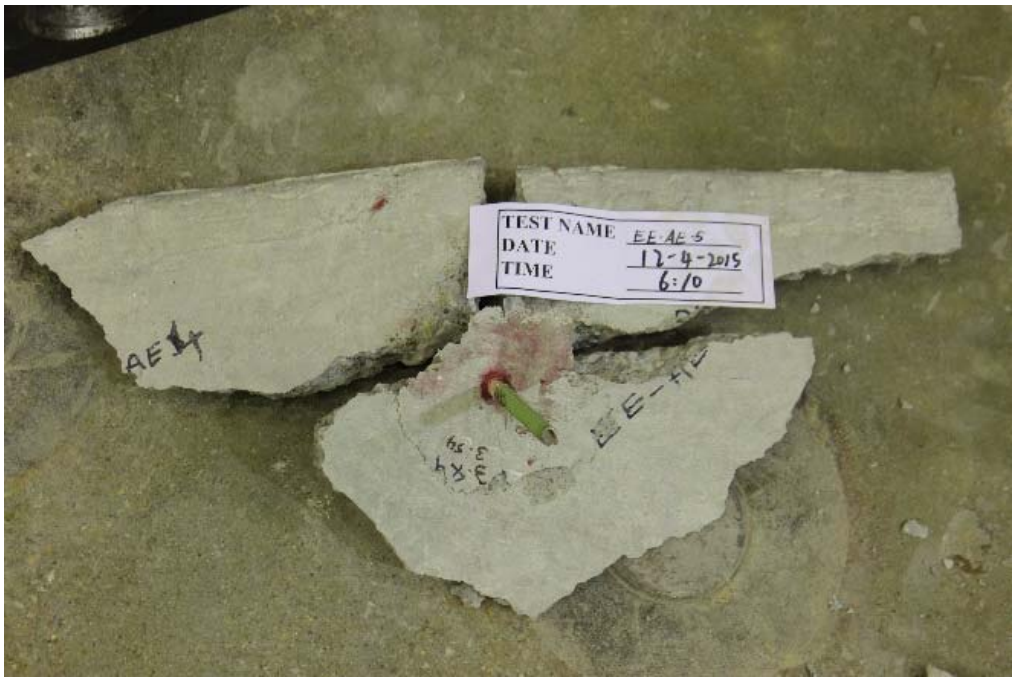

Figure B.63 Specimen details after testing for EE-AE-5

Appendix C – Summary of Phase One[1]

[1] Note phase one was conducted in concrete specimens with a mean compressive strength of 5.8 ksi. This value is outside of the anticipated range for retrofitted bridge rail.

C.1 Raw and Filtered Data

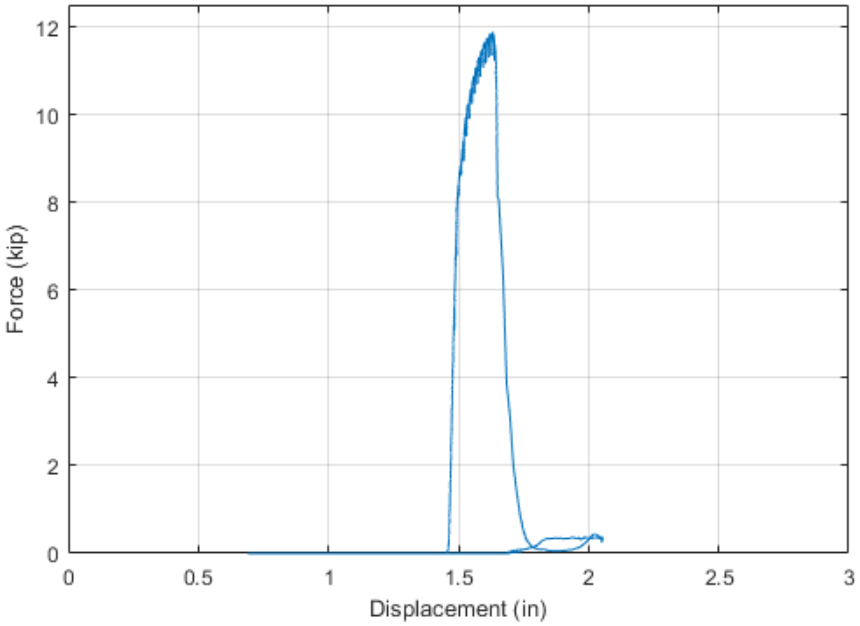

Figure C.1 Unfiltered force versus displacement relationship of BL-AE-1

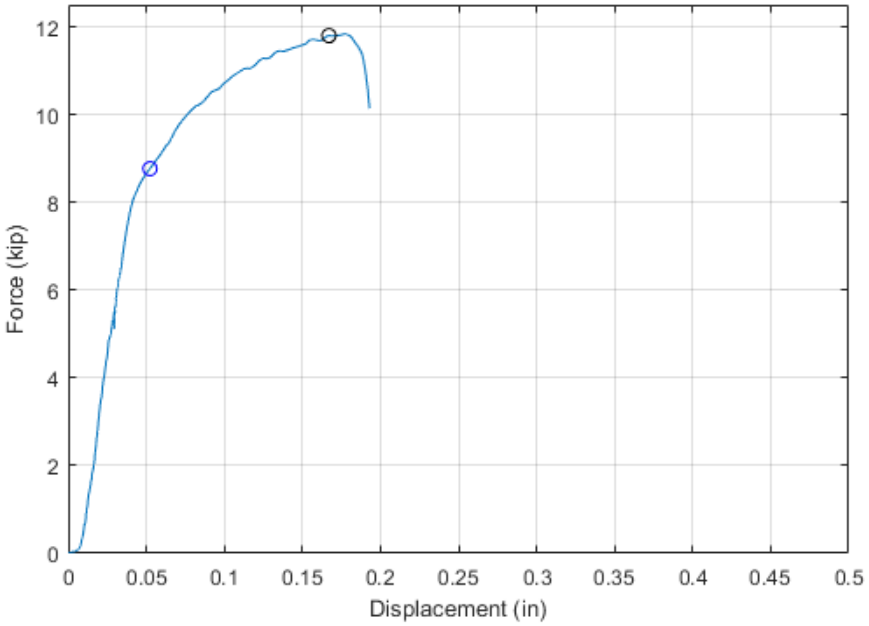

Figure C.2 Force versus displacement relationship of BL-AE-1

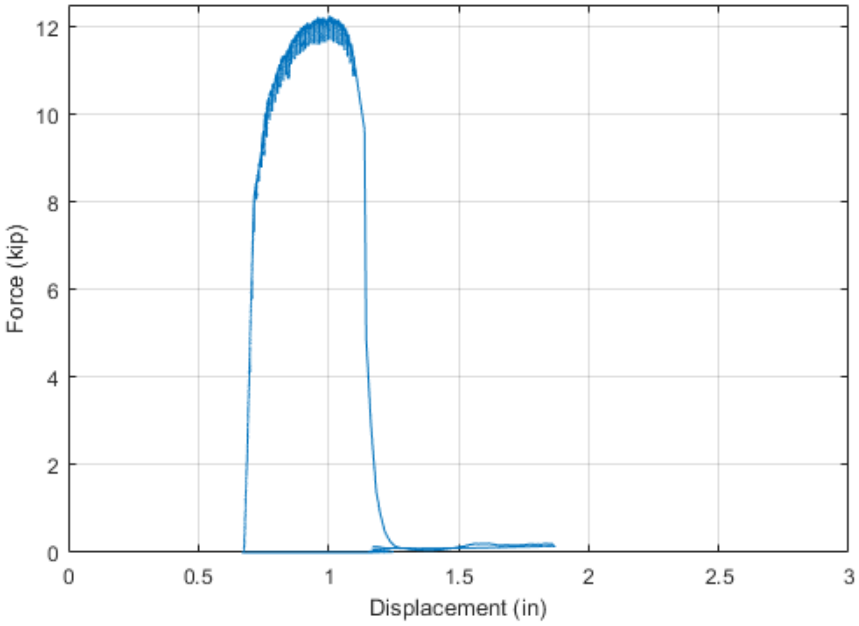

Figure C.3 Unfiltered force versus displacement relationship of BL-AE-2

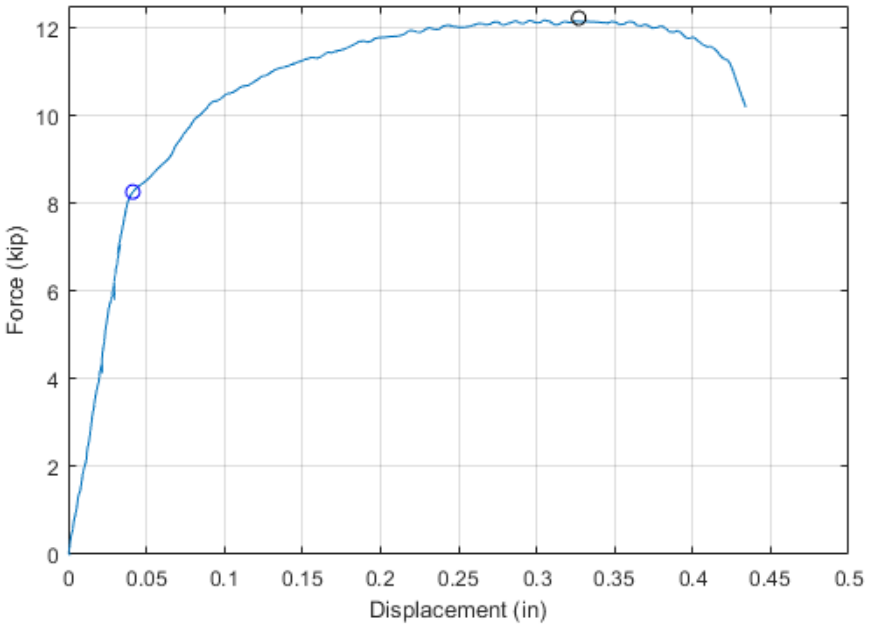

Figure C.4 Force versus displacement relationship of BL-AE-2

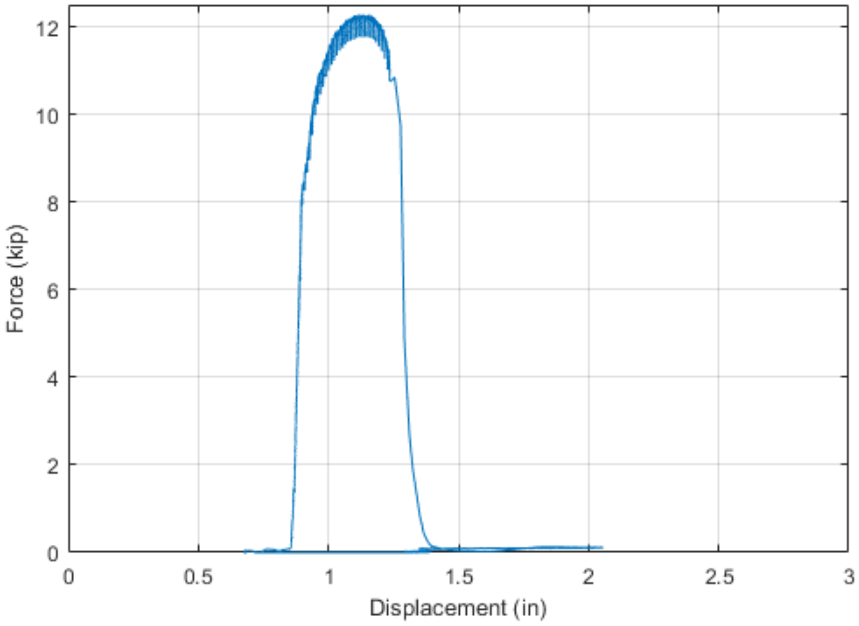

Figure C.5 Unfiltered force versus displacement relationship of BL-AE-3

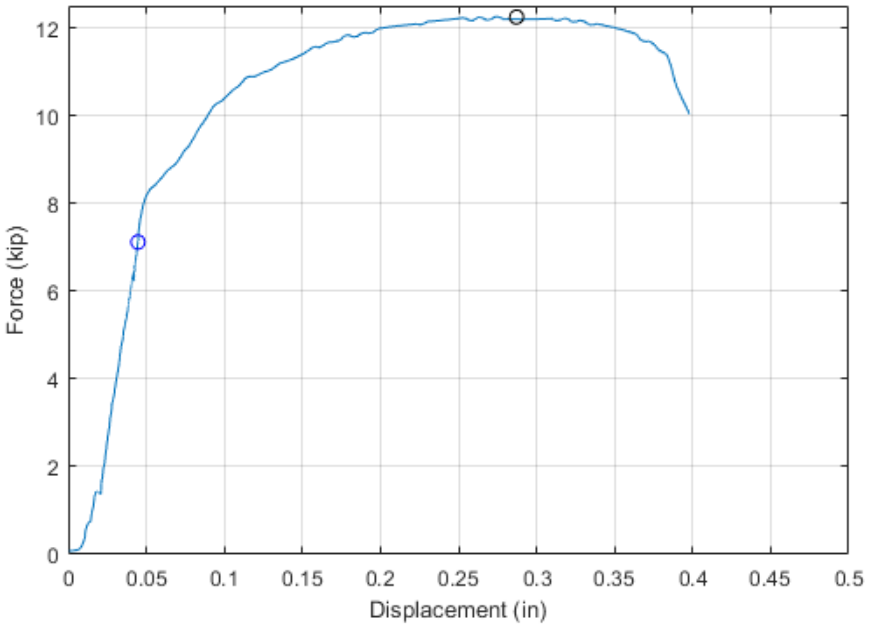

Figure C.6 Force versus displacement relationship of BL-AE-3

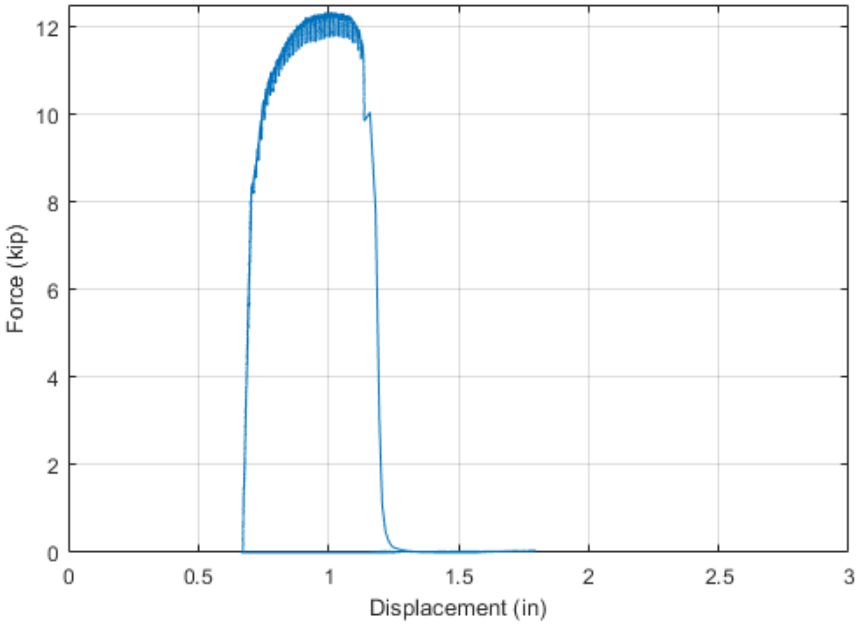

Figure C.7 Unfiltered force versus displacement relationship of BL-AE-4

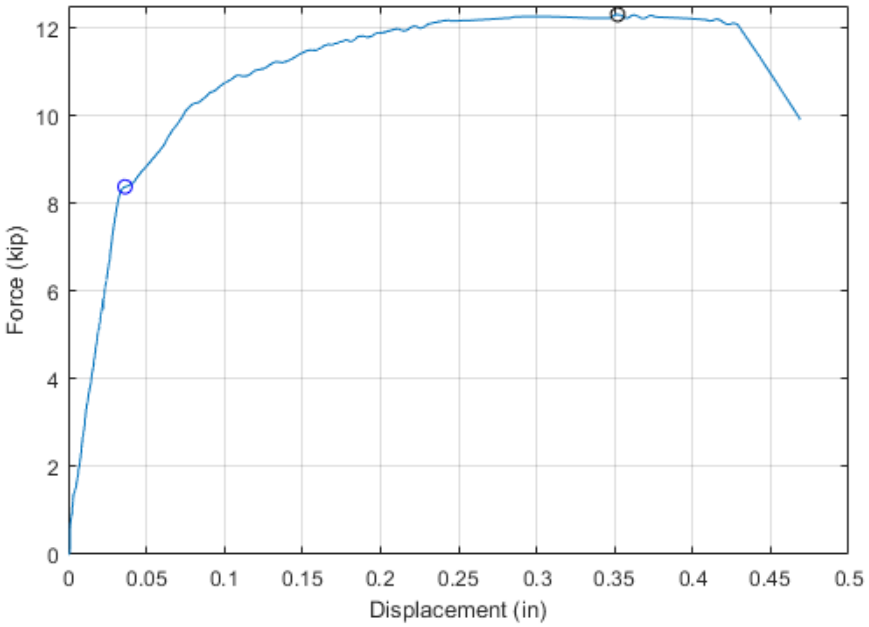

Figure C.8 Force versus displacement relationship of BL-AE-4

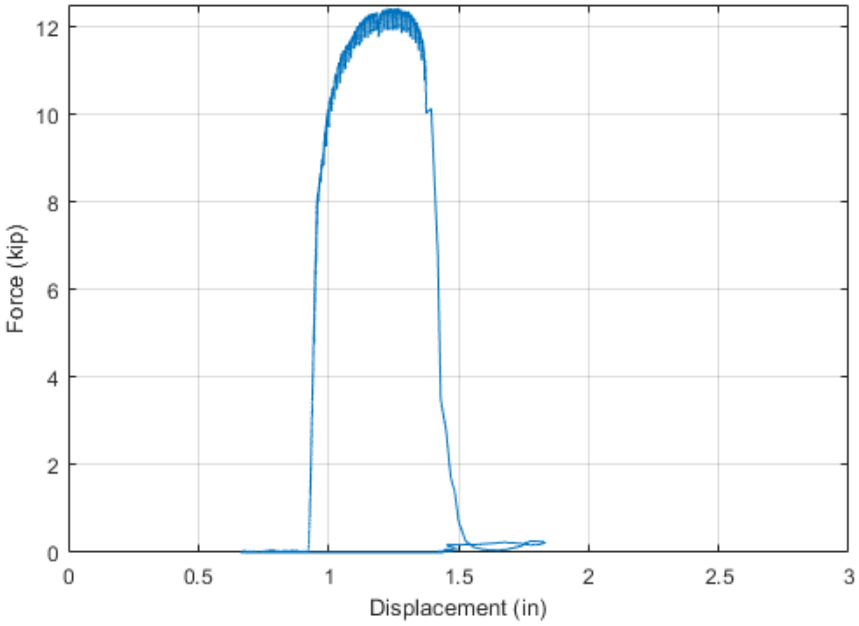

Figure C.9 Unfiltered force versus displacement relationship of BL-AE-5

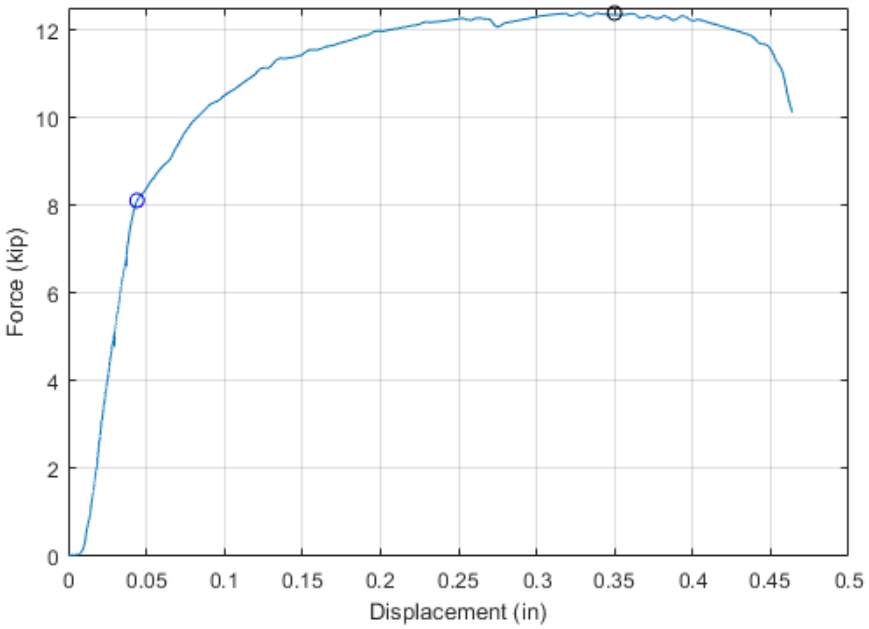

Figure C.10 Force versus displacement relationship of BL-AE-5

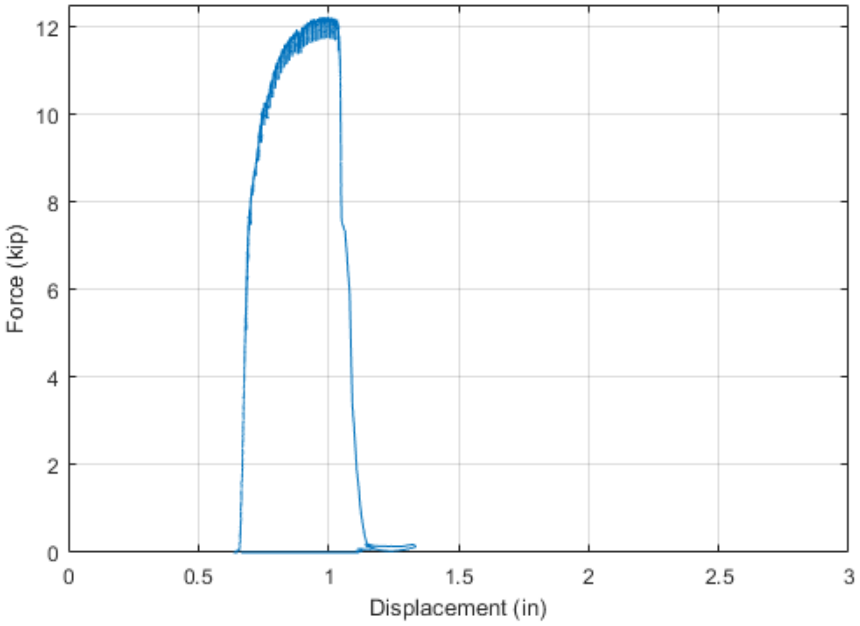

Figure C.11 Unfiltered force versus displacement relationship of BL-AP-1

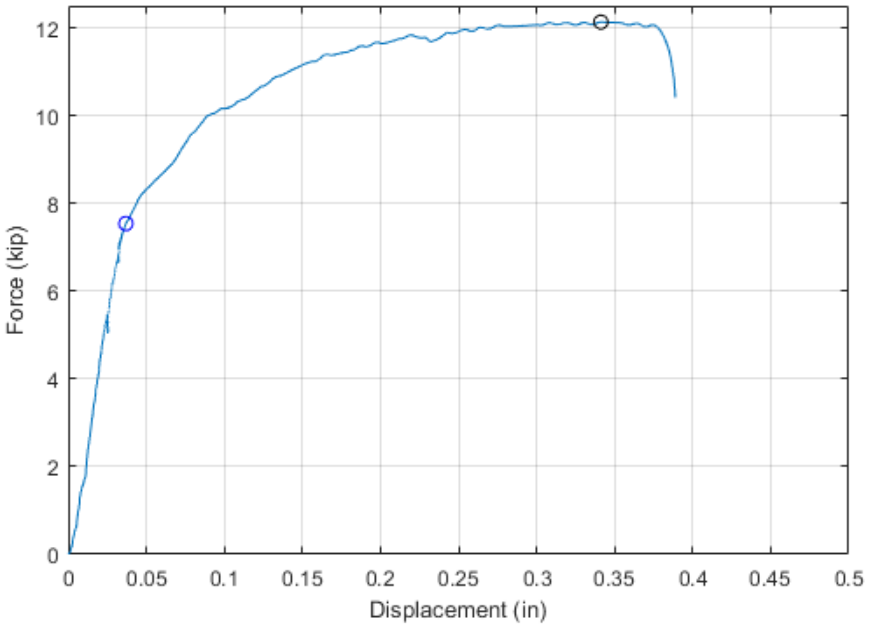

Figure C.12 Force versus displacement relationship of BL-AP-1

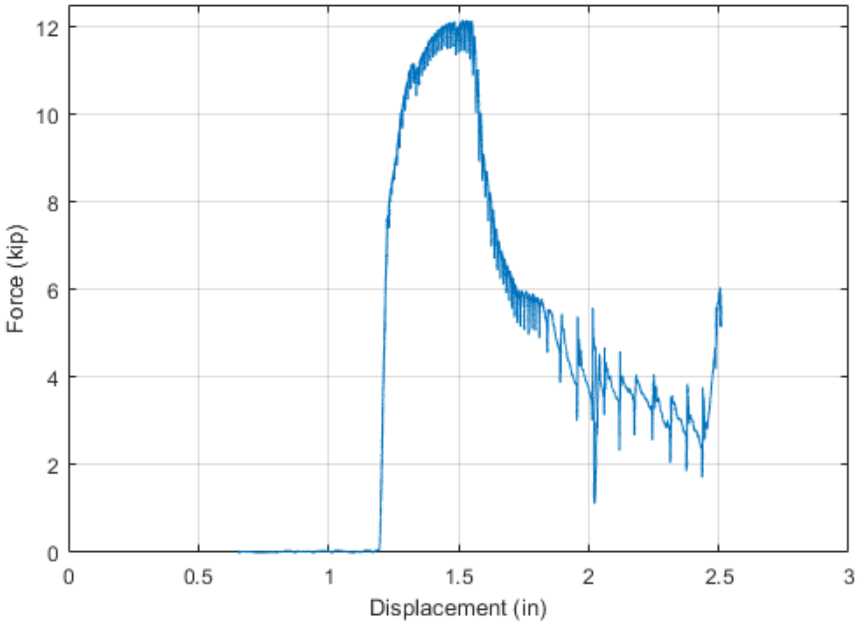

Figure C.13 Unfiltered force versus displacement relationship of BL-AP-2

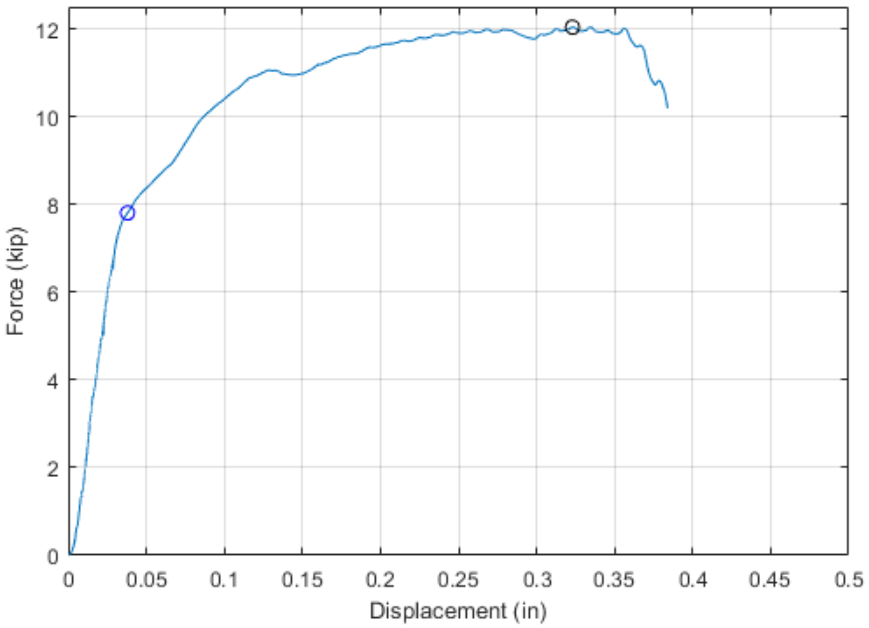

Figure C.14 Force versus displacement relationship of BL-AP-2

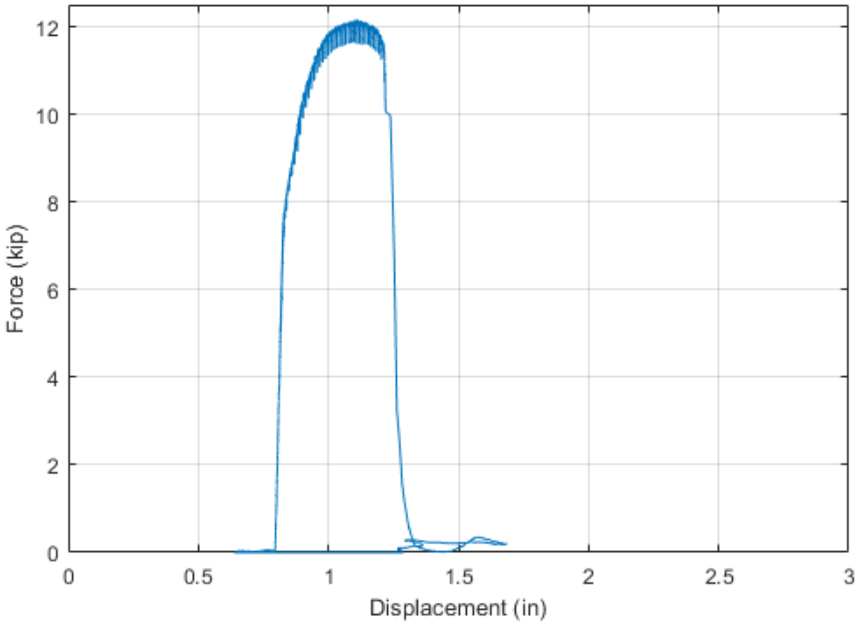

Figure C.15 Unfiltered force versus displacement relationship of BL-AP-3

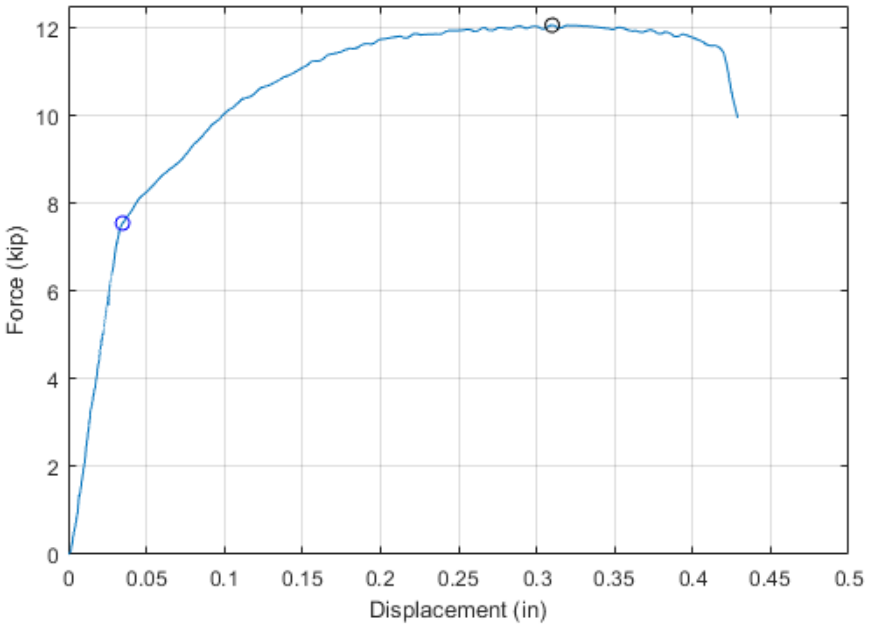

Figure C.16 Force versus displacement relationship of BL-AP-3

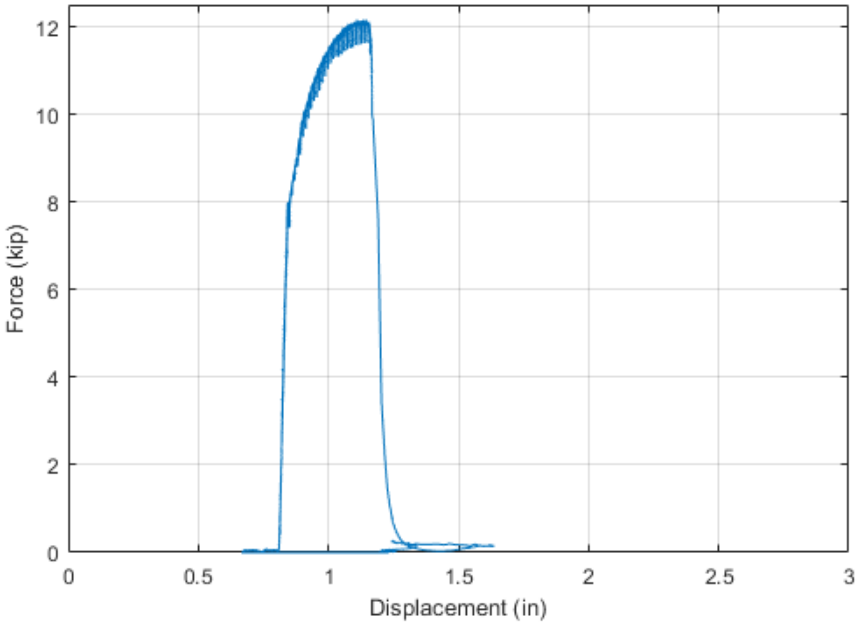

Figure C.17 Unfiltered force versus displacement relationship of BL-AP-4

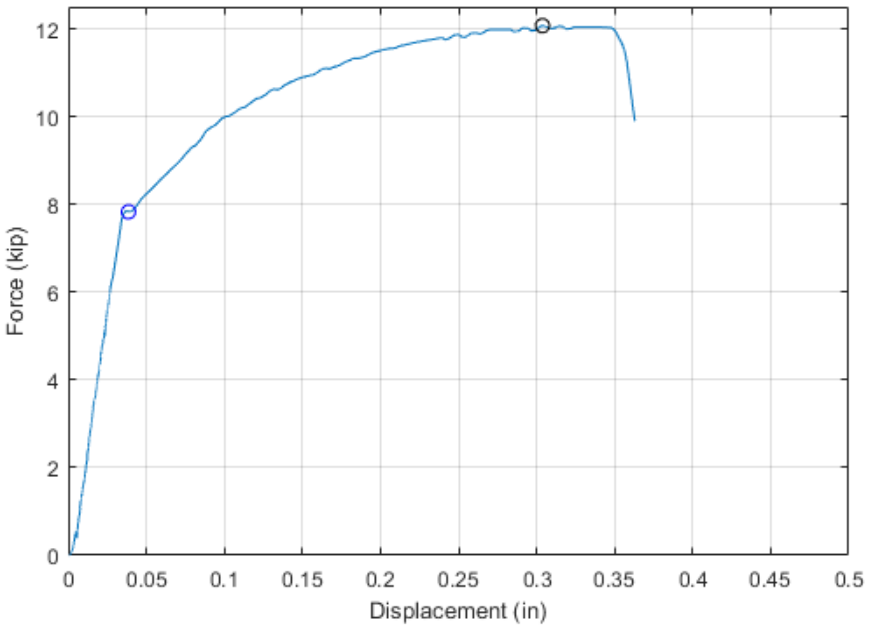

Figure C.18 Force versus displacement relationship of BL-AP-4

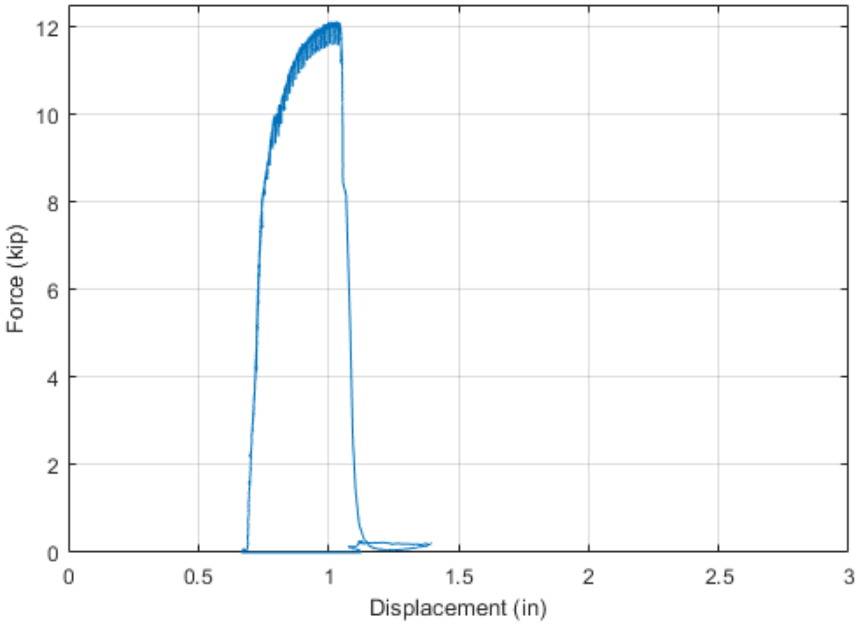

Figure C.19 Unfiltered force versus displacement relationship of BL-AP-5

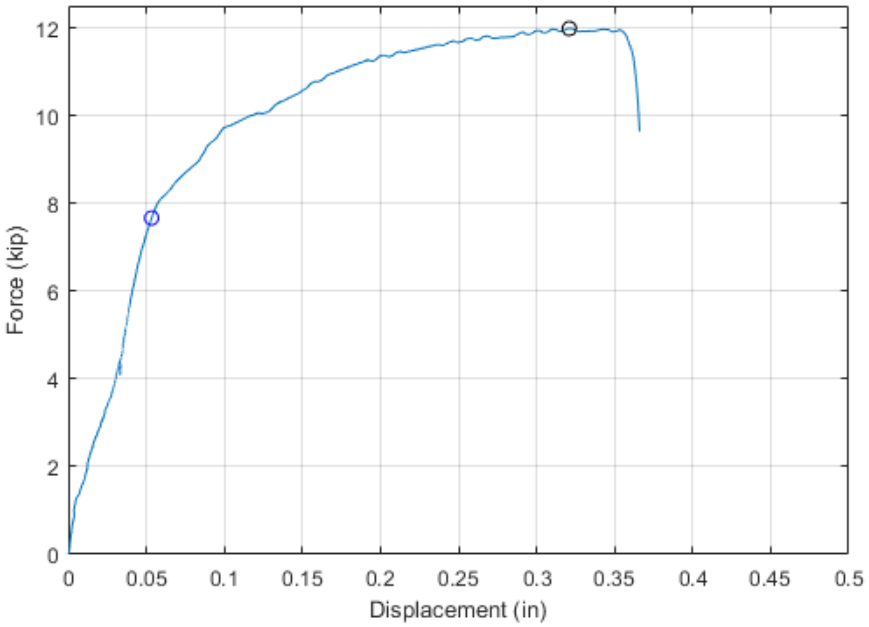

Figure C.20 Force versus displacement relationship of BL-AP-5

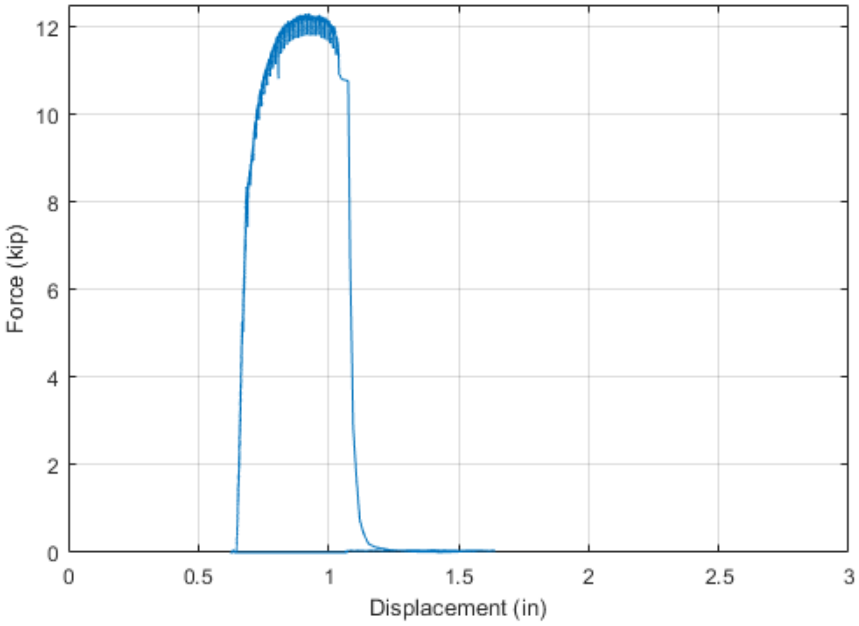

Figure C.21 Unfiltered force versus displacement relationship of CP-AE-1

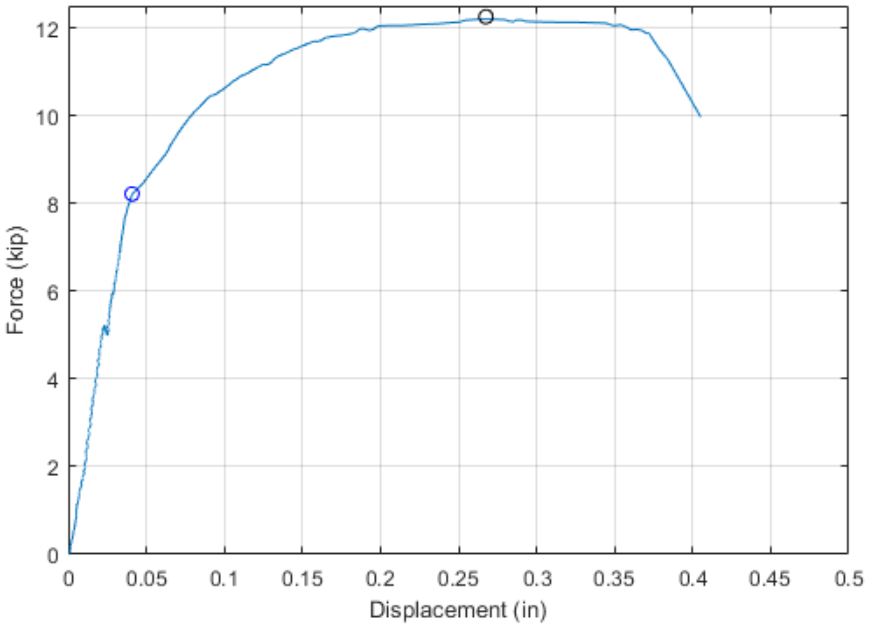

Figure C.22 Force versus displacement relationship of CP-AE-1

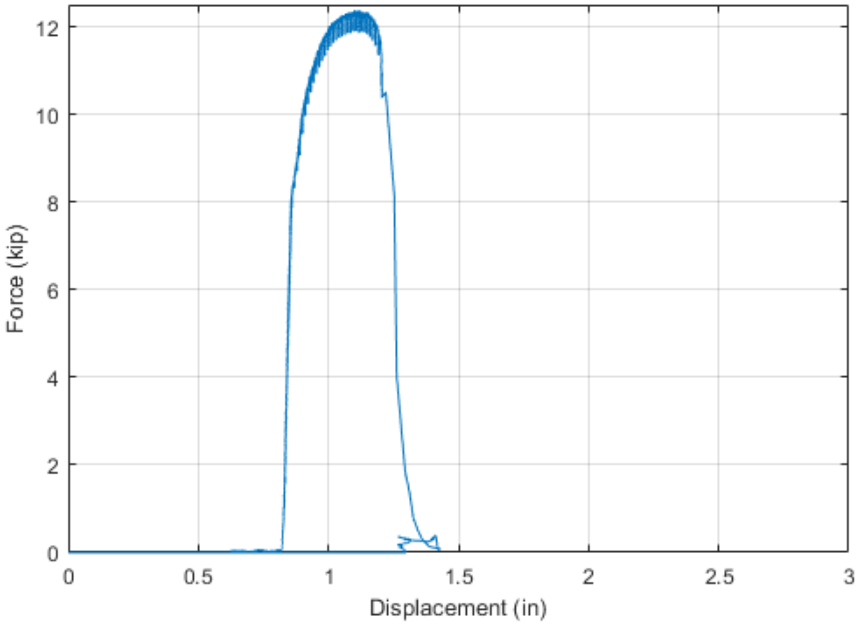

Figure C.23 Unfiltered force versus displacement relationship of CP-AE-2

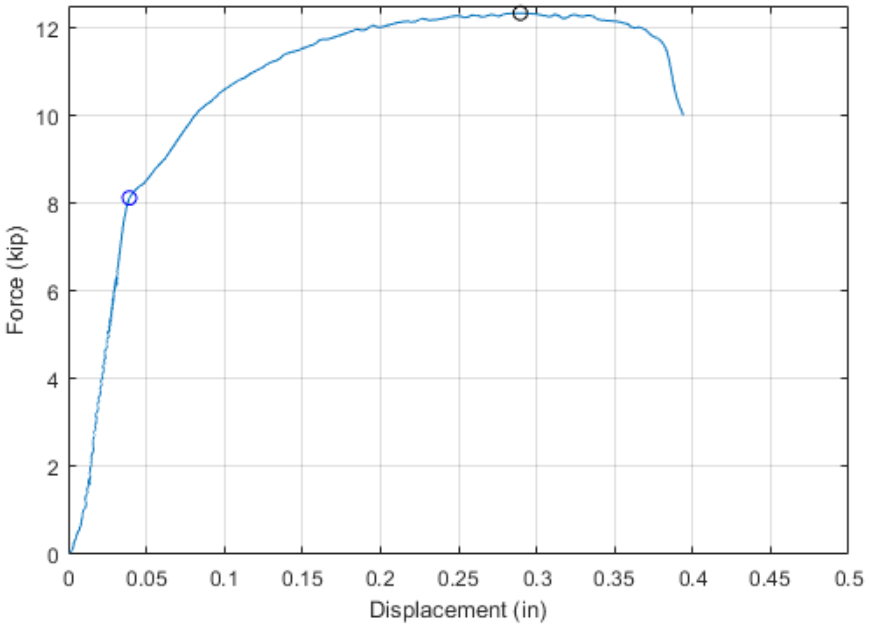

Figure C.24 Force versus displacement relationship of CP-AE-2

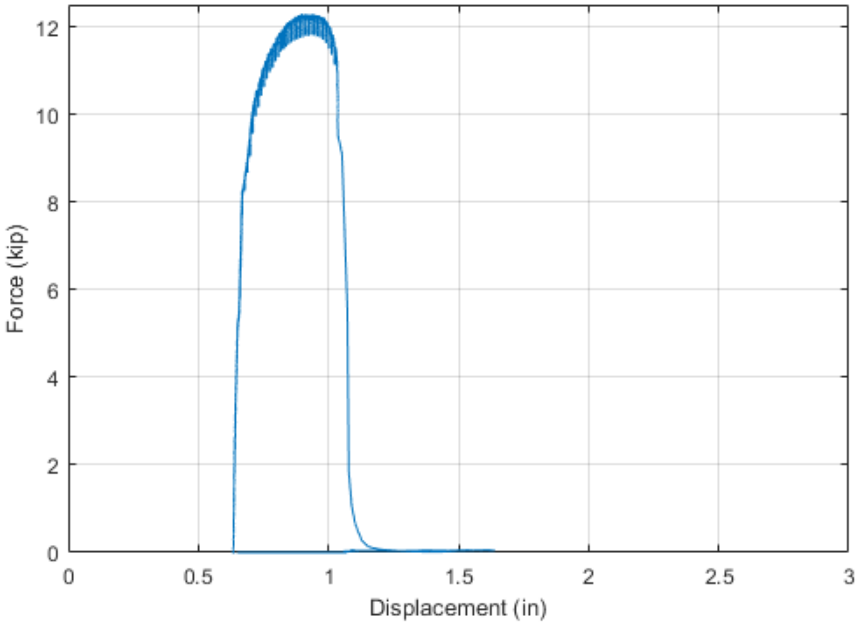

Figure C.25 Unfiltered force versus displacement relationship of CP-AE-3

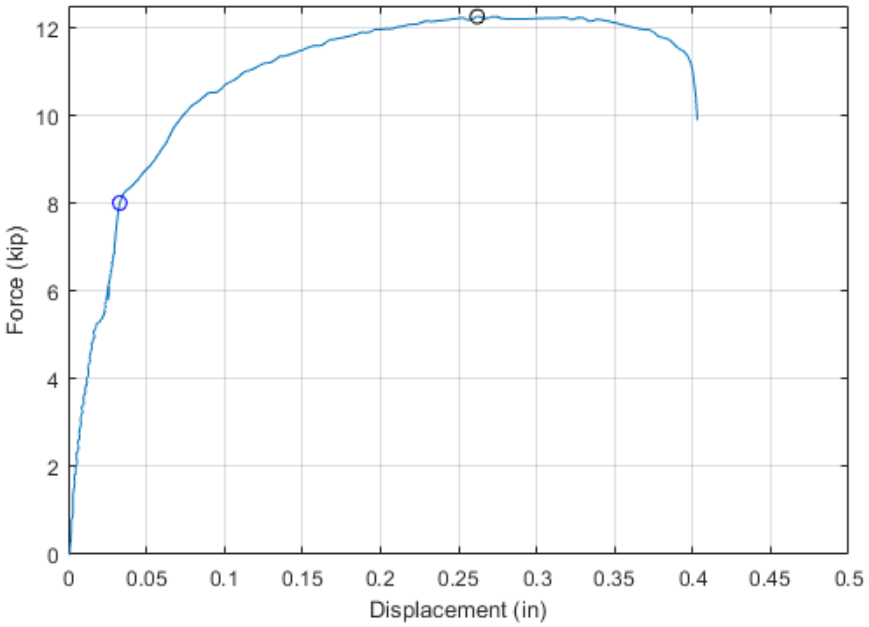

Figure C.26 Force versus displacement relationship of CP-AE-3

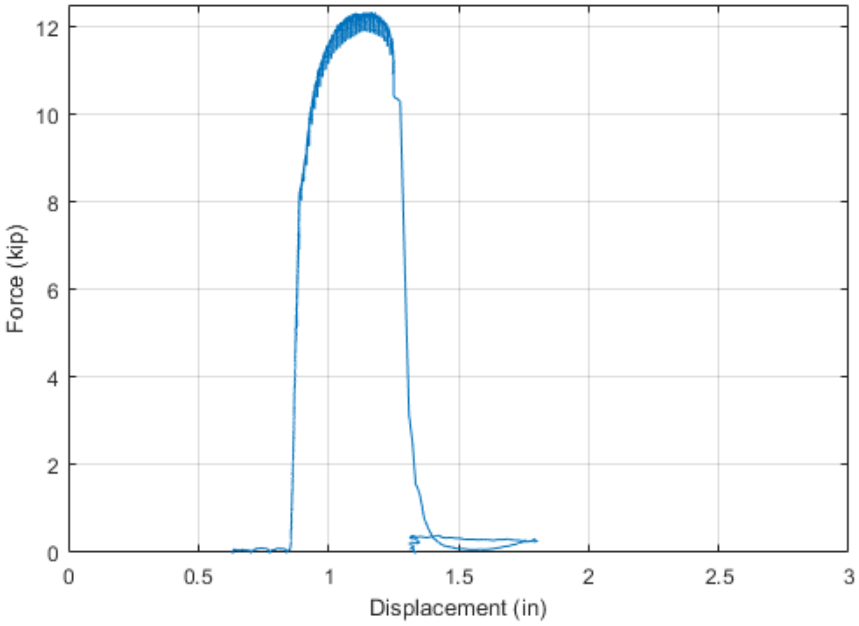

Figure C.27 Unfiltered force versus displacement relationship of CP-AE-4

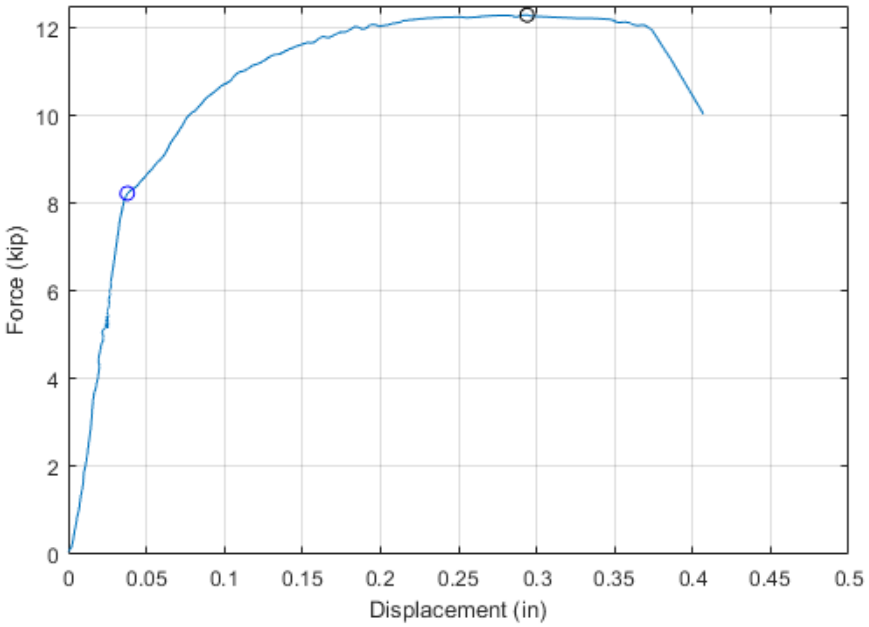

Figure C.28 Force versus displacement relationship of CP-AE-4

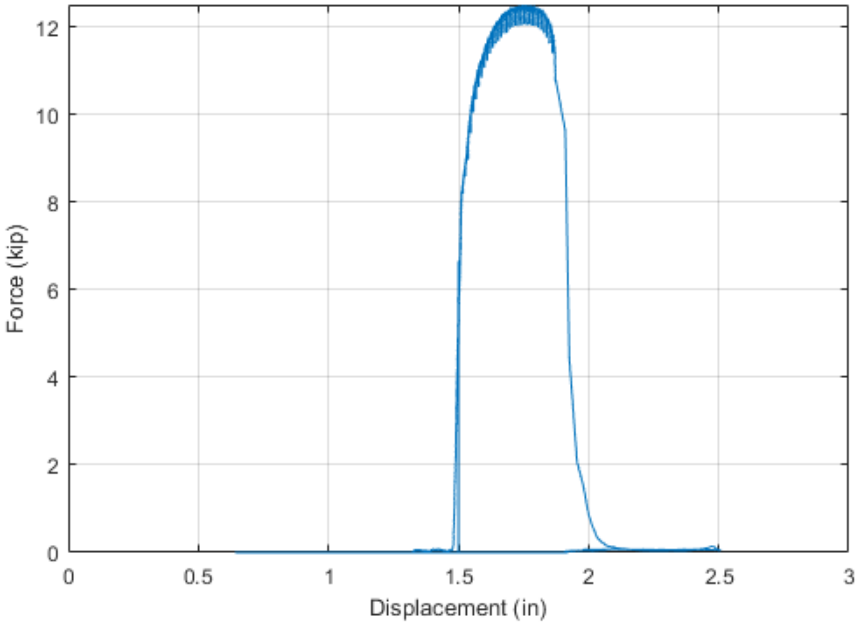

Figure C.29 Unfiltered force versus displacement relationship of CP-AE-5

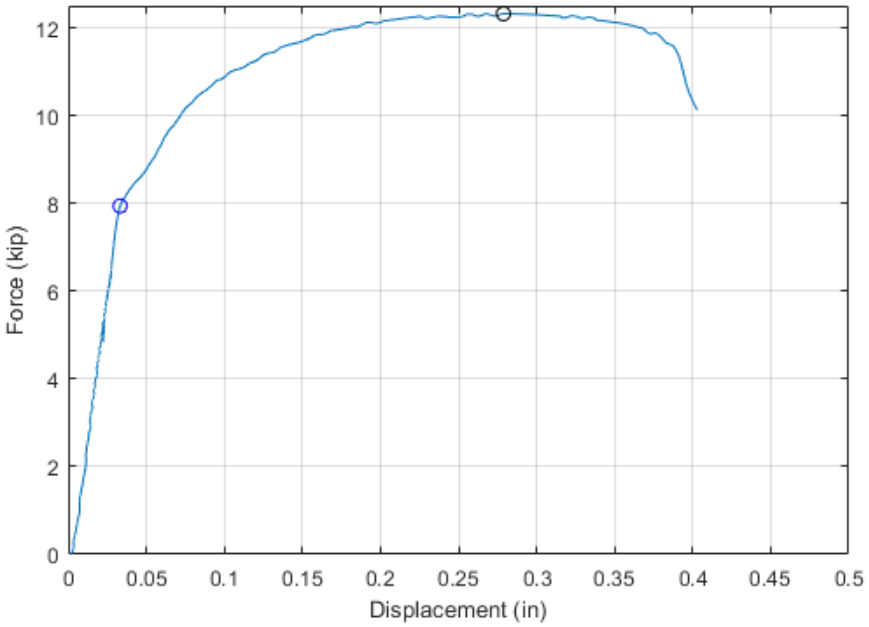

Figure C.30 Force versus displacement relationship of CP-AE-5

C.2 First Derivative and Stiffness Identification

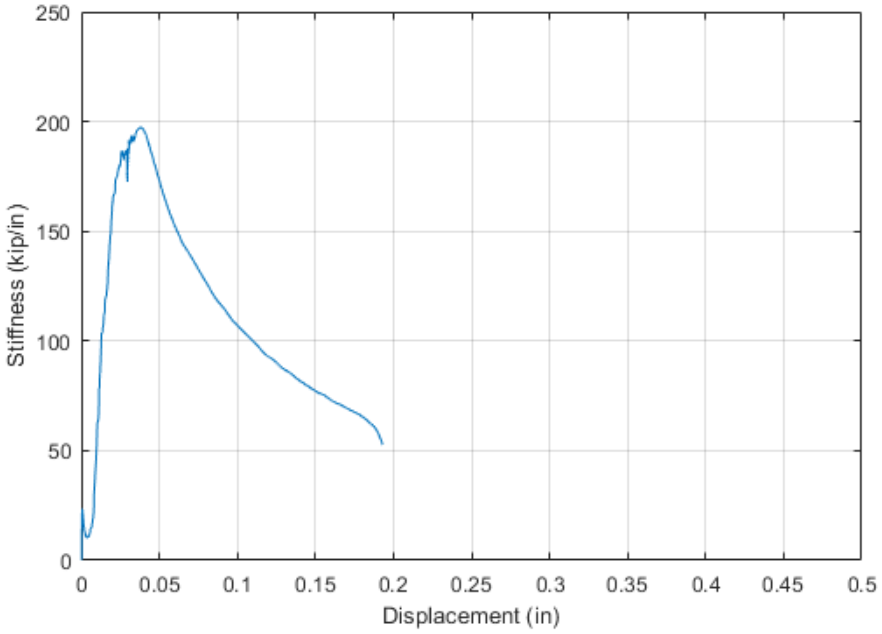

Figure C.31 Tangent stiffness (first derivative) versus displacement relationship of BL-AE-1

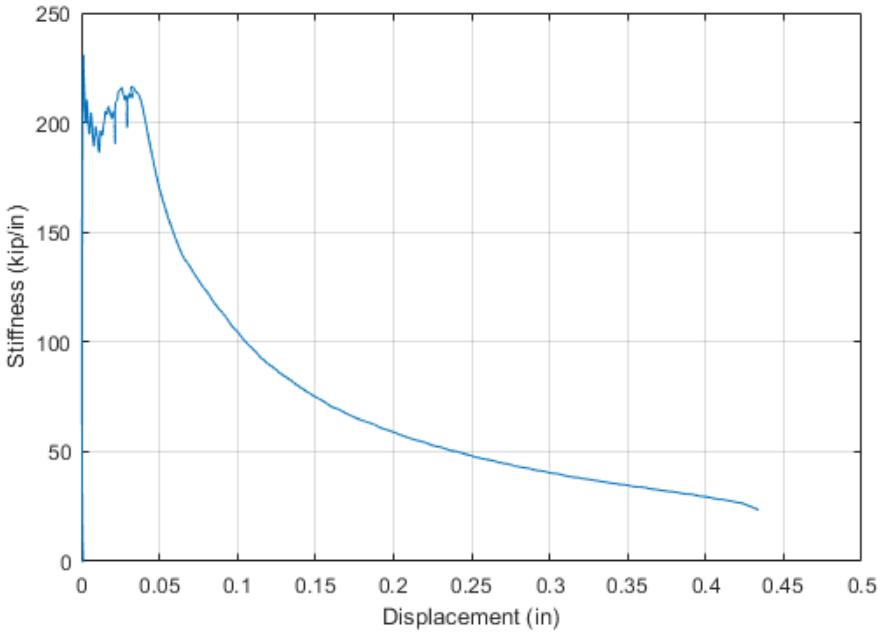

Figure C.32 Tangent stiffness (first derivative) versus displacement relationship of BL-AE-2

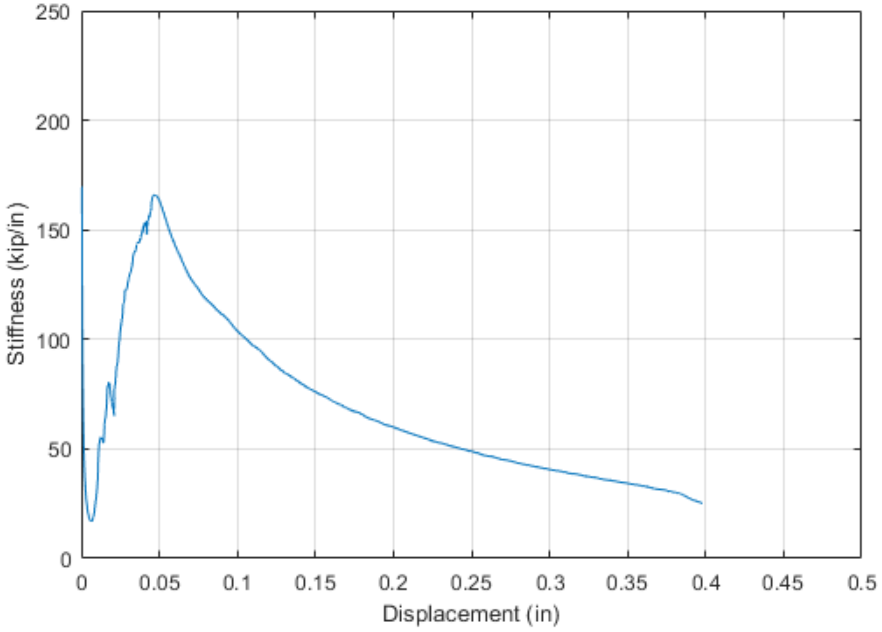

Figure C.33 Tangent stiffness (first derivative) versus displacement relationship of BL-AE-3

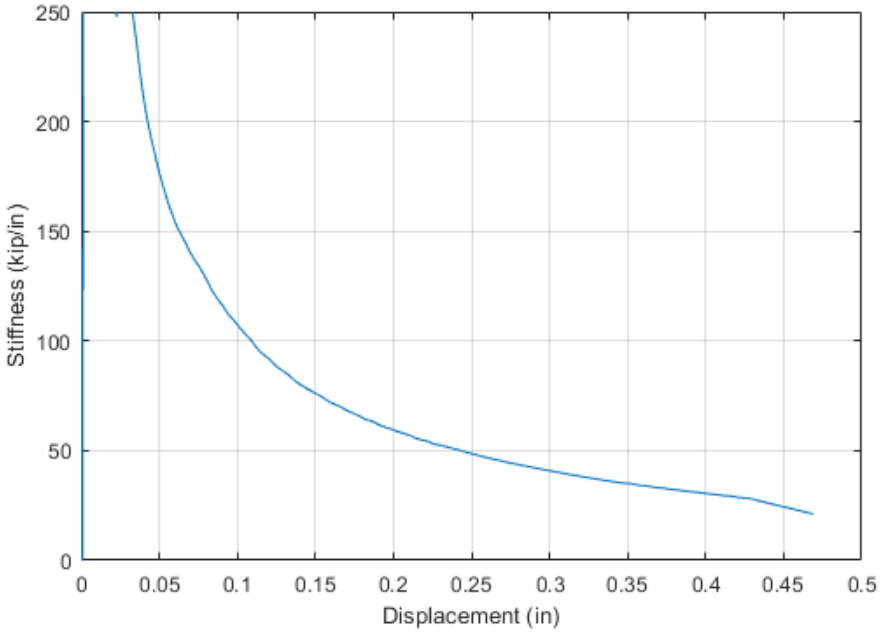

Figure C.34 Tangent stiffness (first derivative) versus displacement relationship of BL-AE-4

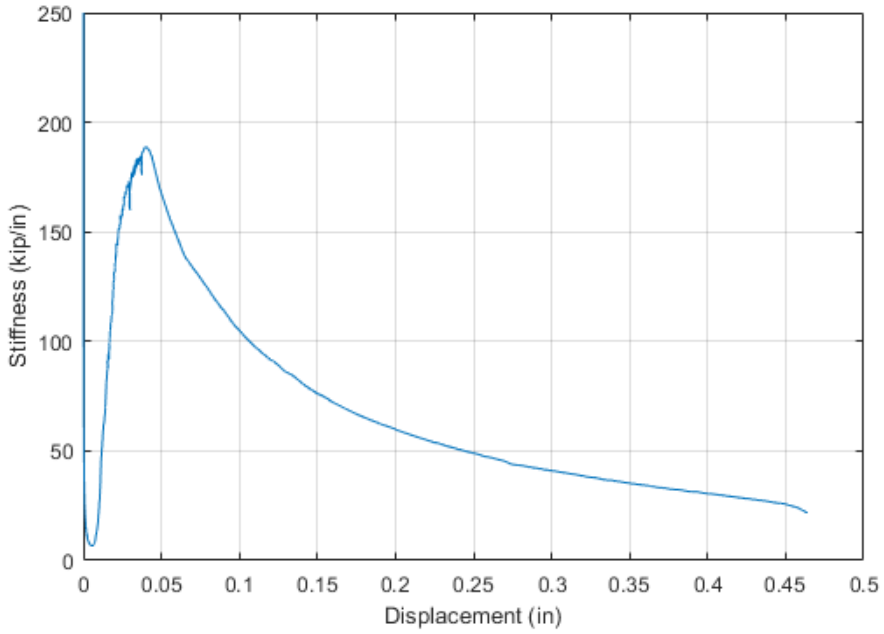

Figure C.35 Tangent stiffness (first derivative) versus displacement relationship of BL-AE-5

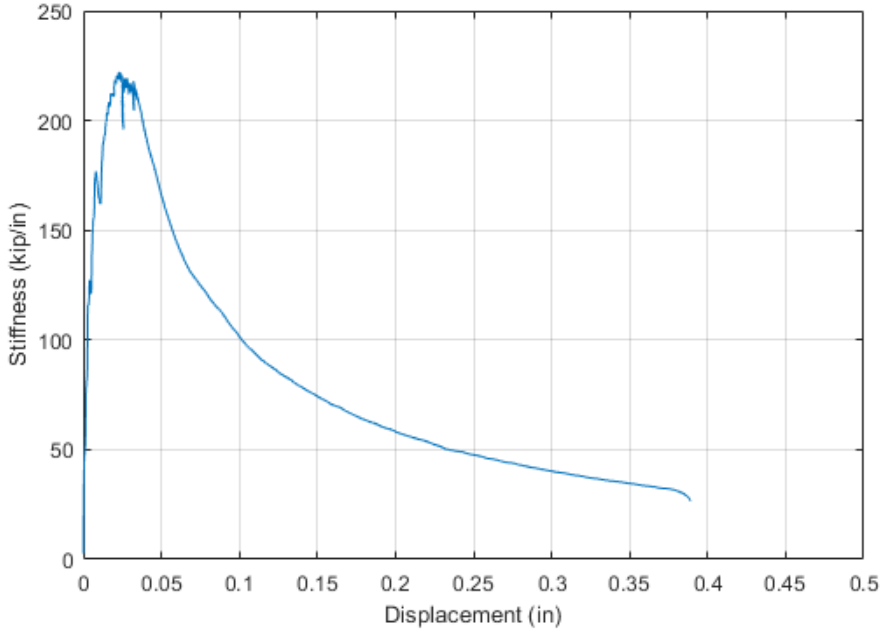

Figure C.36 Tangent stiffness (first derivative) versus displacement relationship of BL-AP-1

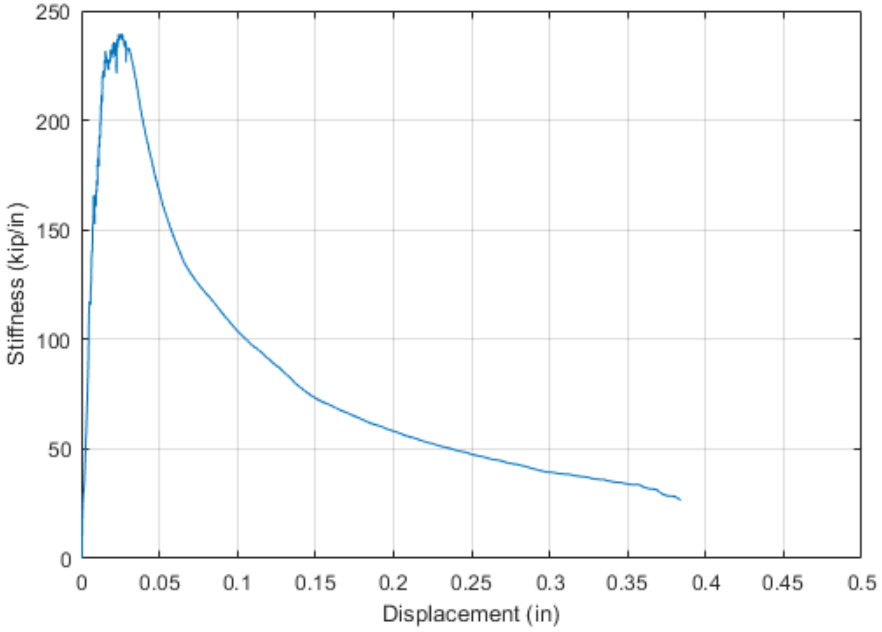

Figure C.37 Tangent stiffness (first derivative) versus displacement relationship of BL-AP-2

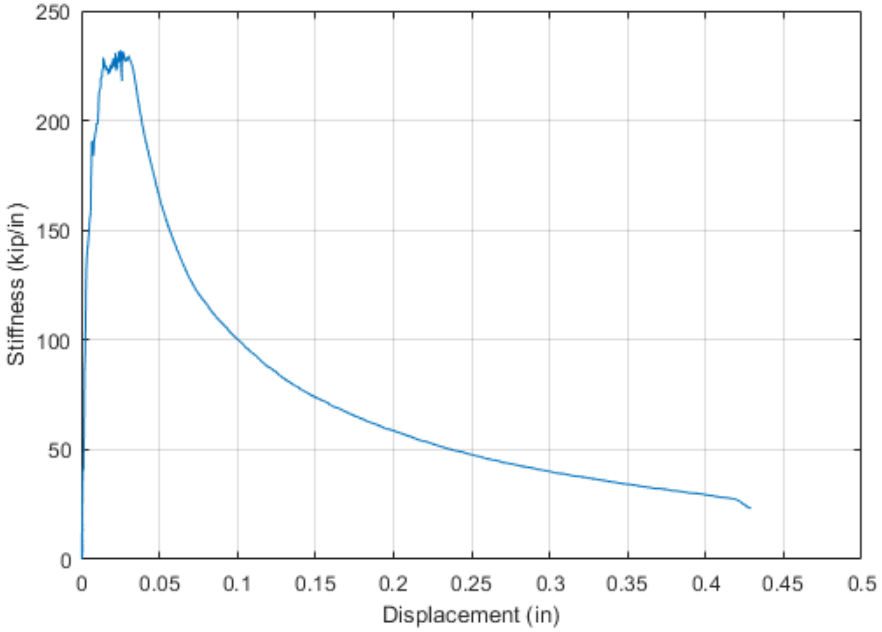

Figure C.38 Tangent stiffness (first derivative) versus displacement relationship of BL-AP-3

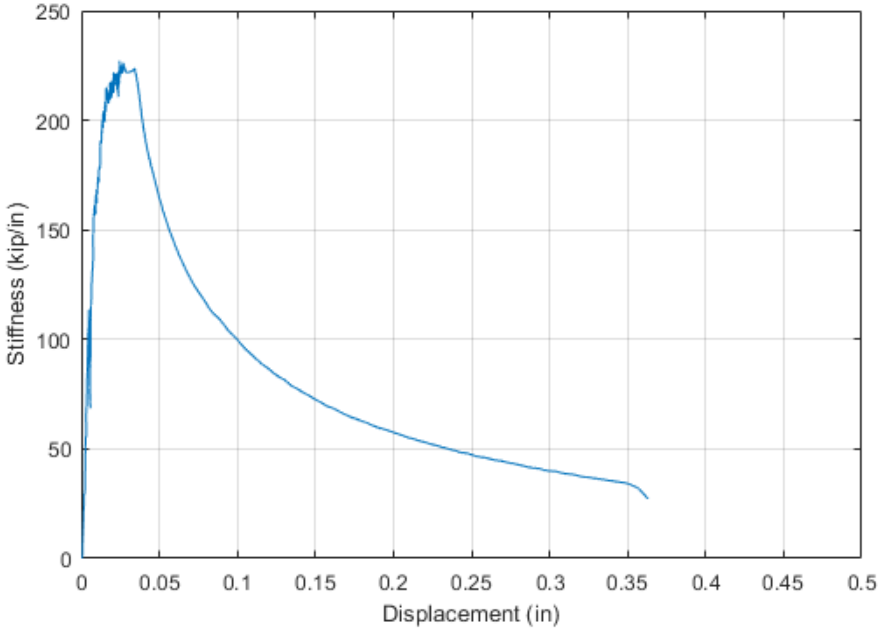

Figure C.39 Tangent stiffness (first derivative) versus displacement relationship of BL-AP-4

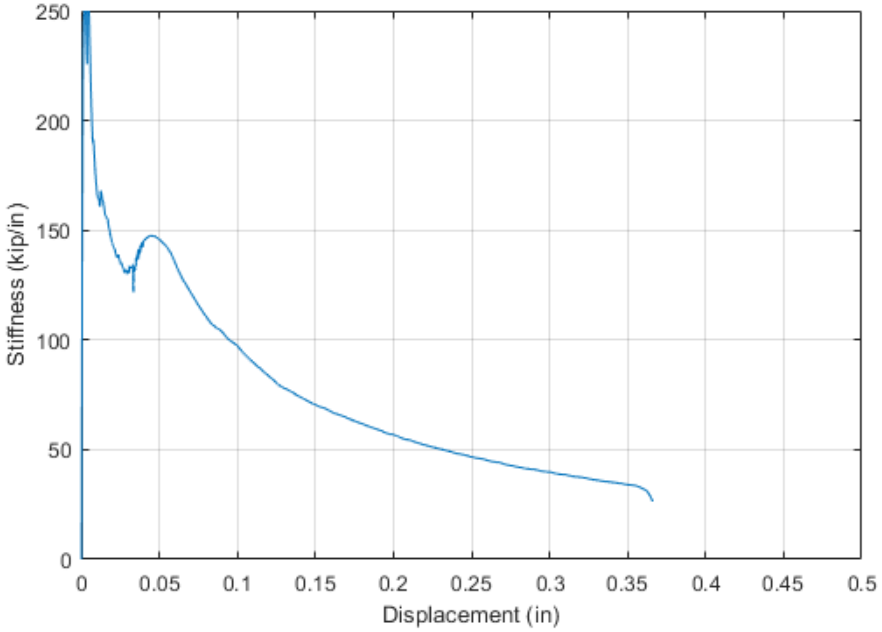

Figure C.40 Tangent stiffness (first derivative) versus displacement relationship of BL-AP-5

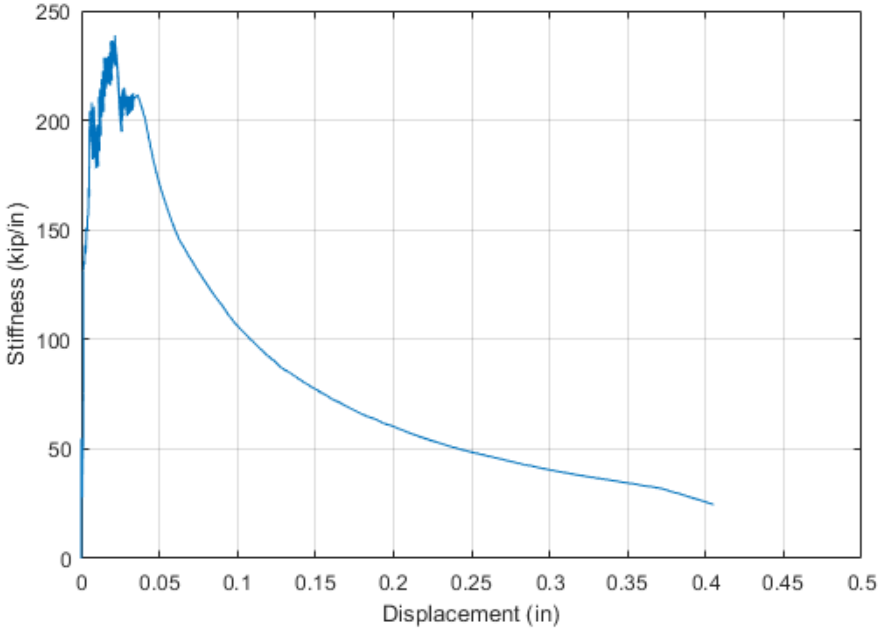

Figure C.41 Tangent stiffness (first derivative) versus displacement relationship of CP-AE-1

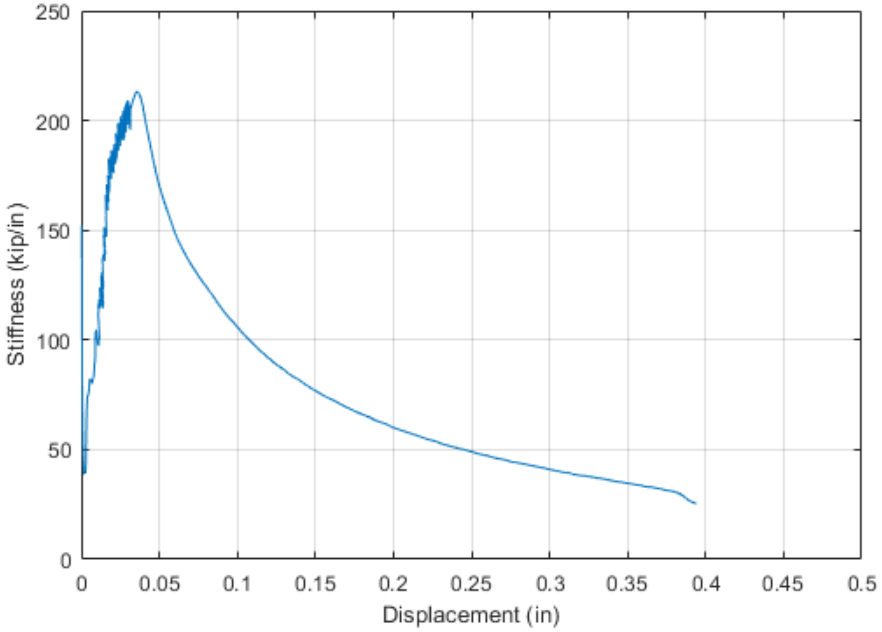

Figure C.42 Tangent stiffness (first derivative) versus displacement relationship of CP-AE-2

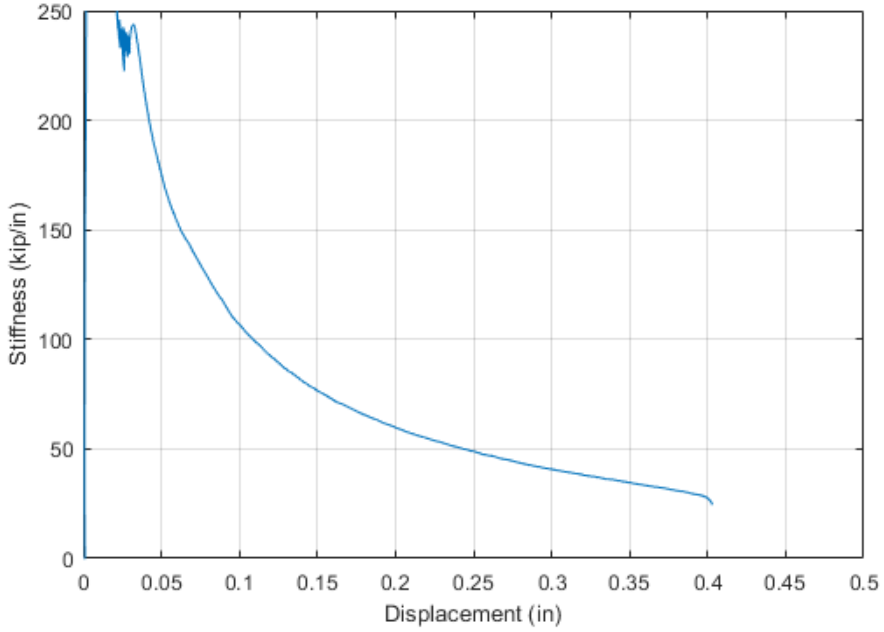

Figure C.43 Tangent stiffness (first derivative) versus displacement relationship of CP-AE-3

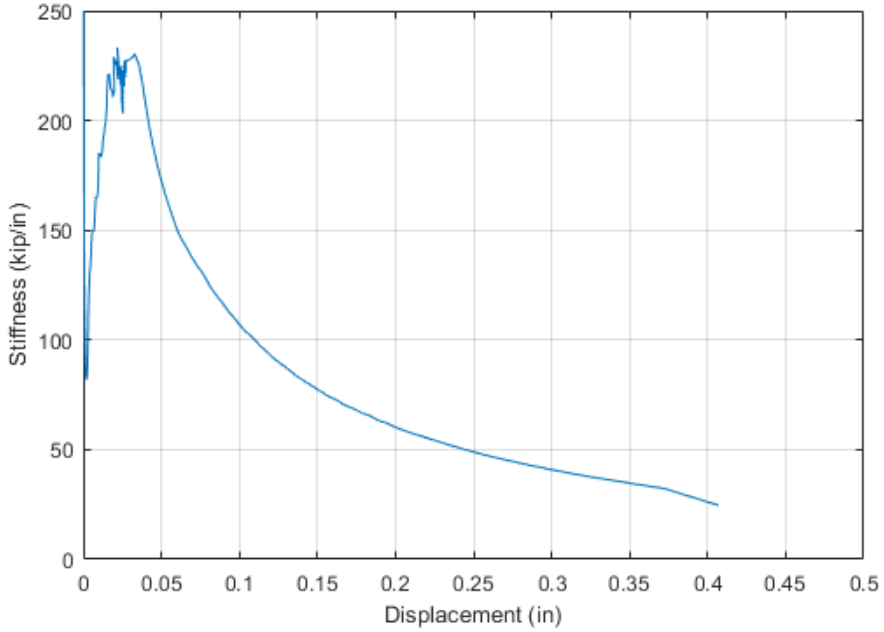

Figure C.44 Tangent stiffness (first derivative) versus displacement relationship of CP-AE-4

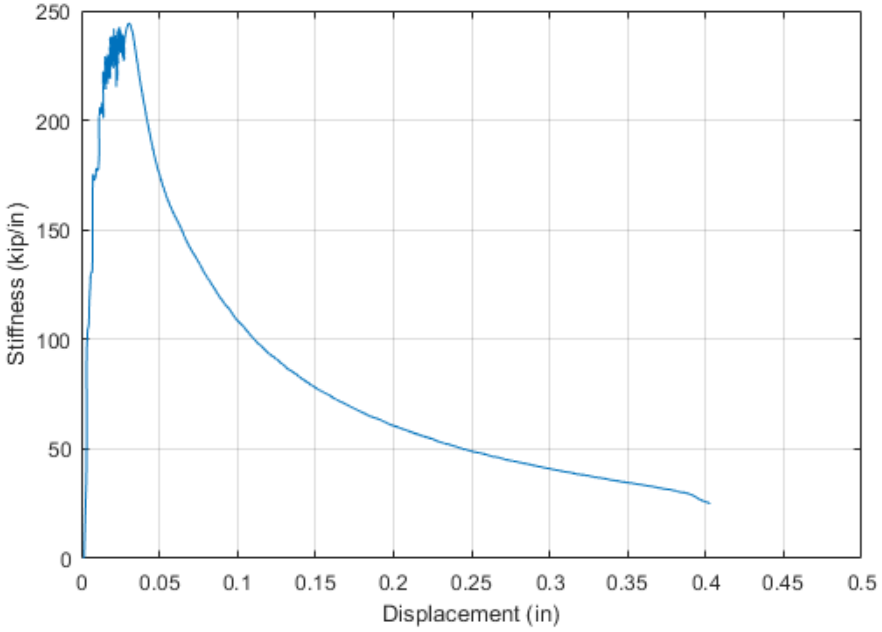

Figure C.45 Tangent stiffness (first derivative) versus displacement relationship of CP-AE-5

C.3 Second Derivative to Indicate Significant Yielding

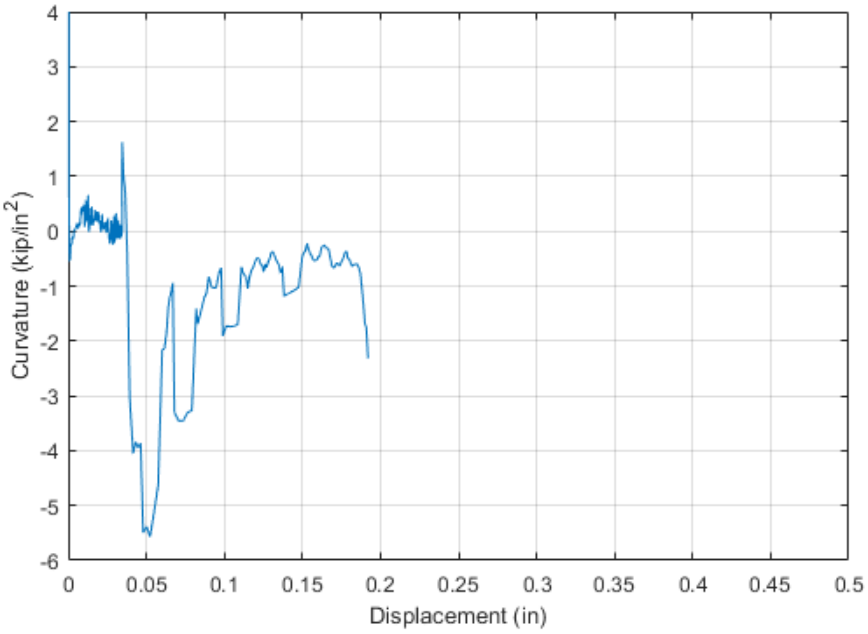

Figure C.46 Curvature (second derivative) versus displacement relationship of BL-AE-1

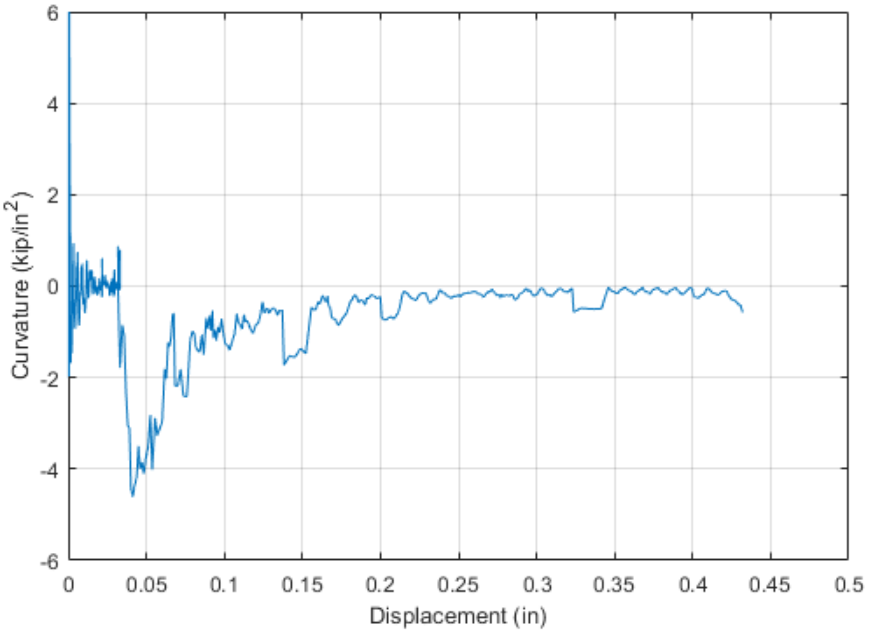

Figure C.47 Curvature (second derivative) versus displacement relationship of BL-AE-2

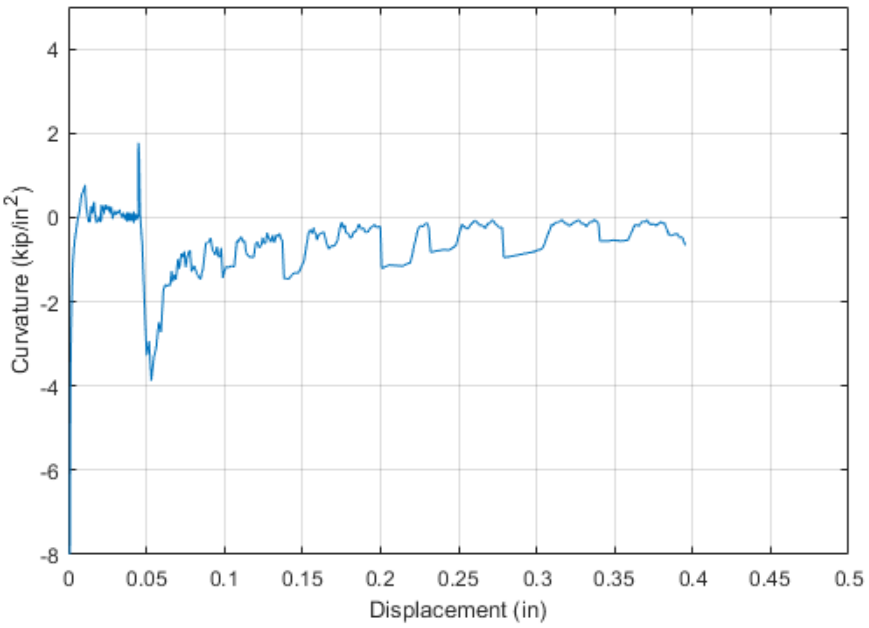

Figure C.48 Curvature (second derivative) versus displacement relationship of BL-AE-3

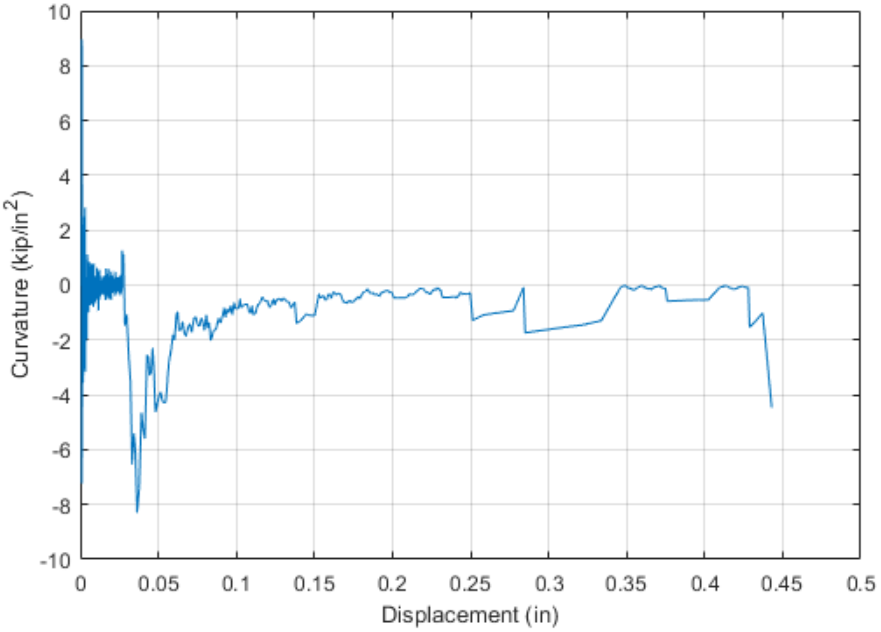

Figure C.49 Curvature (second derivative) versus displacement relationship of BL-AE-4

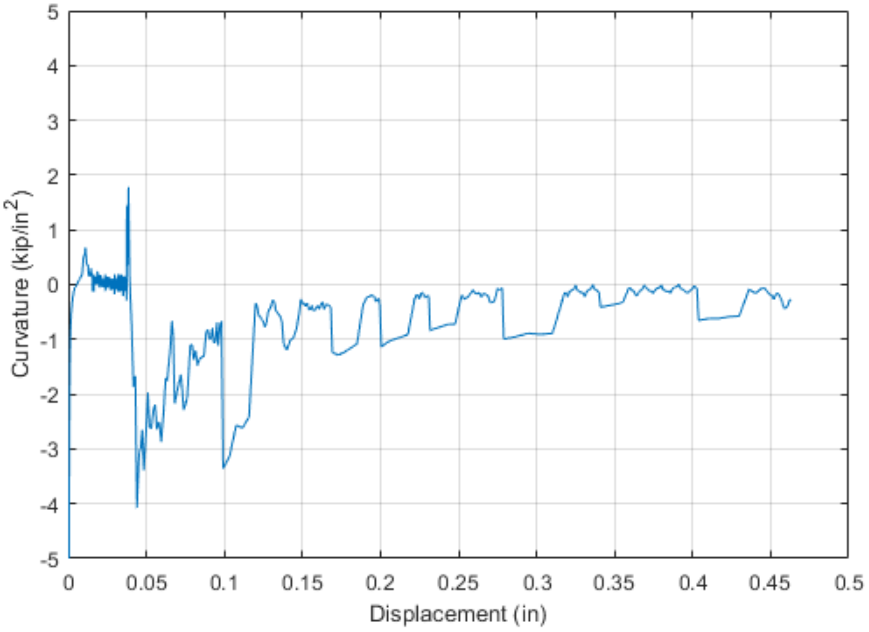

Figure C.50 Curvature (second derivative) versus displacement relationship of BL-AE-5

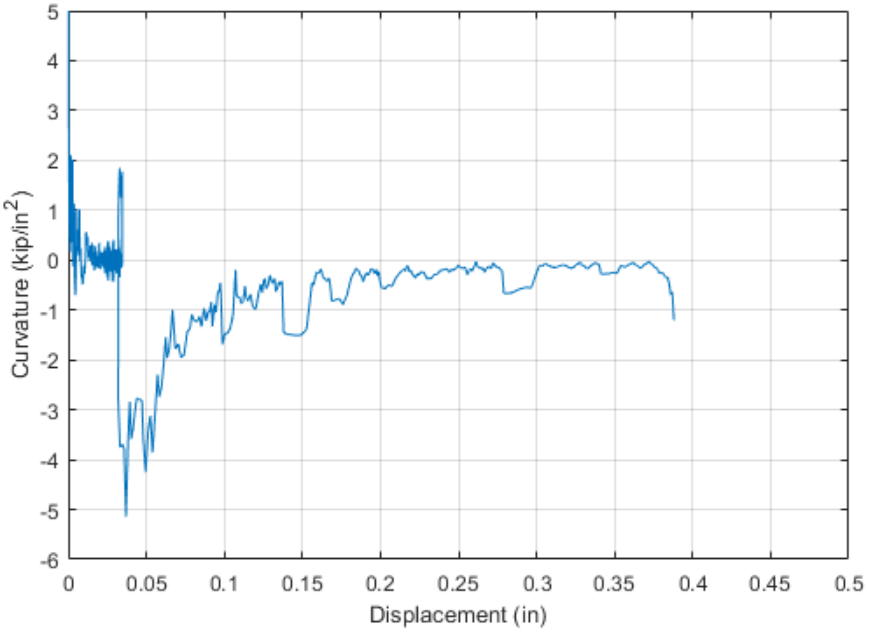

Figure C.51 Curvature (second derivative) versus displacement relationship of BL-AP-1

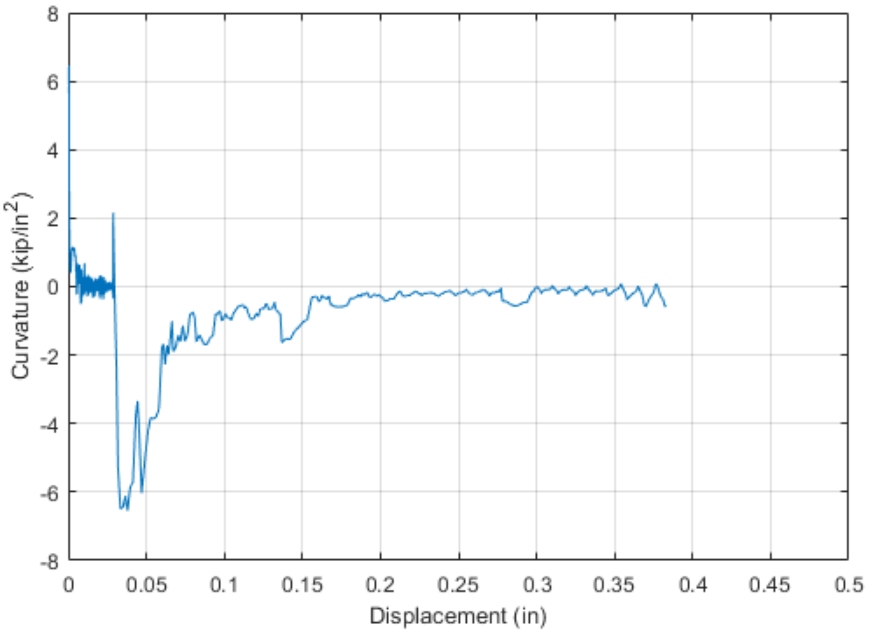

Figure C.52 Curvature (second derivative) versus displacement relationship of BL-AP-2

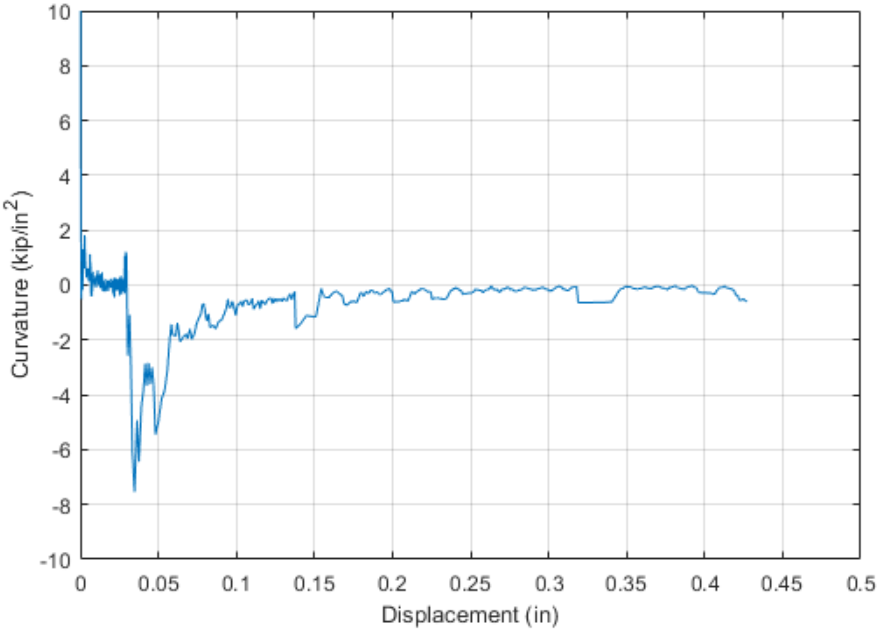

Figure C.53 Curvature (second derivative) versus displacement relationship of BL-AP-3

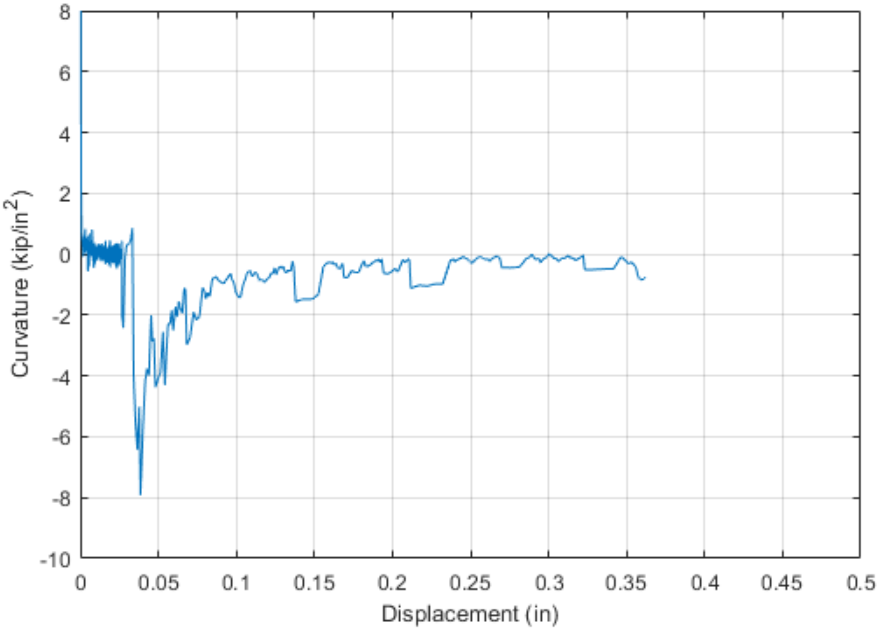

Figure C.54 Curvature (second derivative) versus displacement relationship of BL-AP-4

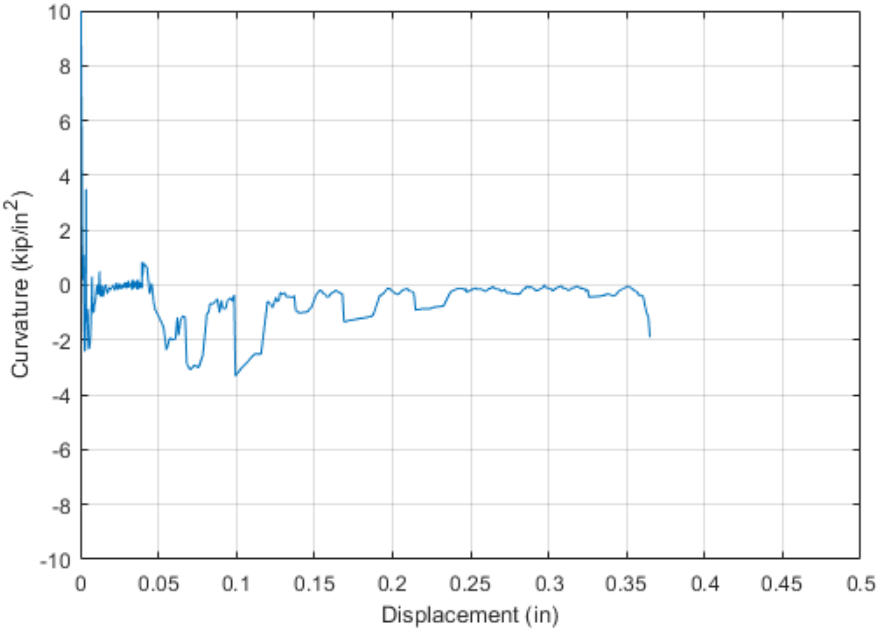

Figure C.55 Curvature (second derivative) versus displacement relationship of BL-AP-5

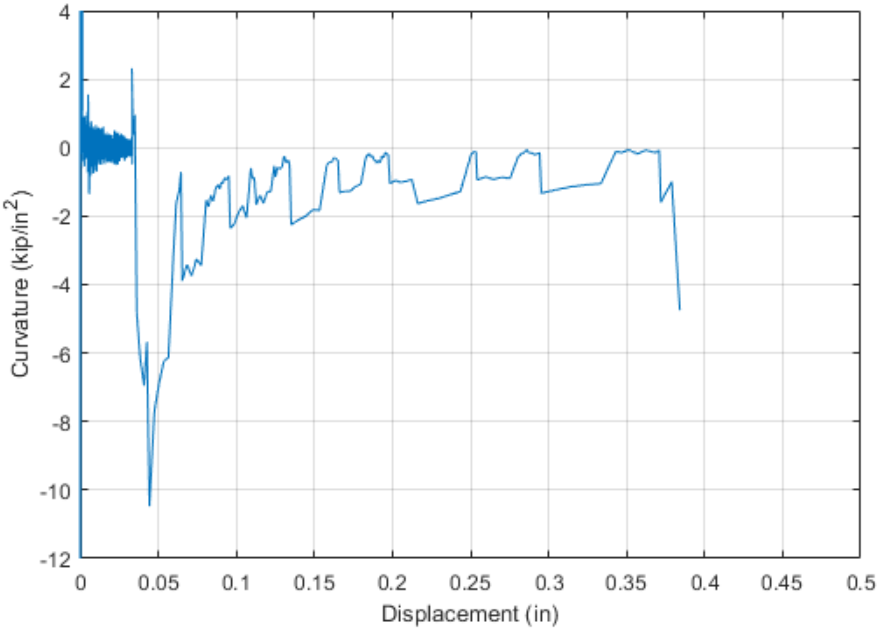

Figure C.56 Curvature (second derivative) versus displacement relationship of CP-AE-1

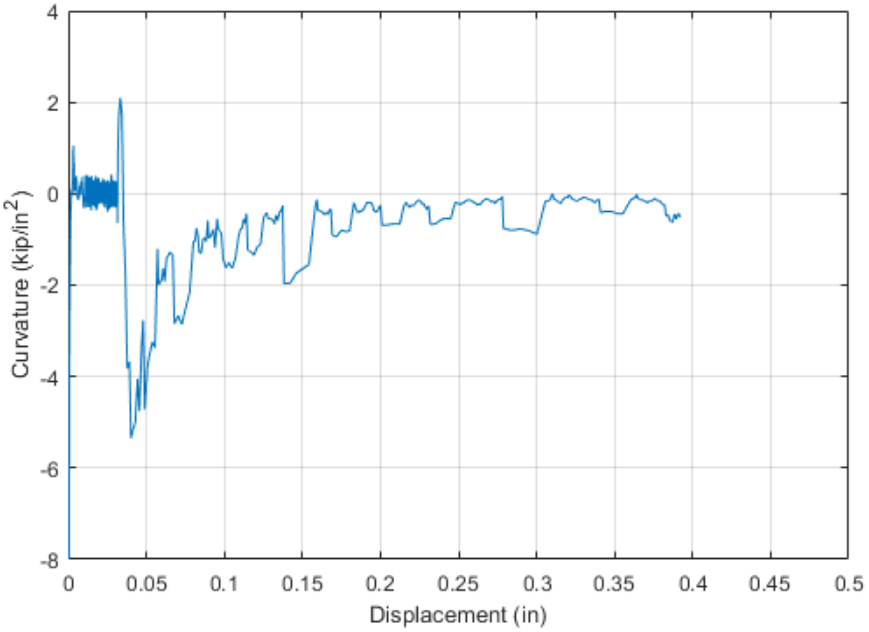

Figure C.57 Curvature (second derivative) versus displacement relationship of CP-AE-2

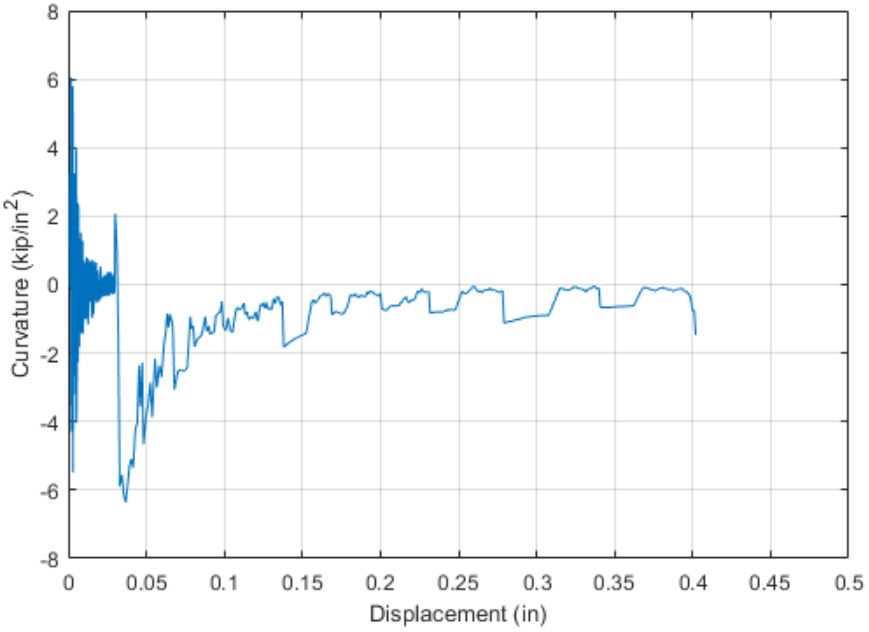

Figure C.58 Curvature (second derivative) versus displacement relationship of CP-AE-3

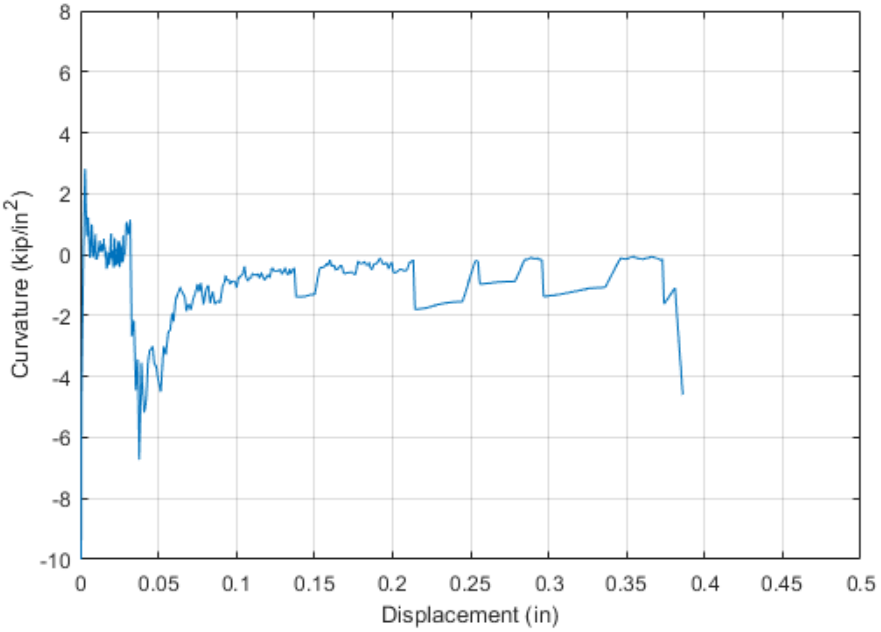

Figure C.59 Curvature (second derivative) versus displacement relationship of CP-AE-4

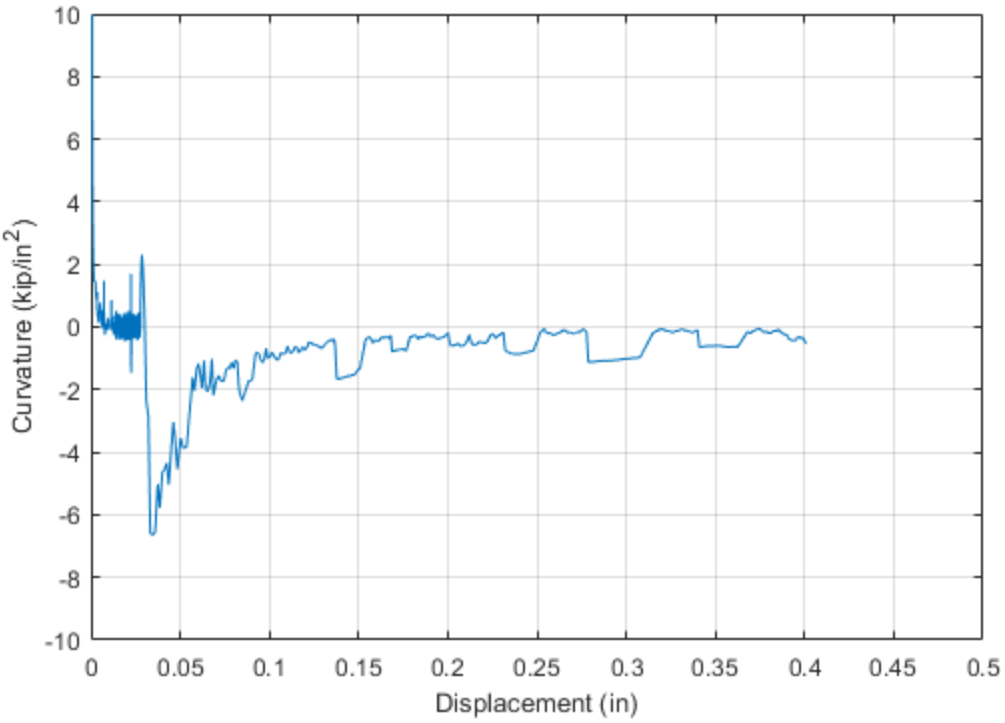

Figure C.60 Curvature (second derivative) versus displacement relationship of CP-AE-5

C.4 Summary of Key Parameters by Configuration

Table C.1 Summary of BL-AE specimens

Test Name	Stiffness (kip/in)	F_y (kip)	Δ_y (in)	F_{max} (kip)	Δ_{max} (in)	F_u (kip)	Δ_u (in)	μ (in/in)
BL-AE-1	197.35	8.07	0.042	11.83	0.178	9.45	0.193	4.60
BL-AE-2	230.81	8.26	0.041	12.17	0.305	9.89	0.437	10.56
BL-AE-3	165.10	8.05	0.043	12.25	0.352	9.74	0.402	9.35
BL-AE-4	230.20	8.38	0.036	12.30	0.352	9.80	0.470	12.92
BL-AE-5	185.60	8.11	0.044	12.38	0.327	9.97	0.466	10.59
Mean	185.58	8.14	0.054	12.11	0.310	10.51	0.385	7.11
Standard Deviation	28.62	0.14	0.0031	0.21	0.073	0.20	0.12	3.08
Coefficient of Variation	0.140	0.017	0.076	0.018	0.24	0.020	0.290	0.320

Table C.2 Summary of BL-AP specimens

Test Name	Stiffness (kip/in)	F_y (kip)		Δ_y (in)	F_{max} (kip)	Δ_{max} (in)	F_u (kip)	Δ_u (in)	μ (in/in)
BL-AP-1	222.04	7.54		0.037	12.13	0.341	9.68	0.389	10.52
BL-AP-2	239.50	7.80		0.038	12.04	0.323	9.63	0.384	10.11
BL-AP-3	231.97	7.55		0.035	12.06	0.310	9.74	0.430	12.29
BL-AP-4	227.10	7.83		0.039	12.07	0.304	9.69	0.365	9.36
BL-AP-5	275.00	7.66		0.053	11.98	0.321	9.59	0.366	6.91
Mean	209.74	7.29		0.039	12.02	0.337	10.36	0.385	9.87
Standard Deviation	18.06	0.12		6.4e-3	0.05	0.068	0.04	0.020	1.75
Coefficient of Variation	0.088	0.018		0.180	0.0045	0.044	0.006	0.068	0.20

Table C.3 Summary of CP-AE specimens

Test Name	Stiffness (kip/in)	F_y (kip)	Δ_y (in)	F_{max} (kip)	Δ_{max} (in)	F_u (kip)	Δ_u (in)	μ (in/in)
CP-AE-1	212.86	8.21	0.041	12.25	0.268	9.63	0.413	10.07
CP-AE-2	213.34	8.12	0.039	12.33	0.302	9.76	0.397	10.18
CP-AE-3	236.72	8.01	0.033	12.26	0.285	9.78	0.403	12.21
CP-AE-4	227.70	8.23	0.038	12.29	0.304	9.75	0.410	10.79
CP-AE-5	244.33	7.94	0.033	12.32	0.279	9.90	0.406	12.30
Mean	221.99	8.16	0.040	12.27	0.285	9.82	0.394	9.85
Standard Deviation	13.98	0.13	0.0036	0.035	0.015	0.096	0.0062	1.08
Coefficient of Variation	0.062	0.016	0.099	0.003	0.053	0.0098	0.015	0.097

C.5 Summary Plots by Configuration

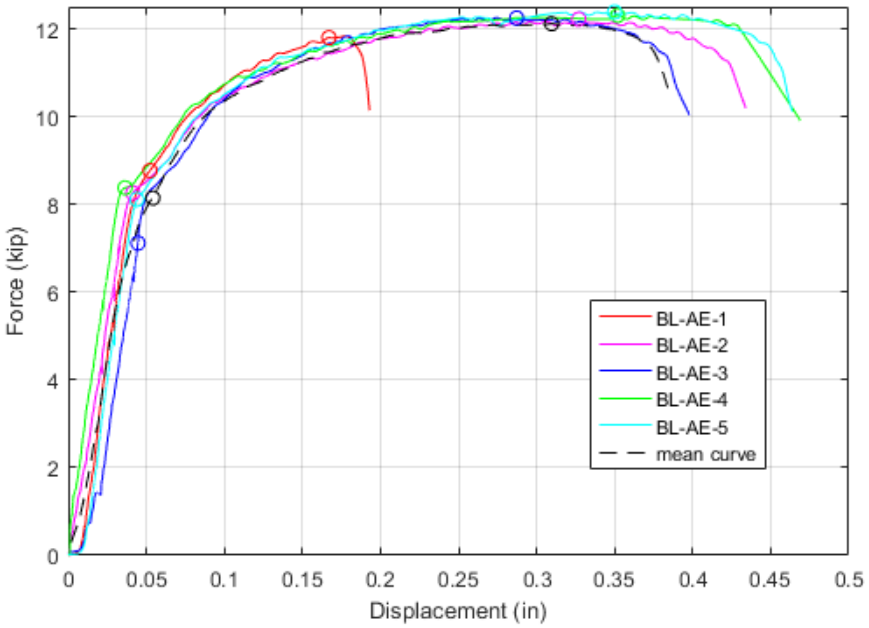

Figure C.61 BL-AE group comparison: individual test specimens against the mean response

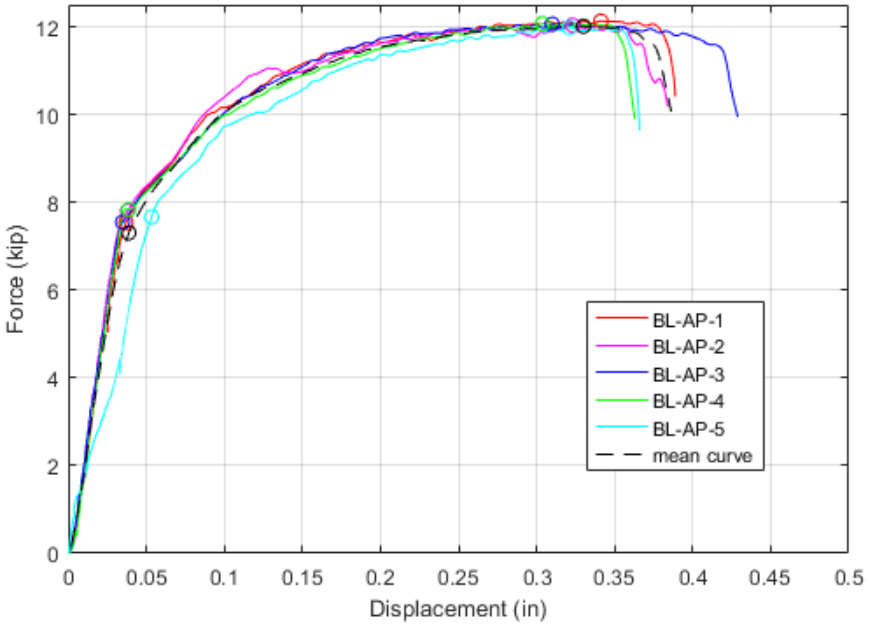

Figure C.62 BL-AP group comparison: individual test specimens against the mean response

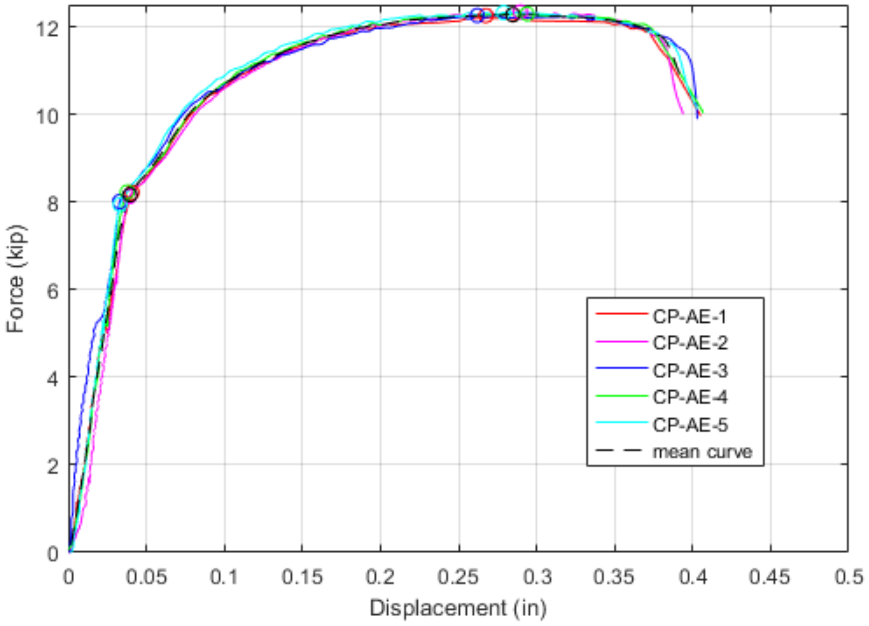

Figure C.63 CP-AE group comparison: individual test specimens against the mean response